Evaluation of Factors Controlling Release and Mobilization of Arsenic in parts of Brahmaputra Floodplain

Thesis submitted

in partial fulfilment of the requirement for the degree of

Doctor of Philosophy

by

Lalsangzela Sailo

Regd. No 05610407

DEPARTMENT OF CIVIL ENGINEERING

INDIAN INSTITUTE OF TECHNOLOGY GUWAHATI

GUWAHATI – 781039, INDIA

October 2011

Statement of originality

I hereby declare that the work presented in this thesis is to the best of my knowledge, original, except as acknowledged in the text. This material has not been submitted, either in whole or in part, for degree\ at any university.

Lalsangzela Sailo

Research Scholar

Department of Civil Engineering

IIT Guwahati.

Certificate

This is to certify that the thesis entitled "Evaluation of factors controlling release and mobilization of Arsenic in parts of Brahmaputra floodplains" submitted by Lalsangzela Sailo (Registration No.05610407) to the Indian Institute of Technology Guwahati for the degree of Doctor of Philosophy is a record of bonafide research work carried out by him under my supervision and guidance. The thesis work, in my opinion has reached the requisite standard fulfilling the requirement for award of the degree of Doctor of Philosophy. This work has not been submitted earlier for the award of any degree or diploma to the best of my knowledge and belief.

(Supervisor)

Chandan Mahanta

Professor

Department of Civil Engineering

Indian Institute of Technology Guwahati

Contents

Title	Page No.
Statement of Originality	i
Certificate	ii
Acknowledgements	iii
Abstract	iv
Contents	vii
List of Figures	xii
List of Tables	xv
Abbreviations	xvii
Chapter 1 **Introduction**	
1.1 Statement of purpose	1
1.2 Objective and hypothesis	2
1.3 Significance of the research work	3
1.4 Thesis structure	4
Chapter 2 **Literature review**	
2.1 General properties of Arsenic	5
2.1.1 Elemental characteristics	5
2.1.2 Toxicity	6
2.2 Sources of Arsenic in the environment	7
2.2.1 Natural occurrence	7
2.2.2 Anthropogenic sources	8
2.2.3 Background *As* concentration in the environment	8
2.2.3.1 Crustal materials	8
2.2.3.2 Groundwater	9
2.2.3.3 Surface water	10
2.2.3.4 Variation of Arsenic concentration in natural water	10
2.2.4 Global Arsenic assessment	11
2.3 Arsenic aquatic chemistry	12
2.4 Geochemical processes in aquifers involving Arsenic	14

2.4.1 Adsorption and desorption 15
2.4.1.1 Arsenic mobilization from Fe-oxides in aquifer sediments 15
2.4.1.2 Arsenic mobilization from Mn-oxides 18
2.4.1.3 Arsenic Sorption to clay minerals 19
2.4.1.4 Competitive anions exchange of Arsenic 20
2.4.1.4.1 Competitive anions exchange with PO_4^{3-} 20
2.4.1.4.2 Competitive anions exchange with HCO_3^- 21
2.4.1.4.3 Competitive anions exchange with SiO_2 21
2.4.1.5 Sorption of Arsenic by cations 22
2.4.1.6 Sorption of Arsenic by calcite 22
2.4.2 Oxidation and reduction 23
2.4.3 Precipitation and dissolution 25
2.4.4 Arsenic mobilization by Natural Organic Matter (NOM) 26
2.5 Immobilization of Arsenic in the aquifer materials 27
2.5.1 Arsenic adsorption by natural sediments 28
2.5.1.1 Langmuir adsorption isotherm 29
2.5.1.2 Freundlich adsorption isotherm 29
2.5.2 Kinetics of *As* adsorption 30
2.5.2.1 Pseudo First-Order kinetic model 31
2.5.2.2 Pseudo Second-Order kinetic model 31
2.5.2.3 Elovich kinetic model 33
2.5.2.4 Intra-particle diffusion model 34
2.5.3 Oxidation kinetics of *As*(III) to *As*(V) 34
2.5.4 Surface Complexation Model (SCM) 35
Chapter 3 **Study area**
3.1 Location and Environmental Conditions 38
3.1.1 Study area in the Darrang district 38
3.1.2 Study area in the Jorhat district 38
3.2 Geological Setting 40
3.2.1 Darrang district 40
3.2.2 Jorhat district 40
3.3 Hydrogeology 41
3.3.1 Darrang district 41
3.3.2 Jorhat district 41

3.4 Previous investigations 41
3.5 Aquifer lithologs 42
Chapter 4 **Methodology**
4.1 Groundwater and sediment sampling 44
4.1.1 Groundwater sampling 44
4.1.2 Sediment sampling 45
4.2 Groundwater analysis 46
4.3 Solid phase analysis 48
4.3.1 Chemical parameters 48
4.3.1.1 pH 48
4.3.1.2 Cation Exchange Capacity (CEC) 48
4.3.1.3 Loss On Ignition (LOI) 49
4.3.2 X-Ray Diffraction (XRD) 49
4.3.3 Scanning Electron microscopy and Energy Dispersive X-Ray 49
4.3.4 Particle size analysis 50
4.3.5 Total metal concentration (EPA – 3052) 50
4.3.5.1 Quality control and quality assurance 50
4.3.6 Selective Sequential Extraction (SSE) 51
4.3.6.1 Recovery through Selective Sequential Extraction 52
4.3.7 Attenuation experiment of Arsenic 52
4.3.7.1 Batch sorption kinetics study 53
4.3.7.2 Oxidation kinetics of *As*(III) to *As*(V) 54
4.3.7.3 Batch adsorption study 55
4.3.8 Validity of the models 55
4.4 Statistical analysis 56
4.5 Geochemical model (PHREEQC) 56
4.5.1 Inverse geochemical model 57
4.5.2 Surface Complexation Model (SCM) 58
Chapter 5 **Results and discussion**
5.1 Groundwater geochemistry 62
5.1.1 Groundwater geochemistry of the study area in Darrang district 62
5.1.1.1 Groundwater composition 64

5.1.1.2 Mineral saturation 66
5.1.1.3 Arsenic and other water quality parameters 67
5.1.2 Groundwater geochemistry of the study area in Jorhat district 69
5.1.2.1 Groundwater composition 72
5.1.2.2 Mineral saturation 73
5.1.2.3 Arsenic and other water quality parameters 75
5.1.2.4 Inverse geochemical modeling at Site_1 79
5.1.3 Comparison with hydrogeochemistry of other contaminated areas 81
5.2 Sediment characteristics 82
5.2.1 Sediment properties 83
5.2.1.1 pH of sediment 83
5.2.1.2 Loss On Ignition (LOI) 84
5.2.1.3 Cation Exchange Capacity (CEC) 85
5.2.1.4 X-Ray Diffraction (XRD) 87
5.2.1.5 Scanning Electron Microscopy (SEM) and Energy Dispersive X-Ray (EDX) 89
5.2.1.6 Specific Surface Area (SSA) 90
5.2.2 Total metal concentration 91
5.2.2.1 Quality control and quality assurance 101
5.2.3 Selective Sequential Extraction (SSE) of Arsenic 102
5.2.3.1 Selective Sequential Extraction (SSE) for Site_1 103
5.2.3.2 Selective Sequential Extraction (SSE) for Site_2 108
5.2.3.3 Selective Sequential Extraction (SSE) for Site_3 110
5.2.3.4 Selective Sequential Extraction (SSE) for Site_4 113
5.2.3.5 Selective Sequential Extraction (SSE) for deep tubewell 114
5.2.3.6 Comparison of SSE with that of other South East Asian countries 116
5.3 Arsenic Remediation Study 119
5.3.1 Sorption kinetics of Arsenic 119
5.3.1.1 Pseudo-First-Order kinetic model 120
5.3.1.2 Pseudo Second-Order kinetic model 120
5.3.1.3 Elovich kinetic model 123

5.3.1.4 Intra-particle diffusion model 125
5.3.2 Arsenic adsorption isotherm 126
5.3.2.1 Effect of pH 128
5.3.2.2 Effect of Phosphate (PO_4^{3-}) 129
5.3.2.3 Effect of Silica (SiO_2) 130
5.3.2.4 Effect of Bicarbonate (HCO_3^-) 130
5.3.2.5 Combined anions effect 131
5.3.3 Oxidation of *As*(III) to *As*(V) 132
5.3.3.1 Conceptual model for *As*-surface interaction 135
5.3.4 Surface Complexation Model (SCM) 138
Chapter 6 **Summary and conclusions** 143
References 148
Appendix
A 1. Groundwater Quality Data from the study areas. 162
A 2. SEM and EDX data from the drillcore 1A of Site_1. 170
A 3. X–Ray Diffraction (XRD) data from drillcore 1A of Site_1. 172
A 4. Total Metal Concentration (mg/kg) of sediments at Site_1 for Cu, Zn, Cd, Cr, Mg, Na, Ca, K along the depth profile. 175
A 5. *As* extraction in mg/kg using SSE from Site_1. 182
A 6. Kinetic study models for *As* adsorption. 183
A 7. Surface complexation model 186

List of Figures

No.	Caption	Page
Figure 2.1	Eh-pH diagram for aqueous *As* species in the system *As*-O_2-H_2O at 25°C and 1 bar total pressure.	14
Figure 2.2	Schematic sequence of geochemical reactions for dissolution of *As* in the groundwater of Bengal Delta.	24
Figure 3.1	Location of the study area in Jorhat district and Darrang district of Assam.	39
Figure 3.2	Lithologs of drilled cores from Site_1 (a) 1B (b) 1C (c) 2F (d) 2G locations.	43
Figure 4.1	Six drilled core of Site_1 (Tokobari) targeting Tubewell 1 and Tubewell 2.	46
Figure 5.1	Piper diagram of the groundwater composition of the (a) Pub-Mangaldai (b) Sipajhar	65
Figure 5.2	Saturation Indices of minerals (a) Pub-Mangaldai, (b) Sipajhar.	66
Figure 5.3	PCA plots of groundwater quality parameters at (a) Pub-Mangaldai (b) Sipajhar.	69
Figure 5.4	Piper diagram showing the composition of groundwater for (a) Site_1 (b) Site_2 (c) Site_3 and (d) Site_4.	73
Figure 5.5	Saturation indices of groundwater samples from (a) Site_1 (b) Site_2 (c) Site_3 and (d) Site_4.	74-75
Figure 5.6	PCA plots of groundwater quality parameters in (a) Site_1 (b) Site_2 (c) Site_3 and (d) Site_4.	77-78
Figure 5.7	Inverse geochemical model of Groundwater quality for Site_1 (a) model-1 (b) model-2.	81
Figure 5.8	Average pH distribution along the depth profile of sediments from Site_1.	83
Figure 5.9	Organic carbon content (LOI) of the sediment samples from (a) 1A (b) 1B (c) 1C (d) 2E (e) 2F (f) 2G sampling locations.	85
Figure 5.10	Cation Exchange Capacity (CEC) of the sediment samples from (a) 1A (b) 1B (c) 1C (d) 2E (e) 2F (f) 2G sampling locations	86-87
Figure 5.11	X-Ray Diffraction (XRD) of sediment samples (a) 1C_50 (b) 1C_70 (c) 1C_150.	88
Figure 5.12	SEM and EDX of soil sediment samples (a) 1C_50 (b) 1C_70 (c) 1C_150.	89
Figure 5.13	Specific Surface Area (SSA) distributions along the depth profile for samples at (a) 1A (b) 1B (c) 1C (d) 2E (e) 2F (f) 2G.	90-91
Figure 5.14	Depth wise distribution of (a) total *As*, (b) total Fe, (c) total Mn of the sediment core samples at location 1A. (d) PCA plot of total metal concentrations for sediment samples at 1A	93-94
Figure 5.15	Depth wise distribution of (a) total *As*, (b) total Fe, (c) total Mn of the sediment core samples at location 1B. (d) PCA plot of total metal concentrations for sediment samples at 1B	95
Figure 5.16	Depth wise distribution of (a) total *As*, (b) total Fe, (c) total Mn of the sediment core samples at location 1C. (d) PCA plot of total metal concentrations for sediment samples at 1C	96-97

Figure 5.17	Depth wise distribution of (a) total *As*, (b) total Fe, (c) total Mn of the sediment core samples at location 2E. (d) PCA plot of total metal concentrations for sediment samples at 2E	98
Figure 5.18	Depth wise distribution of (a) total *As*, (b) total Fe, (c) total Mn of the sediment core samples at location 2F. (d) PCA plot of total metal concentrations for sediment sampled at 2F	99-100
Figure 5.19	Depth wise distribution of (a) total *As*, (b) total Fe, (c) total Mn of the sediment core samples at location 2G. (d) PCA plot of total metal concentrations for sediment samples at 2G	100-101
Figure 5.20	*As* extraction through SSE from sediment core samples at (a) 1A (b) 1B (c) 1C (d) 2E (e) 2F (f) 2G.	104-105
Figure 5.21	Fe extraction through SSE from sediment core samples at (a) 1A (b) 1B (c) 1C (d) 2E (e) 2F (f) 2G.	106
Figure 5.22	Mn extractions through SSE from sediment core samples at (a) 1A (b) 1B (c) 1C (d) 2E (e) 2F (f) 2G.	107
Figure 5.23	*As* extraction through SSE from sediment samples (a) BH6 (b) BH7.	109
Figure 5.24	Fe extraction through SSE from sediment samples (a) BH6 (b) BH7.	110
Figure 5.25	Mn extraction through SSE from sediment samples (a) BH6 (b) BH7.	110
Figure 5.26	*As* extraction through SSEf rom sediment samples at (a) BH1 (b) BH2 (c) BH3.	111
Figure 5.27	Fe extraction through SSE from sediment samples at (a) BH1 (b) BH2 (c) BH3.	112
Figure 5.28	Mn extraction through SSE from sediment samples at (a) BH1 (b) BH2 (c) BH3.	112-113
Figure 5.29	Results of SSE for *As* from sediment samples at (a) BH4 (b) BH5.	114
Figure 5.30	Results of SSE Fe extraction from sediment samples at (a) BH4 (b) BH5.	114
Figure 5.31	Results of Mn extraction from sediment core samples at (a) BH4 (b) BH5.	114
Figure 5.32	Results of SSE from sediment samples of deep borehole for (a) *As* (b) Fe (c) Mn.	116
Figure 5.33	Pseudo-second order kinetics for C_50 with initial *As*(III) 300 µg/l for (a) Type-1 (b) Type-2 (c) Type-3 (d) Type-4.	121
Figure 5.34	Elovich adsorption kinetics model for C_50 sample with initial *As*(III) concentration of 300 µg/l.	124
Figure 5.35	Intra-particle diffusion model for (a) C_50 sample with initial *As*(III) 300 µg/l (b) two linear segment for C_50 sample.	126
Figure 5.36	Adsorption isotherm for (a) *As*(V), (b) *As*(III) for the three sediments samples C_50, C_70 and C_150.	127
Figure 5.37	Effect of pH on adsorption of with initial concentration of 500 µg/l on (a) *As*(V) and (b) *As*(III) for sediment samples.	128
Figure 5.38	Effect of phosphate (P) on adsorption of *As*(V) with initial concentration of (a) 300 µg/l and (b) 500 µg/l for sediment samples.	130
Figure 5.39	Effect of silica (SiO_2) on adsorption of *As*(V) with initial concentration of (a) 300 µg/l and (b) 500 µg/l for sediment samples.	130
Figure 5.40	Effect of bicarbonate (HCO_3^-) on adsorption of *As*(V) with initial concentration of (a) 300 µg/l and (b) 500 µg/l for sediment samples.	131

Figure 5.41	Combined effect of anions on adsorption of *As*(V) with initial concentration of (a) 300 µg/l and (b) 500 µg/l for sediment samples with increasing phosphate (PO_4^{3-}).	131
Figure 5.42	Oxidation kinetics of *As*(III) for soil sample C_50 for initial *As*(III) concentration of (a) 500 µg/l and (b) 300 µg/l.	133
Figure 5.43	43 Oxidation kinetics of *As*(III) for soil sample C_70 for initial *As*(III) concentration of (a) 500 µg/l and (b) 300 µg/l.	133
Figure 5.44	Oxidation kinetics of *As*(III) for soil sample C_150 for initial *As*(III) concentrations of (a) 500 µg/l and (b) 300 µg/l	134
Figure 5.45	Schematic showing multi-steps redox reaction between *As*(III) and Manganese oxides on the surface of sediments.	137
Figure 5.46	The relative composition of Surface complex calculated from the composition of groundwater quality of Site_1 using PHREEQC.	141
Figure A2.1-A2.7	SEM and EDX data from the sediment core at 1A at depth of 3 m, 9 m, 15 m, 21 m, 27.5 m, 33.5 m, 47 m.	170-171
Figure A3.1-A3.8	X–Ray Diffraction (XRD) data from the sediment core at 1A at depth of 3 m, 9 m, 15 m, 21 m, 27.5 m, 33.5 m, 40 m, 47 m.	172-174
Figure A4.1 – 4.	Total metal concentration along depth profile in the sediment cores (a) 1A (b) 1B (c) 1C (d) 2E (e) 2F (f) 2G for	
	A 4.1 Copper (Cu)	175
	A 4.2 Zinc (Zn)	176
	A 4.3 Cadmium (Cd)	177
	A 4.4 Chromium (Cr)	178
	A 4.5 Sodium (Na)	178
	A 4.6 Magnesium (Mg)	179
	A 4.7 Calcium (Ca)	179
	A 4.8 Potassium (K)	180

List of Tables

No.	Caption	Page
Table 2.1	Common physico-chemical properties of arsenic.	5
Table 2.2	Common naturally occurring arsenic bearing minerals and their occurrence in environment.	7
Table 2.3	Natural abundance of *As* (mg/kg) in crustal materials.	9
Table 2.4	Pseudo-second-order kinetic model linear form.	33
Table 4.1	List of the groundwater quality parameters analyzed and name of the experiment or instrument.	46
Table 4.2	List of analytical instruments and their model/manufacturer used for the analysis of groundwater and sediment parameters.	47
Table 4.3	Selective Sequential Extraction (SSE) scheme for sediments.	52
Table 4.4	Surface reactions and thermodynamic constants for PHREEQC surface complexation model with strong (Hfo_s) and weak (Hfo_w) adsorption sites.	59
Table 4.5	Surface reactions and thermodynamic constants for PHREEQC surface complexation model with goethite (Goe_) adsorption sites.	60
Table 5.1	Groundwater composition of Pub-Mangaldai area (units mg/l, except pH and EC µs/cm).	63
Table 5.2	Groundwater composition of Sipajhar area (units mg/l, except pH and EC µs/cm).	64
Table 5.3	Groundwater composition of Site_1 (units mg/l, except pH and EC µs/cm).	70
Table 5.4	Groundwater composition of Site_2 (units mg/l, except pH and EC µs/cm).	70-71
Table 5.5	Groundwater composition of Site_3 (units mg/l, except pH and EC µs/cm).	71
Table 5.6	Groundwater composition of Site_4 (units mg/l, except pH and EC µs/cm).	71-72
Table 5.7	Correlation amongst LOI, SSA and CEC for samples obtained from borehole 1A, 1B, 1C, 2E, 2F and 2G.	84
Table 5.8	Total metal concentrations in the sediment (mg/kg).	92
Table 5.9	Recovery percent of various elements analyzed for JLk-1 and JSd-3 (CRM).	102
Table 5.10	Characteristics of the three sediments with their extraction (SSE) values used for the batch experiments.	119
Table 5.11	Pseudo-second-order kinetic parameters obtained by using linear regression methods for 300 µg/l *As*(III).	121
Table 5.12	Pseudo-second-order kinetic parameters obtained by using linear regression methods for 500 µg/l *As*(III).	122
Table 5.13	Pseudo-second-order kinetic parameters obtained by using linear regression methods for 300 µg/l *As*(V).	122

Table 5.14	Pseudo-second-order kinetic parameters using linear regression methods for 500 µg/l *As*(V).	122-123
Table 5.15	Regression analysis results of the Elovich kinetic model for *As*(III) and *As*(V) with initial concentrations of 300 µg/l and 500 µg/l.	124
Table 5.16	Intra-particle diffusion adsorption model parameters for initial *As*(V) concentrations of 300 µg/l and 500 µg/l.	125
Table 5.17	Freundlich and Langmuir adsorption isotherm parameters for sediments samples.	127-128
Table 5.18	Input parameters for PHREEQC surface complexation model in amorphous Fe-oxides for surface site densities (mol sites/mol Fe) for sample 1A.	138
Table 5.19	Input parameters for PHREEQC surface complexation model in crystalline Fe-oxides for surface site densities (mol sites/mol Fe) for sample 1A.	139
Table 5.20	Model output using *As* extracted from amorphous Fe-oxides for sample 1A.	140
Table 5.21	Model output using *As* extracted from crystalline Fe-oxides for sample 1A.	140
	APPENDIX	
	Groundwater Quality data from the study areas	
	A 1.1 Pub-Mangaldai Darrang district	162
Table	A 1.2 Sipajhar Darrang district	163
A 1.1-A 1.6	A 1.3 Site_ 1 Jorhat district	164
	A 1.4 Site_ 2 Jorhat district	166
	A 1.5 Site_ 3 Jorhat district	167
	A 1.6 Site_ 4 Jorhat district	168
Table A5	*As* extraction in mg/kg using SSE from Site_1 for 1A, 1B, 1C, 2E, 2F and 2G locations.	182
	Kinetics study for 1C_50 sediments with As(III) 300 µg/l	183
Table	A 6.1 Type 1 Pseudo-Second-Order kinetics models	183
A 6.1-A 6.4	A 6.2 Type 2 Pseudo-Second-Order kinetics models	184
	A 6.3 Type 3 Pseudo-Second-Order kinetics models	184
	A 6.4 Type 4 Pseudo-Second-Order kinetics models	
Table A 6.5	Elovich model for 1C_50 sediments with As(III) 300 µg/l	185
Table A 6.6	Intra-particle diffusion model for 1C_50 sediments with As(III) 300 µg/l	185
Table A 7.1	Phreeqc input for SCM model Fe-oxides amorphous	186
Table A 7.2	Phreeqc input for SCM model Fe-oxides crystalline (Goethite)	186
Table A 7.3	Phreeqc model output for SCM model Fe-oxides amorphous	187
Table A 7.4	Phreeqc model output for SCM model Fe-oxides crystalline	189

Chapter 1

Introduction

1.1 Statement of purpose

Arsenic contamination of groundwater continues to be a serious concern for public health affecting millions of people world-wide (Bhattacharya et al., 1997, 2002, 2006, 2007; Nickson et al., 1998, 2000, 2005, 2007; Matschullat, 2000; Berg et al., 2001, 2007, 2008; Friedrich et al., 2001; Nordstrom, 2002; Smedley and Kinniburgh, 2002; Welch and Stollenwerk, 2003; Bundschuh et al., 2005; Naidu et al., 2006; Shrestha et al., 2003; Farooqi et al., 2007; Pfeifer et al., 2007; Nriagu et al., 2007). The floodplains of Ganga-Brahmaputra-Meghna (GBM) covering an area of approx. 5,00,000 km^2 with a population over 500 million are at risk of arsenic (*As*) contamination (Chakraborti et al., 2004). Assam plains which is located in North-Eastern part of India, adjoining Bangladesh and the state West Bengal where severe arsenic toxicity has been recently manifested have similar hydrogeologic setting (Nickson et al., 2007), which has increased the vulnerability to *As* contamination.

Following initial reports of presence of arsenic in groundwater in the Brahmaputra floodplain of Assam in 2004 (Chakraborti et al, 2004; Singh, 2004), the Public Health Engineering Department (PHED) of Assam in collaboration with UNICEF, conducted an "Assessment of Presence of Arsenic in Groundwater in Assam" to identify areas contaminated with arsenic during 2004 - 2005. In this assessment program, 5,729 groundwater samples collected from 192 blocks spreading across 22 districts revealed that 6.3% of the sources did contain arsenic concentration greater than 50 µg/l and 26% at concentration greater than 10 µg/l (Nickson et al., 2007). It was further reported that groundwater in 76 blocks from 18 districts were contaminated with high level of arsenic.

Following the Rapid Assessment, the PHED, Government of Assam initiated Arsenic Screening Program (leading to blanket screening of an estimated 56,180 sources) with technical assistance from IIT Guwahati, in collaboration with UNICEF. 8% of samples were found to have *As* concentration greater than 50 µg/l and 30% at concentration greater than 10 µg/l (Mahanta et al., 2010).

The groundwater *As* contamination in Assam is of special concern to the public as most of the people in the rural areas rely solely on groundwater sources for drinking, domestic and irrigation purposes. The popularity of groundwater as a source comparing surface water source for potable water in Assam is due to the availability of water during dry periods, flooding and water logged period, and lesser inherent risk of water borne diseases like diarrhea, cholera etc. This exposure to high *As* concentration in the drinking water has caused major health hazard risk to a large section of people of Assam. In Bangladesh it has been estimated that if consumption of *As* contaminated water continues, the occurrence of arsenicosis will extend to approx. 20,00,000 cases, that of skin cancer will be approx. 1,00,000, and the incidence of death from cancer induced by arsenic will be approx. 3,000 per year (Yu et al., 2003). However, while a similar large risk is anticipated in the Assam plains as well, relative extent of research in the upper Brahmaputra floodplains have remained almost non-existent.

1.2 Objectives and hypothesis

The present work is an attempt to understand the mechanism and processes involving occurrence, distribution, mobilization and release of *As* in Assam plains focusing upon the major factors that influence *As* release and mobilization. The following objectives were set for the proposed research work:

1. To identify potential location of arsenic in the aquifers in the highly contaminated areas.
2. To determine the influencing parameters present in groundwater and in sediments that control *As* mobilization and release.
3. To investigate the hydrogeochemical processes contributing to arsenic release and mobilization in the aquifers of the study area.
4. To explore processes leading to lowering of *As* concentration in the groundwater with the help of batch sorption and kinetics experiments on sediment samples that may lead to in-situ attenuation mechanism.
5. To predict *As* sorption onto the sediments by surface complexation model using groundwater geochemistry with the available database, that may improve the understanding for attenuation mechanism.

It was hypothesized that the *As* pollution in the study area is geogenic i.e. of natural origin, due to the absence of any evidence of anthropogenic sources. Natural arsenic is believed to be derived from erosion of lithified sediments and crystalline rocks of the Himalayan range and adjacent region (Breit et al., 2003; McArthur et al., 2004). The eroded materials may contain *As* bearing "primary minerals" transported by the large river network of the Brahmaputra (Harvey et al., 2006; Polizzotto et al., 2006, 2008). After the sediments were buried, strong reducing condition could have been established in the alluvial aquifers, which facilitated mobilization and release of *As* into the groundwater.

On the other hand, the current *As* sinks in the sediments are likely to be constituted by sorption onto Fe-oxides and Mn-oxides and clay mineral surfaces and precipitation into various solid phase minerals that could adsorb *As*. The mobilization of *As* in groundwater are anticipated due to particular hydrologic and natural biogeochemical conditions that partition arsenic from the solid to aqueous phase and perhaps transport arsenic into a contaminated aquifer, but have not yet flushed dissolved arsenic from these aquifers (Harvey et al., 2006; van Geen et al., 2008). Chemical heterogeneity may largely influence arsenic partitioning within solid phases, thus affecting its occurrence in dissolved phase. Possible *As* release mechanism may include desorption, dissolution from arsenic-bearing oxides and clay minerals; and the oxidation of minerals containing *As*. Some mobilization of *As* may be enhanced by possible anthropogenic activities resulting in disequilibrium of natural conditions and further arsenic release (Harvey et al., 2002; van Geen et al., 2004; McArthur et al., 2004; Polizzotto et al., 2008). In the present study area this has been found to be of limited possibility due to thin habitation and lack of mining and industrialization.

1.3 Significance of the research work

Numerous research studies have been carried out in the arsenic affected areas of Bangladesh and West-Bengal, which lie adjacent to the Assam floodplains. The alluvial plains of Assam deposited largely by the Brahmaputra River remains unexplored in this region, inspite of reports of wider spread of *As* contamination. The results of the present study are expected to contribute towards the risk assessment of the aquifers and give insight into the major geochemical processes leading to the dissolution of *As* from the sediment phase.

The current *As* sinks identified in the sediments of the Assam plains will lead to an increased understanding of *As* partitioning within the solid phase. The studies on the sediment-water interaction and effects of the various competing anions will increase scientific understanding of *As* mobilization processes within the aquifers.

In order to achieve the objectives, required amount of groundwater samples, sediment samples and hydrogeological data were analyzed and collected, the results of which will contribute towards the overall management of the aquifer systems in the study area for the yield of safe water. This work is expected to make a contribution to the science of arsenic hydrogeochemistry and provide practical knowledge to aid the understanding and future management of the aquifers in Brahmaputra floodplains for sustainable groundwater development and management.

1.4 Thesis structure

The thesis consists of five chapters:

Chapter 1 is the introductory chapter which establishes the background of the study and the need for seeking new insight into the understanding of groundwater arsenic contamination in an unexplored region with the help of state of art scientific tools. Chapter 2 reviews the literature on the arsenic geochemistry including its occurrence in the environment and its mobilization processes in the natural geochemical conditions. The background of basic attenuation experiments (batch sorption experiment) for adsorption, kinetics, oxidation of *As*(III) to *As*(V) and details of surface complexation model have been extensively discussed with the help of available literature. Chapter 3 provides a review of the study areas their environmental conditions, geology and hydrogeology. Chapter 4 outlines the methodology used for collection and analysis of the samples, the experimental conditions, instruments used and tools and procedures followed to arrive at the results and findings. In Chapter 5, efforts has been made to present in a organized way the main elements of the findings of the investigations. It was further divided into three main sections: *Section 5.1* covers the evaluation of the hydrogeochemistry and establishes its relation with arsenic distribution in the aquifers; *Section 5.2* discusses the sediment characteristics and sequential extraction of *As* from the sediment samples; *Section 5.3* covers the attenuation experiments based on batch studies i.e. adsorption kinetics and isotherm, along with oxidation of *As*(III) to *As*(V) and finally the surface complexation model results followed by a synthesis of the results and discussions. Chapter 6 provides a summary and conclusion of the research work, highlighting the salient findings. References contain the bibliography and citations used in the study. Appendices contain the supporting data that were considered to elaborate for inclusion in the main body of thesis.

Chapter 2

Literature review

The grave health consequences of arsenic (*As*) have led to numerous amount of scientific research being conducted on arsenic toxicity, mobility, occurrence, chemical behavior, cycling and bioaccumulation. In recent decades numerous research efforts were made to understand the processes that control *As* mobilization in groundwater systems. The understanding of *As* occurrence in the environment has been reviewed extensively in research reports including Matschullat (2000), Smedley and Kinniburgh (2002), Mandal and Suzuki (2002), Hossain (2006), Bhattacharya et al. (2007), Drahota and Filippi (2009), Sharma and Sohn (2009), Brammer and Ravencroft (2009). Given the amount of published literature on *As*, this review will focus on the topics which are more to *As* issues relevant to the study area. Where possible, references for further reading have been added on aspects that are less critical to this investigation and these are only briefly discussed.

2.1 General properties of Arsenic

2.1.1 Elemental characteristics

Arsenic is the 20th most abundant elements in the earth's crust, 14th in the sea water and 12th in the human body (Mandal and Suzuki, 2002). It is found at low concentrations in most soils and sediments. Arsenic belongs to Group 15 of the Periodic Table and is considered a metalloid (semi-metal) because it resembles a metal in appearance but behaves like a non-metal. It is often referred to as semi-conductor, as it conducts electricity, but less effectively than metals. Few major characteristics of arsenic are listed in Table 2.1.

Table 2.1 Common physico-chemical properties of arsenic

Properties	Values
Atomic Number	33
Atomic Mass	74.92
Melting Point	814 °C
Boiling Point	610 °C
Main Oxidation State	-3, +3, +5, 0
Density	5.73 g/cm^3 (grey) 1.98 g/cm^3 (yellow)
Electro-negativity	2
Atomic Radius	133 pm

Arsenic exists in the environment in the four oxidation states viz. Arsenate *As*(V) or (As^{5+}), Arsenite *As*(III) or (As^{3+}), Arsenic (As^{0}) and Arsine (As^{3-}). In natural water the two main oxidation states i.e Arsenate ions [*As*(V)] which are most prevalent in oxic conditions and Arsenite ions [*As*(III)] are found in anaerobic conditions. Arsenic metal rarely occurs and Arsine (As^{3-}) oxidation state is found only in highly reduced environment. The forms of arsenic are dependent on the type and amounts of sorbents, pH, redox potential (Eh), and microbial activity (Wang and Mulligan, 2006; Bhattacharya et al., 2007; Polizzotto et al., 2006, 2008; Reza et al., 2010a,b).

2.1.2 Toxicity

Arsenic (*As*) is a carcinogenic, mutagenic and teratogenic element. Most *As* compounds are odorless and tasteless and readily dissolve in water. Drinking groundwater with higher *As* concentration can cause skin diseases, cardio-vascular, neurological, hematological, renal and respiratory diseases, as well as lung, bladder, liver, kidney and prostate cancer (Mandal and Suzuki, 2002; Mandal et al.,2003; Wang and Deng, 2009). Most of the *As* ingested is rapidly excreted via kidney within few days, however, high levels of *As* are retained for longer periods of time in the bone, skin, hair and nails of exposed humans (Mandal et al., 2003; Bhattacharya et al., 2007). Methylated arsenic species such as dimethylarsenous acid DMA(III) and monomethylarsenous acid MMA(III) are more acutely toxic and genotoxic i.e mutagenic and teratogenic than their parent compound (Sharma and Sohn, 2009) monomethylarsonic acid MMA(V), dimethylarsenic DMA(V), are found in trace quantities in human urine (Mandal et al., 2003; Bhattachary et al., 2007). The potency of the DNA damage decreases in the order:

DMA(III) > MMA(III) > *As*(III) > *As*(V) > MMA(V) > DMA(V)

The World Health Organization (WHO) has set a provisional guideline limit of 10 µg/l for *As* in drinking water (WHO, 1996), which was subsequently adopted by European Union (1998). United States Environmental Protection Agency (E.P.A) lowered the maximum contaminant level (MCL) for *As* in drinking water from 50 µg/l to 10 µg/l, effective in January 2006. The provisional guideline value for *As* concentration in drinking water of China has been lowered from 50 µg/l to the WHO recommendation of 10 µg/l since 2007. India has endorsed WHO limits of 10 µg/l by the Bureau of Indian Standards (BIS) in September 2003 (Chakraborti et al., 2011) and in Bangladesh, the guideline value for *As* in drinking water is still 50 µg/l.

2.2 Sources of Arsenic in the environment

2.2.1 Natural occurrence

Arsenic occurs naturally in a wide range of minerals in soils and several forms of inorganic compounds. Arsenic is a constituent of more than 200 minerals, which includes arsenate *As*(V) (60%), sulfides and sulfo-salts (20%) and minor amounts of arsenite, arsenate, oxides, silicates and *As* in its native forms. Table 2.2 illustrates that the majority of the arsenic minerals are generally with ore deposits and their alteration products.

Table 2.2 Common naturally occurring arsenic bearing minerals and their occurrence in environment

Mineral	Formula	Occurrence
Adamite	Zn_2AsO_4OH	Oxidation zone mineral, forming near metal ore deposit
Arsenolite	As_2O_3	Secondary mineral formed by oxidation of arsenopyrite native arsenic and other minerals
Arsenopyrite	FeAsS	Mineral veins
Claudetite	As_2O_3	Secondary mineral formed by oxidation of realgar, arsenopyrite and other *As* minerals
Cobaltite	CoAsS	High temperature deposits, metamorphic rocks
Glaucodote	(Co,Fe)AsS	Metalliferous veins with ores of tin, copper and silver – a replacement mineral of arsenopyrite
Native Arsenic	*As*	Hydrothermal veins
Niccolite	NiAs	Veins deposites and norites
Orpiment	As_2S_3	Hydrothermal veins, hot springs, volcanic sublimation products
Pharmacosiderite	$Fe_3(AsO_4)_2(OH)_35H_2O$	Oxidation product of arsenopyrite and other *As* minerals
Realgar	As_2S_2	Vein deposits, often associated with orpiment, clays and limestones, also deposites from hot springs
Scorodite	$FeAsO_4.2H_2O$	Secondary mineral

(Smedley and Kinniburgh (2002), Wang and Deng (2009))

The most abundant *As* ore mineral is arsenopyrite, FeAsS (46 wt.%), orpiment (60.9 wt.%) and realgar (70 wt.%) (Kirk et al., 2010). The main *As* source in nature viz. realgar (As_4S_4) and orpiment (As_2S_3) usually form even at low temperature, whereas arsenopyrite (FeAsS)

only formed under high temperature conditions in the earth's crust (Smedley and Kinniburgh, 2002; Hossain, 2006). Realgar (As_4S_4) and orpiment (As_2S_3) are the two common reduced forms of *As* whereas the oxidized form of *As* occurs in the mineral arsenolite (As_2O_3). However, authigenic arsenopyrite (FeAsS) has been reported in sediments and orpiment has been reported to have been formed by microbial precipitation (Lowers et al., 2007). Arsenic rich pyrite ($Fe(S,As)_2$) rather than arsenopyrite, is probably the most important source of *As* in ore zones (Nordstrom, 2002; Wang and Mulligan, 2006; Wang and Deng, 2009; Kirk et al., 2010).

2.2.2 Anthropogenic sources

Human production and use of arsenic and its compounds can lead to an increased load of this element in the environment. Failure to adequately contain arsenical compounds during or after their use may lead to mobilization of arsenic. Sources of *As* to the atmosphere, soils, sediment, and water include mining and smelting operations; industrial releases; sewage effluent discharges; applications of arsenical pesticides to crops, orchards, and lakes; fertilizer use (including chicken manure); and leaching from arsenic-treated wood products (Mandal and Suzuki, 2002; Ahmed et al., 2004; Bhattacharya et al., 2007).

2.2.3 Background As concentration in the environment

2.2.3.1 Crustal materials

Interaction of groundwater with host rocks drive the multiphase cycling of *As* in aquifer systems. The typical concentrations of *As* in crustal rocks were presented in Table 2.3. The crustal materials are classified according to its formation and type such as igneous, sedimentary, metamorphic rocks and coal. The concentration of *As* igneous rocks as well as metamorphic rocks are relatively lesser than the fine grained and organic rich sedimentary rocks. The *As* concentration in the sedimentary rocks can be more variable. The highest *As* concentrations (20-200 mg/kg) are typically found in organic and sulfide rich shales, sedimentary ironstone, phosphate rocks and some coal (Mandal and Suzuki, 2002; Smedley and Kinniburgh, 2002; Wang and Deng, 2009; McArthur et al., 2004, 2008, 2011).

In sedimentary rocks, high *As* concentration are found in clays and fine grained sediment, rich in sulfide minerals, organic matter, secondary iron-oxides, and phosphates. The concentration of *As* is higher in an order of magnitude for shale comparing sandstone and carbonaceous rocks. *As* strongly sorbed onto Fe-oxides, Al-oxides and Mn-oxides as well as

some clay minerals, which leads to enrichment of *As* in the ferromanganese nodules and manganiferrous deposits (Manning and Goldberg, 1997; Smedley and Kinniburgh, 2002).

Table 2.3 Natural abundance of *As* (mg/kg) in crustal materials

Rock Type	Average *As* concentration (mg/kg) (range)
Igneous	
Ultrabasics	1.5 (0.03-15.8)
Basalts	2.3 (0.18-113)
Granites/silicic rocks	1.3 (0.2-13.8)
Sedimentary	
Shales and Clays	3-15 (upto 490)
Phosphorites	21 (0.4-188)
SandstoneS	4.1 (0.6-120)
Limestone/dolomite	2.6 (0.1-20.1)
Fe-rich sediments	(1-2900)
Evaporites (gypsum/anhydrite)	3.5 (0.1-10)
Metamorphic rocks	
Quartzite	5.5 (2.2-7.6)
Hornfels	5.5 (0.7-11)
Phyllite/slate	18 (0.5-143)
Schist/gneiss	1.1 (<0.1-18.5)
Amphibolite and greenstone	6.3 (0.4-45)
Coal	
Peat	(16-340)
Lignites	7.4±1.4
Bituminous	9.0±0.8

(Smedley and Kinniburgh, 2002)

2.2.3.2 Groundwater

Background *As* concentration in the groundwater for most of the countries are less than 10 µg/l (Edmunds et al., 1989 for UK; Welch et al., 2000 for US) and sometimes substantially lower. Nonetheless, high *As* concentration occurring naturally have been found in many parts of the world and the concentration ranges from <0.5 µg/l to 5000 µg/l (Smedley and Kinniburgh, 2002). High concentrations of *As* are found in variety of environments including both oxidizing (under high pH) and reducing aquifers, and area affected by geothermal, mining and industrial activities (Mandal and Suzuki, 2002; Smedley and Kinniburgh, 2002; Bhattacharya et al., 2007).

Most of the high *As* contaminated groundwater are result of natural occurrences and have been found in different groundwater conditions and environments (Smedley and Kinniburg, 2002; Bhattacharya et al., 2007). The most commonly reported *As* mobilization processes is the reducing conditions from quaternary formation and deltaic regions, where strong neo-tectonic processes have resulted in complex patterns of sedimentation and rapid burial of

large amount of sediment containing fresh organic matter during its development (McArthur et al., 2001, 2004, 2011; Bhattacharya et al., 2007; Wang and Deng, 2009). These areas are characterize by thick sequence of young sediments (alluvial) with *As*(III) forming the predominant species. Oxidizing conditions also favors the higher *As* concentration in the groundwater where *As*(V) predominates with relatively higher pH (Bhattacharya et al., 2006). The concentration of arsenic in precipitation is quite low, with an average of 0.019 µg/l precipitations originating from unpolluted ocean air masses, and 0.46 µg/l for that of terrestrial air masses (Andrea, 1980). The global average *As* concentration value is 1.7 µg/l for dissolved *As* in stream water (Martin and Whitfield, 1983). When rain or snowmelt infiltrates through soils, the chemical weathering of soils and aquifer minerals alters its composition (Appelo and Postma, 2005). The differences in the chemical composition of surface water and groundwater reflect the progress of chemical weathering under varying conditions and for varying durations that are characteristic of these types of natural waters.

2.2.3.3 Surface water

In sea and ocean water *As*(V) predominates due to its oxic environment near surface, though some *As*(III) is invariably present and increasingly important in the anoxic bottom water (Smedley and Kinniburgh, 2002; O`Shea, 2007). The average *As* in oceans water is about 3 µg/l and the average of freshwater in rivers and streams is about 1 µg/l but are highly influenced by drainage areas, base-flow and point contamination sources such as industrial plants, mining near the area (O`Shea, 2007). In lake and river waters, *As*(V) is generally the dominant species, though significant seasonal variations in speciation as well as absolute concentration have been found (Oremland et al., 2000; Smedley and Kinniburgh, 2002). The reduction of *As*(V) to *As*(III) by the biological activity maintain the *As*(III) in the oxic water. Similarly vertical stratification of the water bodies viz. lake causes predominance of *As*(V) in the top oxic layer whereas *As*(III) dominates in the anoxic reducing layer (Oremland et al., 2000). Organic forms of *As* are minor in surface water, but can increase as a results of methylation reactions catalyzed by microbial activity (Oremland et al., 2000). Thus, *As*(V) generally dominates in surface waters but can be affected by stratification, anoxic bottom sediments, microbial interaction and anthropogenic input.

2.2.3.4 Variation of Arsenic concentration in natural water

Several studies have reported daily and seasonal variation in raw water arsenic concentration. The issue of seasonal arsenic measurement variability poses consequences regarding the

interpretation and frequency of well measurements. Previous studies have demonstrated seasonal variability of arsenic levels when measured in surface streams (Cheng et al, 2005). Stream has been hypothesized to be related to deliberate pollution, water pH, and release of other metals, which can adsorb arsenic (Olias et al., 2004). Azeue and Nriagu (1995) found that dissolved arsenic varies with seasonal change, during summer 60% of the arsenic in the hypolimnion is largely present as *As*(III).

Cheng et al. (2005) observed high seasonal variability in the *As* concentration in very shallow aquifer (< 10 m) along with changes in *As* concentration with time. Chakraborti et al. (2004) reported increase in the *As* concentration of many wells in West-Bengal over time. Dhar et al. (2008) observed that shallow and young groundwater are highly vulnerable to redox as well as major ions changes has lesser effect on *As* concentration, while deeper aquifers groundwater was mostly stable over time. The results of change in *As* concentration with seasonal variation have been inconsistent, with some wells showing higher arsenic concentrations during the wet season, some showing higher concentrations during the dry season, and some showing little seasonal change. Nadakavukaren et al. (1984) identified several wells in Oregon in which arsenic concentrations decreased dramatically in the wet season including one well in which arsenic levels fell from over 1000 µg/l during a period of low rainfall to under 400 µg/l during a period of high rainfall. Berg et al. (2001) reported *As* concentration declined between September – December, 1999 and May 2000 in many of 68 wells in four districts of Red River Delta. The reasons why these large heterogeneity in *As* concentrations have been seen in some wells is not entirely clear although mechanisms such as dilution by rainfall or changes in redox conditions due to seasonal changes in pumping rates, groundwater flow, or water table depths, local geology (Harvey et al., 2002, 2005; Zheng et al., 2004; van Geen et al., 2006, 2008; Cheng et al., 2005; Nadakavukaren et al., 1984; Dhar et al., 2008).

2.2.4 Global Arsenic assessment

Arsenic (*As*) has been detected in groundwater in several countries of the world, with concentration levels exceeding the WHO drinking water guideline value of 10 µg/L (WHO, 1996) as well as national regulatory standards (e.g. 50 µg/l of Bangladesh). In Asia, the impact of *As* toxicity has high risk potential because millions of people depend on the groundwater for drinking, cooking and domestic purposes as well as irrigation for example Bangladesh and West Bengal (Bhattacharya et al., 1997, 2002, 2006, 2007; Mukherjee and Bhattacharya, 2001; Smedley and Kinniburgh, 2002; Welch and Stollenwerk, 2003;

Bundschuh et al., 2005; Naidu et al., 2006). Recent studies indicate the occurrence of geogenic arsenic in Central/Middle Gangetic Plains of Uttar Pradesh, Bihar, Jharkhand, Assam (Chakraborti et al., 2004, 2011; Mukherjee et al., 2006; Nickson et al., 2007). In 2001 groundwater arsenic contamination of the sedimentary aquifers of the Terai Belt in Southern Nepal has been noticed (Shrestha et al., 2003). Red river delta and Mekong basin of Vietnam and Cambodia (Berg et al., 2001, 2007, 2008), Pakistan (Nickson et al., 2005; Farooqi et al., 2007), Taiwan (Wang et al., 2007), thus, raising severe constraints on its use as a drinking water resource. However, high arsenic concentration is also reported in groundwaters of Australia, with arsenic concentration well above the drinking water standard of 7 μg/l recommended by the National Health and Medical Research Council and the Natural Resource Management Ministerial Council of Australia (NHMRC/NRMMC, 2004) (Smith et al., 2006; O`Shea et al., 2007). Similarly, in some European Countries viz. Switzerland (Pfeifer et al., 2007) and Hungary (Varsanyi and Kovacs, 2006) contamination of arsenic in patches are reported.Arsenic is also found in widely scattered geographical areas in the United States and Canada (Robinson and Ayotte, 2006; Barringer, 2007) as well as in many other countries of Latin America such as Mexico (Matschullat, 2000; Friedrich et al., 2001; Miller, 2001; Nordstrom, 2002; Nriagu et al., 2007), Argentina (Matschullat, 2000; Smedley and Kinniburgh, 2002; Bundschuh et al., 2005; Bhattacharya et al., 2006; Nriagu et al., 2007), Bolivia (Matschullat, 2000; Nordstrom, 2002; Nriagu et al., 2007), Brazil and Nicaragua (Nriagu et al., 2007; Nordstrom, 2002), where the sources of *As* are geogenic as well as anthropogenic sources (Matschullat, 2000; Nordstrom, 2002; Nriagu et al., 2007).

2.3 Arsenic aquatic chemistry

A comprehensive thermodynamic model including all chemical equilibria important for predicting the distribution of *As* species is natural water is not available at this time (Wang and Deng, 2009); however, the reviews of some pertinent details regarding *As* speciation is important for understanding the distribution of various *As* species in different environment. The Eh-pH diagram (Figure 2.1) of *As* is often used for predicting the stability field of various oxidized and reduced species. The speciation of *As* is largely controlled by the changes in the redox potential of the surrounding solution. *As*(V) is predicted to be thermodynamically stable valence in oxidizing condition, at Eh values greater than approximately -100 mV at pH 8 and greater than 300 mV at pH 4 (Figure 2.1). Below this redox potential is reducing conditions (Eh < -100mV) arsenious acid (H_3AsO_3) exists in various deprotonated forms. In reducing environment, *As*(III) is thermodynamically stable

valence, present either as the H_3AsO_3 species, As-S complexes ($H_2As_3S_6^-$), or *As*(III) solid phases such as As_2S_3 in presence of sulfur or hydrogen sulfide. These compounds are insoluble under neutral or acidic conditions. Arsine gas and free elemental arsenic are formed only under extremely reducing conditions (Smedley and Kinniburgh, 2002) therefore, it is not shown in Figure 2.1 due to uncertainities regarding the appropriate thermodynamic data.

Inorganic *As*(III) and *As*(V) are the major arsenic species in groundwater (Smedley and Kinniburgh, 2002; Wang and Mulligan, 2006).The deprotonation of arsenic species is similar to carbonic acid; it releases protons stepwise as the pH of the solution increases. For arsenate *As*(V), the first dissociation constant of H_3AsO_4, is log K_1= -2.2 ((pK_1) occurs at pH 2.2 which is rarely important in nature);

$$H_3AsO_4 \rightarrow H_2AsO_4^- + H^+; \quad \log K_1 = -2.2 \qquad (2.1)$$

$$H_2AsO_4^- \rightarrow HAsO_4^{2-} + H^+; \quad \log K_2 = -6.9 \qquad (2.2)$$

At pH between, 2.5 and 6.9, $H_2AsO_4^-$ is the predominant form of *As*(V) and $HAsO_4^{2-}$ is the predominant form of *As*(V) between pH > 6.9. These two species are most important in groundwater for *As*(V).

For *As*(III), the fully protonated form is H_3AsO_3 and the first dissociation (pK_1) occurs at pH 9.2;

$$H_3AsO_3 \rightarrow H_2AsO_4^- + H^+; \quad \log K = -9.2 \qquad (2.3)$$

Therefore, at pH < 9.2, the uncharged H_3AsO_3 is the predominant species.

Since, *As*(III) is a neutral, uncharged molecule at the pH of most natural waters, therefore, it is less likely to sorbed strongly to mineral surfaces (Manning and Goldberg, 1997; Dixit and Hering, 2003). This may explain its increased mobility in comparison to *As*(V) which sorbs more strongly under the pH of most natural water. Arsenic exhibits a relatively slow redox transformation and is often therefore responsible for the presence of both *As*(III) and *As*(V) in the same redox environment (Appelo and Postma, 2005).

As(V) should predominate over *As*(III) except in strongly reducing environments, where sulfate reduction is occurring from equilibrium thermodynamic calculations. However, due to bacterially mediated arsenic redox reactions which catalyses the chemical oxidation and reduction to higher magnitude, results in the presence of concomitant *As*(III) and *As*(V) (Smedley and Kinniburgh, 2002).

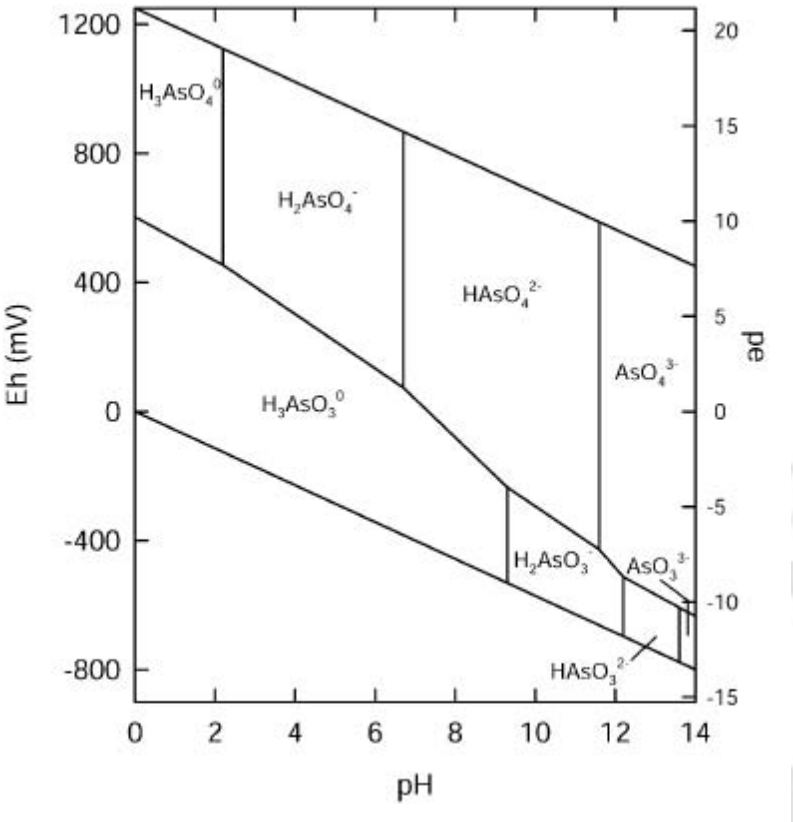

Figure 2.1 Eh-pH diagram for aqueous *As* species in the system *As*-O_2-H_2O at 25°C and 1 bar total pressure (Appelo and Postma, 2005).

2.4 Geochemical processes in aquifers involving Arsenic

The processes controlling the release of *As* to the groundwater have been studied intensively but still they remain a subject of dispute (Horneman et al., 2004; Zheng et al., 2004; van Geen et al., 2008; Halim et al., 2009, 2010; Nath et al., 2008).The aqueous distribution of *As* is often dominated by solution pH; redox potential; composition and interaction with the surrounding solution; and surface reactions on solid particle (both colloids and in-situ matrices) (Dowling et al., 2002; Sracek et al., 2004; Wang and Mulligan, 2006; Charlet el al., 2007; Wang and Deng, 2009). This current section explains the geochemical processes controlling the mobilization of arsenic. The mineral-water interaction which control the *As* in the aquifer systems are broadly divided into four types from geochemical point of view:

- adsorption-desorption,
- oxidation-reduction,
- precipitation-dissolution,
- Natural Organic Matter (NOM).

2.4.1 Adsorption and desorption

Sorption of *As* to solid phases has been proposed as a principal control on its mobility, which can transfer soluble or mobile *As* to particulate phases, subsequently immobilizing it. Sorption is a general term that refers to the partitioning of sorbate, from the aqueous phase to a sorbent, a mineral surface. The oxides of Fe, Al and Mn are ubiquitous in sediments, either in discrete particles or as coating on other minerals, which are characterize by high surface area and are potentially most important *As* adsorbent in the aquifer (Manning and Goldberg, 1997; Smedley and Kinniburg, 2002; Charlet et al., 2007; Stollenwerk et al., 2007; Postma et al., 2007, 2010; McArthur et al., 2004, 2008, 2011). Given the high affinity of Fe-oxides for *As* adsorption much work has focused on them, however similar results have also been reported for other oxides (Wang and Deng, 2009). Lin and Puls (2000, 2003) found the following order of decreasing arsenic affinity on various minerals iron hydroxides > clay > feldspars.

Two types of surface complex models have been recognized (Dzombak and Morel, 1990). Outer-sphere surface complexes are formed through non-specific adsorption, involving the adsorption of anions by simple columbic (electrostatic) interaction with positive charges. Inner-sphere surface complexes are formed through specific adsorption, involving the incorporation of anions as a ligand in the coordination shell of an adsorbent. Researches confirmed that both *As*(III) and *As*(V) may form inner sphere complexes on the surfaces of oxides and clay minerals through ligand exchange with OH^- and OH_2^+ surface function group (Manning et al., 2002; Catalano et al., 2008). *As*(III) may also form outer sphere complexes by simple electrostatic interactions on the surface of Al-hydroxides and sulfide minerals (Dixit and Hering, 2003). Inner-sphere complexes are much stronger than outer-sphere complex bonds, resulting in stronger adsorption, which may make immobilization more persistent (Dzombak and Morel, 1990; Dixit and Hering, 2003; Wang and Mulligan, 2008).

Iron(III) oxides, hydroxides and oxyhydroxides, hereafter will be collectively referred to as iron oxides (Fe-oxides).

2.4.1.1 Arsenic mobilization from Fe-oxides in aquifer sediments

Common oxides of Fe, Al and Mn and silica are widely dispersed in nature as fine particles and surface coatings (Stumm, 1992; Walther, 2010). They have an excellent ability to sorb cations and anions to their surfaces thereby decreasing the mobility of many trace elements in the environment (Dzombak and Morel, 1990; Stumm, 1992). The adsorption of arsenic by Fe(III) and Al-bearing minerals in natural soil and sediment surfaces have been reported by

many researchers (Manning and Goldberg, 1996; Thronton, 1996; Wilkie and Hering, 1996; Fendorf et al., 1997; Raven et al., 1998; Dixit and Hering, 2003; Arai et al., 2005). However, Fe-oxides has higher adsorption capacity than Al-oxides and clay minerals (Manning and Goldberg, 1997; Arai et al., 2001). Adsorption of arsenic species onto Fe-oxides is more highly dependent on its oxidation state than on pH in the range of 5.5-7.5 (Dixit and Hering, 2003). At acidic pH, *As*(V) generally sorbs more favorably than *As*(III), whereas at basic pH, the trend is reversed (Manning and Goldberg, 1997; Manning et al., 2002; Dixit and Hering, 2003). Lower adsorption of *As*(V) at high pH levels can be attributed to an increased amount of electrostatic repulsion between increasing negative *As*(V) oxidation states and negatively charged iron oxide surface. The *As*(III) species present at the same pH levels as the *As*(V) species are less negative charge thereby not exhibiting as much increased repulsion. Hence the effects of *As*(III) adsorption with increasing pH is lesser when compared to *As*(V) (Dixit and Hering, 2003).

The mechanism of reductive dissolution of Fe-oxides and various arsenic bearing oxides is so far the most conceivable and widely accepted theory of *As* mobilization processes in Bangladesh, West-Bengal (Bhattacharya et al., 1997; Nickson et al., 1998; McArthur et al., 2001, 2004, 2008, 2011; Dowling et al., 2002; Harvey et al., 2002, 2005; van Geen et al., 2004; Zheng et al., 2004; Polizzotto et al., 2006, 2008; Nath et al., 2008, 2011; Uddin et al., 2011), Red River Delta of Vietnam and Cambodia (Berg et al., 2001, 2007; Postma et al., 2007, 2010), Nepal (Shrestha et al., 2003; van Geen et al., 2008), Pakistan (Nickson et al., 2005; Farooqi et al., 2007; Baig et al., 2008). The Fe-oxides, such as goethite (α-FeOOH), ferrihydrite (β-FeOOH), and lepidocrocite (γ-FeOOH), have high point of zero charge (PZC) or isoelectric points of about 7.8, 8.5 each respectively and posses net positive charge in most geological environments (Stumm, 1992), thus showing high affinities for anions *As* species. The crystallinity and surface area of the oxides have a significant effect on the adsorption capacity of the *As*. The amorphous Fe-oxides (ferrihydrite) have higher adsorption capacity comparing more crystalline Fe-oxide (goethite) because higher active sorption sites (Dixit and Hering, 2003; Wang and Mulligan, 2006; Postma et al., 2007, 2010; Sharif et al., 2011; Robinson et al., 2011).

Desorption and remobilization of sorbed *As* from Fe, Al and Mn oxides may occur when biogeochemical conditions change. Stumm (1992) illustrated several pathways for Fe-oxides dissolution such as:

a. By protons
b. By bidentate complex formers that forms chelates (e.g. HS^-)

c. By reductant (ligand with oxygen donor atoms e.g. ascorbate)
d. Catalytic dissolution by Fe^{2+} in presence of complex former
e. Light induced dissolution in presence of electron donor such as oxalate.

As(V) may be mobilized from the Fe-oxides at pH above 8, due to increase in electrostatic repulsion on the negatively charged oxide surface, increases the rate of *As*(V) desorption (Dixit and Hering, 2003). Microbial reduction of Fe-oxides in the reducing sediments promotes the dissolution of *As* into the groundwater and microbes also reduces *As*(V) to *As*(III) (Harvey et al., 2002; McArthur et al., 2004). Since, reductive dissolution of Fe-oxides was believed to be the main *As* releasing mechanism in many parts of the world but the poor *As*-Fe correlation was attributed to the formation of secondary minerals viz. Fe(II) or mixed Fe(II)/Fe(III) phases such as siderite ($FeCO_3$), green rust ($Fe(OH)_2$) and magnetite (Fe_3O_4) which can sorbed *As*. Both species of *As* i.e. *As*(III) and *As*(V) sorbed to siderite, green rust and magnetite by forming inner-sphere surface complexes, but no evidence of *As*(III) oxidation as well as reduction of *As*(V) was noticed (Nickson et al., 2000; Jonsson and Sherman, 2008). Adsorption of *As*(III), however, is largely controlled by the oxidized iron content of the mineral (Deschamps et al., 2005).

The source of this *As* rich aquifers has been hypothesized as the mountains of Himalayas (Acharyya et al., 1999; Breit et al., 2003; McArthur et al., 2004; Harvery et al., 2005, 2006; Uddin et al., 2011) during the weathering processes the *As*-rich minerals releases finely divided FeOOH which strongly sorbs co-weathered *As* (Thornton, 1996; Harvey et al., 2002, 2005, 2006; McArthur et al., 2011; Uddin et al., 2011**).** These sediments are then transported to the floodplains of Brahmaputra and Bengal basin during monsoon and flooding event, thus becominga fresh source of *As* to the groundwater once it gets deposited near the surface (Harvey et al., 2006). Some researchers have also indicated that the sediments with high proportion of clay (such as the flood deposits and the surface clay) have much higher concentration of arsenic than in the sand (Acharyya et al. 1999; Reza et al., 2010a,b; McArthur et al., 2008, 2011). Most of the research publication from *As* affected areas of Asia had reported that the concentration of *As* range of sediment in laboratory analysis are not unusually high compared with the average values found elsewhere (Swartz et al. 2004; Harvey et al. 2005**;** Polizzotto et al., 2005; Postma et al., 2007; Berg et al., 2008; Guo et al., 2008**)** suggesting that there is not enough *As* in the aquifer sediment that can explain such high dissolved arsenic concentration in the groundwater.

A study in Munshiganj district lying in the central part of Bangladesh by Harvey et al. (2002, 2005, 2006) suggested that the *As* mobilization may have been associated with the recharge

from the ponds, rivers and rice fields due to large scale irrigation pumping in the area, since, the recharge through rice fields could mobilize *As* from oxides near surface and recharge from the ponds which is the potential source of high organic carbon release sorbed *As* to the groundwater system. However, Nath et al. (2008) found no relation between high *As* concentration and high groundwater pumping. Polizotto et al. (2006, 2008) suggested that *As* may be released at the oxic-anoxic boundary, the dissolved *As* from near surface could be drawn down to the well depth through the aquifer. But contrary to this, Sengupta et al. (2008) observed that surface recharge (via ponds) do not pose any threat to *As* contamination.

McArthur et al. (2004, 2008, 2011) provides a detailed geologic explanation for the high *As* content in the paleao-channel sequence in which gray Holocene sand directly overlies gray-to-brown Pleistocene sand, the gray sand in both contain high *As* groundwater. But the paleaointerfluve sequence where peaty, Holocene, silts overlies a Late Pleistocene paleaosol, which in turn caps brown Pleistocene sand in which groundwater is not polluted by *As*. They termed the paleaosol the Last Glacial Maximum Paleaosol (LGMP).

2.4.1.2 Arsenic mobilization from Mn-oxides

Mn-oxides are widely distributed in natural systems, and are stronger oxidants than Fe-oxides (Stumm, 1992; Manning et al., 2002; Amirbahmann et al., 2006; Stollenwerk et al., 2007). Reductive dissolution of *As* rich Mn-oxides addition to Fe-oxides can release high dissolved *As* into the groundwater (Smedley and Kinniburgh, 2002). Some researcher observed high dissolved Mn concentration concomitant with high dissolved *As* concentration in few areas (Ahmed et al., 2004; van Geen et al., 2004; Zheng et al., 2004; Shamsudduha et al., 2008). In contrary some researchers disagree the hypothesis and stating that the *As* released from the Mn-oxides would have resorbed for Fe-oxides, and thereby, will not have contributed to dissolved *As* concentration (Stuben et al., 2003; Buschmann et al., 2007; Berg et al., 2008). On the other hand, it is possible that all the sorption sites on Fe-oxides have already been occupied (either with *As* or other species), in which *As* release from the reductive dissolution of Mn-oxides will contribute to dissolved *As* concentration in groundwater. Various degradation products of lignin and other plant materials are capable of reducing Mn-oxides thus reduction being thermodynamically more favorable than reduction of Fe-oxides. However, Mn-oxides are less abundant than the Fe-oxides, and hence, the contribution is of less importance. Mn-oxides readily oxidize many natural and xenobiotic organic compounds.

The oxidation of *As*(III) to *As*(V) by Mn-oxides have been reported by many researcher (Section 2.5.3) in sediment. This process in gaining attention since it involves transformation

of *As*(III) to *As*(V) not only decreases the toxicity of *As*, but also enhances *As* removal from drinking water and sequestration to soils and sediments (Amirbahman et al., 2006; Stollenwerk et al., 2007; Sahabi et al., 2009). The oxidation of Fe^{2+} to Fe^{3+} by MnO_2 is an important geochemical reaction (Appelo and Postma, 2005). The oxidized ferric Fe^{3+} forms a surface coating primarily as ferrihydrite and secondarily as jacobsite ($MnFe_2O_4$) on MnO_2 preventing further oxidation, such a coating may also inhibit the oxidation of *As*(III) and organic matter (Han et al., 2011).

2.4.1.4 Arsenic sorption to clay minerals

Clay minerals are ubiquitous in nature, and are largely consist of aluminosilicates with alternating layers of Si-oxide and Al-oxide. *As* sorption onto clay mineral surfaces is influenced by the clay mineral type, surface charge and surface area, in addition to the presence of any other trace elements (Appelo and Postma, 2005). While extensive researches have been conducted on adsorption of *As* on iron oxide, clay mineral adsorption has been studied significantly less despite their abundance in aquifer sediments, soils and particulate matter (Wang and Deng, 2009).

Some researchers suggested the possibility of phyllosilicates (including clay minerals and micas) as *As* fixing phase (Breit et al., 2001; Anawar et al., 2003; Ahmed et al., 2004;Charlet et al., 2007; Chakraborty et al., 2007; Seddique et al., 2008; Reza et al., 2010a; McArthur et al., 2008, 2011). Fe-oxides and Mn-oxides are usually interpreted as secondary minerals formed from the weathering of sediment particles (McArthur et al., 2004). Adsorption of *As* on clay minerals viz. halloysite, kaolinites, illinite and montmorillonite and chlorite is a function of *As* species as well as pH (Lin and Puls, 2000; Wang and Mulligan, 2006). Manning and Goldberg (1997) from laboratory experiment found that ionic strength had little effect on *As*(III) adsorption providing macroscopic evidence for inner-sphere complexation. However, pH has a profound influence on adsorption capability of clay minerals, *As*(V) exhibited higher adsorption affinity than *As*(III) below pH 7. Desorption of both *As*(III) and *As*(V) decreased over time and the two theories were presented to explain this phenomenon (Lin and Puls, 2000):

1. *As* adsorbed onto external clay surfaces may diffuse into internal pores.
2. Loss of hydration water.

Both theories contribute to the strengthened bonding of arsenic with the clay mineral and promoting less desorption of arsenic. Lin and Puls (2000) reported the oxidation of *As*(III) to *As*(V) with aging over time leading to increased affinity of *As*(V) for surface sites over the

more mobile and toxic *As*(III) species. Manning and Goldberg (1997) suspected that the presence of MnO_2 in the clay may have contributed to oxidation, which in turn promotes more strongly bound arsenic in solid phase.

Fine-grained sediments are favorable for the accumulation of Fe-oxides and Mn-oxides as well as organic matter, which are carrier of *As* in sediments (Charlet et al., 2007; Chakraborty et al., 2007; Seddique et al., 2008). Silt-sized micas (biotite and muscovite) effectively adsorbed *As*(V) and *As*(III) onto their surface, where biotite has more reactive site comparing muscovite (Chakraborty et al., 2007). Seddique et al. (2007) proposes release of *As* from biotite via the decomposition of biotite producing Fe^{2+}, eventually the oxidation of byproduct leading to formation of Fe-oxides, and then lowering of redox condition leads to dissolution of *As* into the groundwater of Bangladesh.

2.4.1.4 Competitive anions exchange of As

The mobility, bioavailability and toxicity of arsenic may be influenced by the competitive interaction of other anions. Competition for adsorption sites induced by the presence of other adsorbing anions or cations can significantly influence the adsorption and mobility of *As*(III) and *As*(V) (Wilkie and Hering, 1996; Appelo et al., 2002; Dixit and Hering, 2003; Kent and Fox, 2004; Swartz et al.,2004; Anawar et al., 2004; Stollenwerk et al., 2007; Stachowicz et al. 2008). Various minerals are affected differently and the concentrations and speciation of competitive anions can also influence potential for arsenic sorption. Common competing anions include PO_4^{3-}, CO_3^{2-} and SiO_2. Perhaps the most commonly studied competitive anion with arsenic is PO_4^{3-}, probably due to its application via fertilizer use, increasing its potential to be present in the groundwater systems. The most commonly known competing anions are reviewed below.

2.4.1.4.1 Competitive anions exchange with PO_4^{3-}

Many researchers suggested the competitive anions exchange of sorbed *As* on aquifer matrix by PO_4^{3-} and results in increase dissolved *As* concentration into the groundwater (Acharyya et al., 1999; Wenzel et al., 2001; Smedley and Kinniburh, 2002; Dixit and Hering, 2003; Stollenwerk et al., 2007; Stachowicz et al. 2008). The competition is attributed due to the smaller size and higher charge density of PO_4^{3-} comparing with the *As* (Wenzel et al., 2001). Competitive ligand exchange generally occurs between $H_2PO_4^-$ and HPO_4^{2-} and arsenate ions (Manning and Goldberg, 1997). *As*(V) and PO_4^{3-}sorption on hydrous ferric oxides (Hfo) are

broadly similar, with PO_4^{3-} having a higher affinity for adsorption. The effect of competition of anions exchange with $PO_4^{3-}$is more pronounced on *As*(V) than *As*(III).

Goh and Lim (2004) studied anion competition with arsenic sorption on a bulk tropical soil sample as opposed to singular or synthetic minerals. Phosphate had more profound effect on sorption capacity for both *As*(III) and *As*(V), which may be attributed to its higher negative charge. Goh and Lim (2004) suggested two possible reactions for PO_4^{3-} on surface site: strong inner-sphere complexation and/or accumulation or precipitation of PO_4^{3-} providing electrostatic repulsion on the mineral surface. Both will reduce arsenic sorption and increase its mobilization into groundwater. The competition of adsorption site with SO_4^{2-} is less and rarely affected *As*(V) adsorption capacity but could compete with *As*(III) for sorption site when the pH is below 7 (Meng et al., 2000; Jain and Leoppert, 2002; Goh and Lim, 2005).

2.4.1.4.2 Competitive anions exchange with HCO_3^-

Appelo et al. (2002) examined ferrihydrite sorption capacity and found that carbonate present in common soil and groundwater concentrations significantly replaced arsenic on sorption sites. This has been further confirmed by Anawar et al. (2004) who conducted batch experiments that showed bicarbonate solution were effective in releasing arsenic from Fe-oxides and Mn-oxides. The formation of arseno-carbonate complexes; $As(CO_3)^{2-}$, $As(CO_3)(OH)^{2-}$ and $AsCO_3^+$ which are stable in water. Generally, carbonate exhibits little effect on *As*(III) and *As*(V) adsorption (Meng et al., 2000), but the presence of HCO_3^- can facilitate *As* mobilization from *As* containing sulfide such as orpiment in both oxic and anoxic environment (Kim et al., 2000). Stachowicz et al. (2008) from experiment on goethite found that bicarbonate (HCO_3^-) as very weak competitor of *As*, PO_4^{3-}, therefore, the presence of carbonate ions do not has influence on the competitive release of *As* from the oxides under natural groundwater conditions.

2.4.1.4.3 Competitive anions exchange with SiO_2

Swartz et al. (2004) showed that for a Bangladesh aquifer when silica is incorporated in surface complexation model, the high silica content of the groundwater cause most of the surface complex to become covered predominantly by silica and therefore the ability of HCO_3^- to displace *As* becomes limited. Meng et al. (2000) observed that silica competes with *As* for sorption sites and reduces adsorption of *As*(III) and *As*(V) of ferrihydrite at pH 6.8. In general agreement with the study cited above Goh and Lim (2005) found the ability of anions to mobilize arsenic from fine soil followed the order $PO_4^{3-} > CO_3^{2-} > SO_4^{2-} > Cl^-$.

2.4.1.5 Sorption by Cations

Appelo et al. (2002) reported increase in the *As* adsorption due to increase in cations such as Ca^{2+} and Fe^{2+} due to increase in positive charge on the surface of oxides. Ghosh and Teoh (1995) observed increase in *As*(V) adsorption onto the Al-oxides surface in presence of Ca^{2+} ions at pH above 8. Wilkie and Hering (1996) observed enhanced *As*(V) adsorption due to the addition of Ca^{2+} onto ferrihydrite at pH 9. Meng et al. (2000) reported that the addition of Ca^{2+} and Mg^{2+} to the suspension of ferrihydrite negated part of the competitive effect of silicate on *As* adsorption. The formation of $CaCO_3$ can restrict the development of high pH, thus inhibiting *As*(V) release from oxides and clays. Stachowicz et al. (2008) found that Ca^{2+} and Mg^{2+} ions promote adsorption of PO_4^{3-} which infer that it will also promotes the adsorption of AsO_4^{3-} (*As*(V)) on goethite, the ions has a no significant effects on the adsorption of *As*(III).

Once oxides have an adsorbed load, any change in their surface chemistry or the solution chemistry can lead to release of adsorbed *As*, and thereby increase *As* concentration in groundwater. The extremely high solid/solution ratio of soil and aquifers make them highly sensitive to such changes (Meng et al., 2000).

2.4.1.6 Sorption by calcite

Arsenic incorporation with carbonate mineral structures has received little research attention despite the ubiquitous nature of carbonate material in the environment (Bardelli et al., 2011). The possible role of calcite in sequestering *As* from the groundwater has been considered in number of studies (Goldberg and Glaubig, 1988; Cheng et al., 1999; Sø et al., 2008; Bardelli et al., 2011). Since calcite is ubiquitous mineral in many *As* contaminated aquifers, understanding its role in the uptake of *As* is of high importance.

Cheng et al. (1999) provide one of the few macroscopic investigations of arsenic association with calcite surfaces. Goldberg and Glaubig (1998) observed a maximum surface adsorption of *As* on calcite at around pH 10. Subsequently, Romero et al. (2004) conducted batch experiment of carbonate-rich aquifer material from Zimapan, Mexico, and found arsenic adsorption was greatest (97%) at pH 10.5. These results indicate that arsenic adsorption onto calcite is likely to exert a major control on dissolved arsenic concentrations in the groundwater.

Sø et al. (2008) conducted an experiment of sorption of *As*(III) and *As*(V) onto calcite, and reported that the sorption kinetics of *As*(V) is much greater than *As*(III), similarly fast desorption of *As*(V) was observed which indicated that *As*(V) is not incorporated to the

calcite crystal lattice. The adsorption capacity also depends upon the ionic strength due to electrostatic effect, competing anions present in solution such as PO_4^{3-}, selenite for sorption site and pH affects due to changes in speciation of *As* or protonation/deprotonation (Sø et al., 2008; Bardelli et al., 2011). Spectroscopic studies of *As* adsorption by natural calcite suggested that *As*(III) occur in local environment is capable of substitution of *As*(III) for carbonate in calcite, in contrary *As*(V) seems to be present in poorly crystalline phase, probably adsorbed on Fe-oxides (Bardelli et al., 2011).

2.4.2 Oxidation and reduction

Redox reactions are important for controlling the behavior of many major and minor species in natural water, including *As* (Smedley and Kinniburgh, 2002; Appelo and Postma, 2005). Redox sensitive minor and trace elements such as *As* respond to these changes rather than control them. In oxic environments, release of sediment bound arsenic has been observed in response to elevated concentrations of PO_4^{3-} (Kent and Fox, 2004) and oxidation of sulfide minerals at low pH values (Stumm and Morgan, 1996; Appelo and Postma, 2005). In anoxic environments, sediment-bound arsenic can be mobilized by reductive dissolution or transformation of Fe-oxide coatings and reduction of *As*(V) to *As*(III) (Ahmann et al., 1997; McArthur et al., 2001; Harvey et al., 2002; Horneman et al., 2004; Kent and Fox, 2004; Swartz et al., 2004; van Geen et al., 2004).

Redox process in groundwater typically occur through the addition of an oxidant, like O_2, Fe^{3+}, SO_4^{2-} and NO_3^- to an aquifer containing reductant (Appelo and Postma, 2005). A well-known sequence of reduction reactions occurs when lakes, sediment and aquifers become anaerobic (Stumm and Morgan, 1996; Langmuir, 1997; Appelo and Postma, 2005). The redox reactions involving Fe are more important since they can directly affect the mobility of *As* into the groundwater. The sequence of redox processes begins with consumption of O_2, and an increase in CO_2 from the decomposing of the organic matter (OM). Arsenic bound to organic matter may be released upon its degradation. Next step is the denitrification where the reduction of NO_3^- to NO_2^- to NO and then gaseous N_2O and N_2. The next step is followed by the reduction of Mn(IV) to Mn^{2+}. Manganese reduction generally follows, increasing dissolved Mn^{2+} concentration. Arsenic sorbed onto Mn oxides may be released as a consequence. Then the reduction of hydrous ferric oxides (Fe^{3+}) to Fe^{2+} occur thus increasing Fe^{2+} in solution. The surface of Fe-oxides reduces to Fe^{2+}, which lowers the overall net positive charge of the oxide producing weaker electrostatic bonds between sorbed anions and the oxide surface, leading to desorption of the anion. This process is followed by SO_4^{2-}

reduction to sulfide (S^{2-}) then CH_4 production from fermentation and methanogenesis, and finally reduction of N_2 to NH_4^+. In the process of SO_4^{2-} reduction, the consequent S^{2-} reacts with any available Fe^{2+} to produce FeS and ultimately pyrite, FeS_2. *As*(V) reduction would normally be expected to occur after Fe^{3+} reduction but before sulfate reduction (Smedley and Kinniburgh, 2002).

Bhattacharya et al. (2002) postulated that the principal redox reactions controlling *As* release in the groundwater of the Bengal Delta are given by the following schematic representation (Figure 2.2):

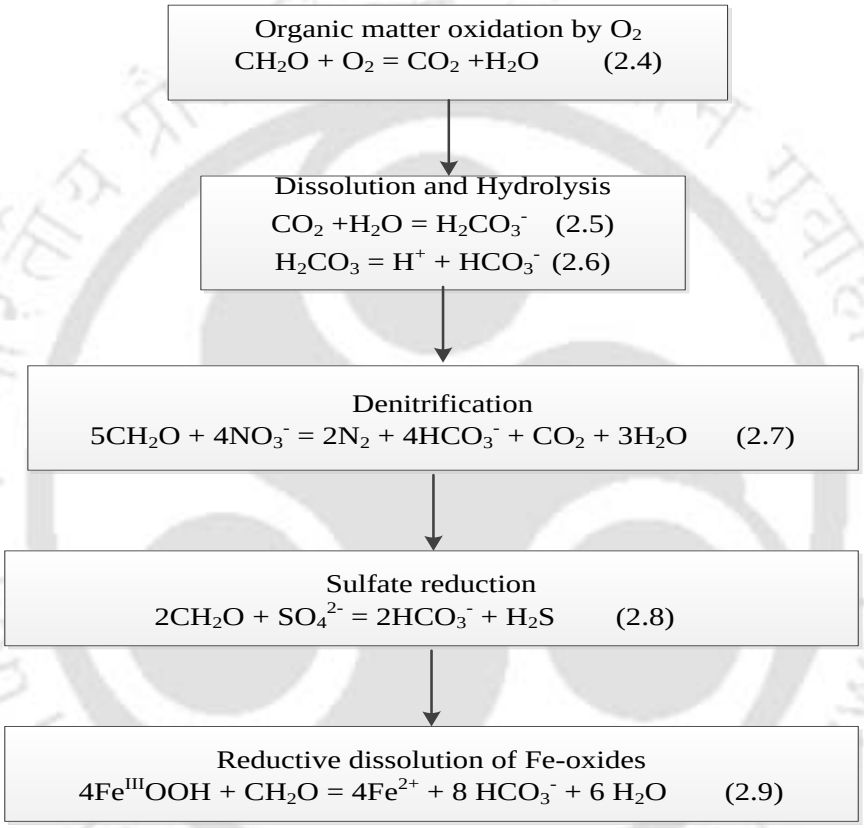

Figure 2.2 Schematic sequence of geochemical reactions for dissolution of *As* in the groundwater of Bengal Delta (Bhattacharya et al., 2002).

The *As* sorbed onto Fe-oxides is highly susceptible to lowering of the redox potential in the geochemical condition. The reductive dissolution of Fe-oxides occurs when the redox potential drops, by reducing Fe(III)-oxides to soluble Fe^{2+} and release the sorbed *As* from the surface of oxides into the solution.

Saunders et al. (2005, 2008) proposed that *As* was mobile under Fe-reducing conditions and immobile under SO_4^{2-} reducing conditions, given an ample supply of necessary electron donors and acceptors. They proposed that *As*-bearing pyrite should be the most important solid phase *As* formed under SO_4^{2-} reducing conditions in natural systems. Recently, *As*-

bearing pyrite has been found in deeper (> 150 m) alluvial sediments in Bangladesh (Lowers et al., 2007) and West-Bengal (Acharya et al., 2000). An indication of a change in redox potential occurring in sediments can be demonstrated by a color change from red/brown/orange (oxidizing conditions) to grey/green/blue (reducing conditions). Additionally, many of the reactions are mediated by biological reaction rather than chemical reactions alone.

The oxidation theory involves arsenic release during pyrite oxidation induced by lowering of the water table during groundwater extraction (Mallick and Rajgopal, 1996). This theory has largely been discounted as a dominant mobilization process given the highly reducing conditions observed in the aquifer. The impact of fertilizer-derived phosphate addition to the aquifer was predicted to release arsenic sorbed to minerals in the aquifer matrix due to competitive anion exchange (Acharyya et al., 1999). However, phosphate transport to the depths in the aquifer is unlikely, which does not account for the high concentrations of arsenic observed in groundwater depth (McArthur et al., 2001).

Harvey et al. (2002) suggest high organic matter content surface water is drawn into the aquifer during irrigation pumping which promotes reduction of Fe-oxides and arsenic release. This has been most recently disputed by McArthur et al. (2004) who found natural organic matter is present in peaty strata throughout the aquifer and that this is the probable source driving reduction (McArthur et al., 2001; Ravencroft et al., 2001). Zheng et al. (2004) suggested that re-oxidation of reducing *As* and Fe enriched water in Bangladesh aquifers was plausible.

2.4.3 Precipitation and dissolution

Numerous theoretical and experimental studies exist on the precipitation of arsenic with various elements, notably sulfides (Thornton, 1996; Nordstorm 2000; Smedley and Kinniburgh 2002; Lowers et al., 2007; Saunders et al., 2008; Kirk et al., 2010). Precipitation results because of the saturation of the aqueous solution with respect to mineral solubility. Precipitation-dissolution reactions involve the growth or erosion of a mineral structure and therefore only involve structural ions, that is, the elements included in the chemical formula of the mineral (Stumm, 1992; Appelo and Postma, 2005; Wang and Deng, 2009). The mineral solubility depends on its solubility products as well as the particle size and crystallinity of the minerals (Wang and Deng, 2009). The rate of dissolution or precipitation can be very slow and thermodynamic equilibrium is therefore often not attained in practical time scales.

Co-precipitation a common natural process also incorporate minor constituents or scavenged *As* into its mineral structure as it forms. Under reducing conditions, *As*(III) may co-precipitate with sulfide as arsenopyrite (FeAsS), realgar (As_4S_4) and orpiment (As_2S_3) (Appelo and Postma, 2005; Lowers et al., 2007; Kirk et al., 2010). Phosphate (PO_4^{3-}) and Fe are co-precipitated during the formation of Fe-oxides (Wang and Deng, 2009). Arsenic precipitation during microbial SO_4^{2-} reduction appears to be important in determining whether *As* accumulates to hazardous levels (Kirk et al., 2004, 2010). Remediation of *As* in most reducing aquifers could be achieved in-situ via injecting SO_4^{2-} into the groundwater, since low concentration of SO_4^{2-} limits the activity of SO_4^{2-} reducing microorganism (Kirk et al., 2004). Saunders et al. (2008) in a field test at the contaminated site of Bangladesh found that decrease in *As* concentration coincide with stimulated SO_4^{2-} reduction.

It has been reported that Arsenian pyrite, $Fe(AsS)_2$, might be most significant reservoir of mineral *As* in nature (Thornton, 1996; Nordstorm 2000; Kirk et al., 2010). Pyrite can incorporate up to a maximum of 8 wt% *As* into its structure, and it was hypothesized to form arsenopyrite (FeAsS) (Morse and Luther, 1999; Kirk et al., 2010). Kirk et al. (2010) observed that *As* precipitation during microbial sulfate and iron reduction in aquifer sediment that the main *As* sequestration occurs as pyrite rather than makinawite ($(Fe,Ni)_{1+x}S$) and greigite (Fe_3S_4). The authigenic pyrite is typically formed when organic matter (OM) is introduced into an iron and sulfur rich system, which causes redox potential to drop. The Fe-oxide is first reduced by the OM to soluble ferrous (Fe^{2+}), and then sulfate is reduced to sulfide. In this course the dissolved *As* concentrations decreases due to complex process that co-precipitate *As* (Lowers et al., 2007). The oxidation of sulfides, however, is not an efficient mechanism for arsenic release into groundwater due to its rapid adsorption onto iron oxide by-products commonly formed upon sulfide oxidation.

2.4.4 Arsenic mobilization by Natural Organic Matter (NOM)

NOM such as humic acid (HA) and Fulvic acid (FA) is an inherently complex mixture of polyfunctional organic acids derived from the decomposition of terrestrial and aquatic animals and plants (Appelo and Postma, 2005). A number of researches have been performed to understand the effects of NOM on the sorption behavior of *As* species and its consequence influence on their mobility.

The presence of organic matter, both in solid and aqueous forms, can influence *As* sorption onto mineral surfaces as it exhibits high surface areas and great affinities for surface sorption. Both *As*(III) and *As*(V) adsorption onto goethite (FeOOH) is reduced in the presence of

dissolved organic matter (Grafe et al., 2001). NOM, such as humic or fulvic acids, form stable complexes with mineral surfaces (Kaiser et al., 1997) thereby blocking arsenic sorption sites on iron oxides, alumina, kaolinite or quartz (Grafe et al., 2001). This has been supported by Bauer and Blodau (2006) who confirmed competition between arsenic and organic anions for sorption sites on synthetic Fe-oxides and natural soils and sediments. Mukhopadhyay and Sanyal (2004) devised stability constants for arsenic-humic/fulvic complexes that were considered stable, which would affect the mobilization/retention of *As* from the sediment. Redman et al. (2002) found that the formation of aqueous complexes of arsenic and natural organic matter dramatically reduced the amount of arsenic sorption onto hematite and displaced already sorbed*As*(III) and *As*(V).

Additionally, the decomposition of other minerals by indirect organic matter influence can affect arsenic mobility. The reductive dissolution of Fe-oxides catalyzed by organic matter oxidation is a prime example. This is because organic matter acts as a reductant, converting Fe^{3+} to Fe^{2+} and therefore inhibiting oxide formation, in addition to inhibiting crystallization. If it is not present then oxide formation and crystallization will occur more easily.

Therefore NOM may contribute to increasing the mobility and potential bioavailability of arsenic via competitive anion exchange mechanisms, inhibition of Fe-oxides formation as well as reduction of *As*(V) to *As*(III) thus increasing the mobility of *As* into the solution.

2.5 Immobilization of Arsenic in the aquifers

Arsenic sorption to solid phases is a complex mechanism currently receiving an increased amount of research attention. Experimental studies using pure mineral phases and high-powered microscopic techniques are providing valuable information for geochemists, material scientists, environmental scientists and pedologists alike. Using the data obtained through these theoretical investigations, predictions regarding arsenic retardation in heterogeneous matrices can be made. A number of arsenic mineral sorption studies are reviewed in order to show the wide range of potential conditions suitable for arsenic surface sorption in the environment.

Sorption of *As* to solid phases has been proposed as a principal control on its mobility, which can transfer soluble or mobile *As* to particulate phases, thus immobilizing it (Smedley and Kinniburgh, 2002; Goh and Lim 2004; Stollenwerk et al., 2007; Robinson et al., 2011; Sharif et al., 2011). *As* (and other trace elements) associated with the solid phase may be present in a variety of different chemical forms – precipitated as a mineral phase; adsorbed onto a mineral surface; incorporated within the crystal structure of a mineral or partitioned into organic

matter (Wang and Deng, 2009; Mulligan et al., 2010). Sorption is a general phrase that refers to the partitioning of sorbate, from the aqueous phase to a sorbent, a mineral surface. The various properties of sorbent i.e natural soils which influence sorption are specific surface area (SSA), surface charge, surface sorption, surface complexation, permanent and variable charge.

2.5.1 Arsenic adsorption by natural sediments

In addition to serving as an *As* source, however, aquifer sediments also act as a sink for dissolved *As*, which can be partitioned from aqueous to solid phases by sorption or co-precipitation processes. The extent of *As* removal from groundwater by aquifer sediments depends on the mechanisms controlling the aqueous-solid partitioning, which are a functions of pore water chemistry, pH, sediment chemistry, and groundwater flow conditions (Welch et al., 2000; Smedley and Kinniburg, 2002; Stollenwerk et al., 2003). Other potential mechanisms of attenuation are sorption of *As*(III) to sediments with or without oxidation, or oxidation of dissolved Fe^{2+} and precipitation of Fe-oxide, with sorption or co-precipitation of *As*. In general, *As*(V) adsorption to mineral oxides is favored at low pH, whereas maximum *As*(III) adsorption occurs at circumneutral pH and decreases with an increase or a decrease in pH (Goldberg, 2002; Dixit and Hering, 2003).

The most common isotherms applied in solid/liquid systems are the theoretical equilibrium isotherm; Langmuir and Freundlich (two parameter models) (Ho, 2004). Simplicity and easy interpretability are some of the reasons for extensive use of these models. At the same time, linear regression has been frequently used to evaluate the model parameters (Ho, 2006). Isotherms are of limited use in describing geochemical systems do not include any structural information regarding adsorbed species as the structure of an adsorbed species largely determines its reactivity, this is particularly limiting when a species may adsorb at a mineral surface with different structures, depending on solution or mineral surface conditions (Koretsky, 2000; Appelo and Postma, 2005). The mobility, bioavailability, and toxicity of *As* in soils may be greatly affected by the presence of competitive anions (*Section 2.4.1.4*). Competing anions such as PO_4^{3-}, Si and HCO_3^- can compete with *As* for adsorption site (Xu et al., 2002; Goh and Lim, 2004; Stollenwerk et al., 2007).

2.5.1.1 Langmuir adsorption isotherm

The Langmuir isotherm also called the ideal localized monolayer model was developed to represent chemisorption (Appelo and Postma, 2005). Langmuir (1918) theoretically examined the adsorption of gases on solid surfaces, and considered sorption as a chemical phenomenon. The Langmuir equation relates the coverage of molecules on a solid surface to concentration of a medium above the solid surface at a fixed temperature. This isotherm is based on the assumption that; adsorption is limited to mono-layer coverage, all surface sites are alike and can only accommodate one adsorbed molecule, the ability of a molecule to be adsorbed on a given site is independent of its neighboring sites occupancy, adsorption is reversible and the adsorbed molecule cannot migrate across the surface or interact with neighbouring molecules (Febrianto et al., 2009). By applying these assumptions and the kinetic principle (rate of adsorption and desorption from the surface is equal), the Langmuir equation can be written in the following hyperbolic form:

$$q_e = q_{max} \frac{K_L C_e}{1+K_L C_e} \tag{2.10}$$

This equation is normally written in different linear forms (Febrianto et al., 2009):

$$\frac{1}{q_e} = \left[\frac{1}{K_L q_{max}}\right]\frac{1}{C_e} + \frac{1}{q_{max}} \tag{2.11}$$

$$\frac{C_e}{q_e} = \frac{1}{q_{max}} C_e + \frac{1}{K_L q_{max}} \tag{2.12}$$

Where q_e is the adsorption capacity at equilibrium (mg/g), q_{max} is the theoretical maximum adsorption capacity of the adsorbent (mg/g) and,K_L is the Langmuir affinity constant (l/mg) and C_e is the supernatant equilibrium concentration of the system (mg/l). This isotherm equation has been most frequently applied in equilibrium study of adsorption, however, it should be realized that the Langmuir isotherm offers no insights into aspects of adsorption mechanism (Koretsky et al., 2000).

2.5.1.2 Freundlich adsorption isotherm

The Freundlich isotherm was originally of an empirical nature, but was later interpreted as sorption to heterogeneous surfaces or surfaces supporting sites of varied affinities. It was assumed that the stronger binding sites were occupied first and that the binding strength decreases with increasing degree of site occupation (Appelo and Postma, 2005). The Freundlich isotherm can describe the adsorption of organic and inorganic compounds on a wide variety of adsorbents (Febrianto et al., 2009).

According to this model the adsorbed mass per mass of adsorbent can be expressed by a power law function of the solute concentration as (Freundlich, 1906):

$$q_e = K_f C_e^{1/n} \quad (2.13)$$

Where K_f is the Freundlich constant related with adsorption capacity (mg/g), n is the heterogeneity coefficient (dimensionless). For linearization of the data, the Freundlich equation is written in logarithmic form:

$$\log q_e = \log K_f + \frac{1}{n} \log C_e \quad (2.14)$$

The plot of $\log q_e$ versus $\log C_e$ has a slope with the value of $1/n$ and an intercept magnitude of $\log K_f$. On average, a favorable adsorption tends to have Freundlich constant n between 1 and 10. Larger value of n (smaller value of $1/n$) implies stronger interaction between the adsorbent and the adsorbate while $1/n$ equal to 1 indicates linear adsorption leading to identical adsorption energies for all sites. Linear adsorption generally occurs at very low solute concentrations and low loading of the adsorbent (Appelo and Postma, 2005).

2.5.2 Kinetics of As adsorption

The type of soil component can drastically affect the rate of metal sorption (Sparks, 1999). Sorption reaction can involve physical sorption, outer-sphere complexation (electrostatic attraction), inner-sphere complexation (ligand exchange), and surface precipitation and can occur on time scales of microseconds to months (Sparks, 1999; Appelo and Postma, 2005). In natural composite soil with different mineral phases, both oxidation and adsorption reactions were considered for the removal of arsenic from solution.

In batch laboratory experiments, arsenic adsorption kinetics onto Fe-oxides have been shown to be relatively fast, with a faster rate observed for *As*(V) at lower pH values, and for *As*(III) at higher pH values (Raven et al., 1998). The extent and kinetics of *As*(V) and *As*(III) adsorption onto Fe-oxides were shown to be dependent on the solute: sorbent ratio (Raven et al., 1998).

The contact time experimental results can be used to study the rate-limiting step in the adsorption process. In soil, the reaction rates and the molecular processes by which these reactions occur where transport is not rate limiting, due to heterogeneity of soils, one is usually determining a combination of chemical kinetics and kinetics events (Spark 1999). Several adsorption kinetic models have been established to understand the adsorption kinetics and rate-limiting step. Various kinetic models, namely, pseudo-first order, pseudo-second-

order, Elovich model and intra-particle diffusion models have been used to test their validity with the experimental adsorption data.

2.5.2.1 Pseudo-First-Order kinetic model

The pseudo-first-order rate expression of Lagergren model is generally expressed as (Lagergren, 1898):

$$\frac{dq_t}{dt} = K_{ad}\,(q_e - q_t) \qquad (2.15)$$

where q_e and q_t are the amount of *As* adsorbed (mg/g) at equilibrium and at any instant of time *t* (min), respectively, and K_{ad} is the rate constant of pseudo first order adsorption operation (min^{-1}). The integrated rate law after application of the initial condition of $q_t = 0$ at *t* = 0, becomes a linear equation as given by:

$$\log(q_e - q_t) = \log q_e - \frac{K_{ad}}{2.303}\,t \qquad (2.16)$$

The plot of $\log(q_e - q_t)$ versus *t* gives a straight line for the pseudo first-order adsorption kinetics, from which the adsorption rate constant K_{ad}, is estimated. The determination of q_e for fitting the experimental data accurately in Eq. 2.16 is difficult tasks. Since in soil-water interaction the sorption process becomes very slow after initial fast response, therefore ascertaining the equilibrium concentration becomes difficult.

Pseudo first-order kinetic equation differs from a true first-order equation in two ways: (i) the parameter, $K_{ad}\,(q_e - q_t)$ does not represent the number of available sites, and (ii) the parameter, $\log q_e$ is an adjustable parameter and often it is found that it is not equal to the intercept of the plot of $\log(q_e - q_t)$ versust, whereas in a true first order model the value of $\log q_e$ should be equal to the intercept. Hence, pseudo first-order kinetic model is used for estimating K_{ad} alone, which is considered as mass transfer coefficient in the design calculations (Gupta and Bhattacharya, 2011).

2.5.2.2 Pseudo-Second-Order kinetic model

Pseudo first-order kinetic model gives only K_{ad} and as q_e cannot be estimated using this model, applicability of the pseudo-second-order kinetics has to be tested for the estimation of q_e with the rate equation given by Ho (1995). Major factors which influence the sorption capacity includes, the initial sorbate concentration (Ho et al., 2004; Ho and McKay, 2000, 2003), the reaction temperature (Ho et al., 2004; Ho and McKay, 2000), the solution pH value (Ho et al., 1995), the sorbent particle size (Ho and McKay, 2003) and dose (Ho and

McKay, 2000, 2003), and the nature of the solute (Ho and McKay, 2000), a kinetic model is concerned only with the effect of observable parameters on the overall rate.

The pseudo-second-order model is based on the assumption of chemisorption of the adsorbate on the adsorbents. This model can be represented in the following form:

$$\frac{dq_t}{dt} = K_2 (q_e - q_t)^2 \quad (2.17)$$

Where, K_2 is the equilibrium rate constant of pseudo-second-order adsorption (g/mg min). From the boundary conditions, $t = 0$ to t and $q_t = 0$ to q_t, the integrated form of the equation is:

$$\frac{1}{(q_e - q_t)} = \frac{1}{q_t} + K_2 t \quad (2.18)$$

The above equation can be re-arranged to obtain a linear form as:

$$\frac{t}{q_t} = \frac{1}{K_2 q_e^2} + \frac{1}{q_e} t \quad (2.19)$$

The plot of t/q_t versus t should give a linear relationship which allows the computation of a second-order rate constant, K_2 and q_e. The pseudo-second order model is based on the assumption that the rate limiting step may be chemical adsorption involving valence forces through sharing or exchange of electrons between the adsorbent and adsorbate (Ho and Mckay, 2000). The rate constant K_2 decreases with the increasing initial adsorbate concentration, thus, higher initial concentration of adsorbate longer time would be required for equilibrium, in turn the K_2 value decreases (Ho and Mckay, 2003; Febrianto et al., 2009; Sen and Bhattacharya,, 2011). Due to the complexity of the problem and numerous different factors, the influence of pH and temperature on K_2 has not been theoretically studied (Gupta and Bhattacharya, 2011).

If the initial sorption rate, h, of a second order process at $t \rightarrow 0$ is defined as $h = K_2 q_e^2$. The initial sorption rate, h, adsorption capacity q_e, and rate constant K_2, can be determined experimentally from the slope and intercept of a plot of t/q_t against t.

The above equation can be rearranged to obtain:

$$q_t = \frac{t}{1/h + t/q_e} \quad (2.20)$$

$$\frac{t}{q_t} = \frac{1}{h} + \frac{1}{q_e} t \quad (2.21)$$

Linear regressions are frequently used to determine the best fitting kinetic models, and the method of least squares is used for finding parameters of the kinetic models. However, the

pseudo-second-order kinetic model can be linearized as four different parameter estimates (Ho, 2004) as shown (Table 2.4) and the most popular form used in Type 1.

Table 2.4 Pseudo-second-order kinetic model linear form.

Type	Linear form	Plot	Parameter
Type 1	$\frac{t}{q_t} = \frac{1}{K_2 q_e^2} + \frac{1}{q_e} t$	$\frac{t}{q_t} \; vs. \; t$	q_e = 1/slope K_2 = slope^2/intercept h = 1/intercept
Type 2	$\frac{t}{q_t} = \left(\frac{1}{K_2 q_e^2}\right)\frac{1}{t} + \frac{1}{q_e}$	$\frac{1}{q_t} \; vs. \frac{1}{t}$	q_e = 1/intercept K_2 = intercept^2/slope h = 1/slope
Type 3	$q_t = q_e + \left(\frac{1}{K_2 q_e}\right)\frac{q_t}{t}$	$q_t \; vs. \frac{q_t}{t}$	q_e = intercept K_2 = 1/(intercept*slope) h = - intercept/slope
Type 4	$\frac{q_t}{t} = K_2 q_e^2 - K_2 q_e q_t$	$\frac{q_t}{t} \; vs. \; q_t$	q_e = - intercept/slope K_2 = slope^2/intercept h = - intercept

2.5.2.3 Elovich kinetic model

The Elovich equation has been widely used in adsorption kinetics, which described chemical adsorption in nature (Sparks, 1999; Wu et al., 2009). This equation is commonly used in chemical adsorption of gases on a solid surface without desorption of the products. The rate decreases with time due to an increase in surface coverage (Wu et al., 2009). This equation has also been commonly used to describe the sorption of pollutants from aqueous solution (Ranjan et al., 2009; Gupta and Bhattacharyya, 2011). The Elovich equation can be written in the form:

$$\frac{dq_t}{dt} = a \exp(-b\, q_t) \qquad (2.22)$$

where a represents the rate of chemisorptions at zero coverage (µg/(g min)) and b is the extent of surface coverage and activation energy for chemisorptions (g/µg).

Given that $q_t = 0$ at $t = 0$ and $q_t = q_t$ at $t = t$, the integrated form of the Eq. 2.23 is given by,

$$q_t = \left(\frac{1}{b}\right)\ln(t + t_o) - \left(\frac{1}{b}\right)\ln t_o \qquad (2.23)$$

where $t_o = 1/ab$. If $t >> t_o$, the above Eq. 2.24 can be simplified as

$$q_t = \left(\frac{1}{b}\right)\ln(ab) - \left(\frac{1}{b}\right)\ln(t) \qquad (2.24)$$

the constant a and b were calculated from the slope and intercept of plot q_t versus ln(t).

2.5.2.4 Intra-particle diffusion model

It is usually difficult to apply simple kinetics equations to describe soil chemical reactions, since the soil sediment surfaces are heterogeneous and one cannot differentiate transport effect from chemical kinetics. The heterogeneity of soils including varying particle sizes, sorption sites, and porosities promotes transport processes (Stumm, 1992; Gupta and Bhattacharya, 2011). Theoretical treatments of intraparticle diffusion yield rather complex mathematical relationships which differ in form as functions of the geometry of the sorbent particle (Ranjan et al, 2009; Gupta and Bhattacharyya, 2011). A functional relationship common to most treatments of intra-particle diffusion is that uptake varies almost proportionately with the half-power of time, $t^{0.5}$, rather than t; a nearly linear variation in the quantity sorbed with $t^{0.5}$ is predicted for a large initial fraction of reactions controlled by rates of intra-particle diffusion (Weber and Morris, 1963). Good linearization of the data is observed for the initial phase of the reaction in accordance with expected behavior if intra-particle diffusion is the rate-limiting step (Pootset al., 1976). According to Weber and Morris (1963), if the rate-limiting step is intra-particle diffusion, a plot of solute sorbed against the square root of the contact time should yield a straight line passing through the origin. The most-widely applied intra-particle diffusion equation is given by Weber and Morris (1963):

$$q_t = K_{id} t^{0.5} + C \qquad (2.25)$$

Where K_{id} is the intraparticle diffusion rate constant (µg/(mg $min^{0.5}$)) and the intercept C, obtained by extrapolation of the linear portion of the plot of q_t versus $t^{0.5}$, back to the axis is taken to be proportional to the extent of the boundary layer thickness. The intra-particle diffusion plots show multi-linearity in the sorption process indicating the number of steps that are operational (Wu et al., 2009; Gupta and Bhattacharya, 2011).

2.5.3 Oxidation kinetics of As(III) to As(V)

Previous studies and researches have shown that the extent and kinetics of *As*(III) oxidation may be attributed to the oxidized solid-phase manganese content of the material (Oscarson et al., 1981; Scott and Morgan, 1995; Manning et al., 2002; Tournassat et al., 2002; Amirbahman et al., 2006; Stollenwerk et al., 2007; Han et al., 2011). In natural systems, the most important abiotic pathway for the oxidation of *As*(III) to *As*(V) is by minerals containing Mn(III) and Mn(IV) (Oscarson et al., 1981; Amirbahman et al., 2006; Stollenwerk et al., 2007; Han et al., 2011). However, oxidation of *As*(III) by Fe(III) hydroxide in lake sediment

has been reported previously (De Vitre et al., 1991), possibly because of the high Fe(III):*As*(III)ratio. The process of oxidation of *As*(III) by manganese oxides leads to the production of Mn(II) (Scott and Morgan, 1995; Manning et al., 2002; Tournassat et al., 2002). The reduction of Mn(IV) to Mn(II) during *As*(III) oxidation proceeds in two steps was observed by X-ray photoelectron spectroscopy (XPS) (Nesbitt et al., 1998), where Mn(IV) cations are reduced to Mn(III). The two newly formed Mn(III) cation accepts two additional electrons from another *As*(III) molecule and reduced to Mn(II) (Eq. 2.27-2.28):

$$2 > \mathrm{Mn(IV)O_2} + \mathrm{H_3AsO_3} + \mathrm{H_2O} \rightarrow 2 > \mathrm{Mn(III)OOH} + \mathrm{H_2AsO_4^-} + \mathrm{H^+} \qquad (2.26)$$

$$2 > \mathrm{Mn(III)OOH} + \mathrm{H_3AsO_3} + 3\mathrm{H^+} \rightarrow 2 > 2\mathrm{Mn^{+2}} + \mathrm{H_2AsO_4^-} + \mathrm{H_2O} \qquad (2.27)$$

The Mn^{2+} and *As*(V) products are released to the solution phase or re-adsorbed on the mineral surfaces. Therefore, transformation of *As*(III) to *As*(V) not only decrease the toxicity but also enhances *As* removal from drinking water and sequestration to soils and sediments.

As(III) oxidation by MnO_2 was found to occur abiotically (Amirbahman et al., 2006; Oscarson et al., 1981); however, several microbial respiratory and non-respiratory enzymatic systems for oxidation of *As*(III) have been reported (Stollenwerk et al., 2007; Oremland et al., 2000). Amirbahman et al. (2006) reported that arsenic oxidation conducted in both in the presence and absence of dissolved oxygen and in sterile condition using 0.1M formaldehyde (bactericide) no differences in the aqueous *As*(III) concentration and *As*(V) production rates were observed. Han et al. (2011) from an experiment of *As*(III) oxidation in acidic conditions conclude that the presence of Fe^{2+} ions as well as Fe-oxides covering MnO_2 inhibits the oxidation rates. Han et al. (2011) observed the formation of secondary Fe compounds viz. schwertmannite, FeOHAs or $FeAsO_4$ particles which plays an important role in sorption and oxidation of *As*(III).

2.5.4 Surface Complexation Model (SCM)

Surface complexation model (SCM) have been used widely as an equilibrium based approach to describe and predict metal cation and anion sorption reactions on surfaces of reactive phases in soils such as oxide and clay minerals (Stumm, 1992; Appelo and Postma, 2005). Electrostatic forces draw ions to a solid where they may chemically bond to the surface (Stumm, 1992; Davis et al., 1998). Fundamental sorption reactions that take place at the metal oxide surface are fully describable by surface complexation theory (Dzombak and Morel, 1990; Goldberg, 1998; Koretsky, 2000; Sposito, 1989). The most prominent *As*

attenuation reaction is surface complexation reaction with hydrous metal oxides (Langmuir, 1997; Miller, 2001; Sracek et al., 2004; Robinson et al., 2011; Sharif et al., 2011). The complexity of soil materials and their surface site heterogeneity hinder the direct identification of the most active mineralogical and organic components. Thus, the determination of "intrinsic" stability constants for molecular-scale metal sorption reactions and estimation of surface site densities for sorption site is problematic (Davis et al., 1998).

SCM are fundamentally based on chemical and physical principles that are controlled by measurable parameters such as specific surface area, surface site-density, electrical and chemical potentials of the surface, and intrinsic surface constants associated with reactive surface sites and adsorbate ions etc (Davis et al., 1998; Miller, 2001). Component additivity (CA) approach is used in SCM, where it is assumed that the surface of adsorbent is composed of a mixture of mineral phase whose properties are known from studies of the individual phases (Davis et al., 1998; Sracek et al., 2004; Sharif et al., 2011). CA approach assumed that one mineral phase dominates adsorption, which facilitate a straightforward equilibrium calculation if the exposed surface area and surface-site density of that mineral phase in the soil or sediment can be quantified (Davis et al., 1998).

Surface complexation models (SCM) use the law of mass action, expressed as an equilibrium constant, to define protonation (K_{s+}), deprotonation (K_{s-}) and ion-specific sorption to a surface (K_{int}). To implement SCM in PHREEQC the sorption constants must be known for each mineral phase and ion modeled. Central of SCM approach is that protonation and disassociation reactions and ion-specific complexation constants are reversible and apply over a range of pH and ionic strength conditions. The equilibrium constants K_{s+} and K_{s-} are determined for protonation-deprotonation reactions at the oxide surface. The protonation reaction with surface, S, are described by two steps reversible process below:

$$SOH + H^+ \Leftrightarrow SOH_2^+ \tag{2.28}$$

$$K_{s+} = \frac{[SOH_2^+]}{[SOH][H^+]} \exp\frac{(F\psi_0)}{(RT)} \tag{2.29}$$

$$SOH \Leftrightarrow SO^- + H^+ \tag{2.30}$$

$$K_{s-} = \frac{[SO^-][H^+]}{[SOH]} \exp\frac{(-F\psi_0)}{(RT)} \tag{2.31}$$

where, F is the Faraday constant (9.65×10^{-4}coulumb/mole), ψ_0 is the surface potential in volts, R is the universal gas constant, and T is the absolute temperature. The exponential

electrostatic term appended to the standard form of the equilibrium mass action equation is used to account for the change in surface potential because of the adsorption of the modeled ion.

The equilibrium constants K_{s+} and K_{s-} allow the surface sorbing properties to change with changing pH. Constants for specific sorbing ions that meet these constraints are referred to as "intrinsic constant" or K_{int}. In order to apply these models to SCM, K_{int} for surface reactions must be known for each surface to be used, each sorbing ion, and each site defined on the surface.

Each protonation state of an oxyanion has a unique K_{int}. For example, K_{int} for Diffuse Layer Model (DLM) surface complexation models have the following forms for arsenate sorbing to a single site:

$$K^1_{As_{int}} = \frac{[SH_2AsO_4]}{[\mathrm{SOH}][H_3AsO_4]} \tag{2.32}$$

$$K^2_{As_{int}} = \frac{[SHAsO_4^-][H^+]}{[\mathrm{SOH}][H_3AsO_4]} \exp\frac{(\text{-F}\psi_0)}{(\mathrm{RT})} \tag{2.33}$$

$$K^3_{As_{int}} = \frac{[SAsO_4^{2-}][H^+]^2}{[\mathrm{SOH}][H_3AsO_4]} \exp\frac{(\text{-2F}\psi_0)}{(\mathrm{RT})} \tag{2.34}$$

The electrical layer geometries of the model differ, but they all reduce to mass action equations that are solved numerically. With respect to broad multicomponent modeling proposed here, the most important part of the commonality and formulation among the SC models is the universal application of the mass law constraint. The mass law formulation allows the sorption reactions to be used in the existing theoretical and mathematical framework of thermodynamic equilibrium models. Surface complexation reaction become part of the general mathematical solution of an equilibrium state between an aqueous solution and a solid sorbing phase.

Chapter 3

Study area

3.1 Location and environmental conditions

3.1.1 Study area in the Darrang district

The study area is located in Darrang district, which is in the central region of Assam state (Figure 3.1). It is approximately at 80 km west of Guwahati. The district lies between 26º25' N and 26º55' N latitude and 91º45' E and 92º20' E longitude and covers an area of 3,465.30 km^2. The two blocks namely Pub-Mangaldoi and Sipajhar were covered for groundwater sampling. Groundwater is the main source of drinking water in this area. The topography of the district is characterized by almost flat plain and higher elevated flat uplands along the foothills of Assam Himalayas (ARSAC, 1990a). The Pub-Mangaldoi area is characterized by large number of ponds and wetlands recharging groundwater and is located near Brahmaputra River bank. Both the study areas have similar younger alluvium soils. It is located on the northern bank of Brahmaputra River. It has been chosen due to strategic importance of the alluvial deposits spreading from upper Assam to lower Assam, which is thought to be the main source of *As*. Samples were collected from the wells located in the Brahmaputra flood plain as well as upstream paleochannels from the north. Due to flat topography of the area and the large deposits of sediment the tributaries changes their course regularly.

The climate of the district is sub-tropical climate with semi-dry hot summer and cold winter. The temperature varies between 10 ºC and goes up to 36 ºC during summer. The mean relative humidity is about 82%. The average annual rainfall 1477.77 mm and most of the rainfall is received during South-West monsoon starting from May/June. The district map is represented by Survey of India topographical sheet number 78N and 83B.

3.1.2 Study area in the Jorhat district

The study area Titabor (Tokobari) in Jorhat District, is situated in the eastern part of Assam state of India between Latitude 26°27.3′ North and 26°30.8′ N, Longitude 94°6.3′ E and 94°9.8′ E as shown in Figure 3.1. The district area is represented by Survey of India topographical sheet number 83J in the scale of 1:250,000. Disai hills located in the southern part of the area is at an elevation of 450 m. Brahmaputra flows on the northern side of the district. The district experiences a hot moist summer with a cool dry winter. The mean annual rainfall in the district is 2,197 mm (ARSAC, 1990b). The soil of the study area varies from

clay loam to sandy loam and pH varies from 4.5 to 5.4 (Barua and Borkakoty, 2003). Land-use /Land-cover mapping of Jorhat district identify the study area under cropland of kharif plant and plantation category (ARSAC, 1990b).

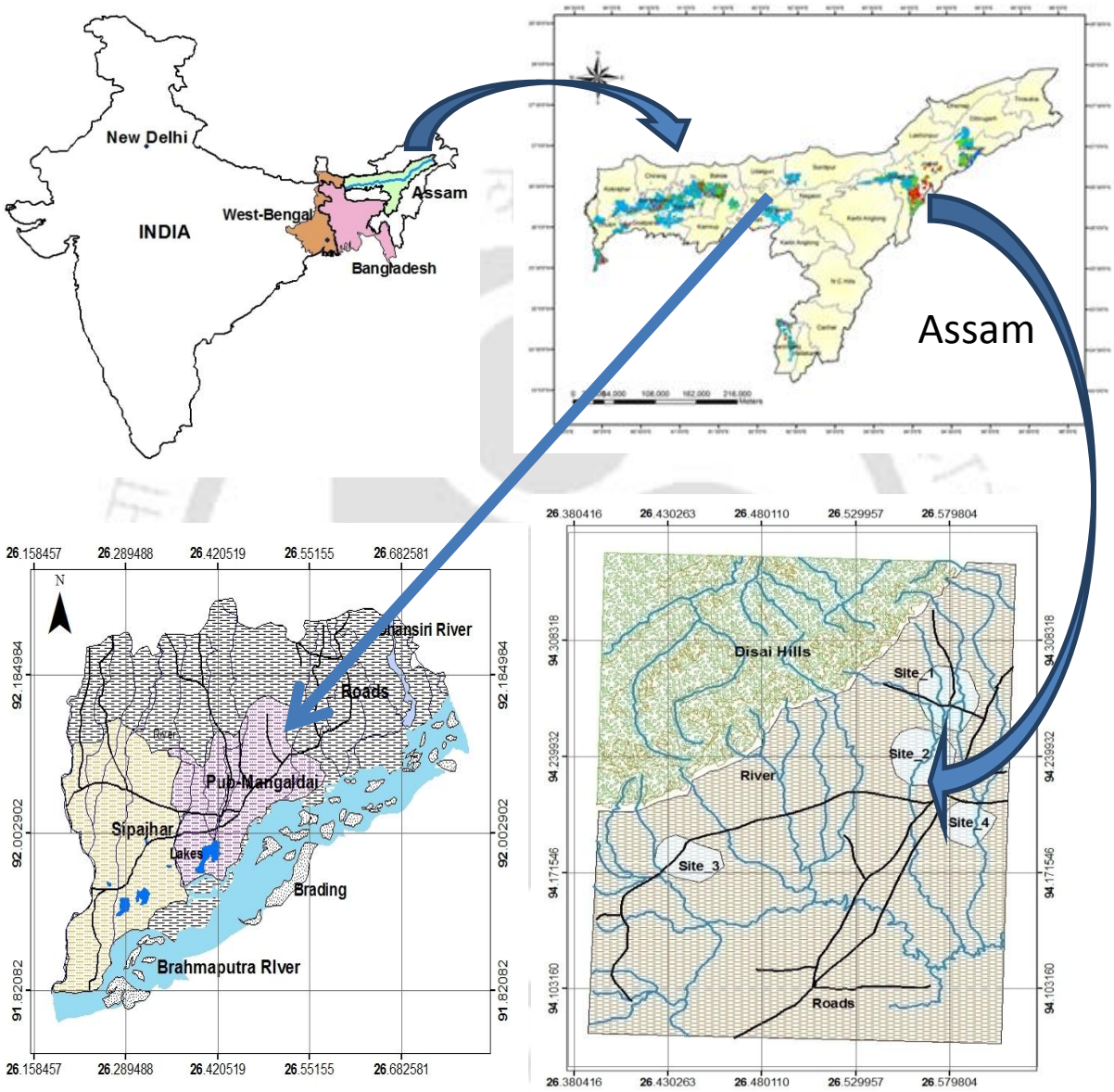

Darrang Jorhat

Figure 3.1 Location of the study area in Jorhat district and Darrang district of Assam.

3.2 Geological setting

3.2.1 Darrang district

Major part of the district is covered by thick deposits of unconsolidated sediments, except in the south-western part where few isolated hillocks consisting of gneissic rocks are exposed. Both new alluvium soils (Entisols) and old alluvium soils (Inceptisols) are found in the district. The study area lies in the new alluvial plains, which are found in the active floodplains bordering the Brahmaputra River and older alluviums which are found further away from the active floodplain zone (CGBW, 2004).

The alluvial deposits are more than 200 m to 300 m in thickness except the inselbergs where alluvial thickness range is 10 m to 30 m (DGM, 1994b). The sub-surface geology comprises of beds of unconsolidated aquifer material throughout the district. The eastern part of the district area has a thick sand cover 21 m to 31 m at the top followed by alternate clay sand/gravel zones. And in the southern part of the district cover the study has a thin clay and silt zone present at the top followed by a thick sand and gravel zone. Two types of aquifer zones encountered in the area are:

(1) Shallow aquifer zone (depth < 50 m below ground level (bgl)).
(2) Deeper aquifer zone (depth between 50 m to 200 m (bgl)).

3.2.2 Jorhat district

The geology of the district can be broadly classified as alluvium except Tiru hills and Disai hills. In this area Barail series (Lower Tertiary formation) is found which consist of carbonaceous materials. Crude oil sources are found in association with Barail series in the Borholla region of the district (DGM, 1994b). The geomorphic unit of the study area comprises of younger alluvial plains. It occupies major part of the district and is at slightly higher elevation than the present day flood plain of Brahmaputra River, which is often inundated by floods. The area has gentle slopes towards the north. The soil types mainly consist of sand, silt, clay and gravel. The area is characterized by high recharge, but sometimes clay lenses form aquicludes (ARSAC, 1990b).

3.3 Hydrogeology

3.3.1 Darrang district

The study areas are located in the younger alluvial plains deposits which covers major portion of the district. The plain is built by the lower reaches of rivers fanning out from the foothill region, abandon river channels, cut-off meanders, natural levees and back swamps (DGM, 1994a). The sub-surface materials mainly consist of gravel, sand, silt and clay. The groundwater occurs both under confined and unconfined condition, the water levels varies from 1.1 m to 7.5 m bgl. The prospect of groundwater in the alluvial is very good due to its high yield. The floodplains of Brahmaputra occur along the river bank covering 2 km to 7 km from the bank towards north. The area is inundated during the rainy season and transported materials are deposited all over the area. The groundwater level in the floodplains varies from 1 m to 3 m. Older alluvium plain occurs as isolated patches in the eastern part of the district, and located at slightly higher elevation.

3.3.2 Jorhat district

Younger alluvial plain occupies major portion of the district and are located at slightly elevation than the present day floodplains. The area has a gentle slope towards north with high prospect for groundwater development due to good yield at shallow depth (< 50 m). The sub-surface material consists of gravels, sands, silts and clays (DGM, 1994b). The depth of hand tubewells are within 40 m to 50 m depth. Old meanders, paleochannels (abandoned channels), natural levees, ox-bow lakes and water bodies are very common in the area (CGWB, 2004). The floodplain of the river Brahmaputra is an east-west trending 5 km to 15 km wide belt, often inundated by the floods. Heavy sediment load and low velocity result in faster deposition of the sediments and formation of innumerable longitudinal channel bars. Older alluvial plains occur mostly along the southern part of the district and also as scattered isolated bodies throughout the district.

3.4 Previous investigation

Very few studies on *As* has been done and reported in Assam plains of the Brahmaputra Basin, and no in depth research work has yet been carried out for deducing sources and mechanisms of *As* release despite strong indication of its wider spread (Mahanta et. al., 2010). Some studies on the Assam floodplains have been outlined in the introduction (*Section 1.1*). Chakraborti et al. (2004) reported the existence of arsenic contamination in the upper Brahmaputra plain in Assam. Singh (2004) reported that 20 out of 24 districts of Assam had

arsenic concentration exceeding 50µg/l, and recently Borah et al. (2008) did a study in Golaghat district of Assam, followed by the wider work of Mahanta et al., (2010). Little published records are available other than these, except occasional newspaper reports.

3.5 Aquifer lithologs

The subsurface sediments were assumed to be key *As* source and its current sinks due to the absence of strong anthropogenic sources in the study areas. The lithological data for deeper aquifer in the study areas were collected from Central GroundWater Board (CGWB, 2004) and Directorate of Geology and Mining (DGM, 1994a, 1994b). To enable the detailed geomorphic reconstruction in the area of high *As* contamination, six boreholes were drilled in the Site_1. The boreholes namely 1A, 1B, 1C, 2E, 2F and 2G were drilled which targets the high *As* containing tubewells T1 and T2 (*Section 4.1.2*). The location of these boreholes were shown on the map provided (Figure 4.1). The sediments were visually logged by collecting the samples every 20ft or 3m in air tight polythene bags. The change in color and texture of the sediment was noted during the drilling operation. The lithological data for deeper aquifer as well as borehole data for drilled core were shown in Figure 3.2.

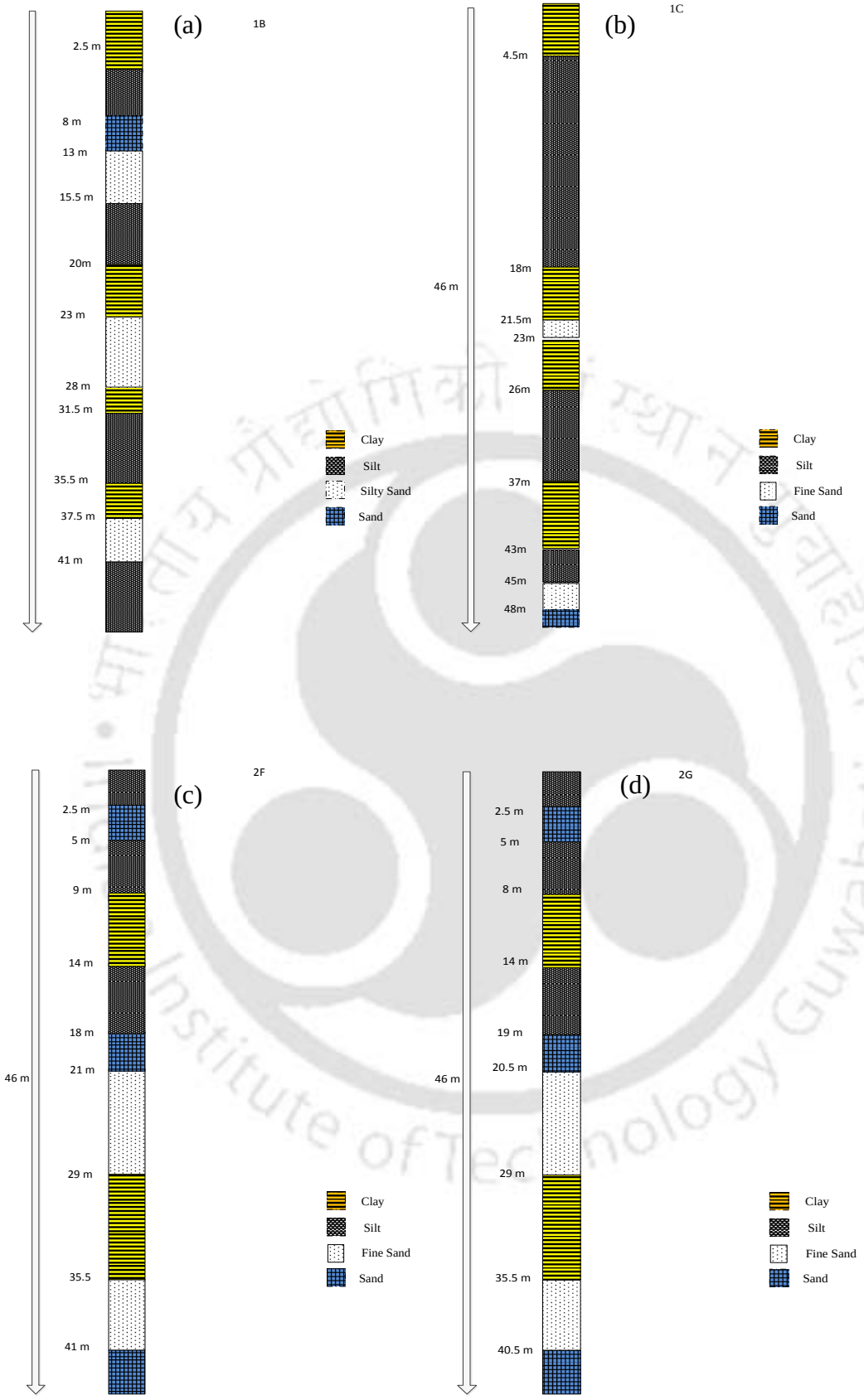

Figure 3.2 Lithologs of drilled cores from Site_1 (a) 1B (b) 1C (c) 2F (d) 2G locations.

Chapter 4

Methodology

4.1 Groundwater and sediment sampling

Groundwater sampling was carried out at Darrang district as well as Jorhat district. In Darrang district a total of 40 and 38 groundwater samples were collected from the two blocks covered viz. Pub-Mangaldai and Sipajhar respectively. In Jorhat district, Titabor blocks which was highly affected with *As* contamination was covered for groundwater and sediment sampling. Four villages were chosen for groundwater and sediment sample collection on the basis of its *As* content and geographical location. The four villages from Titabor blocks were named as:

1. Tokobari village – Site_1
2. Kachukhat village – Site_2
3. Bosagaon village – Site_3
4. Tatigaon village – Site_4

4.1.1 Groundwater sampling

From Darrang district total of 78 samples were collected from existing tube wells in the study area from February 2007 to December 2009 over nine field trips. These tube wells are at different depth, and the geographical locations of the tube wells were determined using a handheld Global Positioning System (GPS). Prior to sampling, tube well was pumped for about 5 min to avoid contamination by stale water. Two samples were collected from each tube well, one acidified samples (pH < 2) using 1:1 HCl and another non-acidified samples in a 500 ml plastic sampling bottles. The physical parameters viz. pH, temperature and Electrical Conductivity were measured directly at site using portable pH meter (pHTestr10-Eutech) and portable Conductivity meter (ECTestr11 - Eutech).

From Jorhat district (Titabor block) a total of 139 samples were collected from existing tube wells in the study area during January 2008 to January 2010 over eight field trips. Out of the total groundwater samples collected, 44 groundwater samples were from Site_1, 35 samples from Site_2, 39 samples from Site_3 and 21 samples were from Site_4. The tubewell were classified as shallow tubewell as the depths were mostly 40 m to 50 m (CGWB, 2004), so obtaining variability in depth was difficult. Similar procedure mentioned above was adopted in the collection and sampling of the groundwater in this study area also. The tube well was

pumped for about 5 minutes to remove the stagnant water thus permitting the fresh water from aquifer to be sampled. Similarly, two samples i.e. acidified and non-acidified samples were collected from each sampling point and the physical parameters viz. pH, temperature and Electrical Conductivity were measured directly at site itself.

4.1.2 Sediment sampling

Sediment sampling was simultaneously done along with the groundwater sampling in the study area of Titabor. Based on the results of groundwater and soil sample analysis from the different site locations, it was decided to drill fresh wells in this high arsenic contaminated location in Site_1 (Tokobari). Six boreholes were drilled during latter part of January 2010 with the help of local drillers provided by the PHED Assam. The borehole samples were collected every 20 ft i.e. approx 3 m and it was drilled to an approximate depth of 46 m to 50 m (150 ft to 165 ft). The sediment samples were identified by location 1A, 1B and 1C which cover the target tubewell-1 which has high *As* concentration in the groundwater (Figure 4.1). In the adjoining location another set of boreholes were drilled and labeled as 2E, 2F and 2G which located near the target tubewell-2 locating in the campus of Tokobari High School (Figure 4.1).

During drilling, the color and texture of sediment was noted and samples were collected in clean sealed airtight polyethylene bags and stored in dark until analysis was done. A total of 13 borehole sediment samples were collected from the study area where 6 borehole samples were from Site_1, 2 soil samples from Site_2, 3 soil samples from Site_3 and 2 borehole samples from Site_4. The soil samples were analyzed for its physical, morphological and chemical properties.

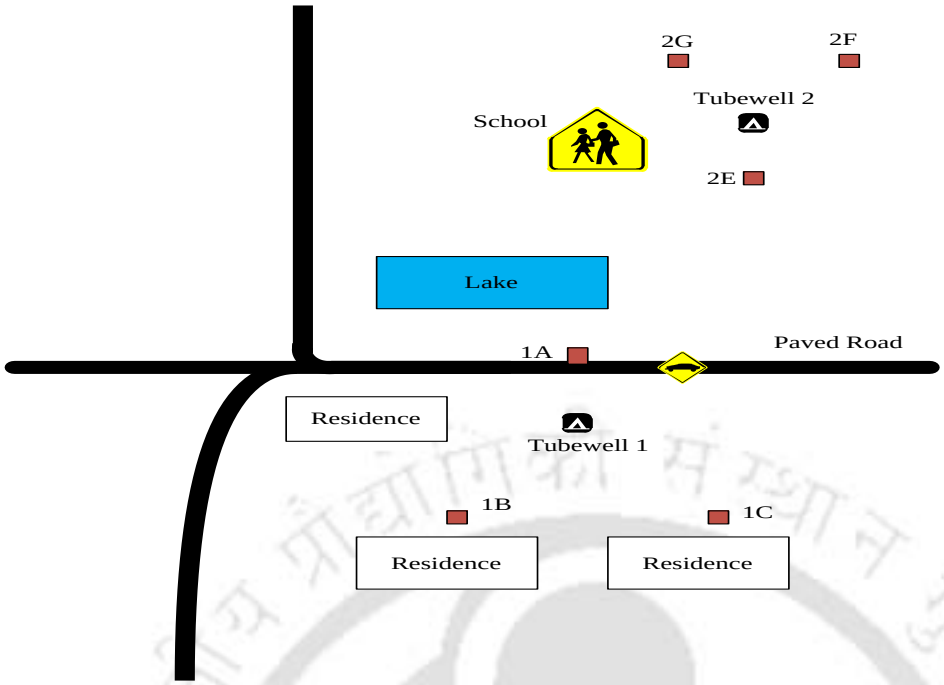

Figure 4.1 location of six drilled cores of Site_1 (Tokobari) targeting Tubewell-1 and Tubewell-2.

4.2 Groundwater analysis

All the analysis of the groundwater quality parameters were carried out in the environmental engineering laboratory of IIT Guwahati. American Public Health Association (APHA, 1998) recommended standard methods were used for the measurement of dissolved ion concentration in the samples as shown (Table 4.1). Major and minor cations viz. Calcium (Ca^{2+}), Sodium (Na^{+}), Magnesium (Mg^{2+}), Potassium (K^{+}), Manganese (*Mn*), Iron (*Fe*), Zinc (Zn^{2+}), Copper (Cu^{2+}), Cadmium (Cd^{2+}), Nickel (*Ni*) were measured with atomic absorption spectroscopy using Spectra Duo, Varian BV(AAS). Arsenic was measured using Hydride Generation Technique in AAS with Vapor Generation Assembly (VGA). The name of the experiment and analytical instrument used for the analysis of water and soil are summarized and tabulated (Table 4.1 and 4.2).

Table 4.1 List of the groundwater quality parameters analyzed and name of the experiment or instrument.

Analysis	Name of the Experiment/Instruments
pH	pH meter
Electrical Conductivity	Conductivity Meter

Alkalinity (HCO_3^-)	Titration Method
Calcium (Ca^{2+})	Atomic Absorption Spectroscopy (AAS)
Magnesium (Mg^{2+})	Atomic Absorption Spectroscopy (AAS)
Sodium (Na^+)	Atomic Absorption Spectroscopy (AAS)
Potassium (K^+)	Flame Photometer
Chloride (Cl^-)	Argentometric Method
Sulphate (SO_4^{2-})	Turbidimetric Method
Fluoride (F-)	UV Visible Spectrophotometer
Phosphate (PO_4^{3-})	Ascorbic Method
Nitrate (NO_3^-)	UV Visible Spectrophotometer
Iron (Fe)	Atomic Absorption Spectroscopy (AAS)
Manganese (Mn)	Atomic Absorption Spectroscopy (AAS)
Lead (Pb^{2+})	Atomic Absorption Spectroscopy (AAS)
Arsenic (*As*)	Vapor Generation Assembly (VGA) of AAS
Chromium (Cr)	Atomic Absorption Spectroscopy (AAS)
Copper (Cu^{2+})	Atomic Absorption Spectroscopy (AAS)
Cadmium (Cd^{2+})	Atomic Absorption Spectroscopy (AAS)
Zinc (Zn^{2+})	Atomic Absorption Spectroscopy (AAS)

Table 4.2 List of analytical instruments and their model/manufacturer used for the analysis of groundwater and sediment parameters.

Instrument	Model/ Manufacturer
Pocket ORP Meter	ORPTestr10-Eutech
Pocket TDS Meter	TDSTestr11 - Eutech
Pocket pH Meter	pHTestr10 -Eutech
Pocket Conductivity Meter	ECTestr11-Eutech
GPS	geko 101, Garmin
Digital pH Meter	µpH system 361, Systronics India
Digital conductivity Meter	VSI 04, India
Microprocessor Based Flame Photo Meter	128 Systronics, Ahmedabad, India
Digital Spectrophotometer	166 Systronics, Ahmedabad, India
UV Visible Spectrophotometer	Cary 50 Bio, Varian
High Speed Research Centrifuge	R24 Remi, Mumbai, India
Analytical Balance	AB304S Metteler Instrument AG, Switzerland
Hot Plate	JSGW, India
Magnetic Stirrer (1/8 HP)	LS 104B
Water Purification System	QRP 380BC, Chemiton, Spain
Mechanical Stirrer	LS04B, ELTEK, Mumbai, India
Horizontal shaker	REICO, Calcutta, India
Incubator shaker	
End over end rotary shaker	Wagner's shaking machine, Reico Pvt. Ltd., Kolkata
Atomic Absorption Spectrophotometer	Spectra Duo, Varian BV, Netherlands
Particle size analyzer	AWM 2000, Malvern instruments, Worcestershire
Scanning Electron Microscopy (SEM)	LEO, 1430 VP, Carl Zeiss, Germany

4.3 Solid phase analysis

The sediment samples collected from the sampling sites were kept in plastic air tight zipper bags and covered with black polyethylene bags till it is brought to the laboratory. Then the samples were air dried. The air dried samples were grounded gently by hand with an agate mortar and pestle, and the powdered samples were used for the following analyses.

4.3.1 Chemical properties

4.3.1.1 pH

The sediment pH was determined on air dried soil sample in ratio 1:5 i.e. soil: 0.01M $CaCl_2$ solution shaken for 30 minutes and measured the pH of supernatant using pH electrode (Hendershot et al., 2008a).

4.3.1.2 Cation Exchange Capacity (CEC)

The amount of exchangeable bases and the cation exchange capacity (CEC) are important properties of soils and sediments. They relate information on a soil's ability to sequester toxic heavy metals. Sorption capability of the soils increases with the increase in specific surface area (SSA) and CEC.

The CEC was estimated by summation of exchangeable bases (Ca, Mg, Na, K). The most widely used method of CEC estimation using 1.00 M ammonium acetate (NH_4OAc) extraction at pH 7.00 was used (Hendershot et al, 2008b).The soil sample is extracted with 1.00 M ammonium acetate (1M NH_4OAc) extraction at pH 7.00. The soil-solution (2g: 20ml) slurry was shaken for 2 hours, and the solution is separated from the solid by centrifuge at 9000 rpm for 5 mins. Samples were collected from the clear supernatant for further analysis. The addition of excess NH_4^+ to the soil displaces the rapid exchangeable alkali and alkaline cations from the exchange sites of the soil particles. The concentration of Na^+, K^+, Mg^{2+} and Ca^{2+} are subsequently analyzed with Atomic Absorption Spectroscopy (AAS).

$$Exch\ Ca^{2+} = \frac{(a-b)*20*mcf}{10*20.04*s}\ \text{meq/100g.} \qquad (4.1a)$$

$$Exch\ Mg^{2+} = \frac{(a-b)*20*mcf}{10*12.15*s}\ \text{meq/100g.} \qquad (4.1b)$$

Where *Exch* is exchangeable, *a* represent mg/l Ca^{2+}, Mg^{2+}, K^+ or Na^+ in the extraction solution, *b* is correction in the blanks, *s* is dry weight of sample (g), *mcf* is moisture correction factor.

4.3.1.3 Loss On Ignition (LOI)

The samples were oven dried at 105 ^{0}C for 24 hours soon after it was brought into laboratory and the resulting loss in weight gives the percent soil moisture content (MC %) in the sample. The organic carbon content in the sediment samples were determined by loss on ignition (LOI), which measures weight loss after burning at specified temperatures. LOI is then calculated using the following formula (Dean, 1974):

$$LOI_{550} = ((DW_{105}-DW_{550})/DW_{105})*100 \quad (4.2)$$

Where LOI_{550} represents LOI at 550 ^{0}C (as percentage), DW_{105} represents the dry weight of the sample before combustion (g) and DW_{550} the dry weight of the sample after heating to 550 ^{0}C (g).

4.3.2 X-Ray Diffraction (XRD)

Mineralogical phases present in the solid residues were identified using X-ray powder diffraction (MAC Science XXP 18) with Cu Kα radiation and a position-sensitive detector. The accelerating voltage was kept at 30 kV and the current at 20 mA. A divergent slit (1^0), a scattering slit (1^0) and a receiving slit (0.3mm) were used to produce the best spectrum. Scans were conducted from 5^0 or 10^0 to 70^0at the rate of 1^0 - 2θ/min. Data were digitally recorded, and peak position and intensity were determined either on screen or using the smoothed and peak finder feature in the software.

Approximate relative abundance ratios of major minerals were estimated from the relative intensities of the most intense and specific peak of each mineral from the XRD chart. Identification of compounds was made by manual search of the JCPDS - International Centre for Diffraction Data (ICDD) as a reference database.

4.3.3 Scanning Electron Microscopy and Energy dispersive X-Ray (SEM and EDX)

The electron microscope work was done at CIF (Centre for Instrumentation Facility) at IIT, Guwahati. The sample to be analyzed with Scanning Electron Microscope – Energy Dispersive X-Ray Spectroscopy (SEM-EDX) was mounted on aluminium stub 2.5 cm in diameter using a double sided carbon tape. It was then placed in sputter coater and coated with thin layer of gold (Au) to make the sample electrically conductive.

Morphological investigations were carried out on a scanning microscopy analyzer (SEM, JOEL JSM-6300F), coupled with an energy dispersive X-ray analyzer (EDX, OXFORD

INCA ENERGY 400). The typical accelerating voltage of SEM was kept at 30 kV, and the EDX was run with a lithium drifted silicon detector at a resolution of 133 keV.

4.3.4 Particle size analyzer

Laser particle size analyser (Mastersizer 2000) was used to find the specific surface area (SSA) of the soil samples. Malvern software assisted with the instrument showed the particle size distribution. The specific surface area (SSA) was calculated by the Malvern software from the results of laser diffraction measurement using the following equation:

$$\text{SSA} = \frac{6\sum\frac{V_i}{d_i}}{\rho\sum V_i} = \frac{6}{\rho D[3,2]} \qquad (4.3)$$

where V_i is the relative volume in class i with mean class diameter of d_i, ρ is the density of the material, and $D[3,2]$ is the surface weighted mean diameter. This was automatically calculated by the laser diffraction system software by assuming that the particles are perfectly smooth, solid spheres.

4.3.5 Total metal concentration (EPA – 3052)

The chemical composition of the sediments was analyzed using Atomic Absorption Spectroscopy (AAS). For total elemental concentrations, the air dried powdered sediments were dissolved in strong acid using EPA – 3052 methods. The digestion of sediment was carried out in PTFE beaker with hood. 0.5 g of sun dried sediment was mixed with 4 ml conc. HCl and 9 ml of conc. HNO_3 and 5 ml of conc. HF acid. It was heated till boiling for 1 hour and 2 ml of H_2O_2 was added to the sample and heated for 30 minutes. Then it was allowed to cool. The final volume was adjusted with distilled water to 50 ml.

4.3.5.1 Quality control and quality assurance

The analytical procedure quality control and assurance measures were implemented by analyzing blanks and replicates. Additional Certified Reference Material of Japanese Geological Survey, JSd-3 and JLk-1 were used for calibration and intermediate check in analytical procedure to evaluate the effectiveness of the digestion procedure. The total metal concentrations database of these (CRMs) i.e. JSd-3 and JLk-1 were obtained from Japanese Geological Survey, http://www.aist.go.jp/RIODB/geostand/ sediment.html.

4.3.6 Sequential Extraction Procedure (SSE)

Metals present in sediments can be associated with several reactive components. The total metal concentration indicating the overall metals in the soils does not provide any information regarding the chemical nature or potential mobility and bioavailability of a particular element (Herreweghea et al., 2003; Hudson-Edward et al., 2004; Baig et al., 2009; Mulligan et al., 2010). Sequential extraction procedure is frequently used to evaluate metal distribution into different chemical forms present in solid phase (Koen et al., 2001; Wenzel et al., 2001; Herreweghea et al., 2003; Hudson-Edward et al., 2004). Conceptually, sequential extraction categorizes metal associated with chemically homogenous fractions that ultimately affect metal availability. Also often criticize due to lack of specificity of extractants and possible readsorption of metals during extraction (Herreweghea et al., 2003; Baig et al., 2009; Mulligan et al., 2010), sequential fractionation can provide useful information to predict the fate of heavy metal in the environment (Herreweghea et al., 2003). Since the stepwise fractionation cannot be quantitatively delineated, the extracted pools are operationally defined. However, thorough optimized sequence has provided useful information on relative lability and may facilitate a reasonable degree of specificity and selectivity for the extraction steps used.

Air dried sediment samples were used in the SSE with solid solution ratios of 1:25 (1 g soil: 25 ml solution). Extraction experiment was carried out in Teflon centrifuge tube, which prevented any loss of sediment between successive extractions. After each extractions step, the mixtures were centrifuged at 10,000 rpm for 10 minutes, the aliquot was transferred into 100 ml specimen tube. A sequential extraction procedure modified by Postma et al. (2007) which is combination of extraction scheme proposed by Wenzel et al., (2001) and Tessier et al. (1979) was used for the sediment extraction. The sequential leaching procedure is summarized in Table 4.3. Seven steps sequential extraction was used with each steps being represented as Ext_1 to Ext_7 and their target phase being specified. The Ext_3 and Ext_4 targeting the carbonate bound *As* and resorbed *As* was applied from Tessier et al. (1979) because carbonate phases could adsorb *As* and the *As* released from the carbonate could adsorb onto Fe oxides so Ext_3 steps was followed by phosphate washing step as shown (Table 4.3).

Table 4.3 Selective Sequential Extraction (SSE) scheme for sediments.

Step	Target phase	Extractant	Extraction conditions	SSR[a]	Wash steps
Ext_1	Non-specifically bound *As*	0.05 M $(NH_4)_2SO_4$	4 hour shaking, 20°C	1:25	-
Ext_2	Specifically bound *As*	0.05 M $(NH_4)H_2PO_4$	16 hour shaking, 20°C	1:25	0.05 M $(NH_4)H_2PO_4$: SSR 1:12.5, 4 hr shaking
Ext_3	Carbonate bound *As*	1M *NaOAc+HOAc*, pH 5	6 hour shaking, 20°C	1:25	1M *NaOAc+HOAc*, pH 5; SSR 1:25; 4 h shaking
Ext_4	Resorbed *As*, release from carbonates	0.05 M $(NH_4)H_2PO_4$	4 hour shaking, 20°C	1:25	
Ext_5	Amorphous hydrous oxide-bound *As*	NH_4-*Oxalate* buffer (0.2M), pH 3.25	4 hour shaking 20°C in the dark	1:25	NH_4-*Oxalate* (0.2M); pH 3.25 SSR 1:12.5; 10 mins shaking in the dark
Ext_6	Crystalline hydrous oxide-bound *As*	NH_4-*Oxalate* buffer (0.2M) + ascorbic acid (0.1M) pH 3.25	30 minutes in a water basin at 96±3°C	1:25	NH_4-*Oxalate* (0.2M); pH 3.25 SSR 1:12.5; 10 mins shaking in the dark
Ext_7	*As* in sulfide minerals	16N HNO_3	Microwave digestion	1:50	

[a]SSR: soil solution ratio (Postma et al., 2007)

4.3.6.1 Recovery of Selective Sequential Extraction

An internal check to SSE mass balance was done by comparing the sum of concentrations for each step in the extraction experiment divided by the total digestion of the trace metals. The recovery of sequential extraction procedure was calculated using the following equation:

$$\text{Recovery (\%)} = \frac{Ext\_1+Exn\_2+Ext\_3+ Ext\_4+Ext\_5+Ext\_6+Ext\_7}{TotalMetal\ Concentration} \times 100 \qquad (4.4)$$

where $Ext\_$ denotes the extraction steps and the Total Metal Concentration is the obtained from *Section 4.3.5*.

4.3.7 Attenuation experiment of Arsenic

The aim of attenuation experiment using batch sorption study was to examine the mechanism and extent of arsenic uptake in laboratory batch experiment using field sediments from drill-core taken at the 1C from Site_1 in order to quantify the ability of natural sediments to attenuate *As*. Three sediment samples from borehole drill core 1C was chosen with different depth viz. 15 m, 21 m and 46 m, which have different distinct color i.e. grey, brown and greenish ash for the batch experiment. These sediments are present in most of the sediment core samples from the Site_1 which is highly affected with *As* contamination. The first grey samples (C_50) corresponds to reduced sediment with low Fe and Mn as shown (Table 5.15).

The second sample namely C_70 brown in color is characterized as oxidized sediment with high concentration of Fe and Mn. The sediment sample C_150 with ash-greenish color have moderate concentration of Fe and Mn, this sample was chosen because it is the sandy soil layers from where most of the well screens are placed.

4.3.7.1 Batch sorption kinetic study

Arsenic removal kinetic tests for *As*(III) and *As*(V) by the soil sediment samples viz. C_50, C_70 and C_150 were conducted in 50 ml polyethylene centrifuge tubes at room temperature (26 +/-2 ºC) by taking 1 gram of air dried soil with 20 ml solution (i.e. 1:20 soil/water ratio). The initial *As* concentration [*As*(III) and *As*(V)] of 300 µg/l and 500 µg/l were used which corresponds to the *As* concentration in the Site_1. The pH was set to 6.5 by using 0.1M HCl or 0.1M NaOH prior to the start of the experiment. Blank samples without *As* were also included in the experiment to verify the desorption of *As* from the sediments. The samples were gently shaken in horizontal shaker at an rpm of 180 for 1440 minutes (24 hours). The tubes along with its duplicates were withdrawn from the horizontal shaker at predefined time interval i.e. 5, 10, 20, 30, 60, 120, 240, 360, 600, 1440 minutes. The tube was centrifuged at 9000 rpm for 15 minutes and supernatant were collected using a syringe. The amount of *As* adsorbed per unit mass of soil sediment (µg/g) was calculated from Eq 4.5 and the sorption percentage using Eq. 4.6. The various adsorption model viz. pseudo-second order kinetic which includes Type-1, Type-2, Type-3 and Type-4 the various linearized forms, Elovich model, Intra-particle diffusion model (*Section 2.5.2*) were fitted for each of the *As* species. It was done in order to get insight into the actual adsorption processes occurring in the sediment samples.

All solutions contained Ca^{2+} 16 mg/l, Mg^{2+} 10 mg/l, K^{+} 3 mg/l which is comparable to the natural condition groundwater of the Site_1 was used in all the batch experiment. In preparing the solutions chloride forms of calcium and magnesium were used in these experiments to avoid adsorption affect from bicarbonates. The pH of the solution was set to 6.5. The stock solutions were prepared from reagent grade i.e. *As*(V) from $Na_2HAsO_4.7H_2O$, *As*(III) from $NaAsO_2$, PO_4^{3-} from K_2HPO_4, SiO_2 (silica) from $Na_2SiO_3.9H_2O$ and HCO_3^{-} from $NaHCO_3$.

The amount of *As* adsorbed per unit mass of soil sediment (µg/g) was calculated from the difference between the concentration of the supernatant and that of the initial solutions using following equation:

$$q_t = (C_i - C_e)\frac{V}{W} \quad (4.5)$$

where $C_i$and C_e are the arsenic concentration in µg/l at initial and equilibrium respectively, V the volume of solution in ml, W is the weight of soil sediment in mg. The amount of the adsorbate adsorption was calculated as follows:

$$S(\%) = \frac{(C_i - C_f)V}{C_i} X\ 100 \quad (4.6)$$

where $S(\%)$ is the *As* adsorption (%), C_i is the initial concentration of the *As*(µg/l), $C_f$is the final concentration of *As* (µg/l).

4.3.7.2 Oxidation kinetic of As(III) to As(V)

The oxidation kinetics of *As*(III) to *As*(V) experiments were carried out under similar condition with the sorption kinetics. Similar solution concentrations representing the groundwater composition were used and similar pH of 6.5 was also maintained prior to the experiment. *As*(III) initial concentration of 300 and 500 µg/l were used, the tubes were rotated in dark by covering with black color polythene in a horizontal shaker at an rpm of 180. The tubes were withdrawn at predefined time interval. Once the supernatant was collected from the tube for analysis of aqueous *As*(III), the remaining solution was decanted and the remnant solid was used for the analysis of solid phase *As*.

Then the solid-bound arsenic species were desorbed by adding 25 mL of 0.2M oxalic acid after the removal of the supernatant (Amirbahman et al., 2006). The tubes were then rotated in the dark for 15 min and centrifuged to remove the supernatant containing the desorbed arsenic species. The solid bound *As* was speciated to *As*(III) and *As*(V) to determine the adsorption and oxidation in the soil sediment samples.

Speciation of *As* species was performed with disposable cartridges (MetalSoft Centre). Speciation of the dissolved arsenic was determined by passing 50 mL of the supernatant through the cartridges at a flow rate of 60 ± 30 ml per minutes using 50 ml syringe. Under our experimental conditions, *As*(V) is present predominantly as $H_2AsO_4^-$ and is removed by the cartridge, whereas *As*(III) is present predominantly as H_3AsO_3 and elutes through the cartridge column.

Speciation of the solid phase *As* species was determined by adjusting the pH of the supernatant from the oxalic acid extract to approximately 4.5 by adding 10M NaOH. The *As*(III) concentration was determined from the eluting solution form the cartridge, and the *As*(V) concentration was determined by the difference between the total arsenic concentration in the supernatant and the *As*(III) concentration.

4.3.7.3 Batch adsorption study

Batch adsorption isotherm experiments were conducted under similar conditions explained for batch kinetics experiments. All batch experiments were performed in duplicate. The study for the sorption isotherm was performed on initial arsenic solution [*As*(V) and *As*(III)] concentrations of 100, 200, 300, 400, 500, 700 and 1000 µg/L using similar stock solution as mentioned in the kinetics experiment (*Section 4.3.7.1.1*). Blank samples without *As* were also included in the experiment to verify the desorption of *As* from the sediment. The samples were gently agitated in horizontal shaker at an rpm of 180 for 48 hours. The supernatant were collected using a syringe and separated from the sediment by centrifuging at 9000 rpm for 15 minutes.

Freundlich and Langmuir adsorption isotherms were fitted on the observed experimental data. The effect of pH was studied on the adsorption of *As*(III) and *As*(V) on the sediment samples where the adsorption at pH 6, 7.5 and 8.5 were measured. 0.1N HCl and 0.1N NaOH were used for adjusting the pH of solution to desired value. The effects of competing anions viz. PO_4^{3-}, SiO_2 and HCO_3^- on the adsorption of *As* was studied. The effects of *As* adsorption by PO_4^{3-} was demonstrated by increasing the concentration of PO_4^{3-} in the solution from 0.5 mg/l to 3 mg/l. Similarly the competing effect of HCO_3^- was studied by increasing the HCO_3^- concentration from 200 mg/l to 500 mg/l. The effect of SiO_2 was studied by increasing its concentration from 10 mg/l to 30 mg/l. The combined effect of anions was studied with solution containing 250 mg/l of HCO_3^-, 15 mg/l of SiO_2 and the concentration of PO_4^{3-} was increased from 0.5 mg/l to 3 mg/l.

4.3.8 Validity of the model

The validity of various adsorption models were tested and quantitatively checked using coefficient of determination (r^2) between the actual experimental results and the model

output. The coefficient of determination, r^2, to test the best-fitting of the kinetic model to the experimental data was calculated using the Eq:

$$r^2 = \frac{\sum(q_m - \overline{q_t})^2}{\sum(q_m - \overline{q_t})^2 + \sum(q_m - q_t)^2} \quad (4.7)$$

where q_m is the amount of *As* ion on adsorbed on the surface of the sediment at any time, t, (µg/mg) obtained from the second-order kinetic model q_t, is the amount of *As* ion on adsorbed on the surface of the sediment at any time t, (µg/mg) obtained from experiment, and $\overline{q_t}$ is the average of q_t (µg/mg).

4.4 Statistical analysis

Principal Components Analysis (PCA) was used for identifying patterns in data, and expressing the data in such a way as to highlight their similarities and differences. PCA is a multivariate procedure, which rotates the data such that maximum variabilities are projected onto the axes (Halim et al., 2010). Essentially, sets of correlated variables are transformed into a set of uncorrelated variables, which are ordered by reducing variability. PCA provides an objective way of finding indices of this type so that the variation in the data can be accounted for as concisely as possible (Halim et al., 2010). The first principal component is the combination of variables that explains the greatest amount of variation. The second principal component defines the next largest amount of variation and is independent to the first principal component. Since PCA is a powerful tool for analyzing data of high dimension where patterns can be hard to find in data, thus it increases the scope of graphical representation (Kazi et al., 2009). SPSS 17.0 statistical software package was used for the analysis of the various data.

4.5 Geochemical modeling (PHREEQC)

The experimental results were modeled using PHREEQC (Parkhurst and Appelo, 1999). The aqueous speciation and saturation indices of different minerals like calcite, dolomite, rhodochrosite, siderite and vivianite were calculated on the basis of the hydrochemical results with the PHREEQC-program. Inverse geochemical modeling and Surface Complexation Model (SCM) using Diffuse Layer Model (DLM) (Dzombak and Morrel, 1990) incorporated in PHREEQC geochemical code was performed and its basic procedure were briefly discussed below:

4.5.1 Inverse geochemical model

The geochemical code PHREEQC (Parkhurst and Appelo, 1999) was used for inverse modeling. This model was used to calculate the water quality changes when the river water located near to the drilling Site_1 was considered to be recharging the groundwater. Since groundwater move along its flow paths below the ground surface it dissolves many chemical species (Appelo and Postma, 2005). Therefore, the chemical composition of groundwater reveals its evolution from the geological minerals interaction in the aquifers. Inverse modeling was carried out with a known initial solution concentration of the river water flowing near the Site_1. The potential mineral phases for the model input were selected from the XRD, SEM and chemical analysis of the sediment samples. These phases were constrained (precipitation/dissolution) using a conceptual model of general trends in chemical data and saturation indices ($log\left(\frac{IAP}{K_S}\right)$ where IAP is ion activity product and K_s is the solubility product constant), the over-saturated phases from the groundwater data were allowed to precipitate.

The inverse model in PHREEQC allows uncertainty limits that are constrained to satisfy the mole balance for each element and valence state, as well as charge balance for each solution within the simulation. The inverse model simulations were constrained within the specified uncertainty limit, which was taken as 7% in the model run. The models were first run using the "minimal" identifier. After checking for adequacy and geochemical consistency, the models were rerun using "Multiple Precision Solver" (default tolerance 1E-12) without "minimal" identifier for details. A set of uncertainty terms was generated for each inverse model by the PHREEQC program to account for uncertainties in the model simulation:

1. The sum of residuals is the sum of the uncertainty of the unknowns weighted by the inverse of the uncertainty limit (for this application <8).
2. The sum of delta/uncertainty is the sum of the adjustments to each element concentration weighted by the inverse of the uncertainty limit (for this application <8).
3. Maximum fractional error in element concentration is the adjustment to any element concentration in any solution (<0.07).

If no adjustments are made, all the three quantities would be zero.

4.5.2 Surface Complexation Model (SCM)

The equilibrium surface complexation model (SCM) of PHREEQC – version 2.17.01 (Parkhurst and Appelo, 1999) was used to simulate the sorbed *As* on hydroferric oxides (Hfo) phases, derived from the selective sequential extraction (SSE) data and then comparing the model output with the observed data. The modeling is confined to the use of diffuse layer model (DLM) (Dzombak and Morrel, 1990) mathematical formulation contained in PHREEQC. The SCM developed assumes that the major anion competing with *As* for sorption sites are carbonates, phosphates, silicates and sulfates. The sorption of common cations which were found in the study viz. Ca^{2+}, Mg^{2+} were included in the model.

The model was assumed to be in chemical equilibrium and steady state conditions. The main factors controlling *As* partitioning in SCM under these assumptions were surface site densities, pH and competing ions (Miller, 2001; Robinson et al., 2011; Sharif et al., 2011). The biotransformation, kinetically limited reactions and sorption by organic matter are assumed to be secondary effects. The assumptions made may not be valid for all systems, but may apply to many. The transferability of laboratory surface complexation modeling to the fields is assumed to be limited to the primary factors, due to simplification of modeling system.

The modeled sorbent were selected as ferrihydrite (Hfo_s and Hfo_w) and goethite (Goe_). Using the surface complexation approach the adsorption of *As* species to Hfo were described by equilibrium mass action equations. Ligand sorption was considered to occur at two sorption sites on ferrihydrite with a sorption density of 0.005 mol/mol Fe for strong site which was denoted as Hfo_s, and 0.2 mol/mol Fe for weak site which was denoted as Hfo_w (Dzombak and Morrel, 1990). Ligand sorption for goethite was considered to occur at only one sorption site with a density of 0.00000384 mol sites/m^2 (Manning and Goldberg, 1996). From Dzombak and Morrel (1990), the specific surface was used as 600 m^2/g for ferrihydrite (Hfo_s and Hfo_w) and, 43.7 m^2/g for goethite (Goe_) (Manning and Goldberg, 1996).

Published physical and chemical properties of surface complex parameters are presented including *As*(III) and *As*(V) in Table 4.4-4.5. The surface reaction considered and thermodynamic constants used for ferrihydrite (Hfo_s and Hfo_w) and goethite (Goe_) are shown in Table 4.4-4.5.

Table 4.4 Surface reactions and thermodynamic constants for PHREEQC surface complexation model with strong (Hfo_s) and weak (Hfo_w) adsorption sites.

Adsorption reaction	Log K	Reference
$Hfo\_sOH + H^+ = Hfo\_sOH^{2+}$	7.29	Allison et al. (1990)
$Hfo\_wOH + H^+ = Hfo\_wOH^{2+}$	7.29	
$Hfo\_sOH = Hfo\_sO^- + H^+$	-8.93	
$Hfo\_wOH = Hfo\_wO^- + H^+$	-8.93	
Arsenite		
$Hfo\_sOH + H_3AsO_3 = Hfo\_sH_2AsO_3 + H_2O$	5.41	Allison et al. (1990)
$Hfo\_wOH + H_3AsO_3 = Hfo\_wH_2AsO_3 + H_2O$	5.41	
Arsenate		
$Hfo\_sOH + H_3AsO_4 = Hfo\_sH_2AsO_4 + H_2O$	8.61	
$Hfo\_wOH + H_3AsO_4 = Hfo\_wH_2AsO_4 + H_2O$	8.61	
$Hfo\_sOH + H_3AsO_4 = Hfo\_sH_2AsO_4^- + H_2O + H^+$	2.81	
$Hfo\_wOH + H_3AsO_4 = Hfo\_wH_2AsO_4^- + H_2O + H^+$	2.81	
$Hfo\_sOH + H_3AsO_4 = Hfo\_sOHAsO_4^{3-} + 3H^+$	-10.12	
$Hfo\_wOH + H_3AsO_4 = Hfo\_wOHAsO_4^{3-} + 3H^+$	-10.12	
Phosphate		
$Hfo\_sOH + PO_4^{-3} + 3H^+ = Hfo\_sH_2PO_4 + H_2O$	31.29	Allison et al. (1990)
$Hfo\_wOH + PO_4^{-3} + 3H^+ = Hfo\_wH_2PO_4 + H_2O$	31.29	
$Hfo\_sOH + PO_4^{-3} + 2H^+ = Hfo\_sHPO_4^- + H_2O$	25.39	
$Hfo\_wOH + PO_4^{-3} + 2H^+ = Hfo\_wHPO_4^- + H_2O$	25.39	
$Hfo\_sOH + PO_4^{-3} + H^+ = Hfo\_sPO_4^{2-} + H_2O$	17.72	
$Hfo\_wOH + PO_4^{-3} + H^+ = Hfo\_wPO_4^{2-} + H_2O$	17.72	
Carbonate		
$Hfo\_wOH + CO_3^{2-} + H^+ = Hfo\_wCO_3^- + H_2O$	12.56	van Geen et al. (1994)
$Hfo\_wOH + CO_3^{2-} + 2H^+ = Hfo\_wHCO_3 + H_2O$	20.62	
Silica		
$Hfo\_sOH + H_4SiO_4 = Hfo\_sH_3SiO_4 + H_2O$	4.28	Swedlund and Webster (1999)
$Hfo\_wOH + H_4SiO_4 = Hfo\_wH_3SiO_4 + H_2O$	4.28	
$Hfo\_sOH + H_4SiO_4 = Hfo\_sH_2SiO_4^- + H_2O + H^+$	-3.22	
$Hfo\_wOH + H_4SiO_4 = Hfo\_wH_2SiO_4^- + H_2O + H^+$	-3.22	
$Hfo\_sOH + H_4SiO_4 = Hfo\_sHSiO_4^{2-} + H_2O + 2H^+$	-11.69	
$Hfo\_wOH + H_4SiO_4 = Hfo\_wHSiO_4^{2-} + H_2O + 2H^+$	-11.69	
Calcium		
$Hfo\_sOH + Ca^{2+} = Hfo\_sOHCa^{2+}$	4.97	Allison et al. (1990)
$Hfo\_wOH + Ca^{2+} = Hfo\_wOCa^+ + H^+$	-5.85	

Table 4.5 Surface reactions and thermodynamic constants for PHREEQC surface complexation model with goethite (Goe_) adsorption sites.

Surface reaction	Log K	Reference
Goethite		
$Goe\_OH + H^+ = Goe\_OH^{2+}$	7.52	Dixit and Hering (2003)
$Goe\_OH = Goe\_O + H^+$	-10.6	
Phosphate		
$Goe\_OH + H_3PO_4 = Goe\_H_2PO_4 + H_2O$	8.05	Sigg (1979)
$Goe\_OH + H_3PO_4 = Goe\_HPO_4^- + H_2O + H^+$	3.40	
$Goe\_OH + H_3PO_4 = Goe\_PO_4^{2-} + H_2O + 2H^+$	-2.20	
Arsenate		
$Goe\_OH + AsO_4^{-3} + 3H^+ = Goe\_H_2AsO_4 + H_2O$	30.94	Dixit and Hering (2003)
$Goe\_OH + AsO_4^{-3} + 2H^+ = Goe\_HAsO_4^- + H_2O$	26.75	
$Goe\_OH + AsO_4^{-3} + H^+ = Goe\_H_2AsO_4^{2-} + H_2O$	20.16	
Arsenite		
$Goe\_OH + AsO_3^{-3} + 3H^+ = Goe\_H_2AsO_3 + H_2O$	39.87	
$Goe\_OH + AsO_3^{-3} + 2H^+ = Goe\_HAsO_3^- + H_2O$	32.34	
Silicate		
$Goe\_OH + H_4SiO_4 = Goe\_H_3SiO_4 + H_2O$	4.35	Sigg (1979)
$Goe\_OH + H_4SiO_4 = Goe\_H_2SiO_4^- + H_2O + H^+$	-3.04	
Carbonates		
$Goe\_OH + 2H^+ + CO_3^{2-} = Goe\_HCO_3 + H_2O$	20.78	van Geen et al. (1994)
$Goe\_OH + H^+ + CO_3^{2-} = Goe\_CO_3^- + H_2O$	12.71	
$Goe\_OH + CO_3^{2-} = Goe\_OHCO_3^{2-}$	3.56	Appelo et al. (2002)
Flouride		
$Goe\_OH + F^- = Geo\_F + OH^-$	-4.54	Sigg (1979)
Sulfate		
$Goe\_OH + SO_4^{2-} + 2H^+ = Geo\_ HSO_4 + H_2O$	13.61	Ali and Dzombak (1996)
$Goe\_OH + SO_4^{2-} + H^+ = Geo\_ SO_4^- + H_2O$	8.19	
$Goe\_OH + SO_4^{2-} = Geo\_ OSO_4^{3-} + H^+$	-6.26	
$Goe\_OH + SO_4^{2-} + Cu^{2+} = Geo\_ OHCuSO_4 + H^+$	9.46	
Ferrous		
$Geo\_OH + Fe^{2+} + H_2O = Goe\_OFeOH^+ + 2H^+$	-10.95	Dixit and Hering (2006)
$Geo\_OH + Fe^{2+} = Goe\_OFe^+ + H^+$	-0.60	
Calcium		
$Geo\_OH + Ca^{2+} = Goe\_OCa^+ + H^+$	-7.18	Ali and Dzombak (1996)
Magnesium		
$Geo\_OH + Mg^{2+} = Goe\_OMg^+ + H^+$	-5.94	Sigg (1979)

The Component Additivity (CA) approach was used in the SCM. It assumed that one mineral phase dominates adsorption, which facilitate a straight forward equilibrium calculation if the exposed surface area and surface-site density of that mineral phase in the soil or sediment can be quantified (Davis et al., 1998; Miller, 2001; Robinson et al, 2011; Sharif et al., 2011). The surface complexation model assumed that amorphous Fe-oxides are the dominant mineral adsorbent phase compared with amorphous Mn(IV) and Al(III) oxides and any crystalline and clay minerals. The sorbent phases ferrihydrite (Hfo_w and Hfo_s) and goethite (Goe_) were quantified from the selective sequential extraction (SSE) which is operationally defined. The surface composition of the sediments was kept in equilibrium with the mean groundwater quality of the tubwell-1 (T-1) and tubwell-2 (T-2) of the Site_1. The PHREEQC input data sets were prepared as explained i.e. groundwater composition, the sorbent phase (Hfo_w and Hfo_s or Goe_) were instructed to interact using the given thermodynamic data sets tabulate (Table 4.4-4.5). The water-mineral ratio for PHREEQC was calculated by assuming the porosity 30% and density of 2.5 g/cm^3. The difference between the modeled *As* and the actual extracted *As* was expressed as percentage difference (%) between extracted *As* and modeled *As*.

Chapter 5

Results and discussion

5.1 Groundwater geochemistry

The study areas in two districts namely Darrang and Jorhat districts were originally selected which were reported to have groundwater arsenic contamination. The field studies in two blocks (Sipajhar and Pub-Mangaldai) in the Darrang district, where arsenic had been reported earlier (Chakraborti et al., 2004; Singh, 2004), exhibited relatively low *As* concentration in most of the samples compared to what had been reported in earlier investigations. The basic groundwater quality of the region was evaluated and explained with respect to understanding acquired about overall water quality. At a later stage, attempt was made to contrast the hydrogeochemical composition of the groundwater studied in the Darrang district with respect to relatively highly arsenic contaminated areas of the Jorhat district, to contrast and compare the influencing factors in the two areas of significant difference in *As* concentration.

In Jorhat district, Titabor division was chosen for reported high arsenic concentrations in the groundwater. In the Titabor study area, to gain comprehensive understanding on the arsenic contamination, four villages were selected namely Tokobari (Site_1), Kachuknat (Site_2), Bosagaon (Site_3) and Tatigaon (Site_4) for groundwater investigations. Subsurface sediments were collected from the sampling sites in these villages in order to gain understanding of the geochemical characteristics of the aquifer matrix. The Tokobari village (Site_1) was found to have highest arsenic concentration in the study area and systematic spatial groundwater sampling was done. The groundwater quality was studied for ionic composition and chemical evolution for assessing the process involved in arsenic contamination in the aquifers.

The groundwater *As* concentration was classified into five different category according to Chakraborti et al. (2010): High affected (> 300 µg/l), Moderately affected (100-300 µg/l), Mildly affected (50-100 µg/l), Very mildly affected (10-50 µg/l), Unaffected or safe (< 10 µg/l).

5.1.1 Groundwater geochemistry of the study area in Darrang district

The major ionic composition of the groundwater samples collected from Darrang district are presented in Table 5.1 and Table 5.2 for the sites Pub-Mangaldai and Sipajhar respectively. The concentration of various heavy metals i.e. Copper, Aluminium, Zinc, Chromium and Cadmium were low and most of the samples showed concentration below detection level (b.d.l) and hence not tabulated. Similar to the findings of other *As* contaminated areas, the spatial variability of groundwater quality parameters were observed. Pub-Mangaldai samples were found to be more mineralized for most of the parameter except for Fe and Na^{+}.

Table 5.1 Groundwater composition of Pub-Mangaldai area (units mg/l, except pH and EC µs/cm).

N = 40	Max	Min	Mean	Median	S D
pH	7.90	6.10	7.15	7.10	0.47
EC	618	102	270	233	120
Na	25.6	4.8	11.7	10.7	5.47
Ca	98.3	13.5	39.2	35	18.7
Mg	25.3	2.43	7.77	5.57	5.75
Fe	25.1	0.30	6.10	4.34	6.20
K	14.5	1.17	4.82	4.42	2.79
Mn	2.1	0.03	0.63	0.52	0.52
Alkalinity	372	60	147	128	74
SO_4^{2-}	34.2	0.20	7.7	5	7.42
Cl	44.5	2.5	15.9	11	11.53
PO_4^{3-}	5.30	0.01	0.80	0.20	1.34
NO_3^{-}	2.10	0.02	0.68	0.48	0.59
As	0.11	0.001	0.02	0.002	0.05

The measurement of pH and EC were done at the respective sampling sites. The values of pH showed that the groundwater was in neutral to slightly alkaline range. The electrical conductivity (EC) varied between 191 µs/cm to 618 µs/cm. The major cations in the sampled groundwater were Ca^{2+} (mean ~ 39.2 mg/l). Alkalinity (HCO_3^{-}) was the major anion in the study area, its values ranging from 60 - 372 mg/l as $CaCO_3$. The 95% confidence level of the As concentration was found to be 0.012. High Fe concentration values (mean ~ 6.1 mg/l) and Mn (mean ~ 0.63 mg/l) characterized the reducing condition of the groundwater. The groundwater in this area is mostly unaffected/ safe (< 10 µg/l) about 6% of the samples collected were moderately affected (100-300 µg/l).

Table 5.2 Groundwater composition of Sipajhar area (units mg/l, except pH and EC µs/cm).

N = 38	Max	Min	Mean	Median	S D
pH	6.80	6.30	6.52	6.55	0.21
EC	269	142	162	162	15.2
Na	26.4	14.3	19.9	20.2	1.27
Ca	33	9.5	19.8	29.3	5.25
Mg	7.64	3.4	4.72	4.39	0.55
Fe	20.3	7.4	11.28	11.95	2.09
K	2.18	0.91	1.34	1.52	0.42
Mn	0.82	0.28	0.50	0.68	0.16
Alkalinity	174	102	123	122	2.83
SO_4^{2-}	17.3	0.74	8.5	7.82	4.54
Cl	17	9	11.38	10.75	1.06
PO_4^{3-}	1.8	0.10	1.16	1.30	0.14
NO_3^-	4.1	0.10	2.17	2.25	0.35
As	0.06	0.001	0.01	0.009	0.01

The groundwater in Sipajhar was characterized by neutral to slightly acidic pH. The electrical conductivity (EC) showed mean value of 162 µs/cm. Cation concentration was dominated by Na^+ having a mean concentration of 19.9 mg/l and Ca^{2+} with almost same mean concentration of 19.8 mg/l. The anions were dominated by HCO_3^- with mean concentration of 123 mg/l as $CaCO_3$, which was followed by Cl^-, SO_4^{2-} and NO_3^- in the groundwater composition. The dissolved Fe exhibited high concentration (mean ~ 11.3 mg/l). The major cations, mainly Na^+, Ca^{2+}, Mg^{2+} and K^+ in groundwater results from weathering of silicate and carbonate minerals, which may be further enhanced by respired CO_2 from organic matter degradation (Zheng et al., 2004; Appelo and Postma, 2005; Walther, 2010). The 95% confidence level of the As concentration was found to be 0.012. In this area approximately 93% of the samples are unaffected/safe or mildly affected (< 50 µg/l).

5.1.1.1 Groundwater composition

To classify the major ions for groundwater and to summarize the major contrasts in hydrogeochemical composition between different water sources, Piper diagrams were developed. Plots of major ions on Piper diagram (Figure 5.1-5.2) indicated that the groundwater was mostly Ca-HCO_3 type and Ca-Na-HCO_3 type. A trend of shift from Ca-HCO_3 type to the transition zone Ca-Na-HCO_3 was observed in Sipajhar (Figure 5.1). The dissolution of limestone, which would provide the Ca^{2+} and HCO_3^- ions, is important in determining the chemistry of the groundwater (Appelo and Postma, 2005; Walther, 2010).

The groundwater anions of the study areas were dominated by HCO_3^- concentration, accounted for more than 85% of the anion concentration. This can be attributed to release from dissolution of carbonate minerals via biodegradation of organic matter:

$$CH_2O \text{ (organic matter)} + O_2 \rightarrow CO_2 + H_2O \quad (5.1)$$

$$CaMg(CO_3)_2 + CO_2 + H_2O \rightarrow Mg^{2+} + 2HCO_3^- + CaCO_3 \quad (5.2)$$

$$CaCO_3 + CO_2 + H_2O \rightarrow Ca^{2+} + 2HCO_3^- \quad (5.3)$$

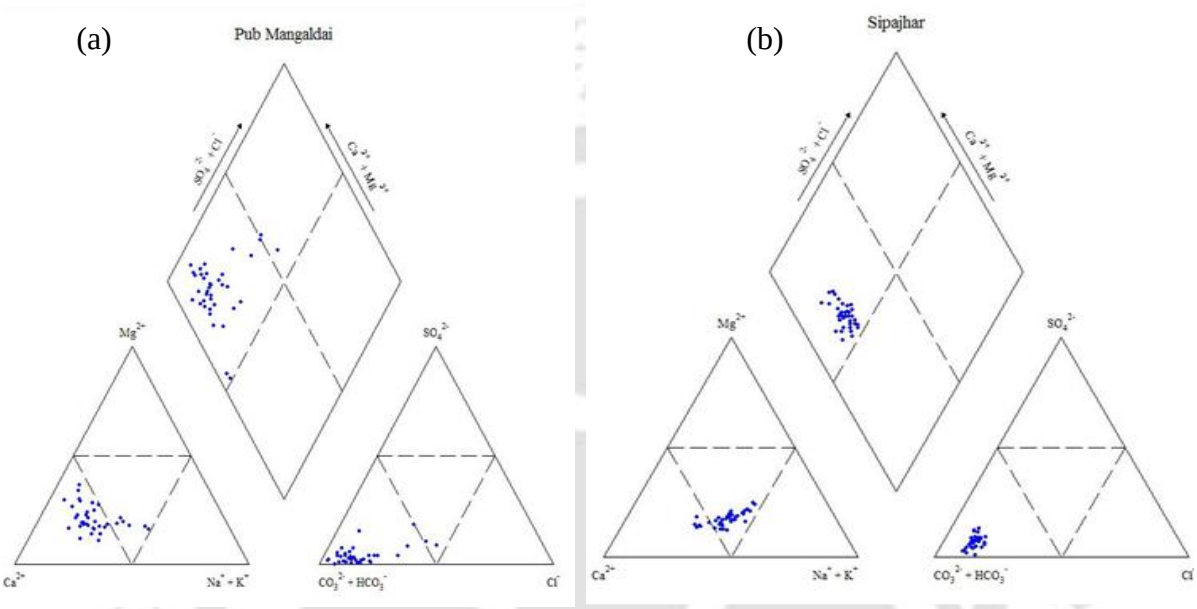

Figure 5.1 Piper diagram of the groundwater composition of the (a) Pub-Mangaldai (b) Sipajhar.

Low NO_3^- and SO_4^{2-} concentrations in aquifers may be due to the processes related to chemically or microbially mediated reduction in presence of organic matter (Eby, 2004; Appelo and Postma, 2005; Xie et al., 2008; Halim et al., 2009, 2010; Walther, 2010). The study area was located on the alluvial plains of Brahmaputra River and has alluvial deposits spreading from upstream to downstream and is assumed to have high concentration of organic matter content. Numerous ponds and wetlands in the area might have contributed organic carbon, thus creating a conducive environment for the sustenance of reducing bacteria. The reduction of NO_3^- and SO_4^{2-} through microbial degradation of organic matter to produce HCO_3^- can be summarized as (Appelo and Postma, 2005; Halim et al., 2009):

$$4NO_3^- + 5CH_2O \rightarrow 2N_2 + 5HCO_3^- \quad (5.4)$$

$$SO_4^{2-} + 2CH_2O \rightarrow 2H_2S + 2HCO_3^- \quad (5.5)$$

5.1.1.2 Minerals saturation

The groundwater was mostly Ca-HCO_3 type and Ca-Na-HCO_3 type, and thus, water-rock interaction and associated chemical reactions (Viz. precipitation, dissolution, cation-exchange, complexation and adsorption) are responsible for the variation of chemical composition in groundwater (Eby, 2004; Appelo and Postma, 2005). The saturation indices of minerals viz. calcite ($CaCO_3$), dolomite ($CaMg(CO_3)_2$), gypsum ($CaSO_4$), rhodochrosite ($MnCO_3$), siderite ($FeCO_3$) and vivianite ($Fe_3(PO_4)_2.8H_2O$) were calculated from PHREEQC have been shown for Pub-Mangaldai and Sipajhar (Figure 5.2a-b).

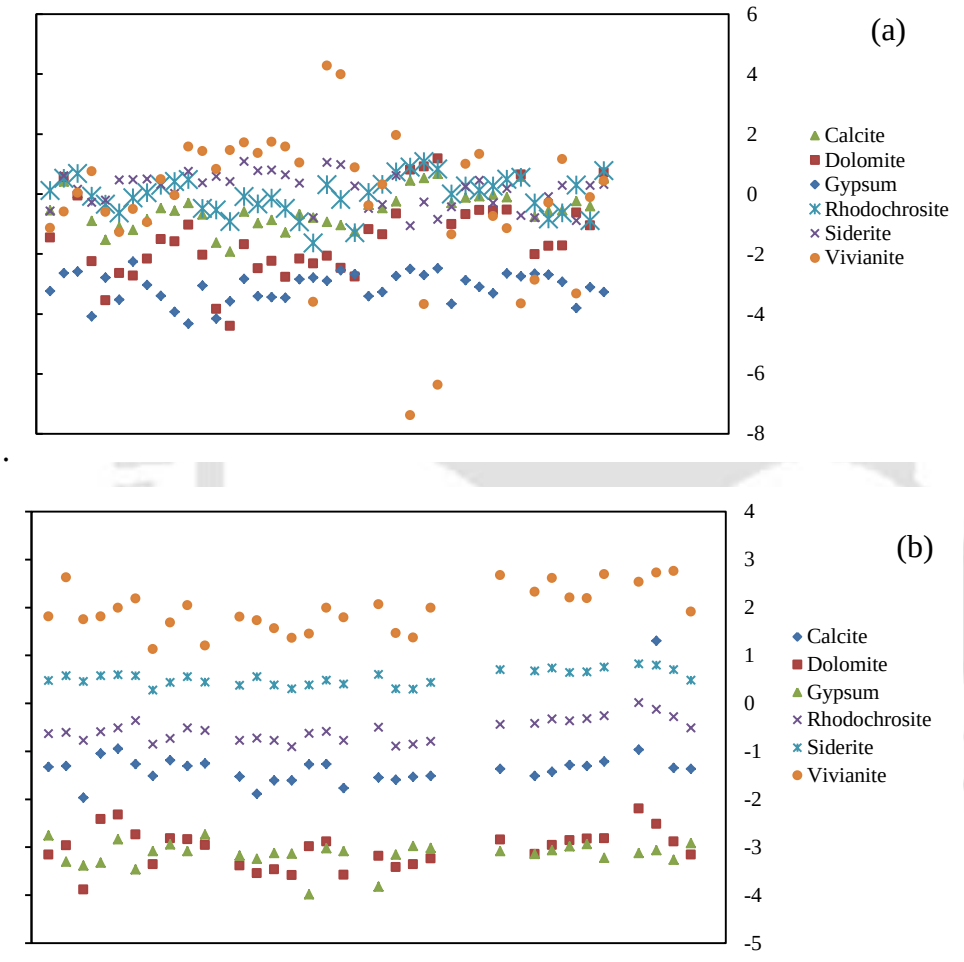

Figure 5.2 Saturation Indices of minerals (a) Pub-Mangaldai, (b) Sipajhar.

The dissolution of carbonate minerals viz. calcite ($CaCO_3$) and dolomite ($CaMg(CO_3)_2$), contributes to Ca^{2+}, Mg^{2+} and HCO_3^- to the groundwater. Gypsum dissolution was noticed in most of the groundwater samples, thus contributing Ca^{2+} and SO_4^{2-} leading to precipitation of calcite at few places and thus increasing CO_2, which leads to somewhat low pH and supersaturation or near equilibrium of groundwater with calcium. This phenomenon is known as common-ion driven precipitation or common ion effect (Langmuir, 1997; Eby, 2004).

Anaerobic decay of organic matter and SO_4^{2-} reduction (both reactions release CO_2) controls the SO_4^{2-} concentration in groundwater and subsequent increase in HCO_3^- (Eq. 5.1,5.5) and decrease in pH. Higher concentration of HCO_3^- than equivalent Ca^{2+} and Mg^{2+} indicates that some HCO_3^- is also coming from processes other than calcite dissolution (Eq. 5.1-5.6), or the Ca^{2+} is getting lost in the cation exchange reactions. Higher concentration Na^+ and Ca^{2+} in the groundwater can also be result of incongruent dissolution of plagioclase feldspars (Eby, 2004; Appelo and Postma, 2005).

5.1.1.3 Arsenic and other water quality parameters

The *As* concentrations in the groundwater are controlled by many complex sets of conditions and biogeochemical processes (Smedley and Kinniburgh, 2002; Dowling et al., 2002; Wang and Mulligan, 2006; Charlet el al., 2007; Wang and Deng, 2009). So, *As* release mechanism may vary with location depending on hydrogeological conditions. Hence, it was important to study the relationship of various water quality parameters such as Fe, Mn, HCO_3^-, PO_4^{3-}, NO_3^-, SO_4^{2-} etc for assessing the likely mechanism of *As* mobilization.

Principal component analysis (PCA) plots were used to deduce the relationship of various groundwater quality parameters in a single plot. PCA plots of dissolved *As*, Fe, Mn, PO_4^{3-} and other parameters of groundwater quality of the study were shown (Figure 5.3a-b). Two principal components (PCs) extracted using correlation matrix revealed the processes influencing the chemical composition of groundwater. First two principal components (PC1 and PC2) which extract highest variation in the dataset were used. In the Pub-Mangaldai (Figure 5.3a) site, the variation explained by first principal component (PC1) is 34.8% and the second principal component (PC2) is 19.6 % i.e. total of 54.4% of variation was explained. In the Sipajhar site (Figure 5.3b) PC1 explains 34.5 % and PC2 explains 15 % of the total variance.

From the PCA plot (Figure 5.3a-b) *As* shows a good correlation with Fe and PO_4^{3-}in both study sites in the Darrang district. Phosphorous phases containing iron (e.g. vivianite ($Fe_3(PO_4)_2{\cdot}8H2O$) and strengite ($FePO_4{\cdot}2H_2O$) are also suspected to be present due to a moderate correlation (r^2=0.5) and higher super-saturation of these minerals. Since the sampling site is located in a cultivated area, anthropogenic sources of phosphate through addition of fertilizers and high input of other components from organic matter rich wetland, domestic waste and lakes in the region is suspected. The higher reducing condition due to organic matter degradation (Eq. 5.1 to 5.5) leading to reductive dissolution of Fe according

to the Eq. 5.6 thus increases Fe and PO_4^{3-} as well as *As* concomitantly into the groundwater (*Section 2.4.2*).

In Pub-Mangaldai it was found that Ca^{2+} is closely correlated with Alkalinity and Mg^{2+}, which may be due to dissolution of minerals viz. calcite and dolomite. Good correlation of Na^+ and Cl^- also points towards the presence of evaporite halite mineral (NaCl) in the region. Iron (Fe) was an important trace metal found in relatively higher concentration with values ranging between 0.3 mg/l to 25 mg/l in the study area. The relatively high average concentration of Fe in Pub-Mangaldai (mean ~ 5 mg/l) and Sipajhar (mean ~ 11.3 mg/l) depicts the reducing condition prevailing in the groundwater. The strong affinity of *As* for iron (Fe) has been well known and reported widely in literature (Dzombak and Morel, 1990; Smedley and Kinniburgh, 2002; Dixit and Hering, 2003) and explained in *Section 2.4.1*. Moderately correlated Fe and Mn in groundwater suggested likelihood of ferromanganese coatings in the aquifer soil matrix which was verified by observed Fe and Mn in the aquifer using SEM and EDX (*Section 5.2.1.5*). Arsenic was found to be closely associated with Fe and Mn (Figure 5.3), similar findings was reported from *As* affected areas of Bangladesh (Shamsudduha et al., 2008; Ahmed et al., 2004; Zheng et al., 2004; Halim et al., 2010). The surface water infiltrating into the upper aquifer of the study area has a high content of organic waste from the domestic waste and from the decomposition of plants and utilization of fertilizer from the fields, and high organic carbon containing alluvial aquifer. These lead to reducing conditions, the Fe-oxides likely get dissolved by the organic matter, resulting the groundwater recharge becoming enriched in Fe^{2+} and HCO_3^- (Appelo et al., 2002):

$$4FeOOH+CH_2O+7H_2CO \rightarrow 4Fe^{2+} + 8HCO_3^- + 6H_2O \qquad (5.6)$$

The redox potential (Eh) of the groundwater in this district was found be about -50 mV to -70 mV, thus implying a reduced condition. And the field speciation of *As* using disposable cartridges (MetalSoft Centre) showed the abundance of *As*(III) species over *As*(V). Thus the Hydrogeochemical data, minerals saturation and the redox environment (*Section 5.1.1.1 – 5.1.1.3*) suggests reductive dissolution of Fe-oxides and Mn-oxides as the dominant *As* release mechanism in Darrang district. The oxidation of organic matter Eq. 5.1-5.6 by bacteria may influences the groundwater *As* concentration by serving as an electron donor for the reduction of Fe-oxides and Mn-oxides in the aquifer sediments.

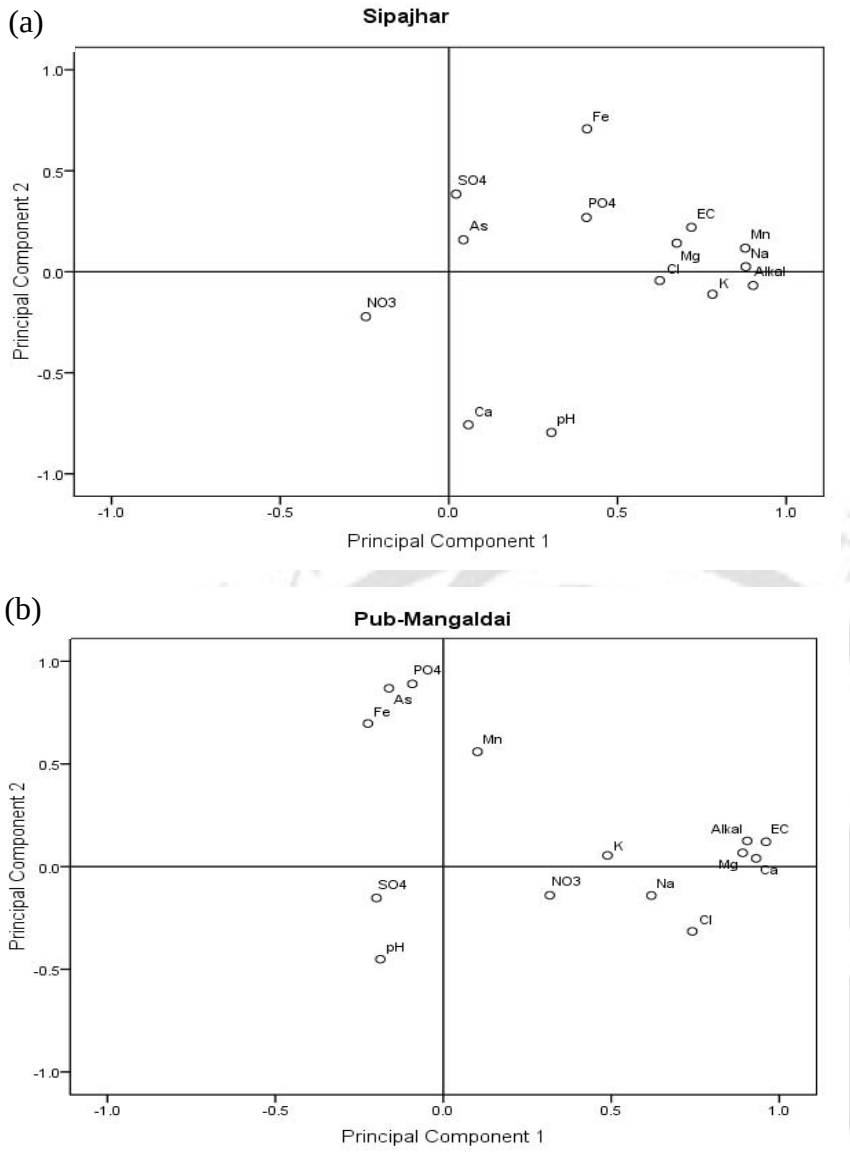

Figure 5.3 PCA plots of groundwater quality parameters at (a) Pub-Mangaldai (b) Sipajhar.

5.1.2 Groundwater geochemistry of the study area in Jorhat district

The major ionic compositions of groundwater samples collected from the study areas viz. Tokobari (Site_1), Kachuknat (Site_2), Bosagaon (Site_3) and Tatigaon (Site_4) are presented in Table 5.3-5.6. The groundwater in the Jorhat district was found to be more mineralized comparing Darrang district. High spatial variation was also observed in the groundwater quality parameters in these different site locations. The major cations in the sampled groundwater were dominated by Na^{+}, and considerable amount of Ca^{2+} was also present in the samples. Alkalinity (HCO_3^{-}) was the predominant anion found in the study area, with Cl^{-}, NO_3^{-} and SO_4^{2-} present as minor anions.

The groundwater quality of Site_1 was found to be moderately mineralized compared to the other study sites (Table 5.3). The pH of the groundwater was found in almost neutral to slightly acidic range, with a mean electrical conductivity (EC) of 309 µs/cm. The cations were largely dominated by Na^+ (mean of 43 mg/l), while the anions were dominated by HCO_3^- (mean of 205 mg/l as $CaCO_3$). The groundwater quality of Site_3 was found to be highly mineralized (Table 5.5). The Fe concentration varied between 0.89 mg/l to 27.3 mg/l (mean ~ 6.6 mg/l). Site_1 was found to be highly affected where about 16% of the sample As concentration is above 300 µg/l and 60% of the samples were found to be moderately affected (100- 300 µg/l). Site_2 about 62% of the samples were very mildly affected (10-50 µg/l) and 34% of the total samples were mildly affected (50-100 µg/l). In Site_3 and Site_4 about 23% and 14% of the samples collected were moderately affected (100-300 µg/l). And majority of the samples in these sites are mildly affected (50-100 µg/l) i.e 36% and 47% respectively.

Table 5.3 Groundwater composition of Site_1 (units mg/l, except pH and EC in µs/cm).

N = 44	Max	Min	Mean	Median	S D
pH	7.10	5.81	6.69	6.74	0.32
EC	486	73	309	335	96.6
Na	117.2	4.71	43.03	40.3	20.4
Ca	26.95	10.77	19.64	19.77	4.40
Mg	14.18	0.84	6.82	6.71	2.56
Fe	40.5	0.68	9.41	7.25	7.58
K	4.80	1.67	2.30	2.04	0.68
Mn	0.77	0.02	0.17	0.16	5.30
Alkalinity	392	48	205	198	59
SO_4^{2-}	72	0.97	10.43	6.83	13.07
Cl	76	3.97	16.25	9.00	18.42
PO_4^{3-}	1.3	0.01	0.49	0.30	0.36
NO_3^-	13.6	0.01	6.04	2.85	4.76
As	0.44	0.01	0.21	0.20	0.11

Table 5.4 Groundwater composition of Site_2 (units mg/l, except pH and EC in µs/cm).

N = 35	Max	Min	Mean	Median	S D
pH	6.90	5.70	6.54	6.60	0.23
EC	302	106	189	166	52
Na	24.2	5.7	15.3	15.5	4.54
Ca	31.6	8.2	21.8	21.8	6.56
Mg	7.27	3.50	5.95	6.13	0.79
Fe	33.17	0.61	16.66	15.01	6.31
K	1.62	0.11	0.94	1.00	0.31

Mn	0.77	0.07	0.24	0.18	0.18
Alkalinity	192	68	154	160	25
SO_4^{2-}	42.9	2.14	10.5	10.2	7.5
Cl	36	6	13.5	12	6.5
PO_4^{3-}	1.60	0.01	0.73	0.60	0.36
NO_3^-	9.80	0.30	4.04	3.50	2.17
As	0.08	0.01	0.03	0.03	0.02

Table 5.5 Groundwater composition of Site_3 (units mg/l, except pH and EC in µs/cm).

N = 39	Max	Min	Mean	Median	S D
pH	7.80	6.40	6.97	6.91	0.31
EC	740	210	375	345	116
Na	140	16	54	47	25
Ca	30.7	9.5	16.7	16.3	3.93
Mg	19.1	5.9	11.2	10.2	3.47
Fe	27.3	0.89	6.6	6.1	4.64
K	2.6	0.46	1.5	1.3	0.55
Mn	1.31	0.02	0.29	0.16	0.30
Alkalinity	500	140	278	262	86
SO_4^{2-}	14.4	0.15	4.30	4.37	2.47
Cl	25.8	1	8.21	5.96	6.03
PO_4^{3-}	3	0.20	1.33	1.20	0.70
NO_3^-	6.80	1.20	3.86	3.70	1.35
As	0.16	0.02	0.07	0.06	0.04

Table 5.6 Groundwater composition of Site_4 (units mg/l, except pH and EC in µs/cm).

N = 21	Max	Min	Mean	Median	S D
pH	7.40	6.40	7.16	7.30	0.29
EC	530	288	422	444	66
Na	86	8.3	52.4	57.1	16.6
Ca	22	7.60	14.30	14	4.18
Mg	18.96	7.03	10.27	10.05	2.36
Fe	18.34	0.59	5.29	1.90	5.83
K	4.80	1.00	1.87	1.20	1.15
Mn	1.13	0.05	0.24	0.20	0.22
Alkalinity	312	120	250	268	50.5
SO_4^{2-}	19.40	1.30	4.29	2.70	4.54
Cl	28	4	9	8	6.12
PO_4^{3-}	14	0.50	1.73	1	2.85

NO_3^-	29.50	4.50	10.82	8.80	5.74
As	0.13	0.02	0.07	0.07	0.03

The 95% confidence level Site_1, Site_2, Site_3 and Site_4 were found to be 0.033, 0.006, 0.013 and 0.013 respectively. Higher concentration of Na^+ in the groundwater can be result of silicate weathering (Appelo and Postma, 2005). The weathering of silicate and carbonate minerals which is enhanced by respired CO_2 from oxic and anoxic organic matter degradation is responsible for higher cations Na^+, Ca^{2+}, Mg^{2+} and K^+ are released into the groundwater (Eby, 2004; Zheng et al., 2004; Appelo and Postma, 2005). The cation Ca^{2+} often comes from carbonate minerals such as calcite and gypsum. The major sources of minerals of Fe^{2+}, Mg^{2+} are quartz, albite, illite and biotite minerals, which were noticed in the X-Ray diffraction (*Section 5.2.1.4*). K^+ comes from orthoclase and clay minerals (Eby, 2004; Walther, 2010). The application of fertilizer for agriculture may be possible sources for NO_3^-, Cl^- and PO_4^{3-} (Manning and Goldberg, 1997; Goldberg, 2002; Goh and Lim, 2005) into the groundwater.

5.1.2.1 Groundwater composition

The hydrogeochemistry of the area has been classified as Na-HCO_3^- type from the Piper diagram (Figure 5.4a-d). The pH values varied from slightly acidic to neutral range. Higher reduced condition characterized by low NO_3^- and SO_4^{2-} concentration in aquifers is probably due to the processes related to chemically or microbially mediated reduction in presence of organic matter shown in Eq. 5.4-5.5 (Halim et al., 2009, 2010). The younger alluvial deposits and the paleochannel of the study area contain organic carbon and thus create a conducive environment for the nourishment of reducing bacteria. Furthermore, strong H_2S odor prevailing in the groundwater indicated the effect of sulfate reduction. Similarly, high alkalinity (HCO_3^-) in the area is probably due to microbial oxidation (Eq. 5.1-5.6) and the dissolution of carbonate minerals ($CaCO_3$) via biodegradation (Eq. 5.2-5.3) of the organic matter.

Concentrations of dissolved HCO_3^- reflect the degree of water-rock interaction in groundwater systems as well as integrated microbial degradation of organic matter (Appelo and Postma, 2005). Groundwater HCO_3^- sources have been discussed (*Section 5.1.1.1*) and high HCO_3^- suggested oxygen free environment (Eq.5.1 to 5.6). The source of dissolved inorganic carbon include a component of respired CO_2 derived from the oxidation of organic matter either due to infiltration through soil or along the flow path of the water. When the

groundwater moves through clay rich sediment, cation exchange results in softening of water where Ca^{2+} and Mg^{2+} in water mutually exchange with sorbed Na^{+}. The divalent ions are more strongly bonded and tend to replace monovalent ions, but high activity of monovalent (Na^{+}) replaces the divalent ions.

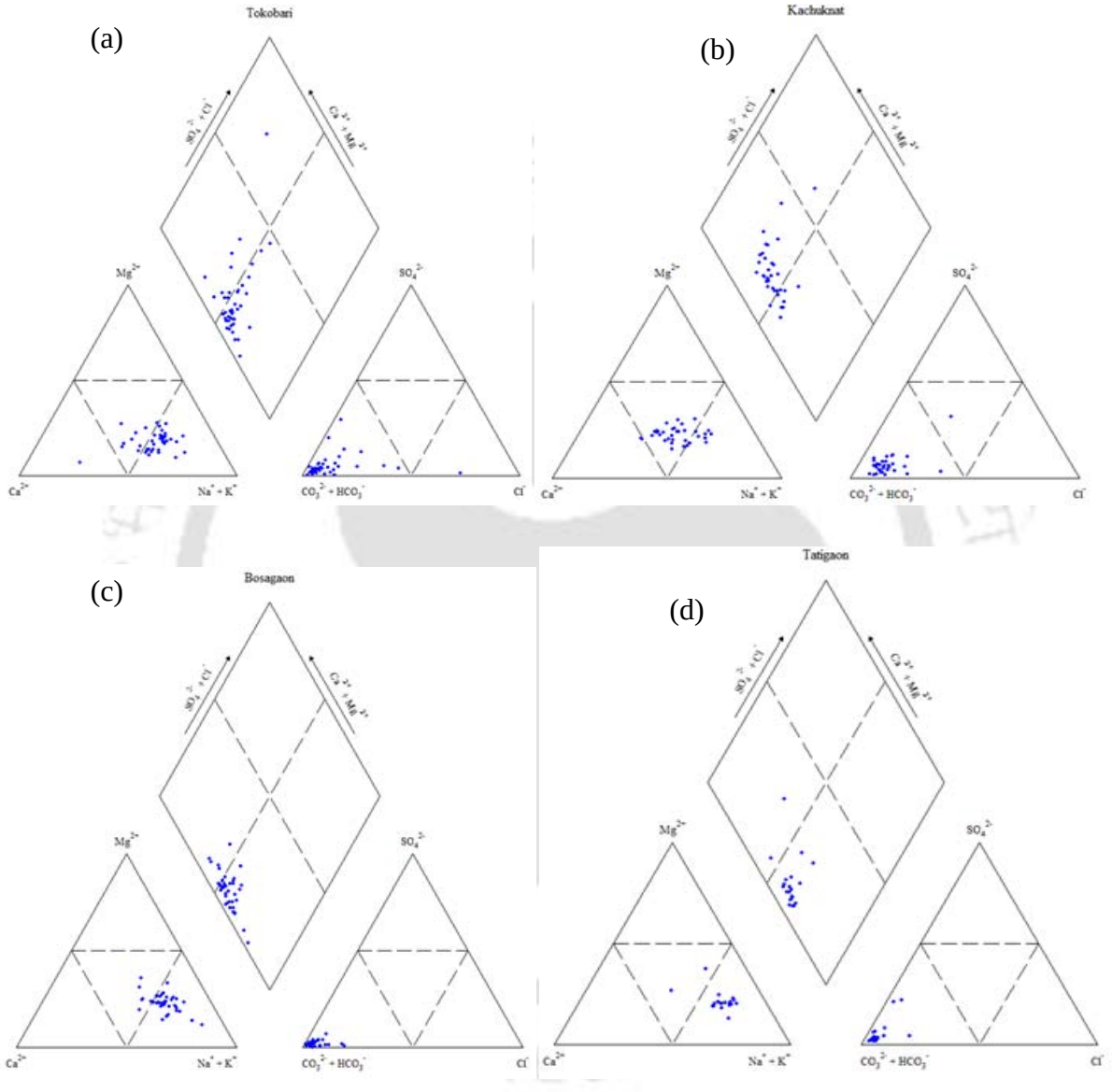

Figure 5.4 Piper diagram showing the composition of groundwater for (a) Site_1 (b) Site_2 (c) Site_3 and (d) Site_4.

5.1.2.2 Mineral saturation

The saturation indices from PHREEQC have been derived (Figure 5.5a-d) for Site_1, Site_2, Site_3 and Site_4. The high degree of sub-saturation of gypsum ($CaSO_4$) is likely to be due to the low concentration of Ca^{2+} in the samples along with low SO_4^{2-} in the study areas.

Similarly, carbonate mineral dissolution viz. calcite ($CaCO_3$) and dolomite ($CaMg(CO_3)_2$) was also observed. The concomitant release of Fe^{2+} and HCO_3^- during the reduction of Fe-oxides (Eq. 5.6) also caused the saturation index of siderite ($FeCO_3$) to increase i.e. to get slightly supersaturated. Similar super-saturation for siderite have been reported in West Bengal (Pal et al., 2002), Bangladesh (Swartz et al., 2004; Polizotto et al., 2006), Vietnam (Postma et al., 2007; Eiche et al., 2008). The concentration of Mn^{2+} in the samples was low (mean ~ 0.23 mg/l), therefore the groundwater was sub-saturated with rhodochrosite ($MnCO_3$) in most of the samples. The saturation index pattern for siderite ($FeCO_3$) and vivianite ($Fe_3(PO_4)_2.8H_2O$) showed a similar pattern. Most of the groundwater remained supers-saturated with hydroxyapatite ($Ca_5(PO_4)_3OH$) and in few cases high degree of sub-saturation was also observed due to low PO_4^{3-} concentration. The distribution pattern of saturation index of hydroxyapatite is of opposite nature to that of siderite and vivianite. Calcite and gypsum solubility and simultaneous SO_4^{2-} reduction with co-precipitation of *As* and sulfide is an important limiting process controlling the concentration of dissolved *As* in groundwater (Sharif et al., 2008).

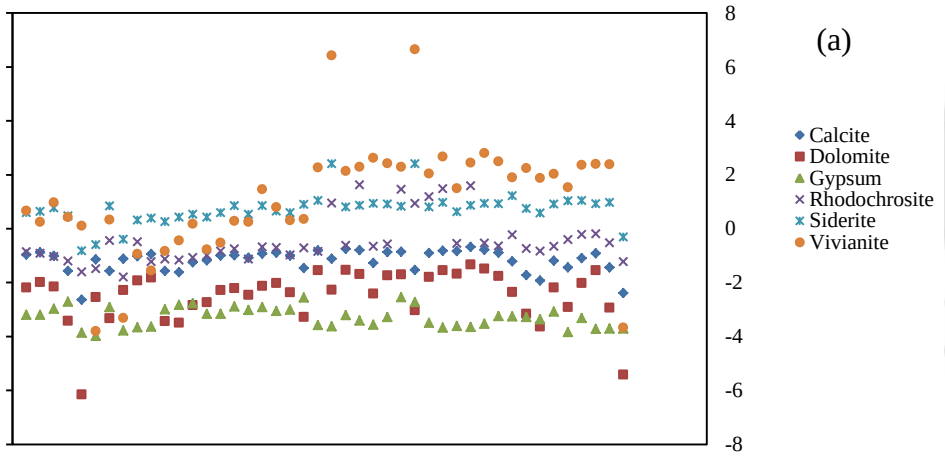

Figure 5.5 (a) Saturation indices of groundwater samples from Site_1.

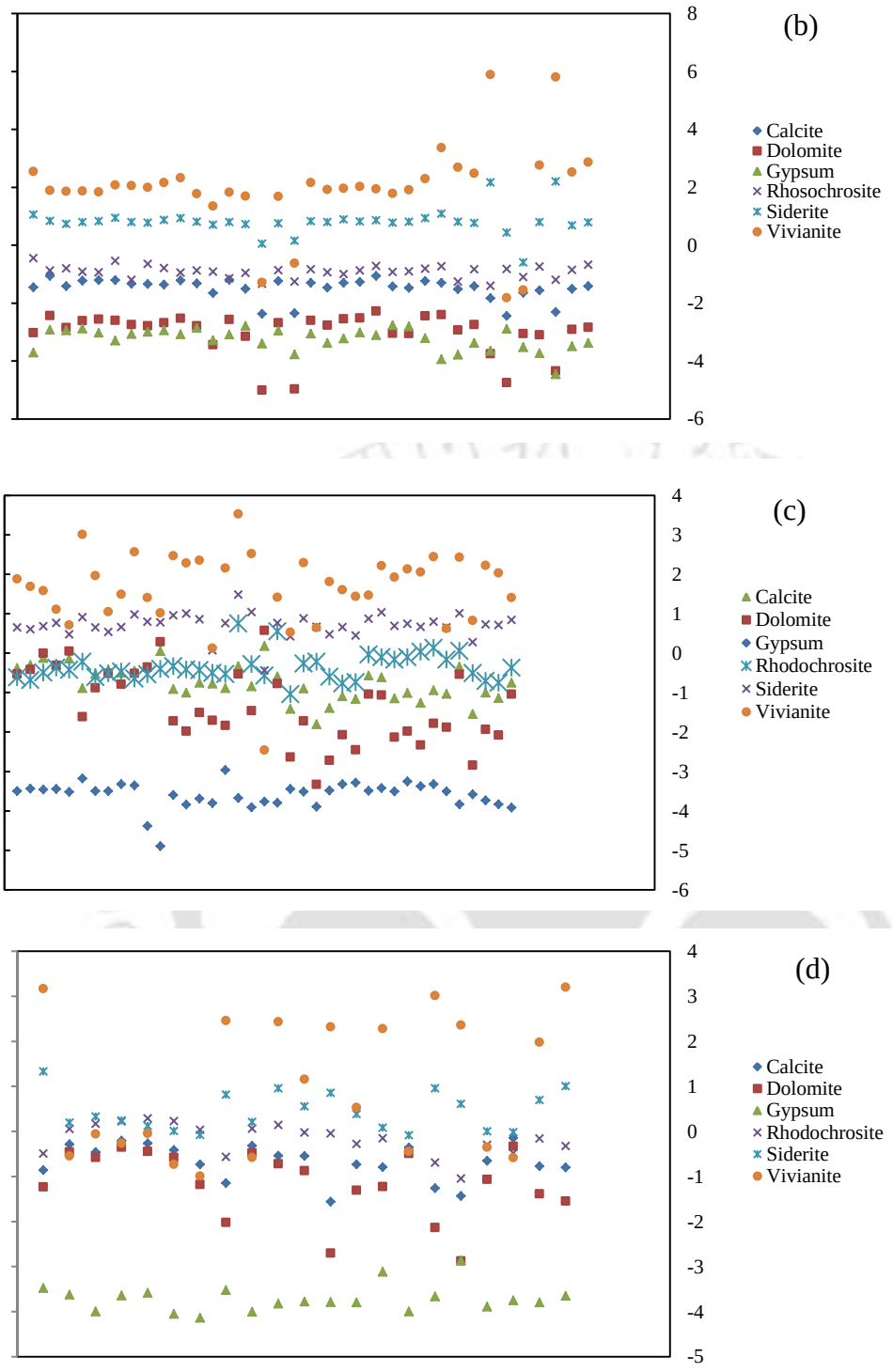

Figure 5.5 Saturation indices of groundwater samples from (b) Site_2 (c) Site_3 and (d) Site_4.

5.1.2.3 Arsenic and other water quality parameters

Concentration of dissolved *As*, Fe, Mn, $PO_4^{3-}$and other groundwater quality parameters of the study area was plotted with Principal Component Analysis (PCA) plots to show the various relationship. PCA plot (Figure 5.6a-d) shows the relationship of *As* with other ions. The first

principal component (PC1) and second principal component (PC2) which extracts the highest variation from the datasets were used in the plots. For Site_1 (Figure 5.6a) the PC1 extracts 26% and PC2 is 24% of the total variation, in the Site_2 (Figure 5.6b) PC1 is 33% and PC2 is about 27.4% of the total variation, in the Site_3 (Figure 5.6c) PC1 extracts to 32%, PC2 is 19%, Site_4 PC1 extracts about 36% and PC2 about 18.4% (Figure 5.6d) of the total variation in the dataset. High correlation of Fe and Mn in most of the sites (Figure 5.6a-d) shows reducing condition existed within the aquifer. The groundwater of Jorhat district was found to have a different nature compared to the Darrang district. In these areas, good correlation of *As* with PO_4^{3-} was seen in the groundwater samples. Further, a moderate relationship was observed between *As* and Ca^{2+} except in Site_2 with low *As* concentration. A moderate to strong relationship was demonstrated between *As*, HCO_3^- and Ca^{2+} in most of the samples.

The relationship that exists between *As*, Ca^{2+}, HCO_3^- was further investigated for the dissolution of carbonate minerals in the sediment using the Selective Sequential Extraction (SSE) method (*Section 5.2.3*). *As* can be adsorbed on to calcite surface, occupying carbonate lattice site (Goldberg and Glaubig, 1988; Cheng et al., 1999; Romero et al., 2004; Sø et al., 2008; Bardelli et al., 2011). Several researchers reported that surface complexation of bicarbonates onto Fe-oxide results in the release of *As* into the groundwater (Appelo et al., 2002; Harvey et al., 2002, 2006; Anawar et al., 2003). Similar high *As* and HCO_3^- are also reported from different parts of the affected countries (Shimada, 1996; Welch et al., 2000, 2003; Berg et al., 2008; Bhattacharya et al., 2006; Halim et al., 2010). The above reported findings provided a backdrop for the study area of Jorhat and these aspects were addressed subsequently (*Section 5.2.3, 5.3.1.4*).

The study areas are located in the rice cultivated land in the vicinity of tea estate. Agricultural activity has direct or indirect effects on the inorganic chemical composition of groundwater viz. PO_4^{3-}, Cl^- and NO_3^- (Appelo and Postma, 2005). The competition of adsorption site of *As* with PO_4^{3-} have been widely published and reported (Manning and Goldberg, 1996; Smedley and Kinniburgh, 2002; Dixit and Hering, 2003, Stollenwerk et al., 2007; Stachowicz et al. 2008). PO_4^{3-} is strongly sorbed on solid phases, including Fe-oxides and Al-oxides in the soils and the amount PO_4^{3-} released in to the water is related to the concentration of PO_4^{3-} that exceeds the capacity of Fe to create insoluble iron phosphate (Manning and Goldberg, 1996). In contrast, PO_4^{3-} may also get released in groundwater due to microbially mediated reductive dissolution of Fe-oxide (Guo et al, 2008, 2011). Strong correlation observed between *As* and PO_4^{3-} in the study area is apparently due to reductive dissolution of Fe-oxides.

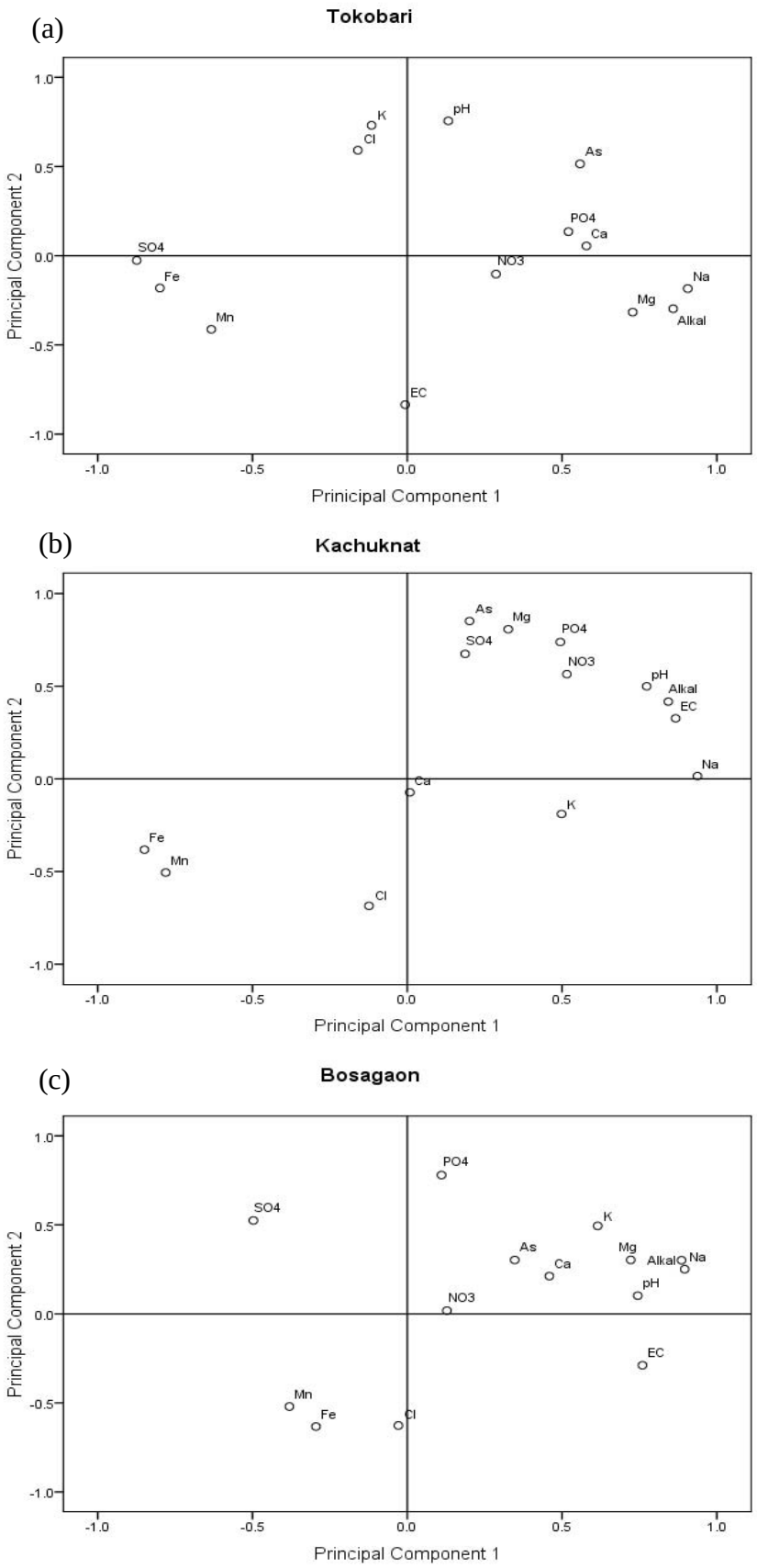

Figure 5.6 PCA plots of groundwater quality parameters in (a) Site_1 (b) Site_2 (c) Site_3.

(d)

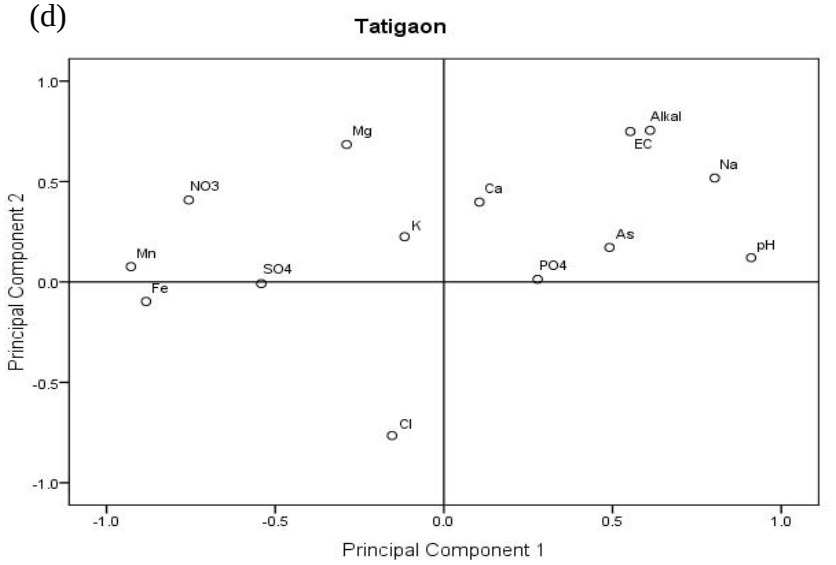

Figure 5.6 (d) PCA plots of groundwater quality parameters in Site_4.

Relatively higher concentration of iron (Fe) was found in the study areas (values ranging from 0.6 mg/l to 40.5 mg/l). The surface water infiltrating into the upper aquifer often flows through high organic content of the younger alluvial deposits. Organic matter from the decomposition of plants and utilization of fertilizer in the field lead to highly reducing conditions. The Fe-oxides are likely to be dissolved by the organic matter according to Eq. 5.6 (Nickson et al., 2000; Appelo et al., 2002), and thus increases groundwater Fe and HCO_3^- concentrations. The precipitation of siderite ($FeCO_3$) shown in Figure 5.2(a-b) and Figure 5.5(a-d) may act as temporary sinks for the *As* in the groundwater. The redox potential (Eh) values from the study areas were found to be highly reducing approx. -230 mv in Site_1 and Site_3. Therefore, co-precipitation of *As* with sulfide minerals may be an important *As* limiting process in the groundwater (Thronton, 1996; Nordstrom 2002; Xie et al., 2008; Kirk et al., 2010; Sharif et al., 2008, 2011).

The PCA plots suggested that Mn have negative correlation with *As* in two sites with higher *As* contamination namely Site_1 and Site_3 (Figure 5.6a,c), while no significant correlation was observed for Site_2 and Site_4 (Figure 5.6c,d). Such negative correlation was observed by few researchers (Stuben et al., 2003; Buschmann et al., 2007; Berg et al., 2007, 2008) implying that MnO_2 reduction occurs at redox potentials that are higher than reduction of Fe-oxides, therefore the dissolved Mn^{2+} may be re-adsorbed onto the surface of Fe-oxides (Belzile, 1988). The dissolved Mn^{2+} has high affinity for the oxidation of *As*(III) to *As*(V) (Manning et al., 2002; Tournassat et al., 2002; Amirbahman et al., 2006; Stollenwerk et al.,

2007; Han et al., 2011). The adsorption capacity of *As*(V) is much higher than *As*(III), removal of *As* through oxidation and adsorption might have taken place. But due to higher organic content in the aquifer systems (*Section 5.2.1.2*) reductive dissolution might have prevailed over other processes, which lead to concomitant release of Fe and *As*. Re-precipitation of Fe phases and the adsorption of Mn by them cause low relationships exhibited among them.

5.1.2.4 Inverse geochemical modeling at Site_1

Inverse geochemical modeling using PHREEQC was performed to calculate water-quality changes during infiltration from the surface water into the groundwater of Site_1. The inverse geochemical modeling was run with a known initial solution concentration of surface water near the drilling location of Site_1 (500 m approx), and the potential mineral phases were made input to the model which were obtained from the sediment analysis (*Section 5.2.1*). Quantification of the processes that lead to the final solution chemistry was done. To do this, the model reconstructs all possible combinations of dissolution and/or precipitation reactions that explain the chemical changes observed between the solutions along the conceptual flow path within a groundwater system and the mineral phases. Inverse modeling output i.e. moles of minerals and gases entering and or leaving the solution (moles/kg of H_2O) to account for the differences in composition are shown in Figure 5.7(a,b).

The USGS geochemical code PHREEQC (Parkhurst and Appelo 1999) was used and following assumptions of inverse models were made (Zhu and Anderson, 2002):

1. Initial and final conditions occur along a single flowpath i.e. they are hydraulically connected.
2. Dispersion and diffusion do not affect dissolved concentrations.
3. Reactions are at steady state.
4. Major reactive mineral phases have been identified in the aquifer material.

Conceptually, the following geochemical reactions were hypothesized to proceed during the groundwater flow, and these were simulated with inverse geochemical models:

- Precipitation or dissolution of calcite, dolomite, and gypsum.
- Dissolution of organic carbon (CH_2O) along the flowpath.
- Reduction of dissolved oxygen in the final groundwater quality.
- Oxidation of pyrite with precipitation of amorphous iron-oxyhydroxide.

- Sulfate reduction with the evolution of hydrogen sulfide (H_2S).

The organic carbon was forced to dissolve in the inverse geochemical model as the groundwater was found to be in highly reduced condition. While simulating the inverse model, two models were obtained, which are shown in Figure 5.7 (a,b). The output of inverse model shows that the geochemical reactions that cause the greatest phase mole-transfer in the simulation were oxidation of pyrite, and subsequent precipitation of iron-oxyhydroxide [$Fe(OH)_3$], and the reduction of sulfate leading to the evolution of hydrogen sulfide (H_2S). Minor mass changes result from apparent dissolution of calcite ($CaCO_3$) and precipitation of gypsum ($CaSO_4$). Gypsum precipitates when the organic carbon is in equilibrium due to the oxidation of pyrite releasing SO_4^{2-} into the groundwater and Ca^{2+} gets released from the calcite dissolution (Figure 5.7a). When dissolved organic carbon gets further dissolved into the groundwater causing higher phase mole transfer for the pyrite dissolution as well as higher $Fe(OH)_3$(a) precipitation and high H_2S (g) formation (Figure 5.7b).

Calcite dissolution is indicated by positive phase-mole transfer. The dissolution of calcite is plausible because the surface water is under-saturated with respect to calcite (-0.43 saturation index-calcite). Model simulation indicates that iron released during pyrite oxidation is precipitated quantitatively as Fe-oxide. Dissolved Fe concentration in recharge water is low (i.e. 0.01 mg/l). Precipitation of Fe-oxide grain coatings is likely in the presence of dissolved oxygen during recharge.

Sulfate reduction is indicated from negative phase-mole transfer values (degassing of hydrogen sulfide gas), and by strong hydrogen sulfide (H_2S) odor emanating from the tubewells during sampling. Sulfate contribution from the stream water as well as gypsum dissolution serves as a source of hydrogen sulfide (H_2S). Microbe mediated sulfate reduction is coupled with oxidation of dissolved organic carbon from recharge water, after dissolved oxygen is consumed (Appelo and Postma, 2005; Sharif et al., 2008).

In this equilibrium model, pyrite is forced to oxidize, and Fe-oxide is forced to precipitate, all under sulfate reducing conditions. It is unlikely that these three reactions co-exist in reality. A better (non-equilibrium) reactive transport conceptual model would simulate pyrite oxidation and Fe-oxide under oxic condition in the surface water. *As* redox environment shifts to sulfate reducing conditions (approx -200 mV) in the groundwater, Fe-oxide would likely become unstable and re-dissolve.

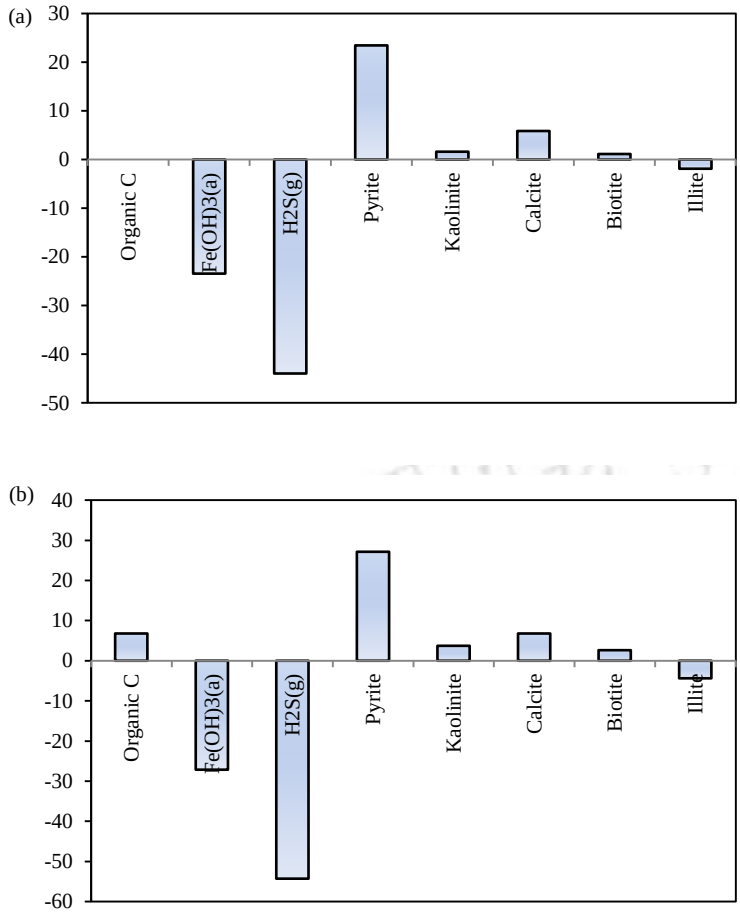

Figure 5.7 Inverse geochemical model of Groundwater quality for Site_1 (a) model-1 (b) model-2

5.1.3 Comparison with hydrogeochemistry of other contaminated areas

The groundwater from *As* contaminated aquifer mainly from quaternary alluvial deposits in Bangladesh and West-Bengal were typically characterized by high concentration of Fe and HCO_3^-, and lower amounts of NO_3^- and SO_4^{2-} in most of the samples, with circum-neutral pH and reduced conditions, with *As* distribution being highly heterogeneous in nature, and *As*(III) being the most predominant form due to the reducing environment of the groundwater (Nickson et al., 1998, 2000; Bhattacharya et al., 2001; McArthur et al., 2001, 2004; Smedley and Kinniburg, 2002; Harvey et al., 2002; Dowling et al., 2002; van Geen et al., 2004, 2006, 2008; Charlet et al., 2007; Nath et al., 2008; Halim et al., 2009, 2010).

Groundwater characteristics within Southern Cambodia, show many similarities to the *As* rich waters of West Bengal and Bangladesh including high but heterogeneous *As* distribution,

higher concentration of Fe, moderate to high HCO_3^-, low SO_4^{2-} (in the majority of samples), circum-neutral pH and reducing conditions (Rowland et al., 2008).

Berg et al. (2008) observed that in Hanoi, Vietnam similar reducing condition with low Eh and high Fe, dissolved organic carbon (DOC) and ammonium was noticed. Kocar et al. (2008) reported a strong correlation between *As*, Fe and alkalinity (HCO_3^-) in Red River Delta, Vietnam (Postma et al., 2008, 2010; Eiche et al., 2008).

The groundwater of the study areas are generally Ca-HCO_3, Ca-Na-HCO_3 and Na-HCO_3 types. High concentration of *As* groundwater in Darrang district are characterized by high concentration of dissolved Fe, Mn and PO_4^{3-}. While in Jorhat district *As* was found to have good correlation with PO_4^{3-} but no relationship was found with Fe and Mn due to the precipitation of secondary Fe minerals such as siderite, vivianite. The groundwaters in both districts were found to have high concentration of Fe and low concentration of NO_3^- and SO_4^{2-} suggests that the groundwater exists in the reducing environment. In this environment, *As*(III) was found to be the major *As* species over *As*(V).

The anions were highly dominated by HCO_3^- accounting to more than 80% of the total anions concentration. The microbial biodegradation of carbonate minerals as well as the NO_3^- and SO_4^{2-} acting as an electron acceptors in the system to allow oxidation of organic matter was believed to be an important contributor to the generation of anoxic conditions that produce high concentration of HCO_3^-.

With head waters in the Tibetan Plateau, the characteristics of the groundwater and sediments in Assam, West Bengal, Bangladesh and Cambodia are somewhat similar. The hydrochemical conditions, minerals saturation and the redox environment suggests reductive dissolution of Fe-oxides as the dominant *As* releasing mechanism in the study areas. Competition of adsorption sites by anions viz. PO_4^{3-} and HCO_3^- to some extent might be responsible for the release of *As* in some affected areas which was further investigated and reported (*Section 5.2.3, 5.3.1*).

5.2 Sediment characteristics

The natural occurrence of arsenic in the aquatic environment is believed to be associated with sediments (Breit et al., 2001, 2003; Harvey et al., 2002, 2005, 2006; Anawar et al., 2003; Ahmed et al., 2004; Charlet et al., 2007; Chakraborty et al., 2007; Seddique et al., 2008; Reza et al., 2010a,b; McArthur et al., 2004, 2008, 2011). However, there has been little evidence of

unusually high level of solid phase *As* in the aquifer materials (Charlet et al., 2007; Guo et al., 2008; Xie et al., 2008). It appears that high dissolved *As* in groundwater may be the result of particular hydrologic and biogeochemical conditions that facilitates its concentration. Many researchers have proposed *As* rich clays deposited during the Holocene in paleochannels as source of *As* to the groundwater (Charlet et al., 2007; Chakraborty et al., 2007; Seddique et al., 2008; McArthur et al., 2008, 2011). Evaluation of the characteristics of sediments can be considered to be of prime importance in understanding release, mobilization and transport of *As* into the groundwater.

5.2.1 Sediment properties

The various physical and chemical properties including spectroscopic characteristics of the sediment samples investigated are briefly discussed in the following section:

5.2.1.1 pH of sediment

The soils in the study area exhibited acidic pH with values ranging between 4.25 to 5.77 (mean ~ 4.75) shown in Figure 5.8. The pH of the sediment (mean 4.75) in the study areas lie in the region of strongly acid reaction i.e. pH range of 4 to 5 (Tan, 2011). Various factors which could lead to acidification of the soils are microbial oxidation of organic matter which releases carbon dioxide (CO_2) into the groundwater that reacts with water forming carbonic acid (H_2CO_3), thus increasing the acidity, organic acids, respiration of plant roots, hydrolysis of Al, nitrification, oxidation of sulfide, fertilizer etc (Tan, 2011). The CO_2 can react directly or indirectly with minerals and organic matter in the aquifers causing precipitation of secondary carbonates and the solubilization of organic matter (Appelo and Postma, 2005).

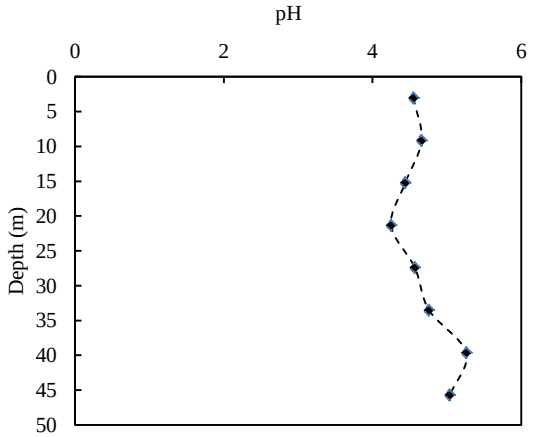

Figure 5.8 Average pH distribution along the depth profile of sediments from Site_1.

5.2.1.2 Loss On Ignition (LOI)

The organic matter content in the aquifer sediment was represented by loss on ignition (LOI). LOI defines the percentage of weight of volatile organic solids at a high temperature (i.e. 550ºC). The organic matter is degraded by micro-organisms, depleting the oxygen in the water, thus creating reducing conditions (Eq. 5.1). The depth profiles of LOI (Figure 5.9) showed heterogeneity along each drilled-core. A significant correlation was observed between the LOI, Specific Surface Area (SSA) and Cation Exchange Capacity (CEC) (Table 5.7).

Table 5.7 Correlation amongst LOI, SSA and CEC for samples obtained from borehole 1A, 1B, 1C, 2E, 2F and 2G.

	LOI	SSA	CEC
LOI	1		
SSA	0.48	1	
CEC	0.58	0.63	1

The organic matter has high affinity for *As* and heavy metal cations because of the presence of ligands or groups that can form chelates with the metals and can also retain heavy metals in exchangeable form (Mulligan et al., 2010). The heavy metal content was found to increase with the increase in the LOI values for most of the sediments; their similar trend was depicted in PCA plots (Figure 5.14b-5.19b, *Section 5.2.2*).

Organic matter presence in the sediment of the study area might play an important role to create anaerobic environments in the shallow aquifers. Thus, the redox potential (Eh), which was found to be mildly reducing to moderately/strongly reducing in the study areas, might have been affected by the presence of organic matter. In the redox process, organic matter (CH_2O) is oxidized to supply the required electrons and the redox-sensitive solutes (NO_3^-, Mn(IV), Fe^{3+} and SO_4^{2-}). The process has been explained in *Section 2.4.2*. The presence of organic matter in the aquifer of *As* contaminated areas has been reported by many researchers globally (Nickson et al., 2000; Ahmed et al., 2004; McArthur et al., 2001, 2004, 2008, 2011; Charlet et al., 2007; Chakraborty et al., 2007; Seddique et al., 2008). The degradation of the organic matter (CH_2O) enhances sequence of redox reactions in the aquifer, and may thereby increase *As* mobilization into the groundwater (Ravencroft et al., 2001; Bhattacharya et al., 2002; Anawar et al., 2003; McArthur et al., 2004).

The higher LOI values also indicates higher water content of sediment. A lower specific gravity of the organic matter can also make the water content higher. In general, the lower the loss on ignition value (LOI), the better the water quality, due to lower leaching of arsenic and heavy metals from sediment (Mulligan et al., 2010). However, from agriculture point of view, a higher content of organic matter is desirable, because of high content of nutrients and water retention capacity of the sediment (Mulligan et al., 2010).

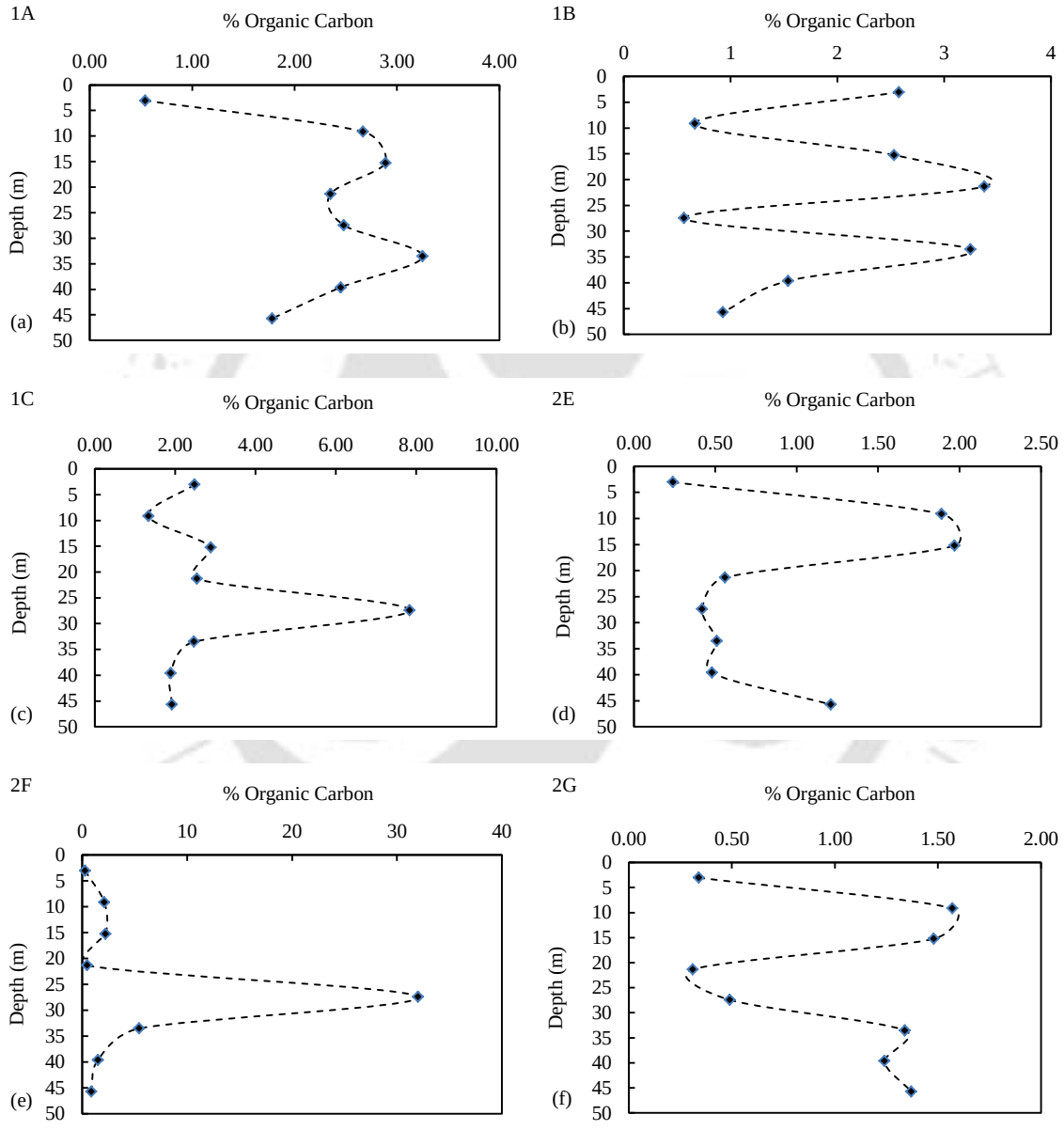

Figure 5.9 Organic carbon content (LOI) of the sediment samples from (a) 1A (b) 1B (c) 1C (d) 2E (e) 2F (f) 2G sampling locations.

5.2.1.3 Cation Exchange Capacity (CEC)

Cation exchange in sediments refers to the exchange of positively charged ions associated with the clay particle surfaces. The process is stoichiometric, and electroneutrality at the clay particle surfaces must be satisfied. The values of CEC along the depth were plotted (Figure 5.10), which showed cation exchange capacity ranging between 0.5 meq/100g to 12.15 meq/100g (mean ~ 4.18 meq/100g). The depth profile of CEC showed a high variability within the soils.

The CEC of a soil depends upon its organic matter content and types of clay presents. In general, the higher the CEC the greater is the ability to retain heavy metals (Appelo and Postma, 2005; Walther, 2010; Mulligan et al., 2010). The type and quantity of clay determines the CEC, which increases with clay content, particularly when it contains a high proportion of 2:1 lattice-type minerals (e.g. montmorillonite) (Appelo and Postma, 2005). A good correlation was observed among the CEC, organic carbon (LOI) and specific surface area (SSA) as shown in Table 5.7.

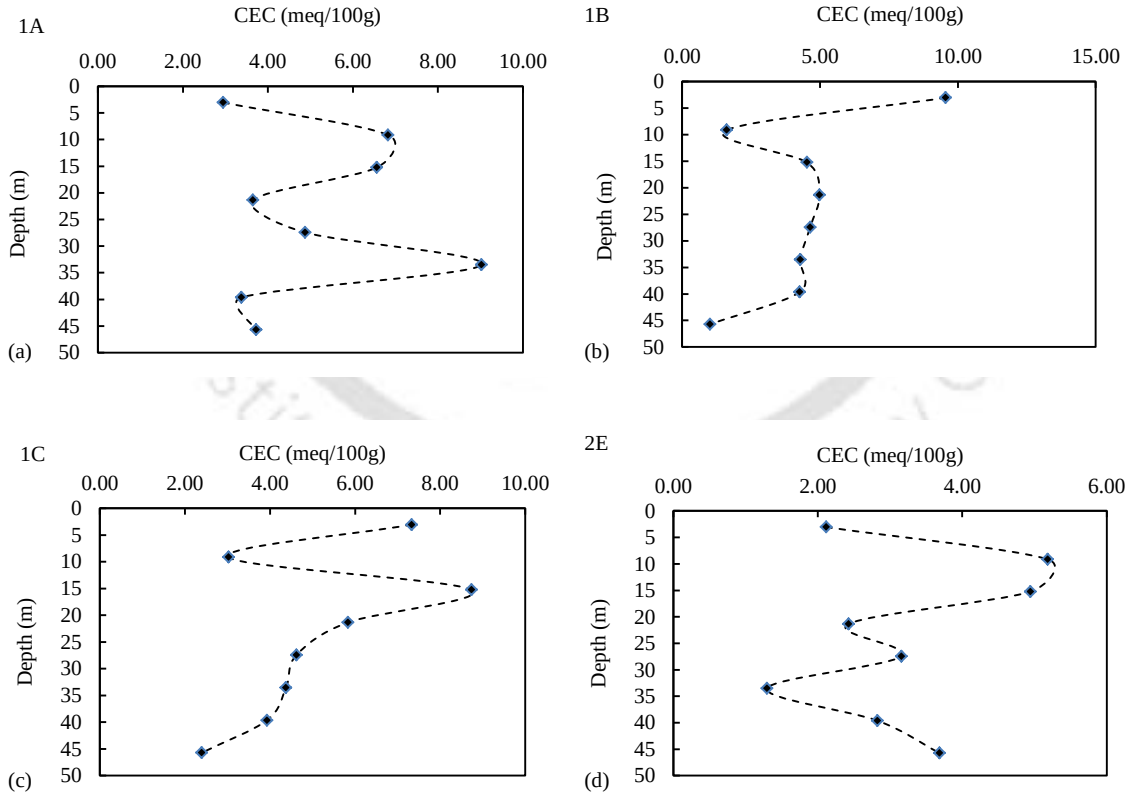

Figure 5.10 Cation Exchange Capacity (CEC) of the sediment samples from (a) 1A (b) 1B (c) 1C (d) 2E sampling locations.

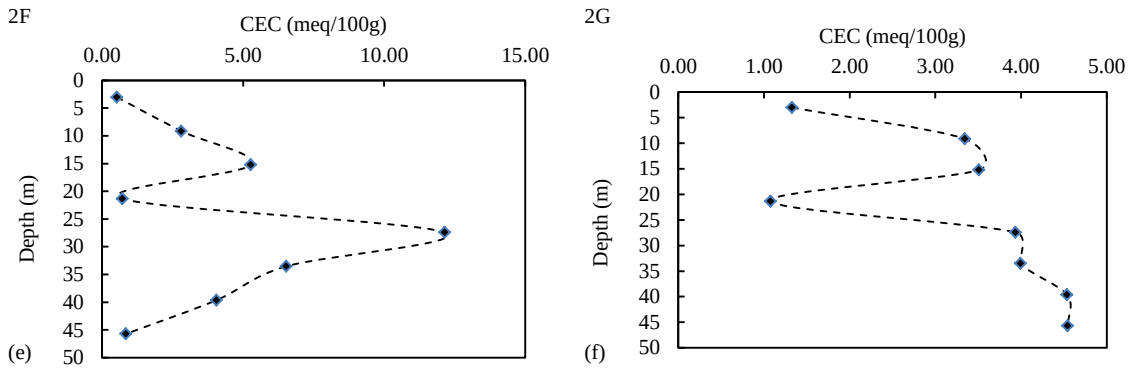

Figure 5.10 Cation Exchange Capacity (CEC) of the sediment samples from (e) 2F (f) 2G sampling locations.

5.2.1.4 X-Ray Diffraction (XRD)

The bulk mineralogy of the sediments was determined at Centre for Instrumentation Facility (CIF), IIT Guwahati, using X-ray powder diffraction (MAC Science XXP 18) with Cu Kα radiation and a position-sensitive detector. The mineralogy of the soil samples were identified by comparing with powder diffraction files (pdf) of Joint Committee on Powder Diffraction Standard (JCPDS) card numbers (9-466) Albite; (25-0155) Mica; (33-1161) Quartz; (13-192) Illite; (06-046) Gypsum; (78-0751) Halite; (33-0311) $CaSO_4$; (47-1743) Calcite; (9-478). The diffractograms obtained from XRD (Figure 5.11a-c) showed the abundance of quartz (SiO_2) for all the soil sediment samples analyzed. The XRD results indicate similarity in the nature of the diffactograms for most of the sediment samples. Presence of mica ($K_2(Fe^{2+}, Mg^{2+})_6(Si_6Al_2)O_{20}(OH)_4$), feldspar ($Na_{0.78}CaO_{0.22}Al_{1.22}Si_{2.78}O_8$), calcite ($CaCO_3$), gypsum ($CaSO_4$), illite $(K,H_3O)(Al,Mg,Fe)_2(Si,Al)_4O_{10}[(OH)_2,(H_2O)]$, halite (NaCl), feldspar ($(Na/Ca/K)Al(Al,Si)_3O_8$) were also found.

Although high heterogeneity was noticed among the sediment samples for its size fractions (SSA) as shown in Figure 5.13 and colors such as brown, grey, dark grey or black and Ash-greenish, no significant variations were found in their mineralogical compositions as shown (Figure 5.11a-c). Currently, not much information is available on the mineralogy of Fe-oxides in the Holocene aquifer sediments to which *As* is supposed to be sorbed (Akai et al., 2004; Polizzotto et al., 2006; Rowland et al., 2008; Postma et al., 2010).

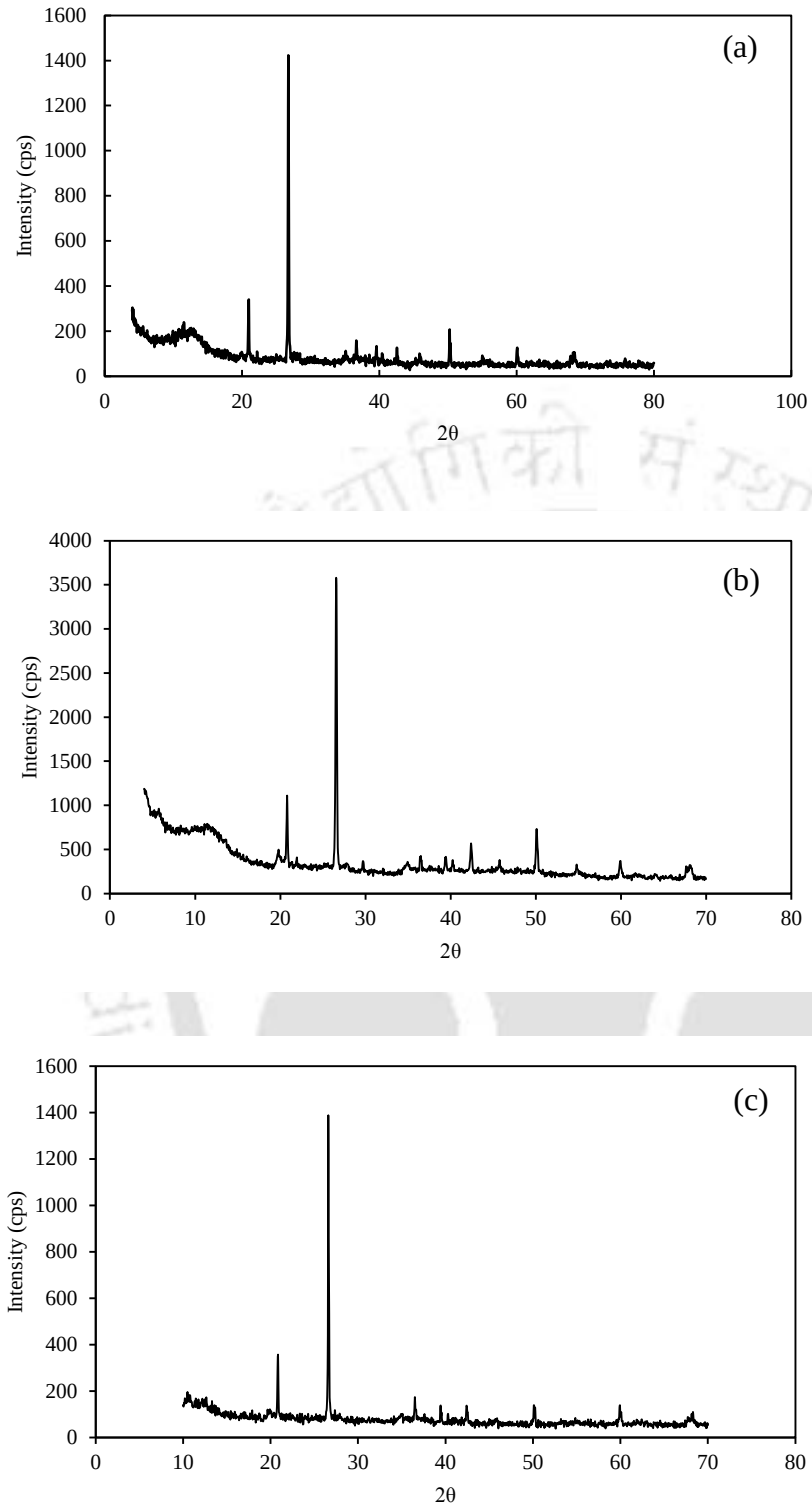

Figure 5.11 X-Ray Diffraction (XRD) of sediment samples (a) 1C_50 (b) 1C_70 (c) 1C_150.

5.2.1.5 Scanning Electron Microscopy (SEM) and Energy Dispersive X-Ray (EDX)

The characterization and observation of elemental composition of sediment samples was conducted with Scanning Electron Microscopy (SEM) and Energy Dispersive X-Ray (EDX) as shown (Figure 5.12a-c). The presence of *As* peaks in the EDX spectra suggested mode of presence as adsorbed and/or co-precipitated. The EDX showed that Fe rich coatings are ubiquitous on mineral constituents such as quartz and aluminosilicate phases in all fractions. Mn was also found to be present in some of the samples suggesting the presence of ferromanganese deposits. It is clear that the solid phase *As* in the bulk sediment is associated with Fe-oxide and Mn-oxide coatings, quartz and aluminosilicates.

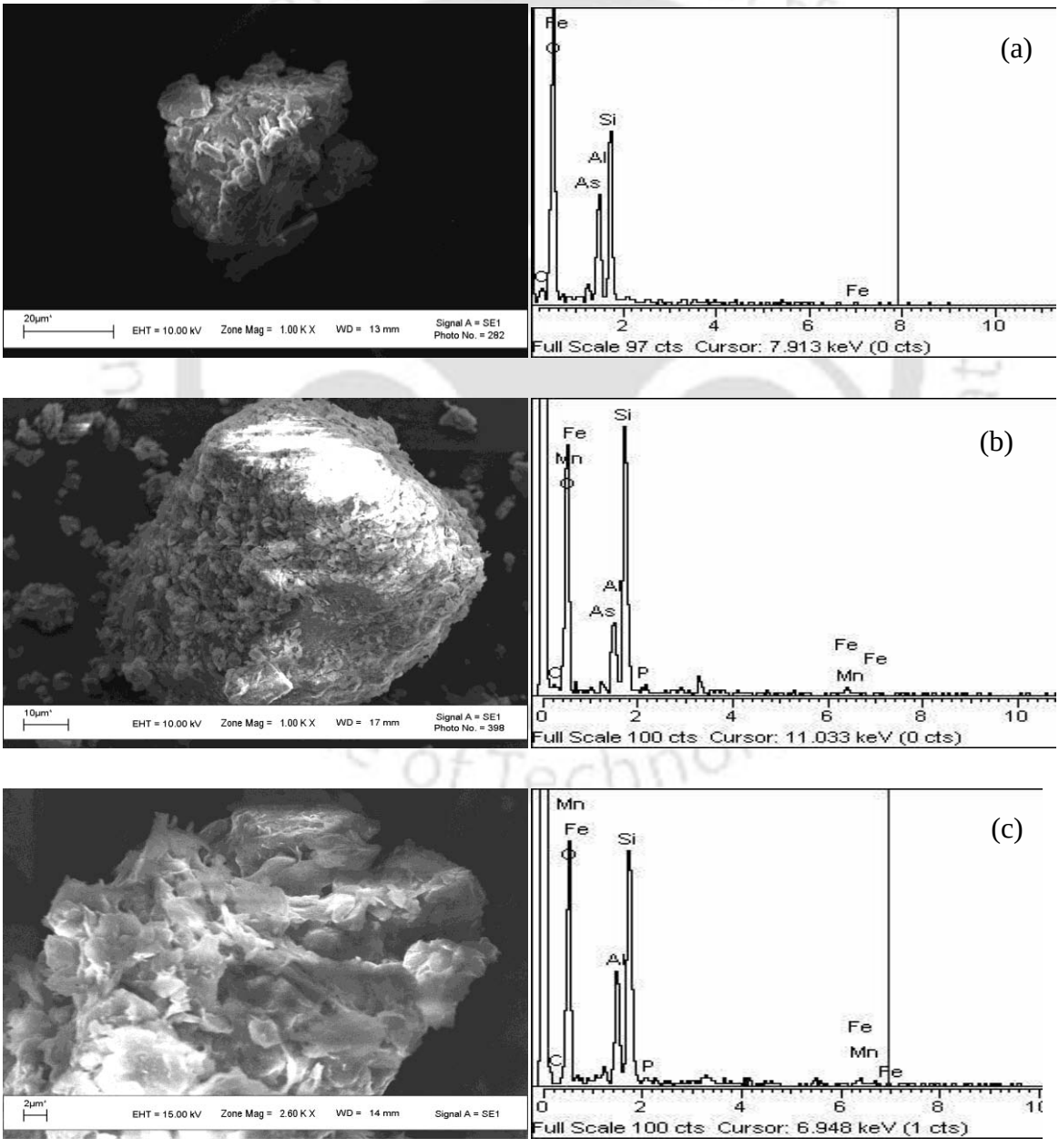

Figure 5.12 (c) SEM and EDX of soil sediment samples (a) C_50 (b) C_70 (c) 1C_150.

5.2.1.6 Specific Surface Area (SSA)

SSA is the total surface area of the solids or particles per unit volume/weight. The determination of SSA was made using Malvern Mastersizer 2000 (*Section 4.3.4*). BET surface area or gas absorption are mainly used for the determination of the amount of gas or liquid (adsorbate) that forms monolayer coating on the surface of the particles in order to evaluate SSA. The current method was used due to non availability of a BET analyzer. In soils, where the particles are porous and have rough surface structure, the BET will be greater than that calculated by laser diffraction (Malvern Mastersizer 2000 Manual). It is clear from Eq.4.3 that as the particle size distribution is more dominated by finer fractions, the specific surface area will increase.

The depth distribution of SSA (Figure 5.13) for all the sediment core drills showed high heterogeneity of the aquifer systems in the study area. A significant positive correlation (Table 5.7) between SSA, LOI and CEC suggested that the fine-grained sediment contained higher amount of trace elements, likely due to their high surface area and corresponding high adsorption capacity (Anawar et al., 2003; Charlet et al., 2007; Chakraborty et al., 2007; Seddique et al., 2008; Reza et al., 2010b). Usually higher SSA are also enriched in phyllosilicates (such as mica) that contain higher amount of P_2O_5, indicating higher concentration of phosphate (Reza et al., 2010b). The fine-grained sediments contained more trace elements because it contained proportionally more feldspar, heavy minerals, clay minerals and authigenic minerals than the coarse-grained sediments, which were dominated by quartz.

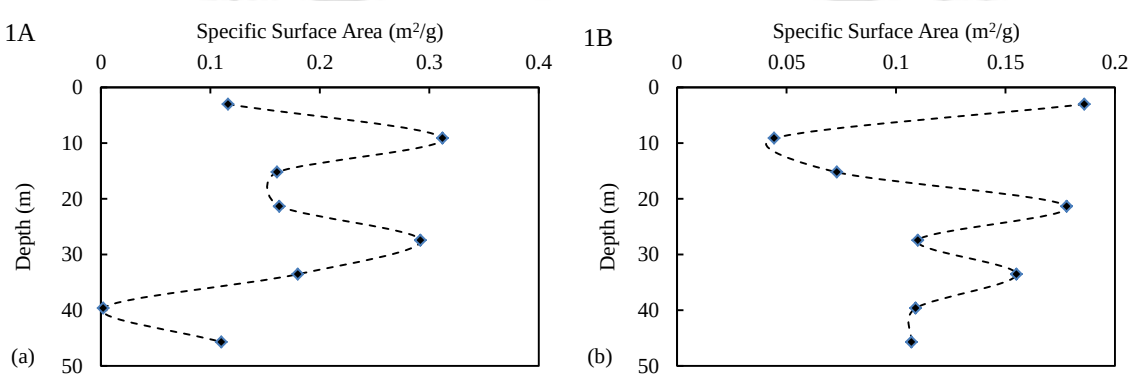

Figure 5.13 Specific Surface Area (SSA) distributions along the depth profile for sediment samples at (a) 1A (b) 1B sampling locations.

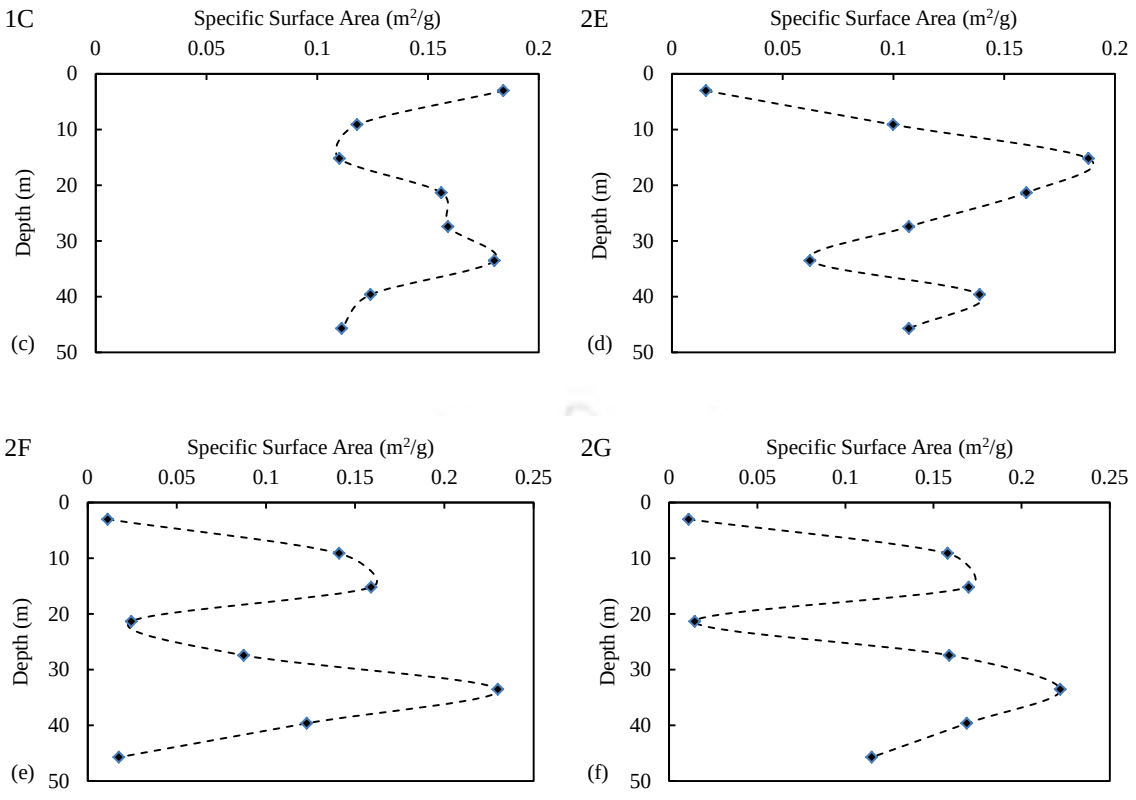

Figure 5.13 Specific Surface Area (SSA) distributions along the depth profile for sediment samples at (c) 1C (d) 2E (e) 2F (f) 2G sampling locations.

The analysis of the sediment samples for its physical, chemical, morphological characteristics suggested high heterogeneity in the samples. The mineralogical composition of the sediments was dominated by quartz and presence of mica, feldspar, illite, gypsum, calcite was observed. The presence of *As* peaks in the EDX spectra suggested mode of presence as adsorbed and/or co-precipitated. The fine grained soil contained higher amount of organic carbon and capacity to adsorbed *As* increases with increase in surface area as well as adsorption capacity.

5.2.2 Total metal concentration

Total metal concentrations (mg/kg) of *As*, Fe and Mn have been shown in Figure 5.14-5.19 along the depth profiles for boreholes 1A, 1B, 1C which surround the target tubewell-1 and 2E, 2F, 2G surrounding the target tubewell-2 (Figure 4.1). The concentration of other metals analyzed in the sediment core viz. Cu, Zn, Cd, Cr, Mg, Na, Ca and K were shown in the Appendix – A4. High variation of concentration ranges were noticed among the sediment core samples from the drilling sites. This shows the higher variability of the alluvial sediment

deposits along with different chemical properties along the horizontal as well as depth profiles.

The composition of sediments derived through total metal digestion using EPA-3052 method is shown in Table 5.8. For comparison, the typical values present in unpolluted soils (Alloway, 1995) are also shown in Table 5.8. Cadmium (Cd) has lowest value of average (mean ~ 8 mg/kg) as well as range (4 mg/kg to 12 mg/kg) showing the lowest deposition as well as mobilization in the sediment materials. The sediment bound *As* concentrations in the contaminated sites range from 6.5 to 45 mg/kg with mean 14.5 mg/kg and median 13.05 mg/kg, which is not unusually high when comparing with normal range in natural soil (0.1 to 40 mg/kg) as well as critical soil total concentration (20 to 50 mg/kg) in soil (Alloway, 1995). The concentration of other heavy metals viz. Mn, Cr, Cu in the soil well within the normal range specified. But the concentration of Cd was found to be higher than the normal range (0.01-2 mg/kg) and fall within the critical soil total concentration (3-8 mg/kg) (Alloway, 1995). The major ions analyzed were dominated by Fe, Ca and K.

Table 5.8 Total metal concentrations in the sediment (mg/kg).

	Max	Min	Mean	Median	Std Dev	Normal range
As	45	6.5	14.5	13.05	6.5	0.1 - 40
Mn	1562	42	405	249	364	20 - 10000
Fe	65600	3602	21705	20864	13105	
Cu	86	1.1	32	26	21	2 - 250
Zn	94	14	39	31.5	21	1 - 900
Cd	12	4	8	8	1.84	0.01 – 2.0
Cr	78	12	37	34	18	2 - 250
Na	11460	2400	6303	6460	1857	
Ca	24200	6074	12119	10643	4623	
K	120600	7660	16854	14201	15892	
Mg	660	10	210	172	137	

The results of total metal concentrations were processed by principal component analysis (PCA). PCA was performed in order to obtain a visual representation of the data set and gain insight into the distribution of the heavy metals by detecting similarities or differences which would be difficult to identify only by looking at the tables. Principal component analysis (PCA) with varimax raw factor loading's rotation was applied using SPSS (1998). The first

two principal components PC1 and PC2 which explain the largest variance in the datasets were used.

The total concentration of *As*, Fe and Mn in the sediments from Site_1 depicted high variability along the horizontal as well as depth profiles. The total metal concentration data for *As*, Fe and Mn at the sediment core 1A was plotted with depth (Figure 5.14a,b,c). At 1A location, the near surface sample at 3 m and 9 m depth had a higher *As* concentration (approx 19.2 mg/kg). A reduction in *As* concentration (10.5 mg/kg) was found at about 15 m due to reduced soil with dark grey color having lower Fe and Mn. At depth 21 m, the *As* concentration increases to about 18.5 mg/kg. Since the sediment at this depth is sandy with smaller specific surface area (SSA), the Fe and Mn concentrations remain lower, but *As* can be strongly adsorbed on the surface of Fe-amorphous and Fe-crystalline oxide. At a depth of 27 m, the concentrations of *As* reduces to 16.5 mg/kg, while the concentration of Fe and Mn increases, which may oxidized *As*(III) to *As*(V) leading to adsorption onto the surface of Fe-oxides. At a depth of approx. 40 m, a coarse sand horizon was encountered, and the *As*, Fe, Mn and other metals analyzed reduced to lower values.

The sediment concentration profiles of 1A core showed that *As* has good correlation with Fe, Mn and other heavy metals as could be seen from the PCA plot (Figure 5.14d). The variance explained by the first two principal components is 73% of the total variance, where a first principal component (PC1) is 55% and the second principal component (PC2) accounts to 18%. The PCA plot suggested that *As* have good correlation with K, Cr and Cd. High correlation was exhibited among Fe, Mn, Ca, Cu and Zn.

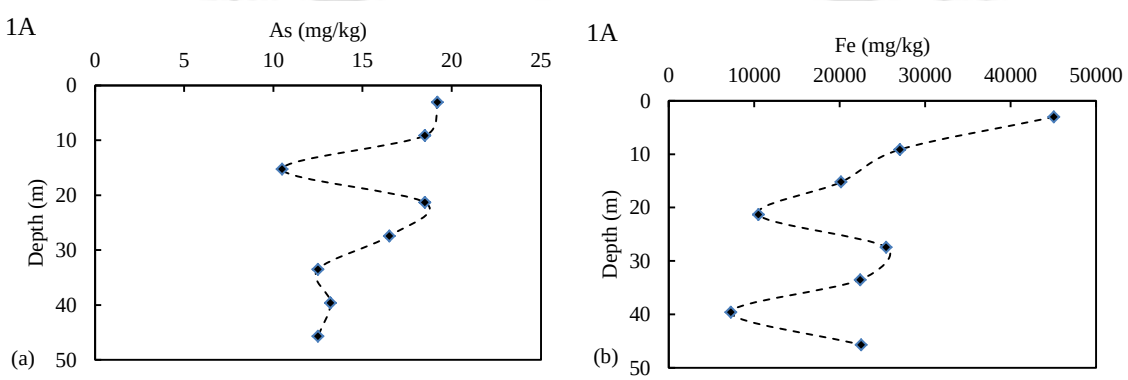

Figure 5.14 Depth wise distribution of (a) total *As*, (b) total Fe of the sediment core samples at location 1A.

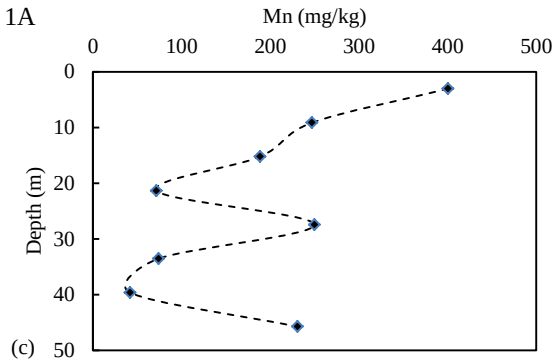

Figure 5.14 (c) Depth wise distribution of total Mn of the sediment core samples at location 1A.

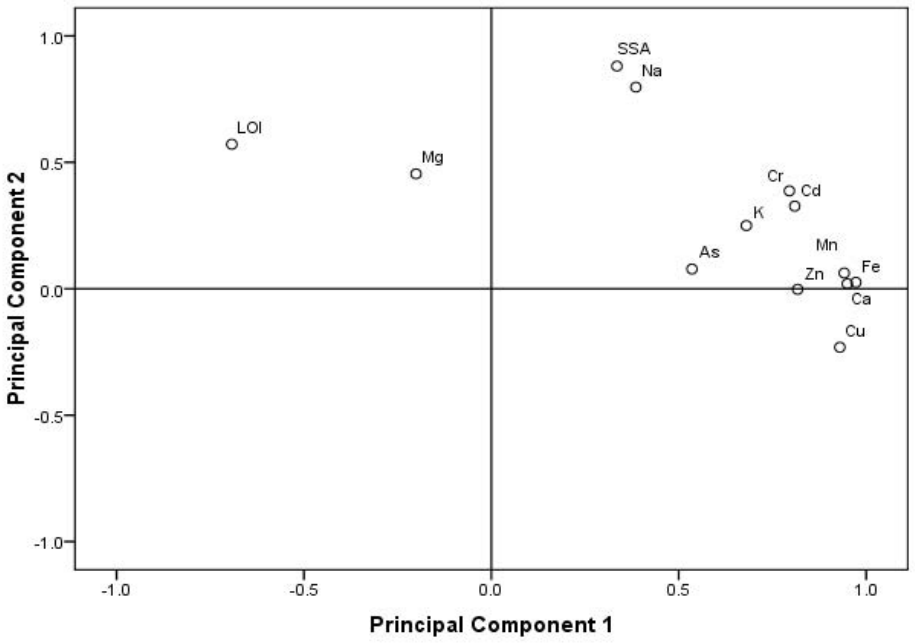

Figure 5.14(d) PCA plot of total metal concentrations for sediment core samples at location 1A.

At drilling site 1B, *As* concentration was found to be highest at near surface i.e. 3 m and 9 m and it gets lesser along the depths as shown (Figure 5.15a). The highest *As* concentration of 20.4 mg/kg was found in the clay layer near surface. The distribution of organic carbon and surface area of the sediment showed a similar trend in the depth profile. The PCA plot (Figure 5.15d) showing relationship of various metals explains total variance of 76%, where PC1 amounted to 54% and PC2 amounted to 22% of the total variance. The PCA plot (Figure 5.15d) for 1B suggested that surface area (SSA) and organic carbon were highly correlated. Iron (Fe) exhibited good correlation with most of the other metal ions viz. Ca, Zn, Cr, Mn and K. Arsenic was found to be correlated with Mn and K in the drillcore 1B.

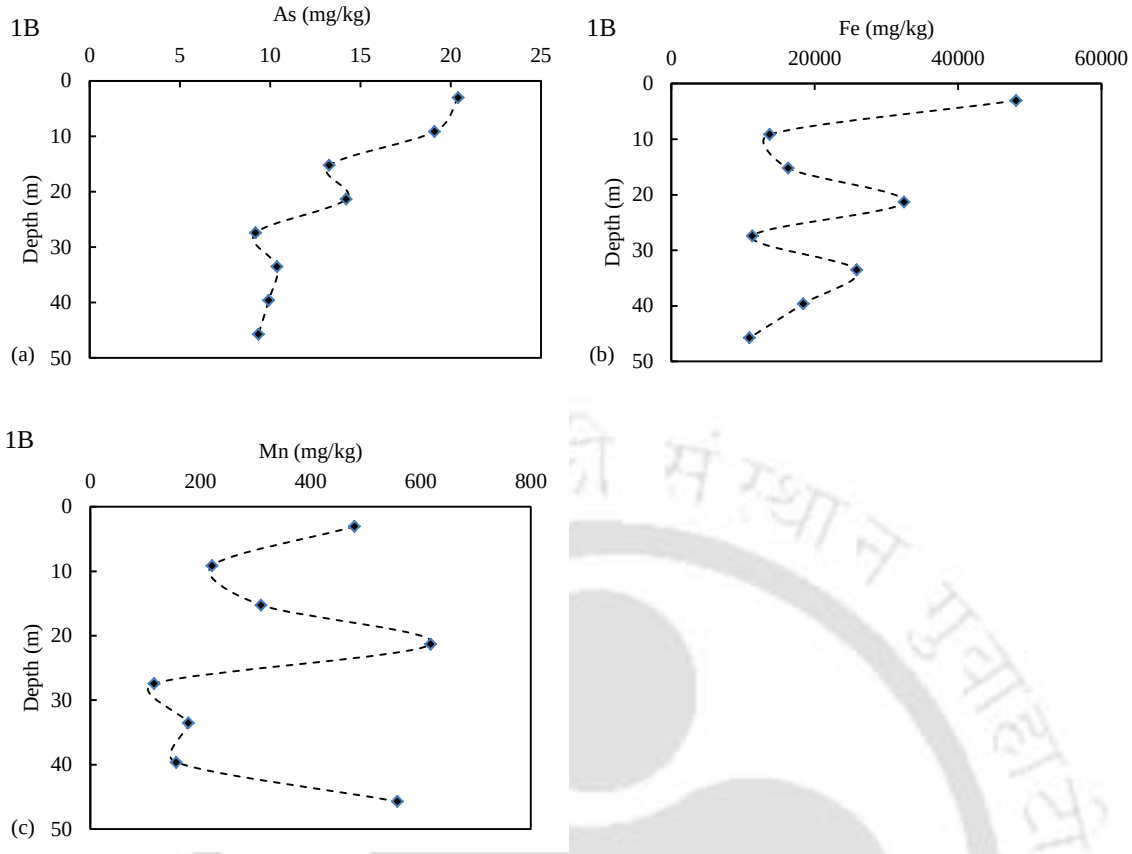

Figure 5.15 Depth wise distribution of (a) total *As*, (b) total Fe (c) total Mn of the sediment core samples at location 1B.

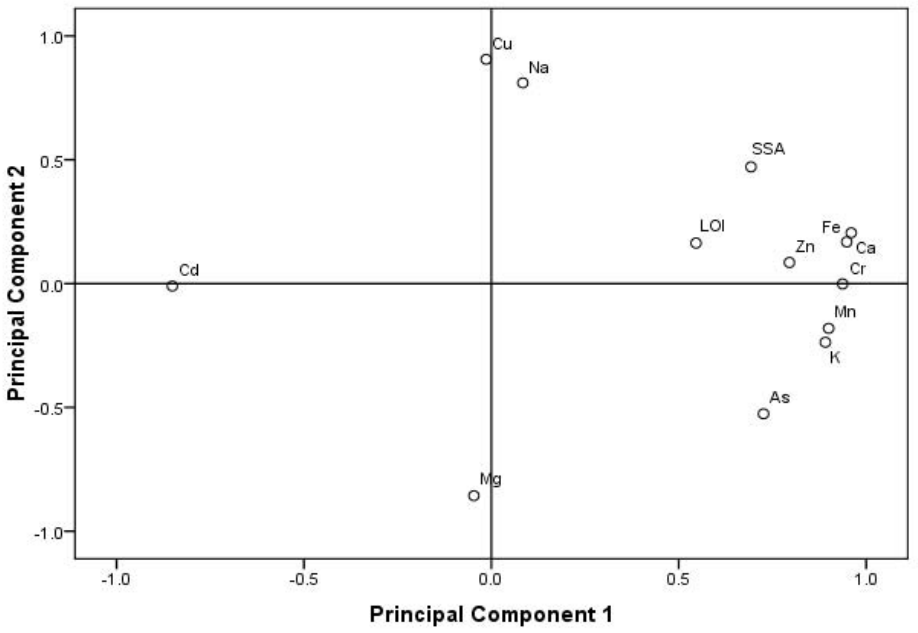

Figure 5.15 (d) PCA plot of total metal concentrations for sediment core samples at location 1B.

Sediment core samples from 1C in Figure 5.16a indicates *As* concentration in the sediments along the depth profile. The distribution of *As* and Fe followed similar pattern along the depths (Figure 5.16a,b). The range of *As* concentration was high (9 mg/kg to 33 mg/kg). The near surface sediments had relatively lower *As* (approx 12 mg/kg), but an abrupt increase in the sediment bound *As* was observed at 21 m. This depth was characterized by high *As* concentration (33 mg/kg) along with high Fe (54,472 mg/kg) and Mn (1008 mg/kg). Lower to this depth at about 27 m, dark color sediment was encountered which had higher organic carbon content (8%) and surface area (SSA) (Figure 5.13c). The reducing environment in the sediment at depth 27 m was characterized by relatively lower concentration of Fe (13,724 mg/kg) and Mn (148 mg/kg).

The PCA plots of drill core 1C (Figure 5.16d) explain 65% of the total variance, where PC1 accounted to 37% and PC2 accounted to 28% of the total variance. The PCA plots suggested a good correlation existed between LOI and SSA. Arsenic was found to be highly correlated with Fe, Mn and Ca. The distribution of other metals ions viz. K, Cr, Cu, Cd, Zn and Na suggested good correlation existed among them (Figure 5.16d).

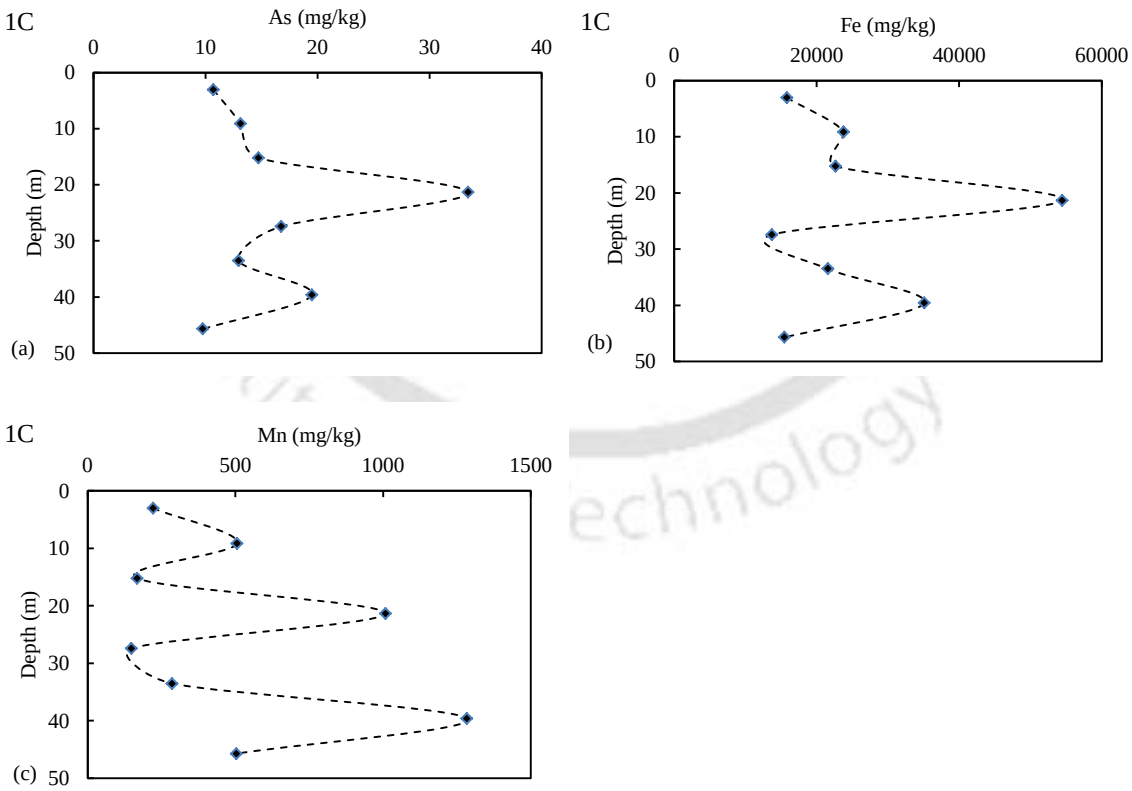

Figure 5.16 Depth wise distribution of (a) total *As*, (b) total Fe, (c) total Mn of the sediment core samples at location 1C.

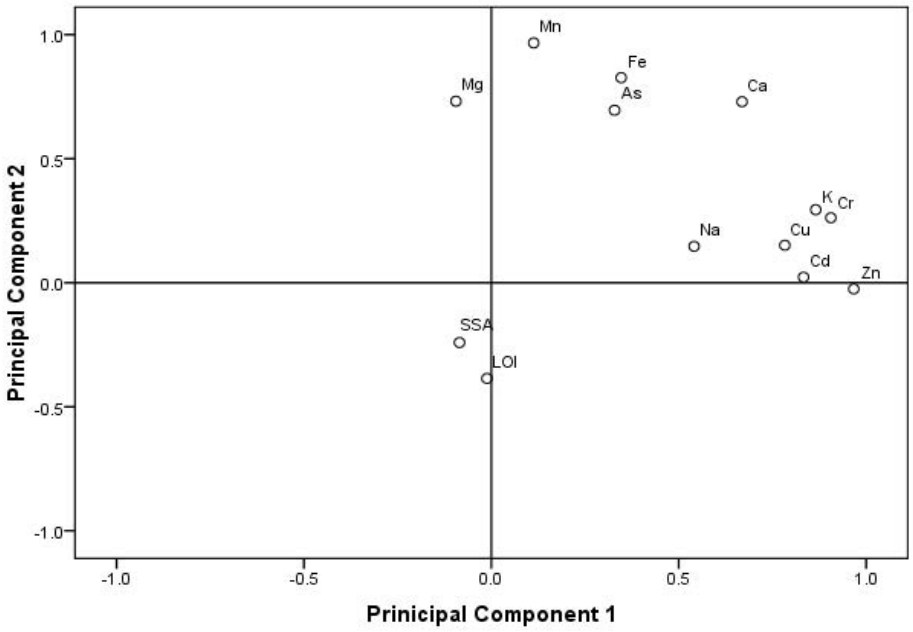

Figure 5.16 (d) PCA plot of total metal concentrations for sediment core samples at location 1C.

The range of *As* concentrations which is bound to sediment in sample 2E varied between 8 mg/kg to 18 mg/kg (Figure 5.17a). The sediment samples near the surface soil had lower *As* (9 mg/kg). This is mark by a band of sandy soil deposits at this depth, where the surface area (SSA) is lowest (Figure 5.13). The highest *As* concentration was at depths of about 15 m and 40 m where the specific surface area (SSA) of the sediment samples were also maximum (Figure 5.13). The depth distribution patterns for Fe, organic C, Ca, Cu, K and Zn followed a similar trend.

The PCA plots (Figure 5.17d) explained a total variance of 80% for the first two principal components viz. PC1 is 41% and PC2 is 39%. The depth profile for sediment samples at 2E using PCA plots (Figure 5.17d) showed that *As* exhibited a good correlation with specific surface area (SSA). Iron (Fe) in the sediment was found to have good correlation with Ca, Cu, LOI and *K*. The distribution of Mn was well correlated with Cr and Cd in drill core 2E.

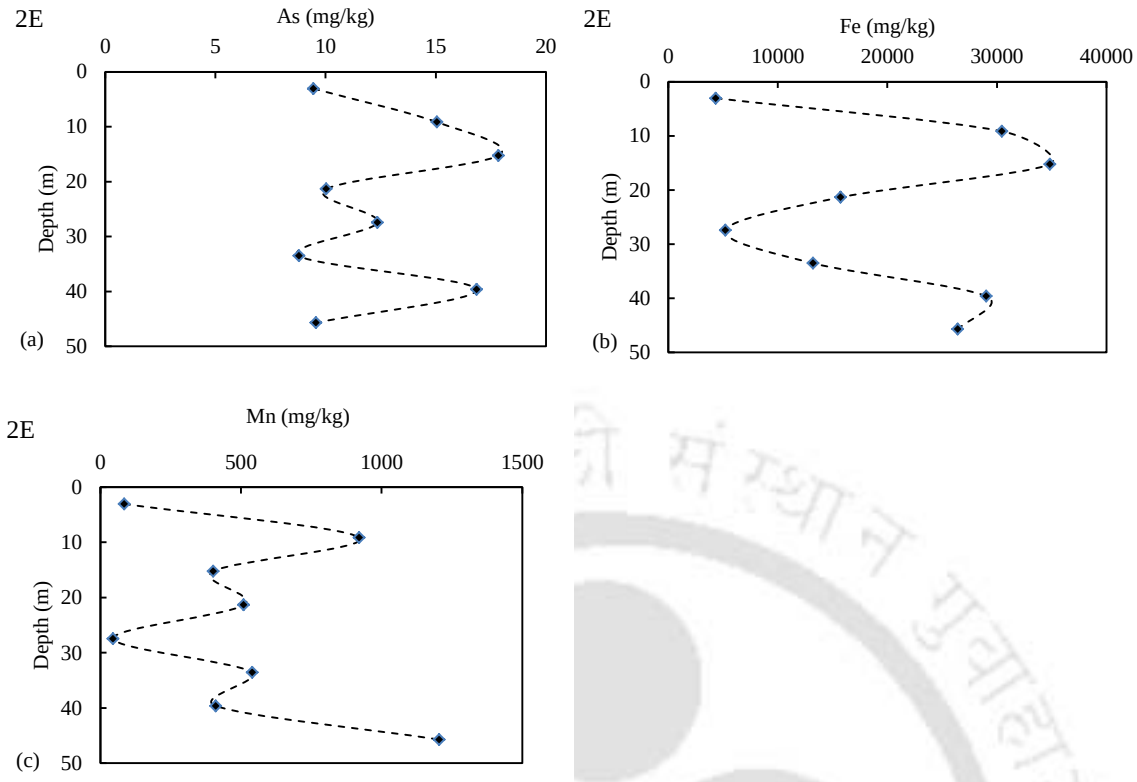

Figure 5.17 Depth wise distribution of (a) total *As*, (b) total Fe, (c) total Mn of the sediment core samples at location 2E.

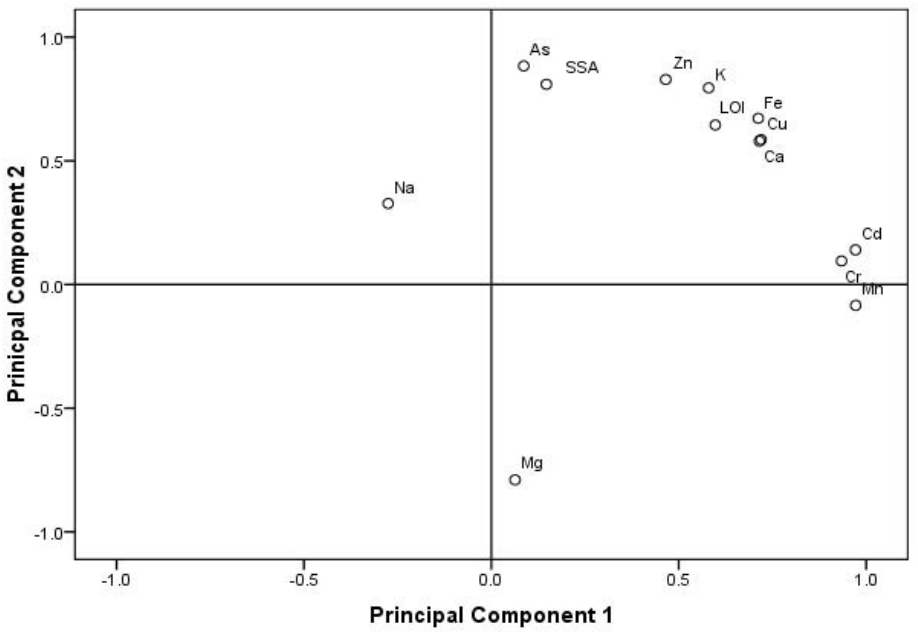

Figure 5.17 (d) PCA plot of total metal concentrations for sediment core samples at location 2E.

The total metal concentration profile for sediment core sample 2F (Figure 5.18a,b,c) depicted high impact from the deposition of a peat layer. The samples from this core had a high range of *As* concentration (6.5 to 45 mg/kg), the highest *As* concentration of 45 mg/kg among all the sediment samples analyzed was found at a depth of 27 m. The associated ions were also found to be maximum i.e. Fe (85,600 mg/kg) and Mn (1,562 mg/kg). At this depth, the organic C was found to be highest of all the sediment samples (31%), as there was a deposition of a peat layer, where the sediment color was black, and plants and tree materials was also found at this deposit.

The PCA plots (Figure 5.18d) explained 81% of the total variance, where variance of 58% was explained by PC1 and 23% by PC2. From PCA plots (Figure 5.18d) exhibited *As* closely related with Cd, Zn and Ca. The distribution of Fe in this drill core has good correlation with surface area (SSA) and LOI. The sediment profile distribution along the depth (Figure 5.18a,b,c) showed a similar trend followed by *As*, Fe and Mn.

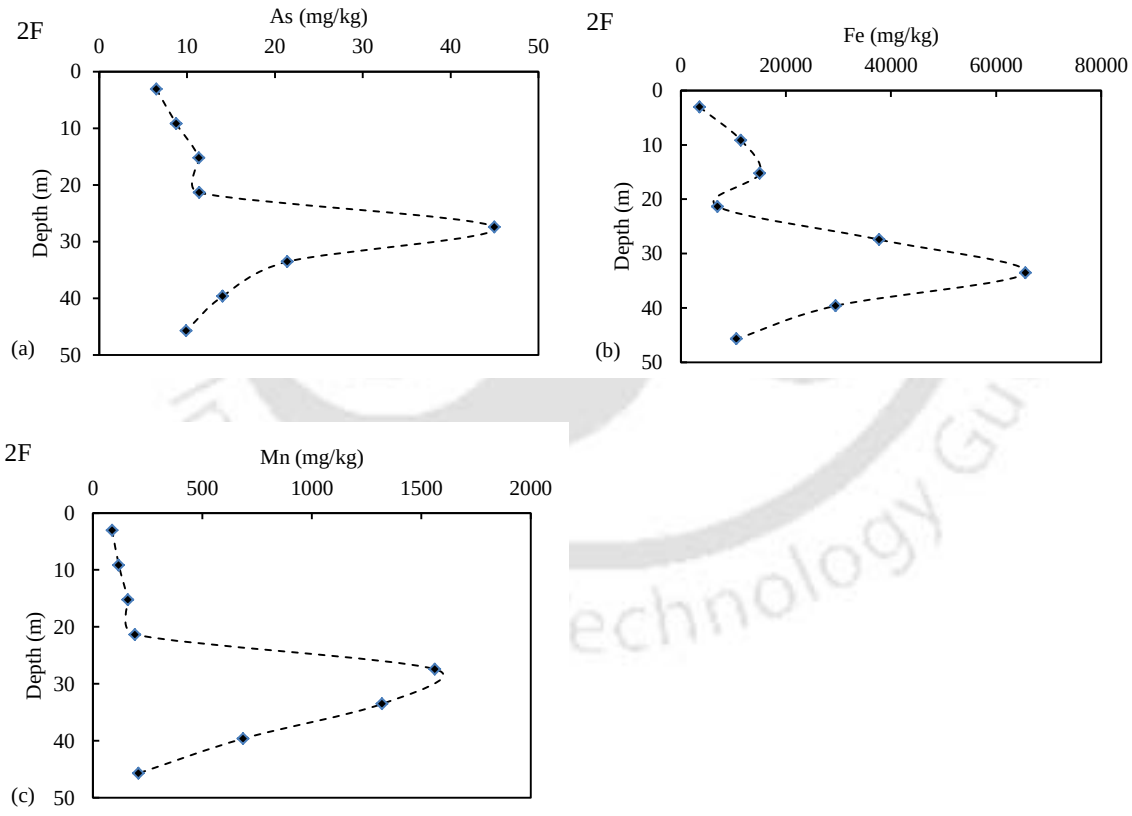

Figure 5.18 Depth wise distribution of (a) total *As*, (b) total Fe, (c) total Mn of the sediment core samples at location 2F.

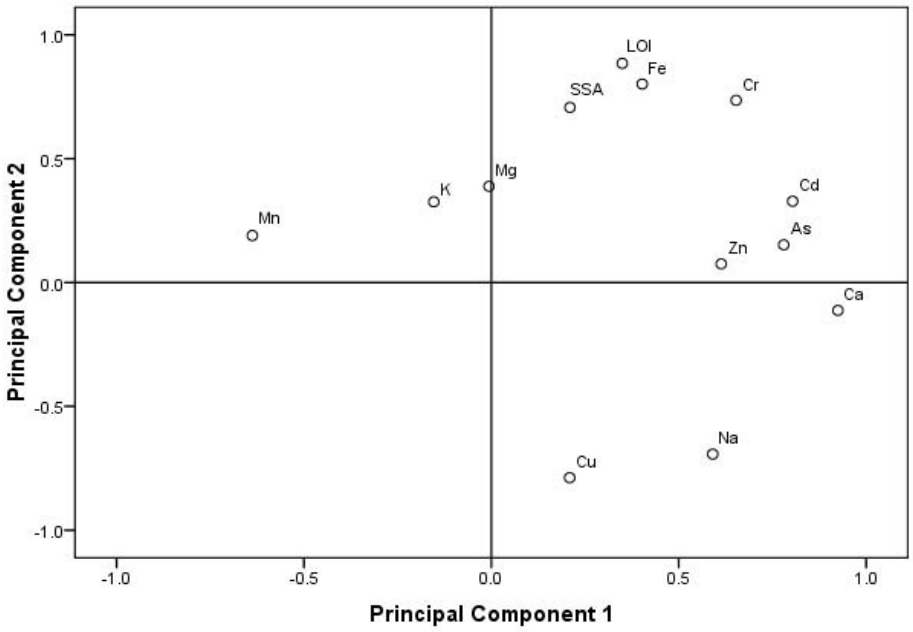

Figure 5.18 (d) PCA plot of total metal concentrations for sediment core samples at location 2F.

The sediment samples from 2G showed variability in the distribution of *As* and other components along the depths of the core (Figure 5.19a,b,c). Sandy layers were found at depths of 3 m and 21 m. The distribution of Fe showed a similar pattern with LOI and surface area (SSA) (Figure 5.9 and 5.16).

The PCA plots (Figure 5.19d) explained 62% of the total variance with the first two principal components viz. PC1 is 32% and PC2 is 30%. The PCA plots (Figure 5.19d) suggested that high correlation existed between *As*, Zn, Cd and Ca. The distribution of Fe, SSA and LOI in the sediment showed good correlation.

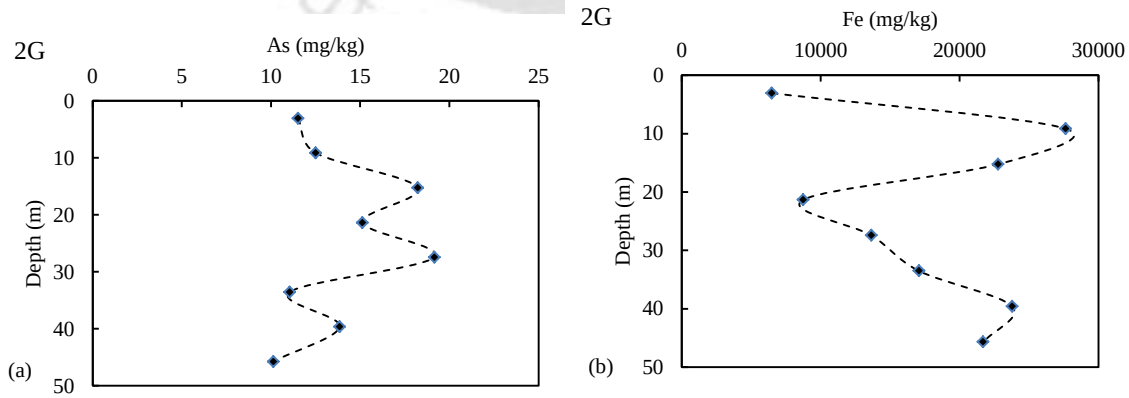

Figure 5.19 Depth wise distribution of (a) total *As*, (b) total Fe of the sediment core samples at location 2G.

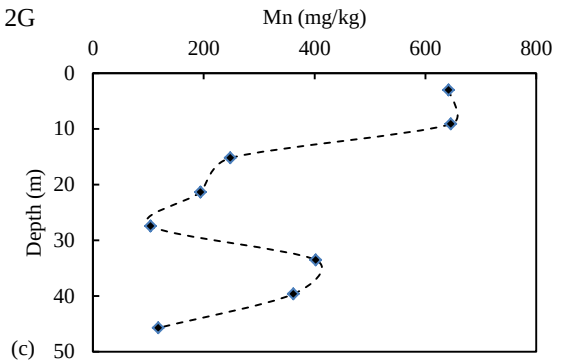

Figure 5.19 (c) Depth profile distribution of total Mn of the sediment core samples at location 2G.

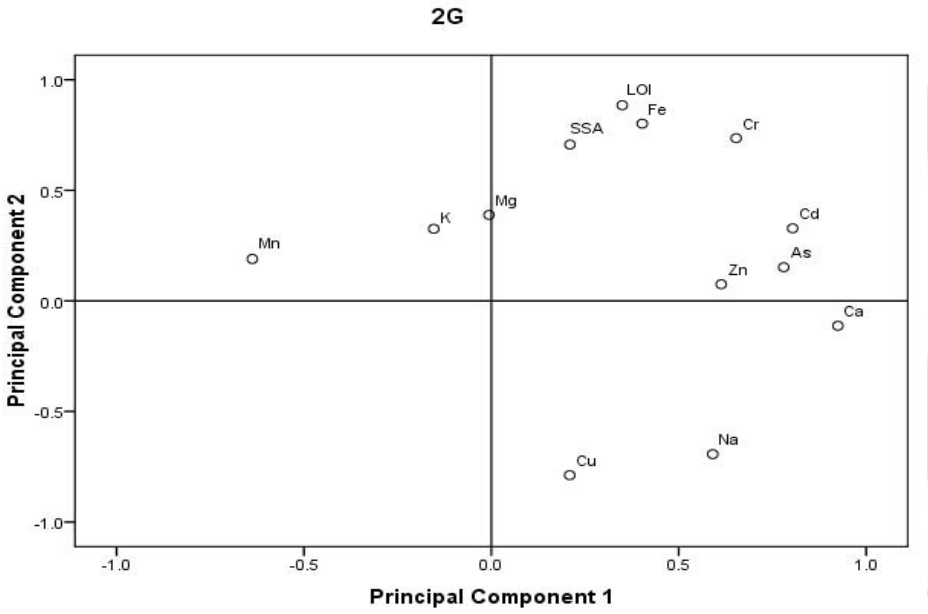

Figure 5.19 (d) PCA plot of total metal concentrations for sediment core samples at location 2G.

5.2.2.1 Quality control and quality assessment

The evaluation of analytical performance in the case of total digestion was made using Certified Reference Materials (CRMs) JLk-1 and JSd-3 of Geological Survey of Japan (GSJ). Table 5.9 shows that the residual percentage of the measured values with the certified values have a good comparability.

Table 5.9. Recovery percent of various elements analyzed for JLk-1 and JSd-3 (CRM).

	Mn (%)	Cu (%)	Zn (%)	Cr (%)	*As* (%)	K (%)
JLk-1	95	90	110.4	90	97.3	91.6
JSd-3	84.3	94	78	108.4	106.5	88.65

As an additional check, the mass balance between the concentrations obtained by total digestion and the sum of steps of sequential extraction Ext_1 to Ext_7 and the residual phase was calculated using Eq. 4.4 (*Section 5.2.3*). The recovery percentage was between 81% and 135% with an average value of 117%, which is generally acceptable. Similar findings of percentage recoveries have been reported (Herrewehge et al., 2003; Biag et al., 2009; Santana et al., 2007; Lopez et al., 2008). Occasional inferior recovery rates compared to the Certified Reference Materials (CRMs) in extraction was attributed to the sub-sample heterogeneity (Herrewehge et al., 2003).

The total metal concentration investigations revealed that the total *As* in the sediment is not unusually high when compared with normal range in natural soil (0.1 to 40 mg/kg) as well as critical total concentration (20 to 50 mg/kg) in soil (Alloway, 1995). The digestion method using EPA-3052 showed good recoveries. The depth profile distribution of the sediments suggested higher heterogeneity along the depth as well as different locations. The nature or trend of the depth profiles for *As*, Fe and Mn exhibited similarities for most of the drill core sediment samples. The complex biogeochemical condition in the subsurface might have driven the *As* dissolution into the groundwater from the sediments. The various fractions of *As* available in the environment was studied in the next section (*Section 5.2.3*) in order to deduce its sources and sinks.

5.2.3 Selective Sequential Extraction Procedure (SSE) of Arsenic

Since the total metal concentrations in the sediments are not necessarily reflective of their bioavailability and mobilization into the groundwater, Selective Sequential Extractions (SSE) were carried out to fractionate the target elements in the solid materials to assess their potential effects (Wang and Mulligan, 2008). The SSE method (Table 4.1) by Postma et al. (2007) was used in the Tokobari village (Site_1). In order to fully comprehend the processes that control dissolved concentration of *As* in the groundwater and its associated key metals i.e. Fe and Mn. These were measured in each of the extraction steps. Six drill core samples

from Tokobari village (Site_1) were analyzed; three sediment samples from Bosagaon village (Site_3), two sediment core samples each from Kachukhat village (Site_2) and Tatigaon village (Site_4) were analyzed.

5.2.3.1 Selective Sequential Extraction (SSE) for Site_1

The studies on SSE for *As*, Fe and Mn are shown in Figure 5.20-5.22 respectively. The results of SSE (Figure.5.20a-f) showed that first step of extraction (Ext_1) using $(NH_4)_2SO_4$, which target non-specifically bound *As*, was in the range of 0.1% to 5% of the total *As* extraction in the samples. The second step (Ext_2) with $(NH_4)H_2PO_4$ targeting specifically bound *As* was significantly high with average of 10% of sum of the total. This suggested that competitive anion exchange with PO_4^{3-} could take place because of smaller size and higher charge density (Wenzel et al., 2001; Berg et al., 2008; Eiche et al., 2008) which is responsible for higher *As* in few tube wells. The high values of Ext_2 range from 2% to 30% could be attributed to the high heterogeneity in the natural soil along with different chemical properties. This extraction steps 3 and 4 (Ext_3 and Ext_4) targets arsenic that are bound to carbonate phases which was very low (< 1%). This shows that carbonate dissolution hardly contributes to *As* leaching in the study area. Therefore, in subsequent SSE procedure for the remaining study sites, these two extraction steps (Ext_3 and Ext_5) were ignored as the main mineralogical composition of the sediment from XRD remained same, although difference in physical and chemical properties of sediment samples were observed (*Section 5.2.1.4*). The oxalate extraction step, which removes adsorbed cations and breaks down Mn-oxides and Fe-oxides, was found to have the highest extraction fraction. The step 5 (Ext_5) extracts *As* from Fe-amorphous hydrous oxide forms a major portion along with step 6 (Ext_6) which targets crystalline Fe-oxide. The Ext_5 contributes to about 16% to 20% of the total *As* extracted and Ext_6 forms about 16% to 28% of the total *As* extracted.

The two sediment core samples of Site_1 (1C and 2F) had a peat layer at about 27 m b.g.l (below ground level), which was characterized by a high organic carbon content of 10% at 1C and 32% at 2F respectively. But these two samples which are at about the same depth (~ 27 m) exhibited different nature i.e. the sample 1C at 27 m depth is low in extractable Fe (3,712 mg/kg), Mn (30 mg/kg) and with total extractable *As* of 18 mg/kg. About 30% of the total *As* extracted accounts to Ext_2 via competitive adsorption with PO_4^{3-}, whereas 25% was extracted from Fe-oxides extraction steps (Ext_5 and Ext_6). The sediment core sample 2F at

similar depth of 27 m was found to have the highest extractable *As* (21.4 mg/kg), Fe (28,727 mg/kg) and Mn (968 mg/kg) concentrations. These two sites (1C and 2F) are located at distance of about 50 m apart. The *As* concentration of the 2F core at 27 m depth was also found to be exceptionally high with a value of 43.4 mg/kg. The Ext_2 step targeting the sorbed *As* accounts to about 5.5% of the totals *As* concentration and Fe-oxides extracting phase (Ext_5 and Ext_6) amounting to about 60% of the total extract for the core 2F.

The residual phase i.e. Ext_7 is the most abundant fraction, which ranges between 30% to 80%. The residual extraction is bound to sulfide and silicate materials in the sediments and cannot be remobilized under normal conditions encountered in the nature (Tessier et al., 1993; Wenzel et al., 2001; Wang and Mulligan, 2008).

The maximum *As* extraction resulted from the Fe-oxides phases for most of the samples in Site_1. A high correlation was observed between the *As* extracted from Fe-oxides phases (Ext_5 and Ext_6) with the amount of Fe extracted from those phases (r^2 0.4 – 0.9). Thus, suggesting that the reductive dissolution of Fe-oxides might be the main process of *As* release into the groundwater and to smaller extent input via competitive sorption with anions. The redox condition responsible for the reductive dissolution in the sediment could be maintained by the organic carbon present in the sediment (*Section 5.2.1.2*).

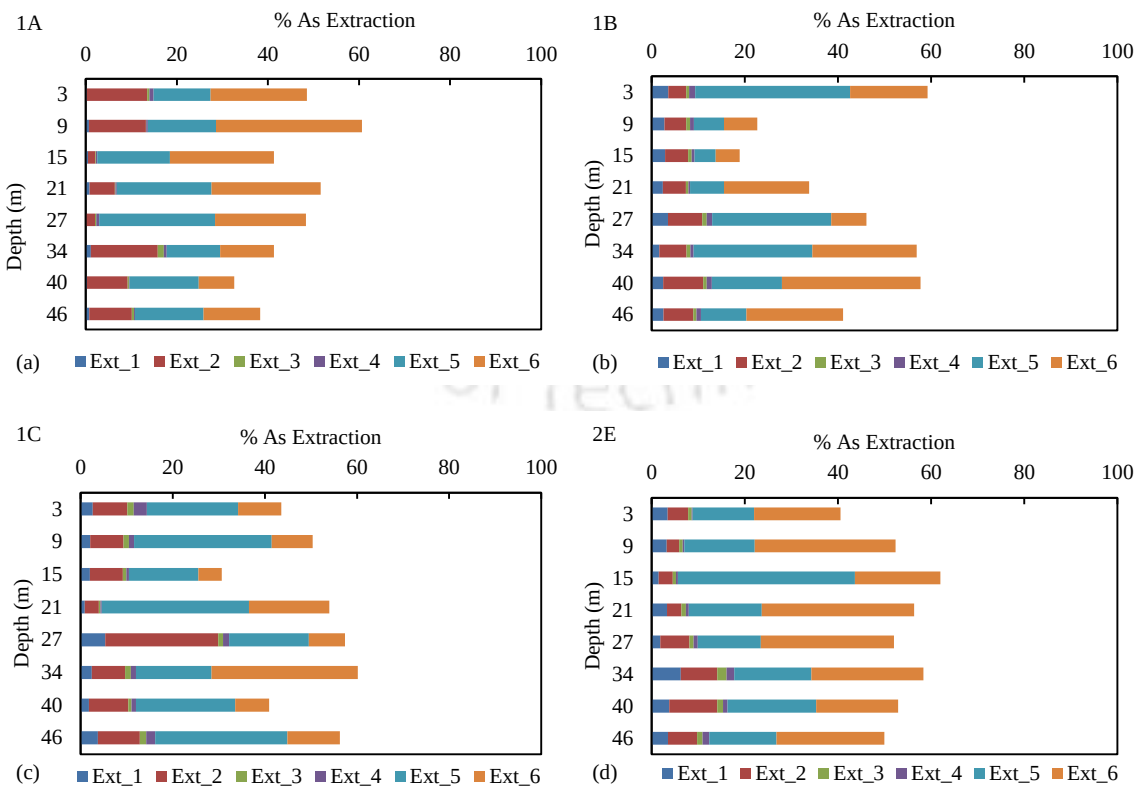

Figure 5.20 *As* extraction through SSE from sediment core samples (a) 1A (b) 1B (c) 1C (d) 2E.

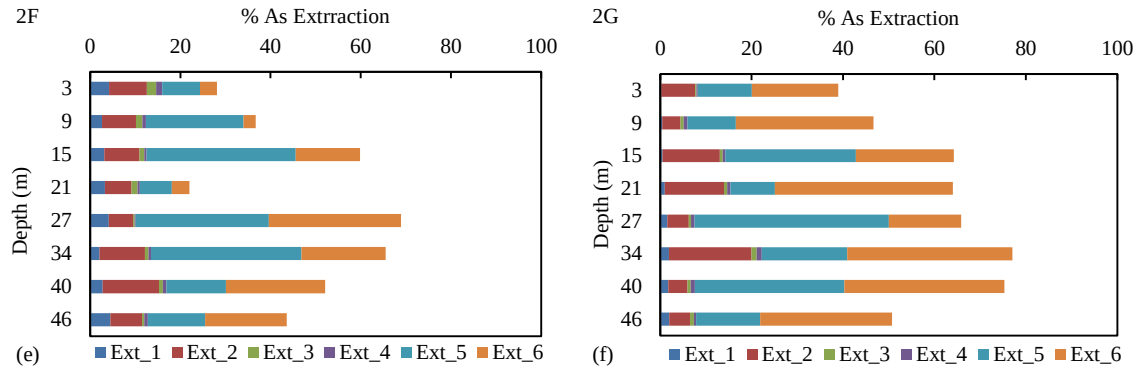

Figure 5.20 *As* extraction through SSE from sediment core samples (e) 2F (f) 2G.

The two steps involving Fe-oxides removal procedure i.e. Ext_5 and Ext_6 recovered, separately, the amorphous or poorly crystalline Fe-oxide and crystalline Fe-oxide fractions. These two steps provided more details on *As* association with different chemical forms of Fe in the soil samples. The Fe-oxides are well known sinks of *As* in the sediments. The dissolution of Fe-oxides in the sediments leads to its increase in the groundwater (*Section 2.4.2*). The results of SSE (Figure.5.21a-f) show that the residual step (Ext_7) contributed to a highest Fe fraction, which is bound to the silicates, sulfides and detrital materials. The heavy metals in this form are not soluble in natural condition and hence may be considered to be held within the mineral matrix (Tessier et al., 1993).

The fractions of Fe for amorphous phase (Ext_5) were highly varying with values ranging from 4% to 59% of the total Fe extracted. The Ext_6 targeting the crystalline Fe also accounted to a highly varying degree with values ranging from 6% to 64% of the sum of Fe extraction. Ext_6 was found to be higher for most of the samples but some anomalies were noticed in sediment samples 1C and 2F, where the fraction of Ext_5 was found to be somewhat higher than Ext_6 (Figure 5.21c,e). Some caution is warranted in the interpretation of extracted Fe in terms of amorphous and crystalline Fe-oxides as even small amount of Fe^{2+}in combination with oxalate will catalyze the dissolution of more crystalline Fe-oxides like goethite and hematite (Suter et al., 1988).

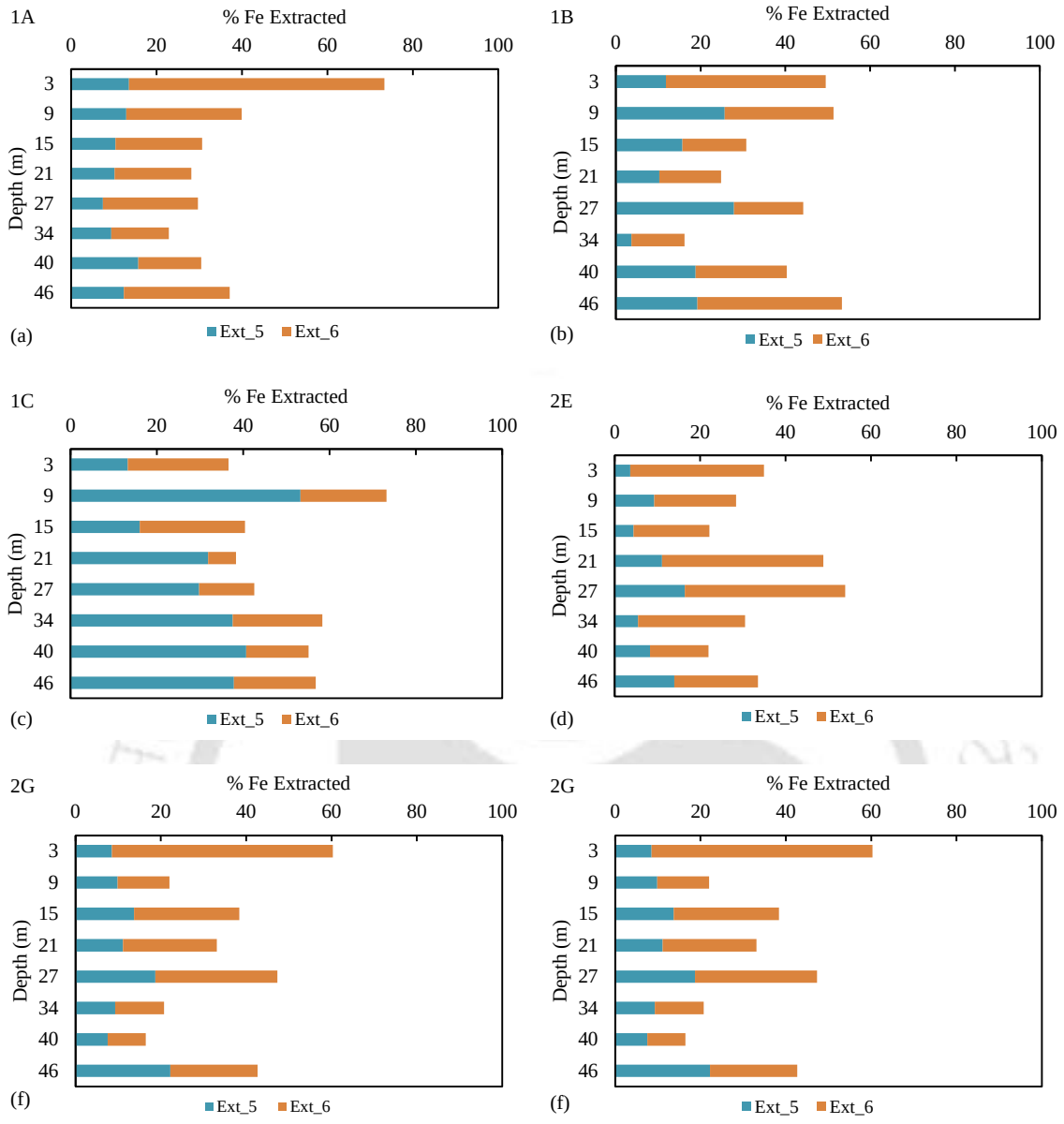

Figure 5.21 Fe extraction through SSE from sediment core samples (a) 1A (b) 1B (c) 1C (d) 2E (e) 2F (f) 2G.

The extraction of Mn (Figure.5.22a-f) suggested that most of the Mn was associated with residual phase (Ext_7) and its distribution was heterogeneous in the sediment. Relatively high concentration of exchangeable manganese in Ext_1 suggested that the metal existed in the reduced form (Tessier et al., 1979). The reduction of Mn was achieved in Ext_1 using $(NH_4)_2SO_4$, and ammonia (NH_4^+) was responsible for the reduction of Mn(III,IV) to Mn^{2+} (Anschutz et al., 2005). Mn^{2+} has higher affinity for surface site and are easily adsorbed on the surface of the fine granules (Amirbahman et al., 2006; Sahabi et al., 2009). Therefore, this might have lead to relatively higher concentration of Mn in the Ext_1.

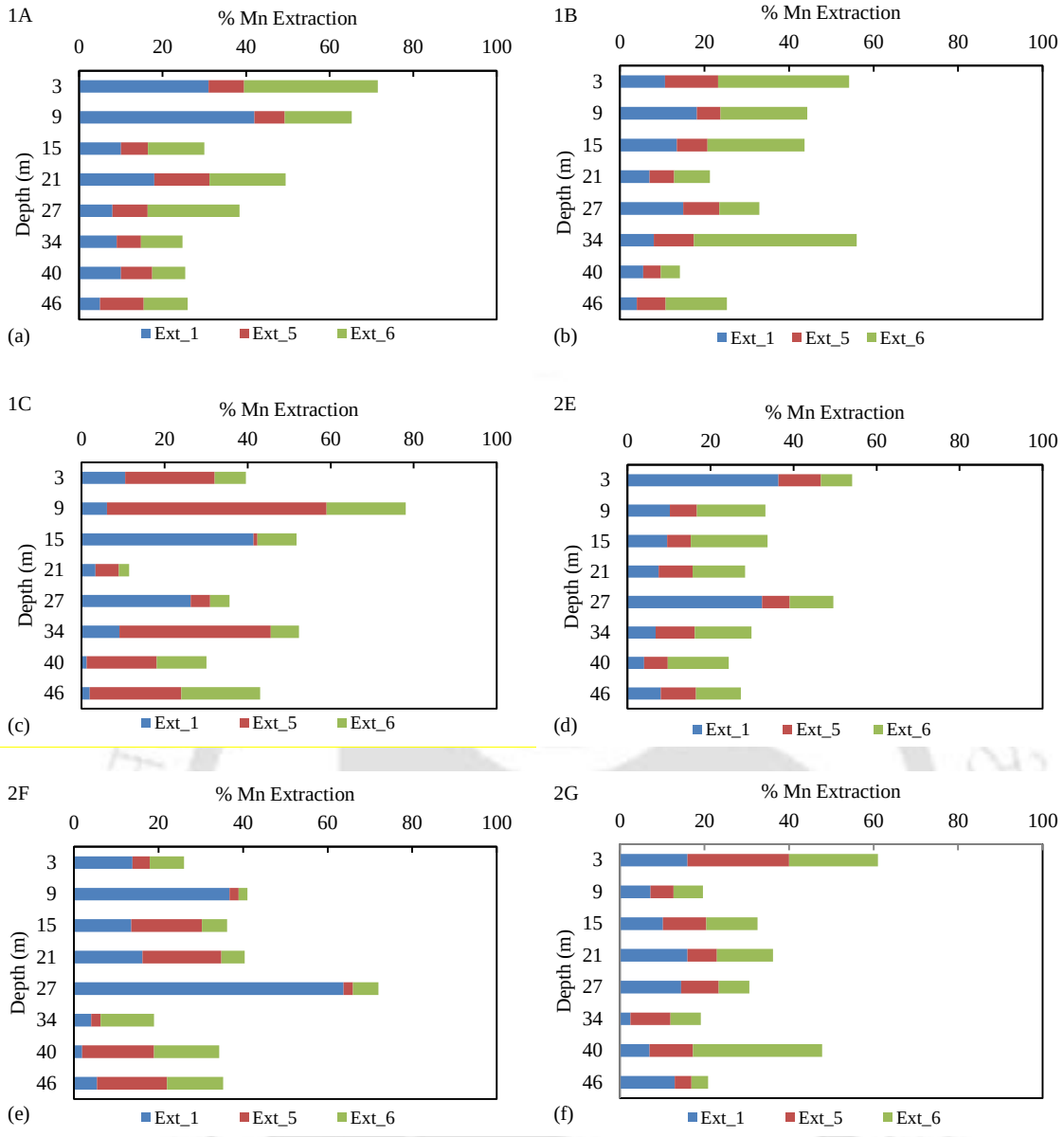

Figure 5.22 Mn extractions through SSE from sediment core samples (a) 1A (b) 1B (c) 1C (d) 2E (e) 2F (f) 2G.

Lower amount of Mn was extracted from Ext_5 which target amorphous phase Fe-oxides. Relatively higher extraction of Mn was observed in Ext_6, which were more crystalline Mn-oxides that would be released if the solid matrix were subjected to more reducing conditions. These oxides (Fe-oxides and Mn-oxides) are well known 'sinks' in the sediment for heavy metals as they can retain substantial amounts of metals and play an important role in controlling the fate of heavy metal mobility in the environment (Silveira et al., 2006; Postma et al., 2007, 2010). These sinks are thermodynamically unstable under highly anoxic circumstances, which may lead to dissolution of the metals into the groundwater. Thus, soil

redox potential can significantly increase dissolved Fe and Mn in the groundwater and plays a major role in the release of *As* into the groundwater.

5.2.3.2 Selective Sequential Extraction (SSE) for Site_2

The sediment core was collected from Site_2 which is located at a distance of about 5 km from Site_1 (Figure 3.1). The groundwater *As* concentration at Site_2 was found to be low (mean 0.03 mg/l) in most of the samples. The results of sequential extraction (SSE) from Site_1 shows that very low amounts of *As* is extracted during the Ext_3 and Ext_4 which targets the carbonates bounds and re-adsorbed from the carbonates, therefore, the sequential extraction scheme proposed by Wenzel et al., (2001) for *As* extraction involving five steps was used. The two SSE steps viz. Ext_3 and Ext_4 account carbonate bound *As* from the sediments were very low (< 1%) from Site_1 and due to similarity of mineralogical composition exhibited via XRD analysis (*Section 5.2.1.4*). Therefore, to optimize the extraction procedure the two steps (Ext_3 and Ext_4) were omitted for the other remaining samples in the study areas (i.e. Site_2 to Site_4). The fractionation steps were renamed as follow:

1. Step_1 - target phase - Non-specifically bound *As* (Ext_1).
2. Step_2 - target phase - Specifically bound *As* (Ext_2).
3. Step_3 - target phase - Fe-Amorphous Hydrous Oxides (Ext_5).
4. Step_4 - target phase - Fe-Crystalline Oxides (Ext_6).
5. Step_5 - target phase - Residual phase of *As* (Ext_7).

Borehole sediment samples (BH6 and BH7) were collected and analyzed from the drilling core at Site_2. The fractionation profiles of *As* (Figure. 5.23a,b) showed that high concentration of *As* was found in the residual fraction (Step_5) which accounts for more than 80% of total *As* extracted. This fraction remains immobile in natural environmental condition. The extraction Step_3 (Fe-amorphous oxides) and Step_4 (Fe-crystalline oxides) form lesser amount in the extractible fraction (< 20%). Similarly, at this site, a high organic carbon content (12% in LOI) layer was encountered at similar depth (approx. 27 m) with that of 1C and 2F of Site_1. The highest extraction of *As* at this depth (approx. 27 m) was with Step_2 (~ 10% for BH6 and ~ 12% for BH7) which targets the specifically bound *As* at the adsorption site. The total *As* in the sediment (Step_1+Step_2+Step_3+Step_4+Step_5) in Site_2 has a mean 18 mg/kg and median 15.15 mg/kg, which is comparable with that of

Site_1. But the sum of extractable fractions (Step_1 to Step_4) accounts only to about 10% to 20% of the total *As* extracted. Therefore, in spite of relatively high *As* in sediment, the environmental available fraction was found to be low. Since most of the *As* are attached to the soil mineralogical structures and silicate materials which is not readily available to the natural environment, it may be the cause of lower arsenic in this area even though lying adjacent to a high arsenic contaminated area.

The extraction of Fe (Figure. 5.24a,b) shows most of the Fe are associated with the residual fraction of Step_5 with values ranging between 55% to 70% of the total Fe in the sediments. The residual phase Fe is bound to mineral structure as stated in the above section. The highest extractible Fe is in the form of Fe-amorphous hydrous oxides i.e. in Step_3 (~ 30%). Lesser amount of Fe-crystalline oxides in Step_4 (~ 7%) were extracted from the total.

For Mn, the highest abundant phase was found to be the residual fraction (Step_5) (Figure.5.25a,b). The exchangeable fraction in Step_1 extracts a low concentration of Mn in most of the samples (< 10%). But high exchangeable fraction (~ 38% and 31%) of Mn (Step_1) was observed in the sediment sample at a depth of 27 m. Since, this sediment is dark in color with high organic content (~ 12% for BH6 and ~ 9.5% for BH7), therefore substantial amount of Mn might be present in reduced form, which is easily extracted by Step_1. For a sample at depth of 27 m similar trend of high Mn extraction with Step_1 was observed at Site_1 (*Section 5.2.3.1*). The highest extraction of Mn was observed in Step_3 (values ranging between 8% to 40%) which target the amorphous phases of Fe-oxides, which suggested that the Mn in the sediment might be bound or sorbed onto amorphous Fe-oxides phases.

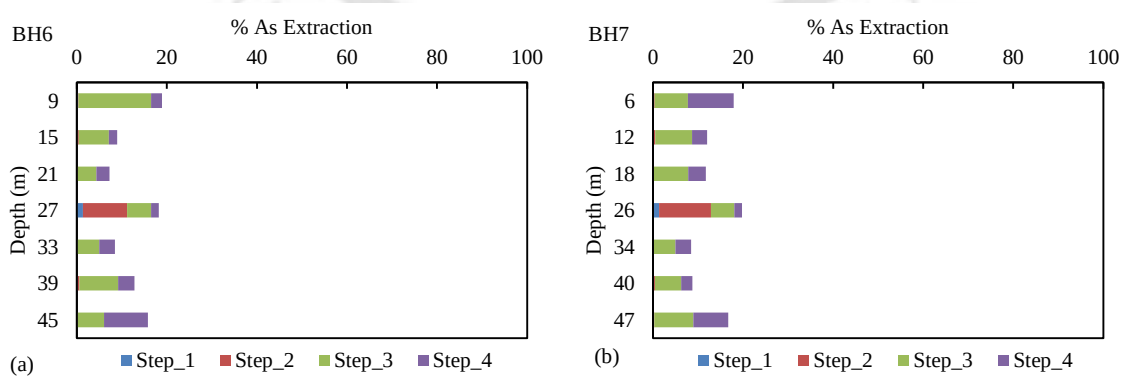

Figure 5.23 *As* extraction through SSE from sediment samples (a) BH6 (b) BH7.

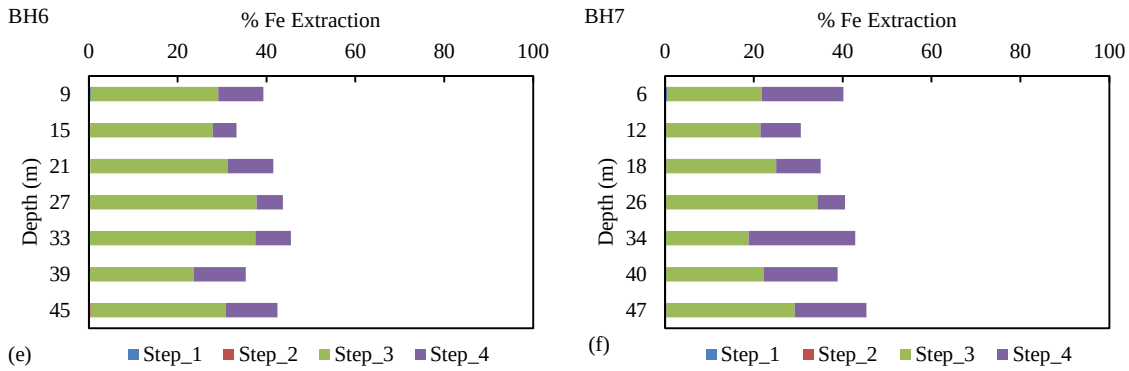

Figure 5.24 Fe extraction through SSE from sediment samples (a) BH6 (b) BH7.

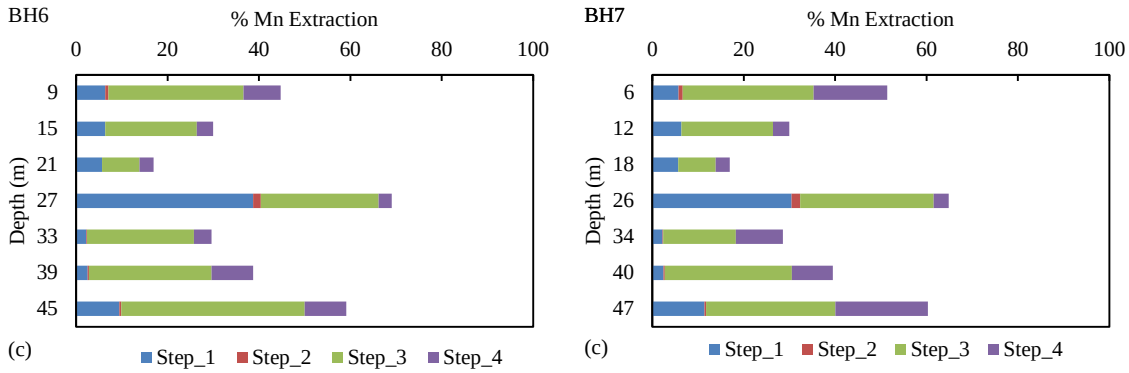

Figure 5.25 Mn extraction through SSE from sediment samples (a) BH6 (b) BH7.

5.2.3.3 Selective Sequential Extraction (SSE) for Site_3

From Site_3, three boreholes samples (BH1, BH2 and BH3) were collected and analyzed. The total extractable *As* which is the environmentally available fraction of *As* accounted to about 25% to 60% with a mean fraction of 44% (Figure 5.26a-c). The fraction obtained out of Step_3 and Step_4 contributed highest fraction of total *As* with a values ranging between 18% to 51%. The two fractions (Step_3 and Step_4) targets the Fe-oxides (i.e. amorphous and crystalline) phase for dissolution of *As* in the groundwater. The fraction of non specifically bound *As* (Step_1) was found to be very low i.e. < 1% of the total *As*. The fraction obtained out of Step_2 was significant with values ranging between 2% to 24% of total *As* extraction. The distribution of *As* phases in the sediments are highly variable due to the heterogeneity of the sediment. Additional *As* in the form of residual fraction in Step_5 bounds to pyrite and silicates, forms about approximately 37% to 72% of the total *As* extracted.

The total *As* concentration in the sediment at Site_3 (mean ~ 9 mg/kg) was found to be much lower than that other study areas viz. Site_1 with a mean of 16 mg/kg, Site_2 mean

concentration of *As* was 18 mg/kg and Site_4 with a mean concentration of 19 mg/kg. The groundwater *As* concentration in the tubewells at boring sites (BH1, BH2 and BH3) were found to be 70 µg/l to 100 µg/l, which was much higher than Site_4 (BH4 and BH5) where *As* concentrations were less than 20 µg/l in the tubewells from the drilled core. Thus it implied that inspite of lower concentration of *As* in the solid phase, the complex biogeochemical conditions in the subsurface might have driven the dissolution of *As* into the groundwater (*Section 5.1*) in these areas at Site_3.

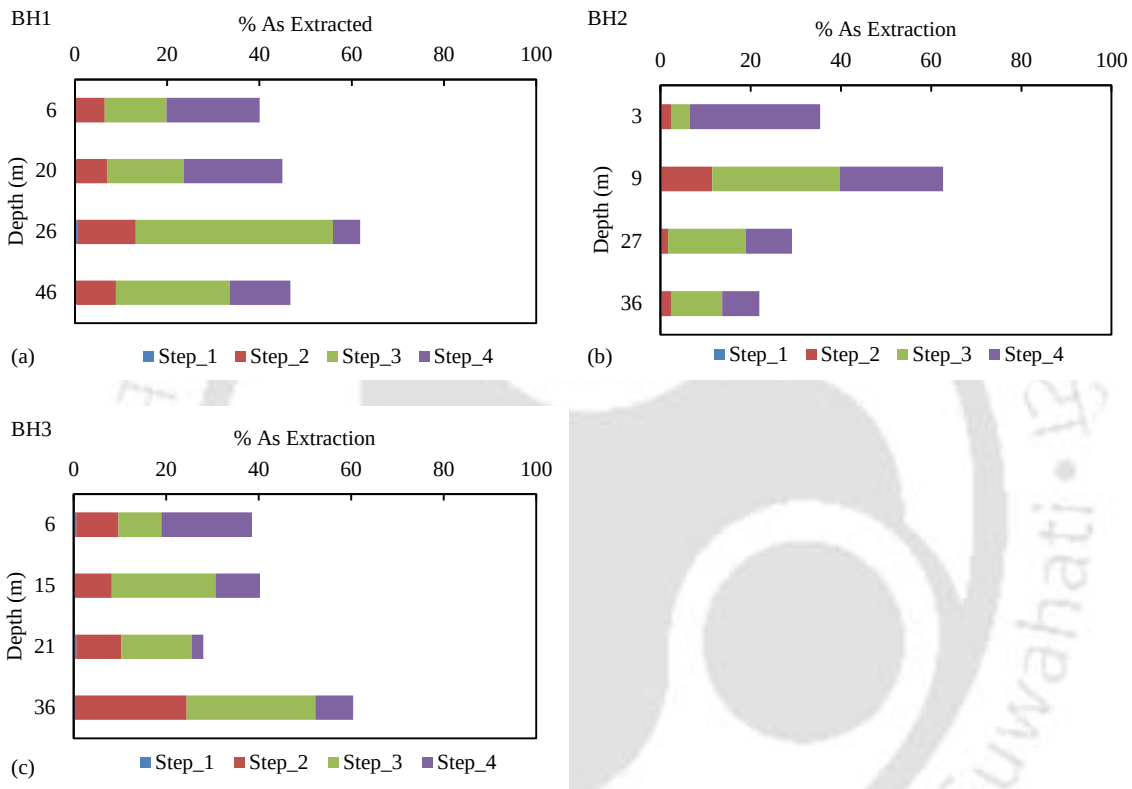

Figure 5.26 *As* extraction through SSE from sediment samples (a) BH1 (b) BH2 (c) BH3.

The extraction of Fe (Figure.5.27a-c) showed that most of the Fe were associated with the residual fraction of Step_5, which was bound to the minerals structure. The highest extractible Fe is in the form of Fe-amorphous hydrous oxides i.e. Step_3 (values ranging between 6% to 50% of total Fe extraction) and the more crystalline Fe-oxides in Step_4 accounts lower fraction, with values ranging between 3% to 25% of total Fe extraction.

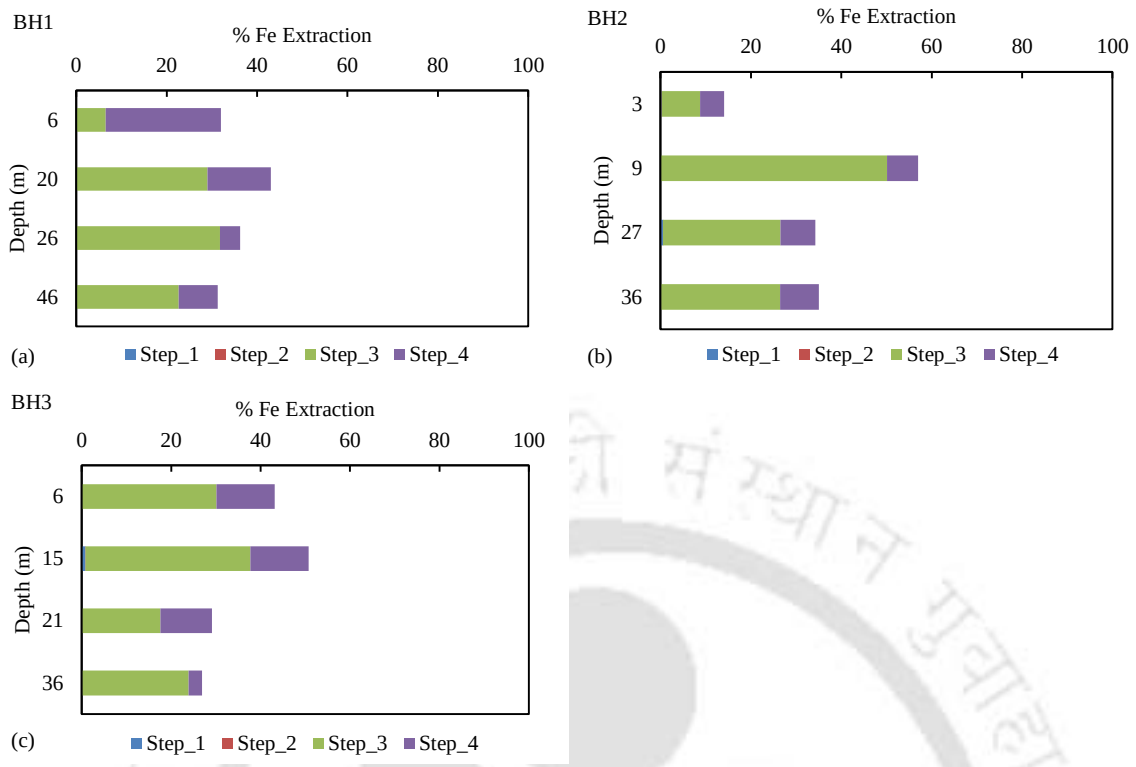

Figure 5.27 Fe extraction through SSE from sediment samples (a) BH1 (b) BH2 (c) BH3.

The Mn extraction profiles along depth showed high variability (Figure. 5.28a-c). The highest abundant Mn phase was found to be the residual fraction (Step_5). The lower value of Step_1 extraction (< 10% except at BH3 sample at depth 15 m ~ 20%) suggested that Mn is in more stable form. A higher value of extraction was achieved in Step_3 (values ranging between 10% to 59% of the total Mn extraction) suggesting more crystalline Mn-oxides dissolved with Fe-amorphous hydrous oxides phase in the sediments.

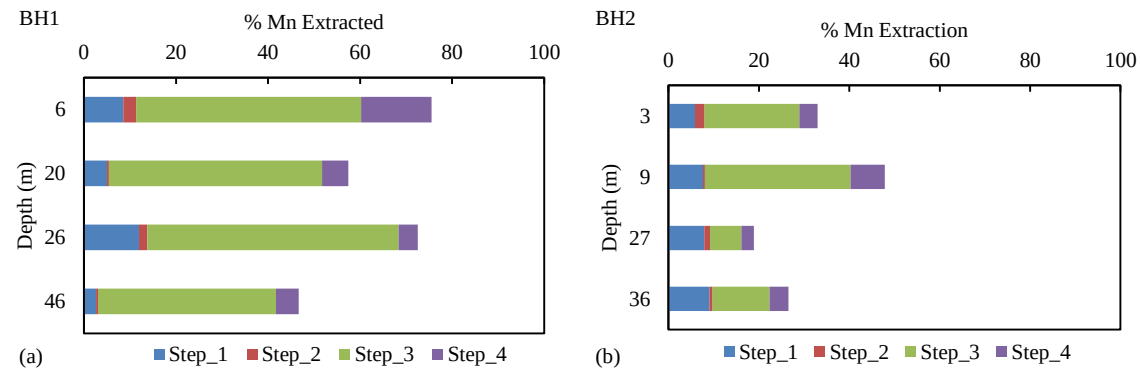

Figure 5.28 Mn extraction through SSE from sediment samples (a) BH1 (b) BH2.

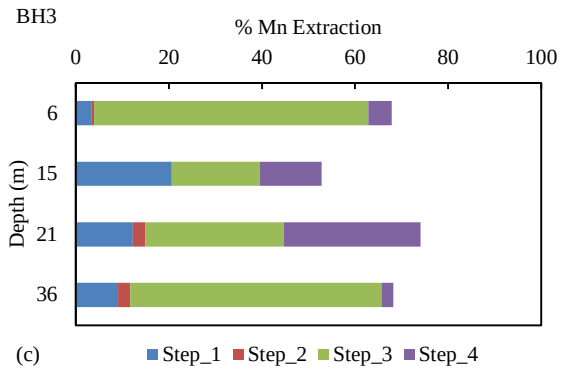

Figure 5.28 (c) Mn extraction through SSE from sediment samples BH3.

5.2.3.4 Selective Sequential Extraction (SSE) for Site_4

The fractionation profile for *As* (Figure 5.29a,b) for the two sediment core samples (BH4 and BH5) showed that a very high *As* concentration was bound to the residual phase (Step_5). The sum of *As* extractable steps accounts for relatively lower amount of total *As* (< 20%) similar to that of sediment core from Site_2. The extraction Step_3 (extracting 2% to 5% of the total *As* extraction) and Step_4 (extracting 4% to 16% of total *As* extraction) targeting Fe-amorphous and Fe-crystalline oxide were found to be the dominant phases in the sediment. The sediment core samples BH4 and BH5 are located at a distance of 10 m apart. The groundwater samples collected from the newly installed tubewells showed low *As* concentration ranging between 1 to 20 µg/l which may be due to low environmentally available fraction of *As*.

The Fe concentration profiles along the depth (Figure 5.30a,b) exhibited high variation with values ranging from 5540 to 73700 mg/kg, showing the heterogeneity of sediment in its chemical properties. Extraction Step_3 targeting amorphous Fe-oxides with values ranging between 6% to 71% of total Fe dominated over Step_4 with values ranging between 3% to 50% of the total Fe, for the sediment core samples BH4 and BH5. The highest abundant fraction obtained was residual fraction (Step_5) of Fe in the sediment samples.

The extraction of Mn (Figure 5.31a,b) showed that the fraction of Step_1 has a high amount of dissolved Mn^{2+} due to the reduction (*Section 5.2.3.1*). The environmentally available fraction (Step_1+Step_2+Step_3+Step_4) of Mn was found to be higher (i.e. > 60% of the total fraction of Mn) in these samples. Significant amount of Mn was also extracted with Step_3 (values ranging between 12% to 74% of the total Mn extracted) and lesser amount

was extracted with Step_4 (values ranging between 5% to 15% of the total Mn extraction) suggesting that most of Mn were associated with amorphous Fe-oxides phases in the sediment.

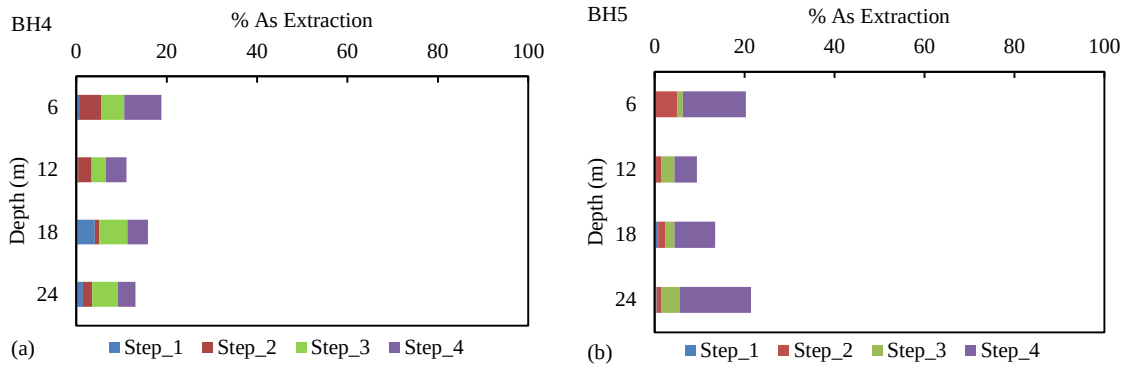

Figure 5.29 Results of SSE for *As* from sediment samples (a) BH4 (b) BH5.

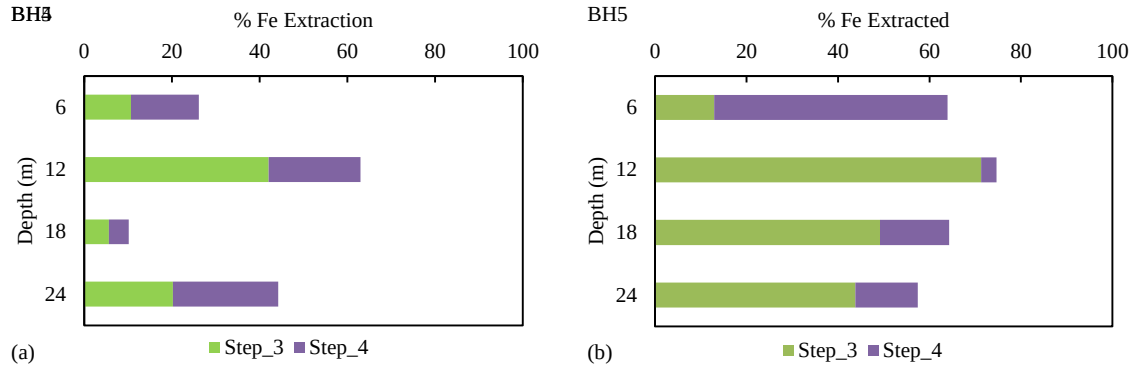

Figure 5.30 Results of SSE Fe extraction from sediment samples (a) BH4 (b) BH5.

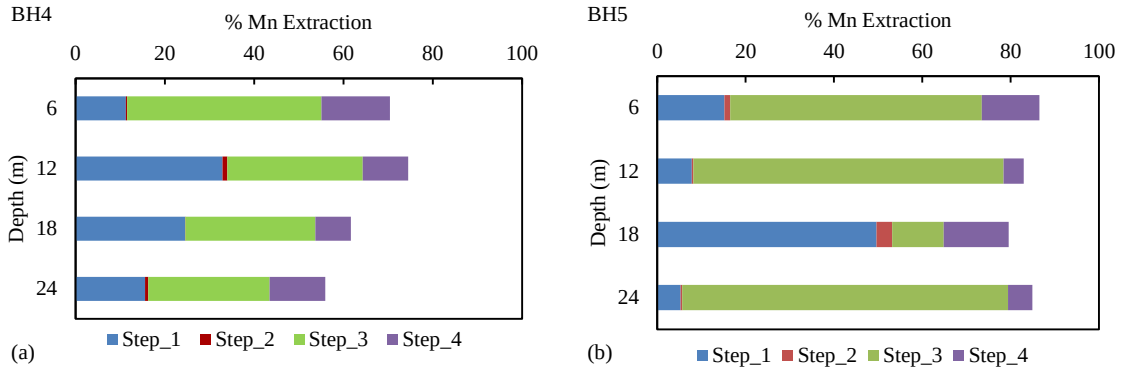

Figure 5.31 Results of Mn extraction from sediment core samples (a) BH4 (b) BH5.

5.2.3.5 *Selective Sequential Extraction (SSE) for deep-tubewell*

Selective sequential extraction (SSE) of *As* was performed on sediment core collected from deep tube-well sample with a depth of 100 m below ground level (bgl). This was done in order to evaluate the option of groundwater supply from deeper aquifer as source for safe *As* groundwater. The *As* distribution profile (Figure 5.32a) in this sediment core of deeper

aquifer clearly indicated its presence. Thus, understanding of release and mobilization process is important for control of *As* contamination in this region.

The fractionation profiles of *As* (Figure. 5.32a) suggested that residual fraction in Step_5 was the most abundant phase. Major fraction of *As* was extracted from Step_3 with values ranging between 2% to 46% of total *As* extracted, which is bound to Fe-amorphous hydrous oxide in most of the sediment samples. The Step_4, targeting the Fe-crystalline oxide also account for significant concentration with extracted fraction values ranging between 3% to 51% of the total *As* extraction. Step_1, which accounts for non-specific bound *As* is very low (< 4%). Step_2 targeting specific bound *As* was generally low most of the samples and was highly variable with values ranging from as low as 0.5% to 13% of the total *As* extraction. The extraction of Fe (Figure 5.32b) showed that Step_3 and Step_4 constituted high fraction of Fe for most of the samples. The Fe associated with the residual phase (Step_5) is the most abundant fraction. The highest extractible Fe was in the form of Fe-amorphous hydrous oxides obtained from Step_3 with values ranging between 10% to 72% of the total Fe extracted. The fraction which was bound to more crystalline Fe-oxides (Step_4), accounted for significant fraction with values ranging between 6% to 47% of the total Fe extracted. In the deeper aquifer (50 m to 100 m), the fraction in Fe-oxides (amorphous) was found to be more than that in the crystalline form of Fe.

The exchangeable fraction in Step_1 forms a significant concentration of Mn, with extracted fraction of Mn ranging between 6% to 53% of the total Mn extraction. High variability in concentrations was observed at different depths in the sediments (Figure 5.32c). The Step_3 (extracted fraction ranging between 1% to 58% of the total Mn extracted) and Step_4 fraction values ranging between 1% to 24% of the total Mn extraction also accounted for substantial amount of concentration of Mn. The residual extraction at Step_5 for Mn showed high variability with values between 10% to 80% showing heterogeneity of the subsurface sediments.

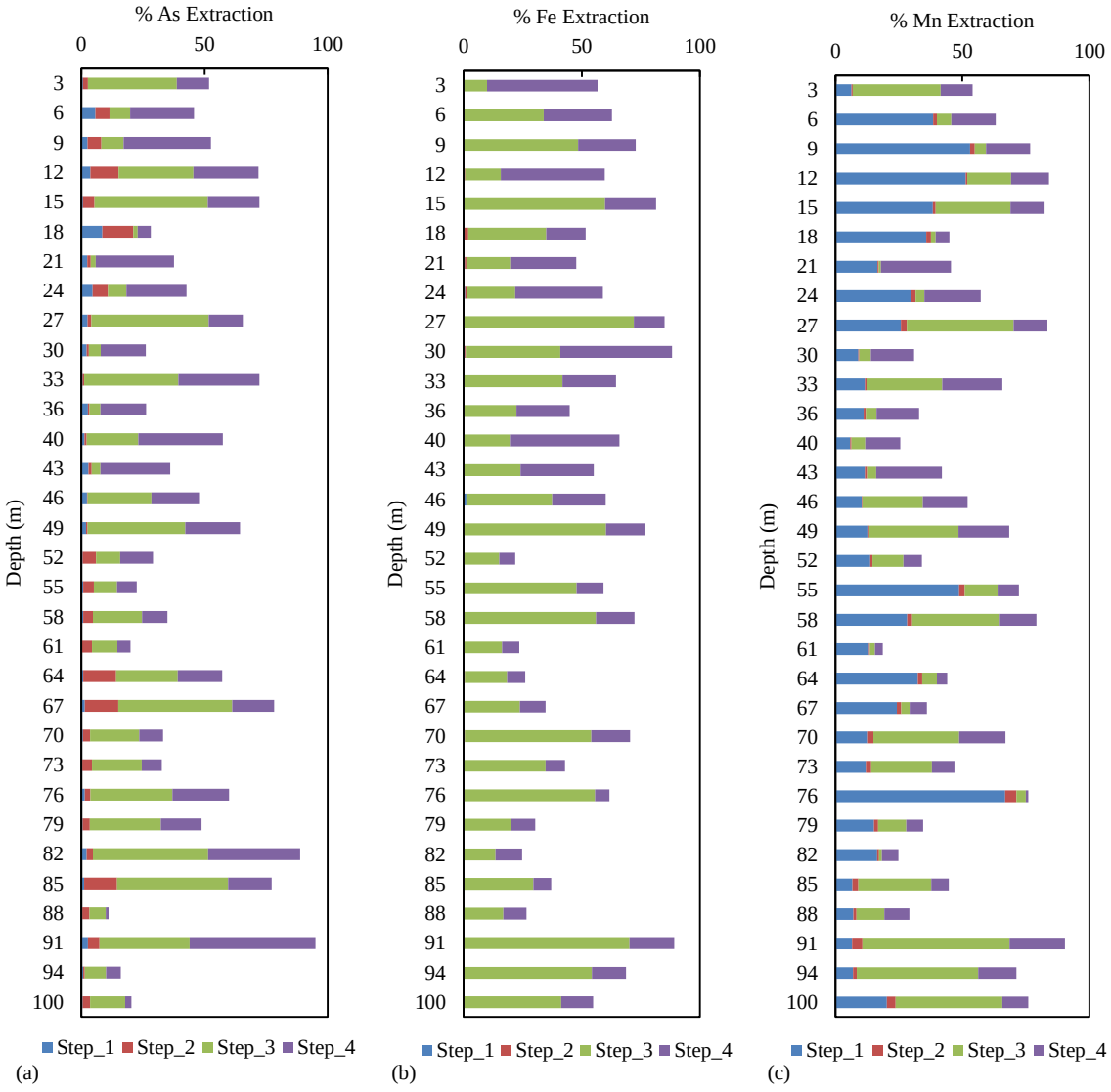

Figure 5.32 Results of SSE from sediment samples of deep borehole for (a) *As* (b) Fe (c) Mn.

5.2.3.6 Comparison of SSE with that of other South East Asian countries

It was found that the magnitude of the extracted values differed but the trend in its relationship with *As* bearing phases was quite similar when compared with *As* contaminated sites of South East Asian countries (Gault et al., 2003; Swartz et al., 2004; Charlet et al., 2007; Guo et al., 2008; Postma et al., 2007; Xie et al., 2008). *As* fractions in individual soil depends strongly on the extractant and extraction procedure employed (Wang and Mulligan, 2008). Small modification of the sequential extraction procedure could yield significantly variable results among laboratories (Hudson-Edward et al., 2004) but the trend in

characterization of distribution into the main soil fractions should agree (Wang and Mulligan, 2008).

Postma et al., (2007) used the same sequential extraction procedure in Dan Phuong, Vietnam and reported total *As* between 7 µg/g to 20 µg/g and total Fe around 20 mg/g. They found that the extraction steps (Ext_5 and Ext_6) targeting the amorphous and crystalline Fe-oxides extracts maximum *As*, and both of these extraction steps had approximately equal amount of extraction of *As* from the total fraction. The Fe in the sediment showed that more than 50% of total iron was associated with Fe-oxides.

Swartz et al., (2004) using extraction procedure proposed by Koen et al. (2001) for extracting *As* from Bangladesh sediments reported total *As* concentration generally to be less than 3 µg/g and total Fe about 20 mg/g. They reported a good correlation of *As* extracted with extractant targeting crystalline Fe-oxides (r^2 = 0.65) where about 20% to 50% of *As* amounts to extractable fraction out of total *As* in the sediment. About 10% of total Fe extracted was associated with amorphous Fe-oxides and 30% extraction was associated with crystalline Fe-oxide.

Charlet et al., (2007) from sequential extraction experiment using modified extraction steps from Koen et al. (2001), Kotska and Luther (1994) and Tessier et al (1979) found that the total *As* concentration in the sediment was 3.0 ± 0.4 ppm and major portion of *As* was associated with Fe-oxides (34% ± 8%) and acid volatile sulfides. Carbonates amounted to 19% ± 7% of total *As* extracted.

Selective Sequential Extraction (SSE) carried out on the sediment samples from Red River delta, Vietnam reported high *As* extracted from strongly adsorbed and ionically bound *As* (i.e. phosphate extraction > 50%) and lesser amount was extracted from *As* bounds to carbonates, Mn-oxides and very amorphous Fe-oxides (Eiche et al., 2008; Berg et al., 2008).

Xie et al., (2008) carried out a sequential extraction study on Datong basin, China using the method proposed by Koen et al. (2001). The amount of extractable *As* cumulatively accounted between 40% to 80% of the total solid-phase *As*. The extractable Fe ranged between 19% to 38% fraction of the total solid-phase Fe. The *As* concentration vary from 4.9 to 118 mg/kg with an average *As* concentration of 18.6 mg/kg. The extractable fraction of *As* and Fe shows a moderate correlation (r^2 = 0.46). Correlation with other geochemical

parameters was found to be low, which indicated that *As* is associated predominantly with iron (Fe) bearing minerals.

Guo et al. (2008) reported sediment *As* range from 7.3 to 73.3 mg/kg (average ~ 18.9 mg/kg) in the Hetao Basin, Inner Mongolia. They concluded that the *As* affected area has slightly higher average values (~ 20.8 mg/kg), than the low *As* area (average of 13.6 mg/kg) the sequential extraction results suggested that about 60% to 86% of total *As* was extracted with extractable Fe-oxides and Mn-oxides.

In our study area Site_1, which is high *As* contaminated, showed total arsenic concentration to be between 6 mg/kg to 43.4 mg/kg with an average of 16.05 mg/kg and total Fe about 25 mg/g. The *As* extracted by amorphous and crystalline Fe-oxides accounted to highest extractable fraction range between 32% to 50% of total *As* extracted. In this high *As* contaminated area (Site_1), the residual *As* accounted for about 60% while the adjacent location Site_2 with low *As* groundwater, demonstrated higher residual concentration fraction of 80%, i.e. the available *As* in natural environment is lesser than 20% of total *As* extracted. A high correlation was observed between the *As* extracted from Fe-oxides phases (Ext_5 and Ext_6) with the amount of Fe extracted in those phases (r^2 0.4 – 0.9). Similar relationship has been reported by many researchers (Gault et al., 2003; Swartz et al., 2004; Guo et al., 2008; Postma et al., 2007; Xie et al., 2008).

The results indicated that *As* extraction is dominated by fractions which target the Fe-amorphous oxides as well as Fe-crystalline oxides since *As* has a strong affinity for Fe-oxide minerals, phyllosilicate or coatings on the feldspar and quartz. The study of scanning electron microscopy (SEM) also demonstrated the universal presence of Fe-oxides on the sediment samples (*Section 5.2.1.5*). The XRD analysis results showed the presence of quartz, phyllosilicates (mica, illite, chlorite, biotite), calcite, gypsum and feldspar (*Section 5.2.1.4*). Since the total extracted *As* is not unusually higher, high dissolved *As* in the groundwater are possibly not due to the elevated total solid phase *As* concentrations in the sediments alone. Rather the geochemical conditions i.e. redox, suboxic to anoxic conditions as well as the hydro-geochemical condition existing in the area, which was found to be consistent with the mechanism of reductive dissolution of Fe-oxides via respiration of organic matter, thus releasing the associated adsorbed or co-precipitated *As*, as has been widely accepted in other case studies (Shimada, 1996; Bhattacharya et al., 1997, 2006, 2007; Nickson et al., 1998,

2000; Harvey et al., 2002, 2006; McArthur et al., 2004, 2008, 2011; Nath et al., 2008) appears to be the influencing factors in the present case.

5.3 Arsenic attenuation study

The *As* concentration in groundwater is usually controlled by natural geochemical processes, where adsorption-desorption reaction of *As* species on mineral play a key role. These adsorption and desorption process mainly control the speciation of *As* thus affecting its mobility, toxicity, and bioavailability. Therefore, the adsorption-desorption processes are also important for the natural remediation, water purification technologies, with the aim of removing *As* from water (Wang and Deng, 2009). The viability of aquifers to release low-*As* water depends on the capacity of these sediments to remove *As* from the groundwater that could infiltrate from the zone of high organic content and strongly reduced sediment. Three sediment samples namely C_50, C_70 and C_150 from drill core 1C were chosen for the batch attenuation studies. These sediments are present in most of the sediment core samples from the Site_1 which is highly affected with *As* contamination. The first grey samples (C_50) corresponds to reduced sediment with low Fe and Mn as shown (Table 5.10), sample C_70 brown in color was characterized as oxidized sediment with high concentration of Fe and Mn and sample C_150 with ash-greenish color have moderate concentration of Fe and Mn. The various characteristics of the sediment samples used for batch attenuation experiments were shown (Table 5.10) and brief explanation was provided (*Section 4.3.7*).

Table 5.10 Characteristics of the three sediments with their extraction (SSE) values used for the batch experiments.

Sample ID	Color	Depth (m)	Reductively extracted Fe (mg/kg)	Reductively extractedMn (mg/kg)
C_50	Grey	15	3000	8
C_70	Brown	21	28000	200
C_150	Ash-Greenish	46	7000	160

5.3.1 Sorption kinetics of Arsenic

Adsorption process can be controlled by different kinds of mechanism such as mass transfer and chemical reactions. To determine the adsorption mechanism, several adsorption models were applied to evaluate the experimental data. For this purpose pseudo second-order kinetic model from type 1 to type 4 (Ho, 2006), Elovich model and intra-particle diffusion model (Weber and Morris, 1963) were fitted to the experimental data. The phenomenon whereby

ions are transferred from liquid phase to a solid phase usually involves the following steps (Poots et al., 1976):

1) Boundary layer mass transfer across the liquid film surrounding the particle.
2) Internal diffusion/mass transport within the particle boundary as pore and/or solid diffusion.
3) Adsorption within the particle and on the external surface.

Allard et al., (1986) proposed further three pathways by which sorption may occurs unto the surface:

1) Physical adsorption which is considered rapid and reversible and is due to non-specific forces of attraction (e.g. Van der Waals forces)
2) Electrostatic adsorption due to coulombic forces of attraction between charged solute species and the adsorbing phase – this process is usually rapid and largely reversible
3) Specific adsorption due to the action of chemical forces of attraction which leads to surface bonding at a specific site on the solid phase – this process can be slow and partly irreversible.

The adsorption process of *As* on natural soil was found to be rapid (Barrachina et al., 1996; Goh and Lim, 2004). It was found that about 80% of total *As* adsorption was observed at initial 30 minutes.

5.3.1.1 Pseudo First-Order kinetic model

The applicability of Lagergen model or pseudo first order kinetics (Lagergren, 1898) was tested for the adsorption of *As* by linear plot of log ($q_e - q_t$) versus t for the pseudo first-order adsorption kinetics (Eq. 2.16-2.17), from which the adsorption rate constant, K_{ad}, was estimated. The coefficient of determination (r^2) from the plots of each dataset revealed low correlation ($r^2 < 0.50$). A comparison of experimental kinetic data and theoretical data indicated a poor simulation by the Lagergen model revealing that the sorption process may be more complex than pseudo-first-order kinetics.

5.3.1.2 Pseudo Second-Order kinetic model

In order to distinguish the kinetics equation based on concentration of solution from the sorption capacity of solids, the second-order rate equation (Eq. 2.18-2.22) has been called a pseudo-second-order. It was developed on the basis that chemisorptions is the operative

reaction mechanism (Ho and McKay, 2000). The coefficients were determined from linear plots in accordance to the Table 2.4. The linearized form takes different type of kinetics (Type-1 to Type-4 according to Table 2.4) in the pseudo-second-order. The coefficient of determination (r^2) show better correlation between the observed and simulated values for pseudo second order kinetics. The plots for the determination of parameters of pseudo-second-order kinetics have been shown (Figure 5.33a-d) and the obtained parameters result have been tabulated (Table 5.11 – 5.14).

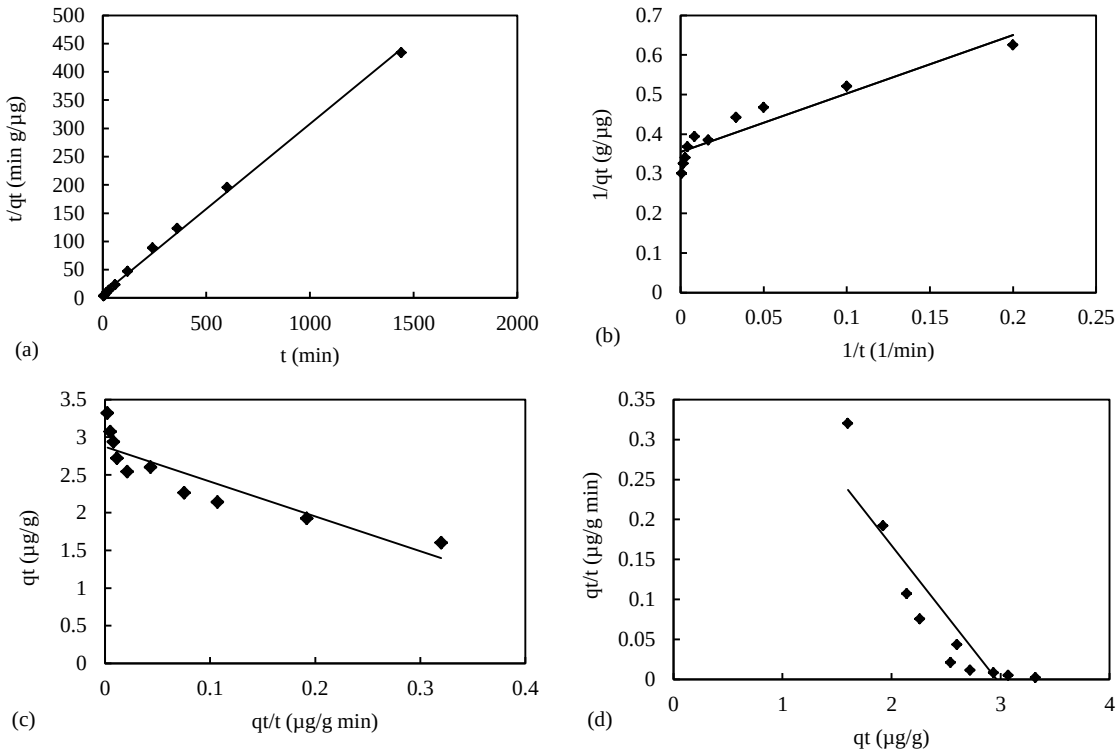

Figure 5.33 Pseudo-second order kinetics for C_50 with initial *As*(III) 300 µg/l for (a) Type-1 (b) Type-2 (c) Type-3 (d) Type-4.

Table 5.11 Pseudo-second-order kinetic parameters obtained by using linear regression methods for 300 µg/l *As*(III).

Type	parameters	C_50	C_70	C_150
Type 1	q_e (µg/g)	7.14	9.26	7.94
	K_2 (g/µg min)	3.87E-03	2.71E-03	4.13E-03
	h (g/µg min)	0.20	0.23	0.26
	r^2	0.74	0.77	0.66
Type 2	q_e (µg/g)	5.71	6.90	6.41
	K_2 (g/µg min)	4.08E-02	3.48E-02	6.93E-02
	h (g/µg min)	1.33	1.65	2.85
	r^2	0.69	0.50	0.45
Type 3	q_e (µg/g)	5.83	7.20	6.49
	K_2 (g/µg min)	3.56E-02	2.79E-02	6.36E-02
	h (g/µg min)	1.21	1.45	2.68
	r^2	0.50	0.55	0.50

Type 4	q_e (µg/g)	6.12	7.88	7.06
	K_2 (g/µg min)	2.48E-02	1.50E-02	2.82E-02
	h (g/µg min)	0.93	0.93	1.41
	r^2	0.72	0.59	0.51

Table 5.12 Pseudo-second-order kinetic parameters obtained by using linear regression methods for 500 µg/l *As*(III).

Type	parameters	C_50	C_70	C_150
Type 1	q_e (µg/g)	6.37	10.87	6.02
	K_2 (g/µg min)	6.32E-03	1.23E-02	1.91E-02
	h (g/µg min)	0.26	1.46	0.69
	r^2	0.62	0.62	0.62
Type 2	q_e (µg/g)	5.35	10.10	5.62
	K_2 (g/µg min)	1.33E-01	1.03E-01	1.47E-01
	h (g/µg min)	3.82	10.53	4.65
	r^2	0.40	0.50	0.59
Type 3	q_e (µg/g)	5.39	10.12	5.63
	K_2 (g/µg min)	1.22E-01	9.85E-02	1.46E-01
	h (g/µg min)	3.55	10.09	4.63
	r^2	0.50	0.50	0.50
Type 4	q_e (µg/g)	5.75	10.30	5.82
	K_2 (g/µg min)	5.04E-02	5.17E-02	8.20E-02
	h (g/µg min)	1.67	5.48	2.78
	r^2	0.44	0.54	0.58

Table 5.13 Pseudo-second-order kinetic parameters obtained by using linear regression methods for 300 µg/l *As*(V).

Type	parameters	C_50	C_70	C_150
Type 1	q_e (µg/g)	10.00	11.36	10.31
	K_2 (g/µg min)	9.29E-03	7.54E-03	2.54E-02
	h (g/µg min)	0.93	0.97	2.70
	r^2	0.66	0.66	0.73
Type 2	q_e (µg/g)	9.35	10.10	9.90
	K_2 (g/µg min)	1.07E-01	7.15E-02	9.11E-02
	h (g/µg min)	5.18	7.30	8.93
	r^2	0.48	0.48	0.86
Type 3	q_e (µg/g)	9.31	10.17	9.92
	K_2 (g/µg min)	5.94E-02	6.60E-02	8.80E-02
	h (g/µg min)	5.15	6.83	8.66
	r^2	0.50	0.50	0.50
Type 4	q_e (µg/g)	9.48	10.66	9.99
	K_2 (g/µg min)	4.55E-02	3.28E-02	7.49E-02
	h (g/µg min)	4.08	3.73	7.49
	r^2	0.77	0.66	0.86

Table 5.14 Pseudo-second-order kinetic parameters using linear regression methods for 500 µg/l *As*(V).

Type	parameters	C_50	C_70	C_150
Type 1	q_e (µg/g)	16.95	18.52	17.24
	K_2 (g/µg min)	7.75E-03	3.66E-03	8.92E-03
	h (g/µg min)	2.23	1.26	2.65

	r^2	0.59	0.63	0.71
Type 2	q_e (µg/g)	15.87	16.67	16.39
	K_2 (g/µg min)	1.07E-01	4.29E-02	3.76E-02
	h (g/µg min)	27.03	11.90	10.10
	r^2	0.31	0.57	0.75
Type 3	q_e (µg/g)	15.58	16.64	16.35
	K_2 (g/µg min)	1.27E-01	4.07E-02	3.72E-02
	h (g/µg min)	30.85	11.28	9.95
	r^2	0.26	0.55	0.65
Type 4	q_e (µg/g)	16.58	17.25	16.68
	K_2 (g/µg min)	3.21E-02	2.34E-02	2.69E-02
	h (g/µg min)	8.84	6.97	7.49
	r^2	0.34	0.60	0.69

The best fit for the adsorption kinetics model for various linearized regression model (Table 5.11-5.14) shows that Type 1 fitted best for most of the sediment samples at different concentrations. The moderate r^2 (coefficient of determination) for most of the samples reveals that the adsorption kinetics model cannot solely described with pseudo-second order, since more complex mechanisms might be involved.

According to the theoretical concept, the rate coefficient K_2 (g/µg min) decreases with increasing initial adsorbate concentration. When the *As* concentration was low in the solution, adsorption was very fast due to availability of active sorption sites and less competition. With increasing concentration, the active sorption sites became lesser and thus adsorption rate reduced consequently decreasing the rate coefficient (K_2) (Gupta and Bhattacharya, 2011). Similar trend was noticed when the initial concentration was increased from 300 µg/l to 500µg/l for the samples with *As*(V) solution (Table 5.13-5.14). *As*(III) solution did not follow the dependence of initial concentrations on the values of rate coefficient (k_2) (Table 5.11-5.12), independence of initial concentration on rate coefficient (k_2) have also been reported (Plazinski et al., 2009).

5.3.1.3 Elovich kinetic model

Elovich adsorption kinetic model was found to be the best suitable kinetic model to describe the adsorption behavior of *As* on the sediment. The model parameters were calculated from the linear plot of q_t versus ln(*t*) (Figure 5.34) and the values were listed in Table 5.15. The Elovich constants *a* and *b* are defined as initial rate constant, '*a*' represents the rate of chemisorptions at zero coverage (µg/g min) and '*b*' is the extent of surface coverage and activation energy for chemisorptions (g/µg).

The adsorption process of *As* was found to be rapid. It was found that about 80% of total *As* adsorption was observed at initial 30 minutes. Similar adsorption process was reported by Barrachina et al. (1996) and Goh and Lim (2004) on natural geological materials. Elovich model was used by Barrachina et al. (1996) and Goh and Lim (2004) to explain the adsorption process of *As*(III) and *As*(V) on sediment.

Goh and Lim (2004) analyzed the tropical soil from Singapore and reported the Elovich model parameter for *As*(V) as , a = 4.3E03 and b = 0.0366 with r^2 = 0.995 and *As*(III) a = 4.78E02 and b = 0.0516 with r^2 = 0.985. The values obtained from our experiments (Table 5.15) revealed that there is no consistency in the values of Elovich coefficients for the sediment samples. Similar inconsistencies for the Elovich coefficient have been reported by various authors and sometimes, apparently abnormal values are also found (Gupta and Bhattacharyya, 2011).

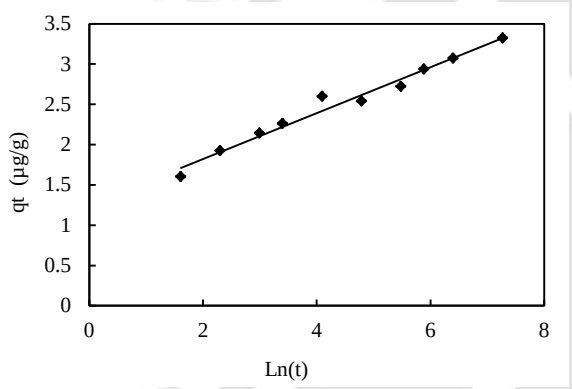

Figure 5.34 Elovich adsorption kinetics model for C_50 sample with initial *As*(III) concentration of 300 µg/l.

Table 5.15 Regression analysis results of the Elovich kinetic model for *As*(III) and *As*(V) with initial concentrations of 300 µg/l and 500 µg/l.

As Species	Initial Conc.	parameters	C_50	C_70	C_150
As(III)	300 µg/l	a (µg/(g min))	2.72E+01	1.21E+01	5.52E+02
		b (g/ µg)	1.62	1.12	1.9
		r^2	0.97	0.97	0.88
As(III)	500 µg/l	a (µg/(g min))	2.51E+04	2.92E+08	1.02E+08
		b (g/ µg)	3.08	2.55	4.52
		r^2	0.89	0.89	0.76
As(V)	300 µg/l	a (µg/(g min))	7.73E+05	1.59E+05	7.74E+09
		b (g/ µg)	2.15	1.76	2.98
		r^2	0.89	0.94	0.91
As(V)	500 µg/l	a (µg/(g min))	4.71E+11	1.11E+06	4.66E+06

	b (g/ µg)	2.08	1.17	1.3
	r^2	0.81	0.93	0.84

5.3.1.4 Intra-particle diffusion model

Due to the heterogeneity of sediments with varying particle sizes, sorption sites and porosities promote transport processes. Thus, pore diffusion or intra-particle diffusion was also suspected to play a significant role along with surface adsorption. Intra-particle diffusion model of Weber and Morris (1963) were fitted to the experimental data. The plots of q_t versus $t^{0.5}$ (Figure 5.35) do not pass through the origin, but the straight line observed confirms the presence of intra-particle diffusion. A deviation from the origin shows that intra-particle transport is not the only rate limiting step. The values of K_{id} (µg/g $min^{0.5}$) are listed in Table 5.16. The large intercept in the plot indicates the greater contribution of the surface sorption in the rate controlling step. This reveals that the mechanism of metal ion adsorption by sediments is complex and both the surface adsorption as well as the intra-particle diffusion contributes to the rate determining step.

Table 5.16 Intra-particle diffusion adsorption model parameters for initial *As*(V) concentrations of 300 µg/l and 500 µg/l.

As Species	Initial Conc	parameters	C_50	C_70	C_150
As(III)	300 µg/l	K_{id} (µg/(g $min^{0.5}$)	0.096	0.412	0.086
		C (µg/g)	3.81	4.38	4.86
		r^2	0.86	0.94	0.89
As(III)	500 µg/l	K_{id} (µg/(g $min^{0.5}$)	0.054	0.06	0.033
		C (µg/g)	4.39	8.95	4.95
		r^2	0.94	0.79	0.66
As(V)	300 µg/l	K_{id} (µg/(g $min^{0.5}$)	0.06	0.088	0.045
		C (µg/g)	7.85	8.488	8.91
		r^2	0.71	0.86	0.63
As(V)	500 µg/l	K_{id} (µg/(g $min^{0.5}$)	0.079	0.134	0.107
		C (µg/g)	14.37	14	14.01
		r^2	0.83	0.87	0.62

The multi linearity of the plot (Figure 5.35b) showed that different mechanism of adsorption takes place for sample C_50. The initial step portion was attributed to the surface adsorption occurring instantaneously or boundary layer diffusion of sorbate molecules, while gentle

slope portion was attributed to the intra-particle diffusion which was slow and likely to be rate-controlled (Ho and McKay, 2003; Wu et al., 2009; Gupta and Bhattacharyya, 2011).

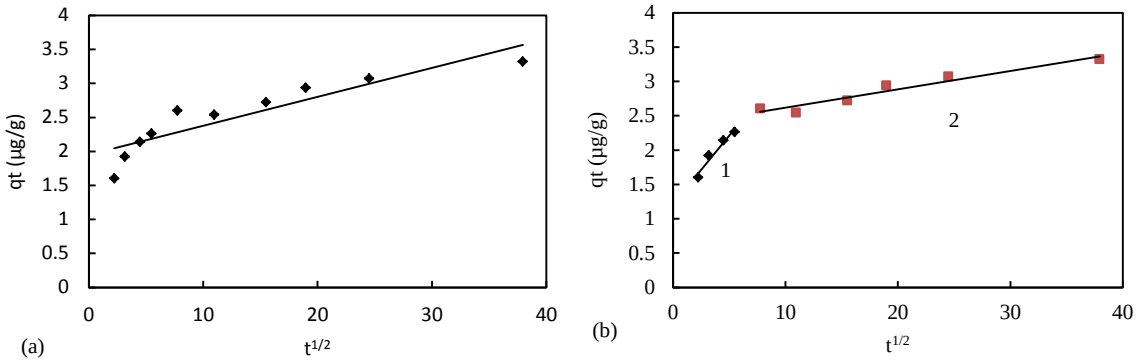

Figure 5.35 Intra-particle diffusion model for (a) C_50 sample with initial *As*(III) 300 µg/l (b) two linear segment for C_50 sample.

Batch experiments suggested that the sediment samples were able to adsorbed *As*(V) and *As*(III) at circum-neutral pH, where the groundwater existed in the study area. The sediment sample C_70 exhibited highest *As* adsorption capacity, as this sample had highest Fe and Mn content and C_50 grey sediment (reduced) showed lowest adsorption capacity. The adsorption kinetics could be best described with Elovich kinetics model. Significant correlation was observed for intra-particle diffusion model. The rate determining step was found to be controlled by both surface sorption as well as intra-particle diffusion. The application of Elovich model demonstrated that the rate determining steps may be chemisorptions.

5.3.2 Arsenic adsorption isotherm

The adsorption isotherms for the three types of sediment samples (C_50, C_70 and C_150) are shown (Figure 5.36). Freundlich and Langmuir adsorption isotherm were fitted into the experimental data for different initial *As* concentrations. The similar stock solution with the average concentration which simulated the natural groundwater condition was used in the experiment.

Batch adsorption experiment revealed that the highest adsorption capacity was exhibited by C_70 sediment sample, which is consistent with the highest Fe and Mn extraction from that sample (Table 5.10). Lower adsorption was observed for samples C_50 and C_150, and they have nearly comparable adsorption capacity. Thus, in order to obtain a low *As* groundwater oxidized sediment with higher Fe content is essential. The adsorption of *As*(V) was found to be higher than *As*(III) and the adsorption behavior of *As*(V) and *As*(III) onto Fe(III) oxides

minerals is similar at pH 6.5 to 8 (Dixit and Hering, 2003). While the adsorption of *As*(III) to Fe-oxides amorphous is greater at pH higher than 7, adsorption of *As*(V) is higher at low pH i.e. below 6 (Goldberg, 2002; Dixit and Hering, 2003). Since the pH of the groundwater was found to be near neutral condition, it is expected that the oxidized sediments will also have significant capacity to adsorb *As*(III) as shown in Figure5.36a,b.

The values of Freundlich and Langmuir adsorption isotherm parameters were tabulated (Table 5.17). Freundlich isotherm is frequently used to model adsorption on solids with multiple types of surface sites or on heterogenous solids such as soils (Sposito, 1989). The Freundlich isotherm was seen to fit better in the adsorption isotherm.

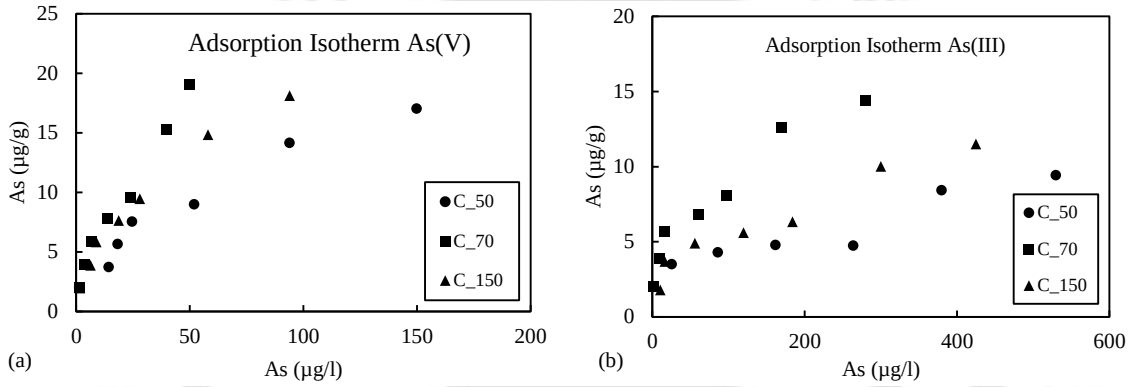

Figure 5.36 (a) Adsorption isotherm for *As*(V), and (b) Adsorption isotherm for *As*(III) for the three sediments samples C_50, C_70 and C_150.

The PHREEQC model output for adsorption isotherm was found to over predict the adsorption of the samples when considering the amorphous Fe-oxides having properties of Hydroferric oxides (Hfo). The amount of Hfo was determined from the sequential extraction step targeting the amorphous Fe-oxides which were operationally defined. Since the sediment in the study area contains high Fe fractions in the amorphous and crystalline Fe-oxides, along with the super-saturation of Fe mineral phases in the aquifer materials may be potential *As* sinks and source of dissolved species. The deviation of simulated model from the observed data indicates that most of the Fe extracted in amorphous and crystalline phase does not possess the surface complexation properties of Hydroferric oxides (Hfo). Therefore, in subsequent surface complexation model (SCM) only 10% of the extracted amorphous and crystalline Fe-oxides were assumed to have properties of Hydroferric oxides (Hfo).

Table 5.17 Freundlich and Langmuir adsorption isotherm parameters for sediments samples.

As Species	Isotherm	parameters	C_50	C_70	C_150
As(III)	Freundlich	log K_f	0.2	0.25	-0.02

		$1/n$	0.24	0.36	0.42
		r^2	0.66	0.95	0.89
As(V)	Freundlich	log K_f	0.17	0.184	0.21
		$1/n$	0.47	0.626	0.52
		r^2	0.94	0.97	0.97
As(III)	Langmuir	q_{max}	7.7	15.6	12.5
		K_L	0.013	0.023	0.012
		r^2	0.69	0.87	0.85
As(V)	Langmuir	q_{max}	21.7	26.3	22.2
		K_L	0.02	0.03	0.03
		r^2	0.95	0.85	0.97

The quantification of *As*(III) was complicated by the fact that some of the *As*(III) was oxidized to *As*(V) (Amirbahman et al., 2006; Stollenwerk et al., 2007). In the batch adsorption study of *As*(III), low concentration of aqueous *As*(V) was found. The experiment revealed that the oxidation might have taken place on the solid phase (sediment) oxidative sites and get adsorbed to the surface without releasing the *As*(V) into the solution (*Section 5.3.3*).

5.3.2.1 Effect of pH

The effect of pH on adsorption of *As*(III) and *As*(V) on the sediment samples have been studied at pH 6, 7.5, 8.5 (Figure 5.37a,b). The pH range chosen corresponds to the natural groundwater conditions existing in the study area (pH range from 6 to 7.25). It was observed that with increase in pH to 8.5 the *As*(V) adsorption reduces 10%, 4.5% and 5.5% for sediment samples C_50, C_ 70 and C_150 (Figure 5.37a). *As*(III) adsorption increase as pH increases, slight increase in adsorption were noticed viz. 6% for both C_50 and C_150, while 3.5% for C_70 sediment samples (Figure 5.37b). Minimal effect of *As*(V) adsorption on Fe-oxides was noticed near neutral pH (Meng et al., 2000; Stollenwerk et al., 2007).

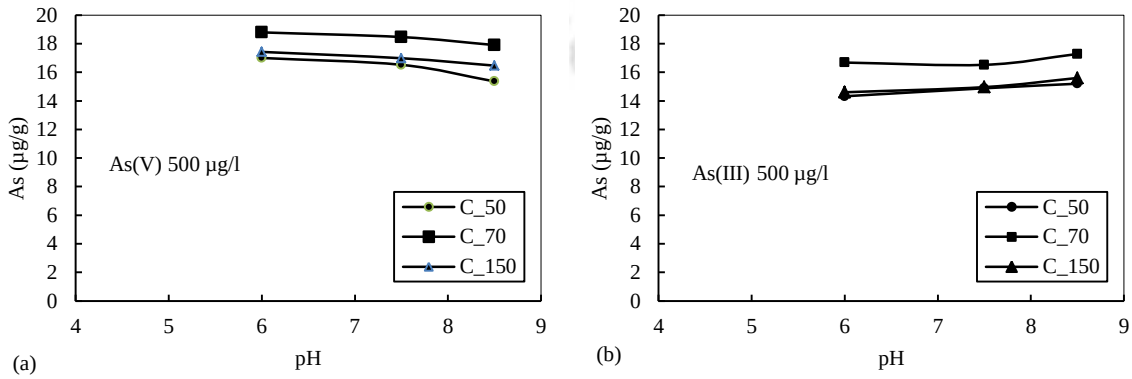

Figure 5.37 Effect of pH on adsorption of with initial concentration of 500 µg/l on (a) *As*(V) and (b) *As*(III) for sediment samples.

At pH less than pzc (point of zero charge i.e. pH 4.6) (Stumm, 1992) the positive charge surfaces on the soil sediment would likely to prefer the adsorption of the charged *As*(V). Due to high Fe-oxides in the sediment samples and the pzc for Fe-oxides is in the pH range of 6 to 8 (Stumm, 1992) the adsorption of *As*(V) is preferred over *As*(III). The decrease in concentration of *As*(V) with increase in pH implies decrease in surface charged density due to increase of OH^- resulted in the electrostatic repulsion with oxyanions *As*(V) comparing with *As*(III) which has less negative character (Goldberg, 2002; Dixit and Hering, 2003; Goh and Lim, 2004). Thus, it was clear that the adsorption of *As* by sediment was dependent on the variable charge developed on the sediment particle surface.

5.3.2.2 Effect of Phosphate (PO_4^{3-})

As and PO_4^{3-} exhibits competition for adsorption site on Fe-oxides and sediment (Manning and Goldberg, 1996; Goh and Lim, 2004; Stollenwerk et al, 2007). PO_4^{3-} has higher affinity for adsorption due to its smaller size and higher charge density (Wenzel et al., 2001; Mulligan et al., 2010). In the batch experiment a strong competition for adsorption sites between *As*(V) and PO_4^{3-} was observed in the samples when the concentration of PO_4^{3-} was increased from 0.5 mg/l to 3 mg/l (Figure 5.38). The decrease in *As*(V) adsorption depends on the ratio of PO_4^{3-}/*As*(V) in the solution (Stollenwerk et al., 2007). The competition for adsorption site by PO_4^{3-} was proposed to be main *As* releasing mechanism by few authors (Zheng et al., 2005; Berg et al., 2008; Eiche et al., 2008). A highest reduction in the adsorption capacity was noticed in the reduced sediment sample C_50 (grey color sediment). The reduction in adsorption of *As*(V) with 500 µg/l initial concentration were 16%, 11% and 13% for C_50, C_70 and C_150 respectively (Figure 5.38b) and with initial *As*(V) concentration of 300 µg/l were 13%, 9% and 14% respectively (Figure 5.38a). The reduction of surface potential due to the formation of inner sphere complex with Fe-oxides, also reduces the adsorption of *As*(V) due to electrostatic repulsion of similar charge on the sediment surface (Goh and Lim, 2004). Therefore, the accumulation or precipitation of PO_4^{3-} on sediment might also promote the formation of negatively charged surface sites, which reduces the surface potential. Thus, reduces the *As*(V) adsorption capacity of the sediment through electrostatic repulsion.

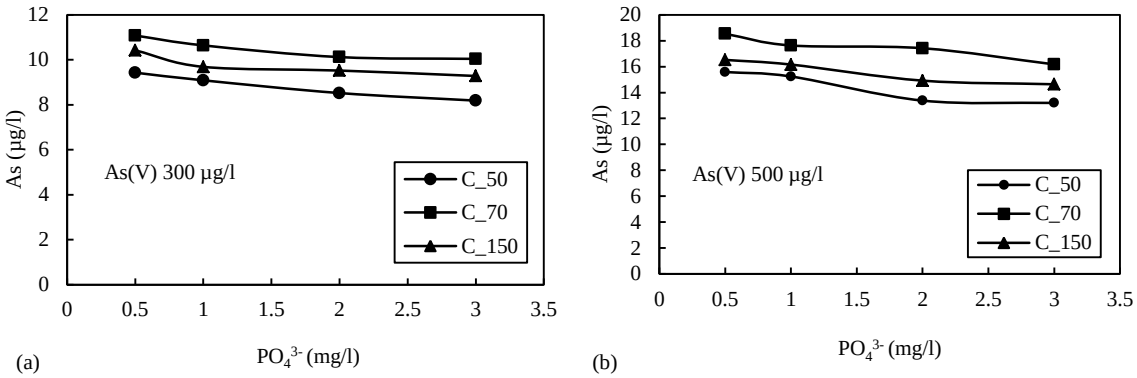

Figure 5.38 Effect of phosphate (P) on adsorption of *As*(V) with initial concentration of (a) 300 µg/l and (b) 500 µg/l for sediment samples.

5.3.2.3 Effect of Silica (SiO_2)

The competition of adsorption sites between *As* and silica has been reported in Bangladesh (Swartz et al., 2004) and Mexico (Miller, 2001). The effects of silica on the adsorption of *As*(V) was also studied by varying the silica concentration viz. 10, 20, 30 mg/l. The experimental results (Figure 5.39a,b) shows that silica has lesser effect on *As*(V) adsorption on the sediment sample. The reduction in the *As*(V) adsorption when silica concentration increases from 10 to 30 mg/l for initial *As*(V) 500 µg/l concentration were 10% for both C_50 and C_150, 7% for C_70 (Figure 5.39b) and with initial concentration of 300 µg/l these were 8% for C_50 and 4% for both C_70 and C_150 (Figure 5.39a).

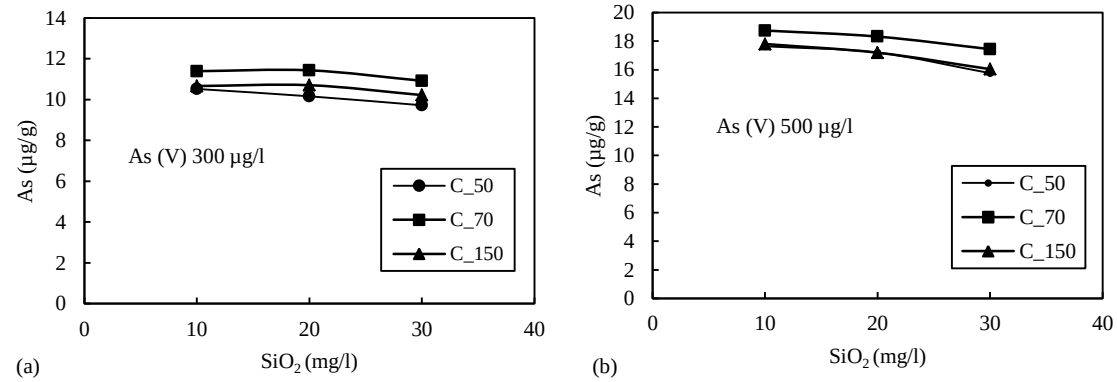

Figure 5.39 Effect of silica (SiO_2) on adsorption of *As*(V) with initial concentration of (a) 300 µg/l and (b) 500 µg/l for sediment samples.

5.3.2.4 Effect of Bicarbonate (HCO_3^-)

Bicarbonate is the most abundant constituent in groundwater from our study area. Since, in the shallow aquifer of Bangladesh, high arsenic concentration was attributed to HCO_3^- (Appelo et al., 2002; Anawar et al., 2004; Harvey et al., 2002, 2006). The effects of HCO_3^- concentration in the groundwater for *As*(V) adsorption have been investigated by increasing

the concentration of HCO_3^- from 200, 300, 400 and 500 mg/l (Figure 5.40a,b). The results showed that bicarbonate has lesser pronounced effect on the adsorption. About 5% decrease in adsorption was observed in the sediment with increased in the bicarbonate concentration, for initial *As*(V) concentrations of 300 µg/l (Figure 5.40a) and 500 µg/l (Figure 5.40b). The sources and distribution of HCO_3^- has already been mentioned (*Section 5.1.2.1-5.1.2.2*).

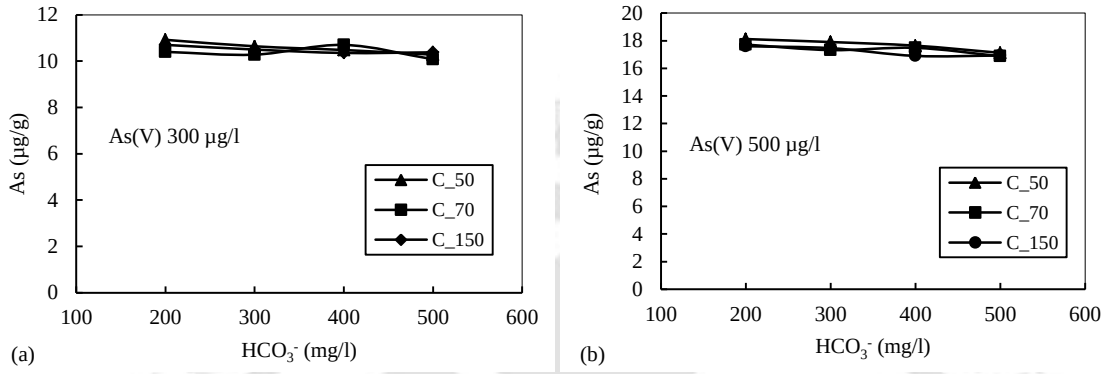

Figure 5.40 Effect of bicarbonate (HCO_3^-) on adsorption of *As*(V) with initial concentration of (a) 300 µg/l and (b) 500 µg/l for sediment samples.

5.3.2.5 Combined anions effect

The competitive nature of anions present in the groundwater was tested using a solution that could closely simulate the actual groundwater conditions in the Site_1. In addition to the cation concentrations, the concentration of major anions viz. HCO_3^- = 250 mg/l, SiO_2 = 15 mg/l were also included. The concentration of PO_4^{3-}, which has highest effect on the adsorption capacity, was varied from 0.5 mg/l to 3 mg/l. The competition of adsorption sites for *As* with other anions has been shown (Figure 5.41a,b). The decrease in the adsorption capacities observed for initial *As*(V) 500 µg/l were 22%, 18% and 15% for the samples C_50, C_70 and C_150 respectively (Figure 5.41b) and *As*(V) 300 µg/l initial concentration were 31%, 26% and 18% respectively (Figure 5.41b) due to the competitive anions.

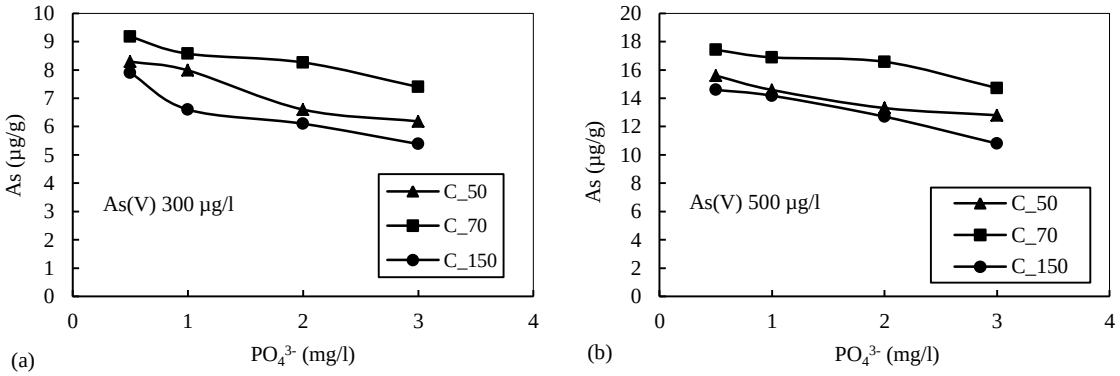

Figure 5.41 Combined effect of anions on adsorption of *As*(V) with initial concentration of (a) 300 µg/l and (b) 500 µg/l for sediment samples with increasing phosphate (PO_4^{3-}).

Batch adsorption study revealed that both *As*(III) and *As*(V) were adsorbed by the sediment samples at circum-neutral pH. *As*(V) exhibited higher adsorption than *As*(III). The minor reduction in adsorption of *As*(V) with increasing pH (6 to 8.5) suggested electrostatic repulsion due to soil surface charge density. The sediment sample C_70 demonstrated highest *As* adsorption capacity, as this sample had highest Fe and Mn content. PO_4^{3-} was found to have highest competition with *As*(V) adsorption on the reduced sediment (C_50) as well as moderate sediment (C_150) and showed lesser effects on oxidized sediment (C_70). The competition of adsorption sites for the anions considered generally followed the order $PO_4^{3-} > SiO_2 > HCO_3^-$. The combined effects of anions showed highest reduction in the adsorption capacities of the sediment samples.

5.3.3 Oxidation of As(III) to As(V)

The sediments from the study areas contain a range of reactive functional groups that originate from the mixture of mineral phases and their surface coatings. The surface coatings were generally comprised of Fe, Al and Si, with lesser amounts of Mn as can be seen from the SEM/EDX, likely in the form of Fe(III) hydroxides, Al hydroxides and silicates, and Mn oxides (*Section 5.2.1.5*). From the batch experimental study, it was found that the sediments can adsorb *As*(III) and *As*(V) (*Section 5.3.3*). Therefore, it was necessary to quantify redox speciation of arsenic in both dissolved and solid phases. The characteristics of the sediment samples viz. C_50, C_70 and C_150 were given in Table 5.10.

The oxidation kinetics of *As*(III) for initial concentration of 500 µg/l and 300 µg/l for three different types of sediments namely C_50, C_70 and C_150 are shown in Figure 5.42-5.44. The sediment sample C_50 shows that the removal of aqueous *As*(III) was very low for initial concentration of 500 µg/l and 300 µg/l. It can be seen (5.42a,b) that the greater aqueous *As*(III) removal (25%) from the solution takes place via adsorption (higher solid *As*(III)) and lesser amount (16%) in oxidation of *As*(III) to *As*(V), which is in the form of solid *As*(V) in the sediment. At lower initial concentration of 300 µg/l, the aqueous *As*(III) removal is higher from the solution, where adsorption and oxidation both form almost equal removal of about 23% from the solution.

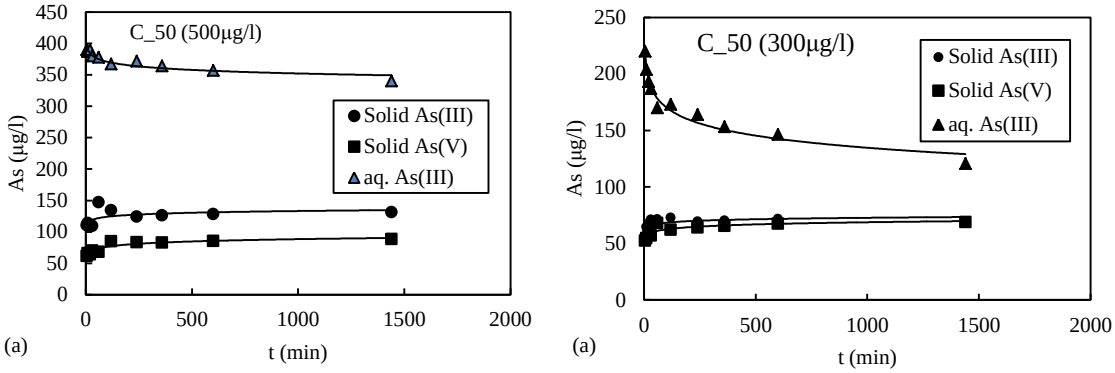

Figure 5.42 Oxidation kinetics of *As*(III) for soil sample C_50 for initial *As*(III) concentration of (a) 500 µg/l and (b) 300 µg/l.

The oxidized sediment sample C_70 have highest capacity to oxidize *As*(III) to *As*(V). The decrease in aqueous *As*(III) concentration with time (Figure 5.43a,b) was caused by a combination of oxidation and adsorption. The sediment of this zone has high concentration of Fe and Mn (Table 5.10). The Fe-oxides (amorphous and crystalline) have high affinity for *As* sorption (Manning and Goldberg, 1996; Smedley and Kinniburgh, 2002; Dixit and Hering 2003; Arai et al., 2005). The aqueous *As*(III) removal from the solution was found to be highest among the sediment samples tested. It was observed that oxidation as compared to adsorption, was clearly the dominant mechanism for aqueous *As*(III) removal. From sample C_70 with an initial concentration of 500 µg/l and 300 µg/l of *As*(III), about 40% and 60% respectively was removed via oxidation of *As*(III) to *As*(V) while 30% and 33% through adsorption onto the sediment samples respectively.

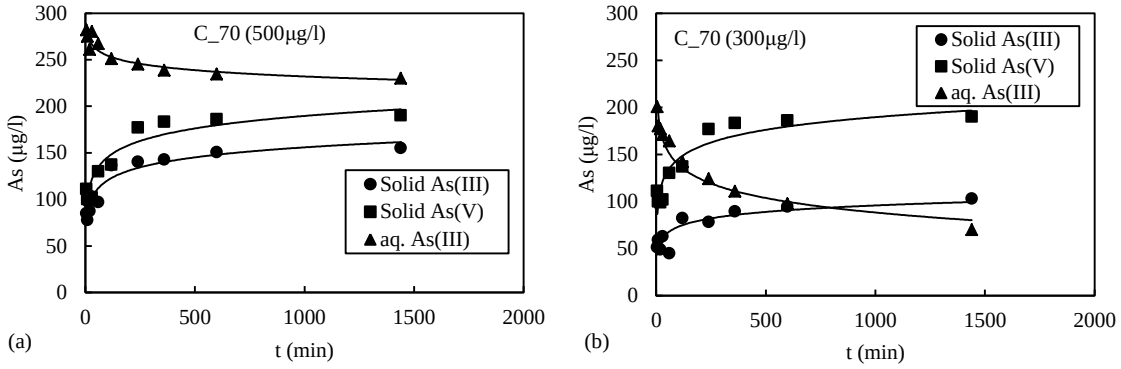

Figure 5.43 Oxidation kinetics of *As*(III) for soil sample C_70 for initial *As*(III) concentration of (a) 500 µg/l and (b) 300 µg/l.

The sediment sample C_150 has moderate Fe and Mn concentration. The removal mechanism of *As*(III) from solution is shown (Figure 5.44a,b). Sediment sample C_150 was

found to have highest aqueous *As*(III) removal via oxidation and lower amount of adsorption. For an initial *As*(III) concentration of 500 µg/l and 300 µg/l, the oxidation of *As*(III) to *As*(V) accounted to 30% and 27% whereas the adsorption of *As*(III) onto the aquifer material accounted to 15% and 23% respectively.

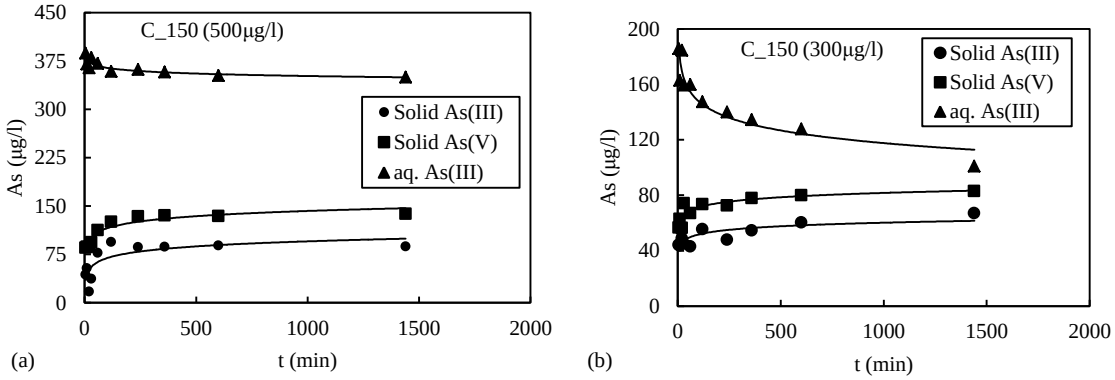

Figure 5.44 Oxidation kinetics of *As*(III) for soil sample C_150 for initial *As*(III) concentrations of (a) 500 µg/l and (b) 300 µg/l.

It is clear from the various plots (Figure 5.42-5.44) that *As* displayed varying transformation rates depending on the aquifer material. The disappearance of the aqueous *As*(III) and formation of solid *As*(V) and solid *As*(III) were highest for soil sample C_70. Slower kinetics with higher aqueous *As*(III) was found in C_50 sediment sample. C_150 sediment sample showed higher oxidation in solid phase via oxidation site and lesser direct adsorption on adsorption site as solid *As*(III). The oxidation kinetics reaches steady state before 600 minutes in all the samples and 80% of total aqueous *As*(III) was achieved at the initial 30 minutes of the experiment.

Mass balance of arsenic species was achieved as a summation of solid-phase *As*(III) and *As*(V) concentrations and total aqueous *As*(III) concentration. In all the samples, mass balance was within ± 15% of the initial *As*(III) concentration. This suggested that 15 minutes of 0.2M oxalic acid extraction is an effective method for desorption of *As* species from aquifer materials (Amirbahman et al, 2006; Stollenwerk et al., 2007). Oxidation of *As*(III) to *As*(V) by Mn-oxides in natural sediments have been reported (Amirbahman et al, 2006; Stollenwerk et al., 2007; Han et al., 2011). Tournassat et al. (2002) attributed differences in *As*(III) oxidation rate to the degree of crystallinity and structure of manganese minerals. Geochemical modeling software PHREEQC indicated that oxidation of *As*(III) by Fe(III)aq and amorphous ferric hydroxide ($Fe(OH)_3$ (aq)) is thermodynamically favorable. However,

As(III) is predicted to be more stable in presence of more crystalline Fe-oxides and found no evidence of oxidation by either $Fe(III)_{aq}$, ferrihydrite or goethite (Manning et al., 1998).

5.3.3.1 Conceptual model for arsenic-surface interaction

The kinetics of aqueous *As*(III) removal by the aquifer materials does not show simple first-order kinetics (*Section 5.3.1*) similar to the previous observations (Chui and Hering, 2000; Amirbahman et al., 2006; Sahabi et al., 2009). Conceptually, this suggests that *As*(III) removal and oxidation by aquifer material may be understood as a multi-step surface process involving the following steps (Amirbahman et al., 2006; Sahabi et al., 2009):

1) Transport of *As*(III) to the surface,
2) *As*(III) adsorption onto the surface sites,
3) Oxidation of *As*(III) to *As*(V) at the surface,
4) Release of produced *As*(V) from the surface,
5) *As*(V) adsorption to other surface sites following its production and release into solution.

Alternatively, outer-sphere electron transfer may occur between oxidative sites and *As*(III) through their respective coordination sheaths (Amirbahman et al., 2006). Adsorption of *As*(III) involves the displacement of surface-bound OH^- and H_2O species via a ligand exchange mechanism, whereby the *As*(III) anion forms an inner-sphere complex at the mineral surface (Manning et al., 1998; Nesbitt et al., 1998; Arai et al., 2001). The surface spectroscopic and proton balance studies indicated that *As*(III) oxidation via birnessite (MnO_2) proceeds via a two steps (Eq. 2.27 and 2.28) in reduction of Mn(IV) to intermediate Mn(III) followed by further reduction to Mn^{2+} (Nesbitt et al., 1998; Tounassat et al., 2002).

Further, some fraction of Mn(III)/(IV) may reside in Mn-substituted goethite (Appelo and Postma, 1999). The actual composition and crystal structure of MnO_2 in these sediment is unknown; Mn-oxides in natural systems are often complex minerals characterized by poor crystallinity and mixed oxidation state (Appelo and postma, 1999; Postma and Appelo, 2000). Oxidation of *As*(III) was assumed to take place via reduction of MnO_2 (Oscarson et al., 1981; Stollenwerk et al., 2007; Sahabi et al., 2009):

$$MnO_2 + H_3AsO_3 + H^+ \rightarrow Mn^{2+} + H_2AsO_4^- + H_2O \qquad (5.7)$$

The stoichiometry of the MnO_2 reduction (Eq. 5.7) could not be confirmed because of re-adsorption of Mn^{2+} and the buffering capacity of sediment with respect to H^+ (Amirbahman et al., 2006; Stollenwerk et al., 2007; Sahabi et al., 2009). The dissolved Mn^{2+} concentrations were low as reported from experimental studies with synthetic Mn(IV), that dissolved Mn(II) remained very low at pH values above approx. 5.8 (Scott and Morgan, 1995). These suggested that the released Mn^{2+} ions adsorb to MnO_2 and other constituents of the solid material is extensive. This resulted in positive charges on the surface of the MnO_2 leading to enhanced arsenate adsorption (Sahabi et al., 2009).

As(III) oxidation theory proposed by Manning et al (2002) on synthetic birnessite (MnO_2) was used. It was assumed that surface manganese oxides are directly involved in the redox reaction between *As*(III) and sediment samples, the adsorptive sites and oxidative sites can be represented by the generic terms SOH and SMnOOH respectively. SOH represents different surface sites of varying affinity for arsenic such as Fe oxides, organic matter and solvated cations such as Ca^{2+}; and SMnOOH represents manganese-oxides rich binding sites bearing a surface manganese oxide molecule. The simple non-stoichiometric equations can be written as (Oscarson et al., 1981; Amirbahman et al, 2006; Sahabi et al., 2009) follows:

$$S - OH + H_3AsO_3 \overset{weak\ oxidant}{\longleftrightarrow} S - OAsO_2H_2 + H_2O \qquad (5.8)$$

$$S - O - Mn - OH + H_3AsO_3 \overset{strong\ oxidant}{\longleftrightarrow} S - O - MnOAsO_2H_2 + H_2O \qquad (5.9)$$

A schematic representation of multi-step reaction of *As*(III) with MnO_2 proposed from previous studies (Oscarson et al., 1981; Tounassat et al., 2002; Amirbahman et al, 2006; Sahabi et al., 2009; Han et al., 2011) was developed (Figure 5.45). Due to the nearly equilibrium of the solid *As*(V) produced via oxidation (Figure 5.42-5.44), the proposed conceptual model does not consider the regeneration of the oxidative surface sites. This was supported by the fact that the produced Mn^{2+} remains associated with the MnO_2 surface (Scott and Morgan, 1995) to significant extent, which would mask the surface sites for further reaction (Amirbahman et al., 2006). Spectroscopic studies revealed that some *As*(V) may also remain on the Mn-oxides surface following its production (Manning et al., 2002; Deschamps et al., 2005). A schematic Figure 5.45 showed the conceptual mutli-step redox reaction for the oxidation of *As*(III).

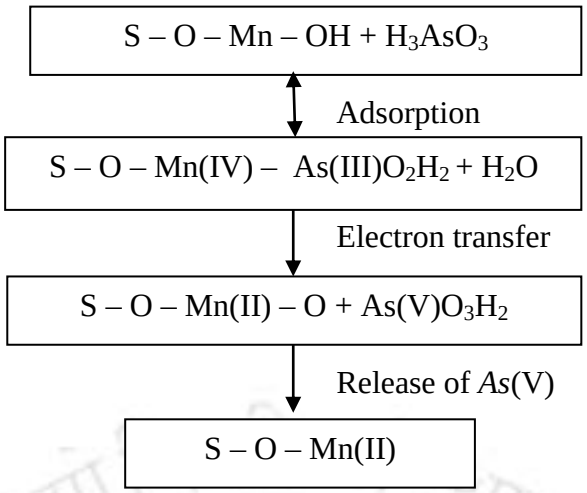

Figure 5.45 Schematic showing multi-steps redox reaction between *As*(III) and Manganese oxides on the surface of sediments.

Step 1 The fraction of *As*(III) was directly adsorbed to the sediments and some fraction diffused to the coating of MnO_2 for oxidation.

Step 2 The diffused *As*(III) gets oxidized to *As*(V) by MnO_2.

Step 3 The oxidized *As*(V) diffused out of the coating and released into the solution. The newly produced *As*(V) could be readsorbed onto the surface of sediments containing Fe-oxides.

The *As*(V) released from the surface of the oxidative site may get readsorbed onto the surface of sediment containing Fe-oxides (Stuben et al., 2003; Buschmann et al., 2007; Berg et al., 2008). The oxidized ferric Fe^{3+} forms a surface coating primarily as ferrihydrite and secondarily as jacobsite ($MnFe_2O_4$) on MnO_2 preventing further oxidation, such a coating may also inhibit the oxidation of *As*(III) and organic matter (Han et al., 2011).

Thus, the oxidation of *As*(III) via MnO_2 is one the most effective pathways to reduce the toxicity as well as mobility of *As* in the subsurface environment. Therefore, targeting oxidized sediment with high concentration of Fe-oxides and Mn-oxides might make natural attenuation of *As* viable in the study areas.

5.3.4 Surface Complexation Model (SCM)

The adsorption of *As* on the sediments was simulated as surface complexation reactions on oxides of iron using Diffuse Layer Model (DLM) of Dzombak and Morrel (1990). The equilibrium surface complexation model (SCM) of PHREEQC (Parkhurst and Appelo, 1999) was used to predict the differences between sorbed *As* on Hfo (Hydroferric oxides) phases as well as goethite (more crystalline phase), which were derived from the selective sequential extraction (SSE) data and the modeled simulations.The model was run using *As* data extracted from SSE which targets the amorphous Fe-oxides and more crystalline Fe-oxides. Therefore, the mineral phases were quantified using the operationally defined wet-chemical extractions for determining Hydroferric oxides (Hfo) surface population on the sediment (Swartz et al., 2004; Stollenwerk et al., 2007; Sharif et al., 2011; Robinson et al., 2011). The Hfo surfaces were defined as individual components of a multicomponent site distribution derived from the SSE results. The concentration of iron in the sediments targeting the two phases (ferrihydrite and goethite) were used to back-calculate the amount of Hfo that was present on the surface of the sediment grains shown in Table 5.18-5.19. Rather than truly defining the surface area of the available mineral phases, the extraction and subsequent calculations estimate the potential number of sorption site forming metal atoms (Miller, 2001).The amount of observed arsenic from the SCM of PHREEQC was compared with the arsenic concentration from the same extraction step. The best fit models were those that provide results that are internally consistent with the ratios of arsenic and Hfo forming elements found in the extractions. The SCM modeling was carried out with DLM option and it was assumed that the system was in chemical equilibrium.

Table 5.18 Input parameters for PHREEQC surface complexation model in amorphous Fe-oxides for surface site densities (mol sites/mol Fe) for sample 1A.

Sl. no.	Sample Id	Depth m	Amor. Fe(mg/kg)	Ferrihydrite g/kg	HFO_ w	HFO_s	Goe_
1	1A -10	3	5000	33.38	7.50E-02	1.88E-03	5.57E-03
2	1A -30	9	2885	19.26	4.33E-02	1.08E-03	3.22E-03
3	1A -50	15	1890	12.62	2.84E-02	7.09E-04	2.11E-03
4	1A -70	21	930	6.21	1.40E-02	3.49E-04	1.04E-03
5	1A -90	27	1595	10.65	2.39E-02	5.98E-04	1.78E-03
6	1A -110	33	1510	10.08	2.27E-02	5.66E-04	1.68E-03
7	1A -130	40	1310	8.74	1.97E-02	4.91E-04	1.46E-03
8	1A -150	46	1965	13.12	2.95E-02	7.37E-04	2.19E-03

Table 5.19 Input parameters for PHREEQC surface complexation model in crystalline Fe-oxides for surface site densities (mol sites/mol Fe) for sample 1A.

Sl. no.	Sample Id	Depth m	Cryst. Fe (mg/kg)	Ferrihydrite g/kg	HFO_ w	HFO_s	Goe_
1	1A -10	3	22000	146.85	3.30E-01	8.25E-03	2.45E-02
2	1A -30	9	6040	40.32	9.06E-02	2.27E-03	6.73E-03
3	1A -50	15	3710	24.76	5.57E-02	1.39E-03	4.14E-03
4	1A -70	21	1650	11.01	2.48E-02	6.19E-04	1.84E-03
5	1A -90	27	4770	31.84	7.16E-02	1.79E-03	5.32E-03
6	1A -110	33	2160	14.42	3.24E-02	8.10E-04	2.41E-03
7	1A -130	40	1225	8.18	1.84E-02	4.59E-04	1.37E-03
8	1A -150	46	3945	26.33	5.92E-02	1.48E-03	4.40E-03

The fractionation of Fe has already been explained (*Section 5.2.3*). High concentrations of amorphous as well as crystalline Fe-oxides were found in the sediment from the study area. The amorphous Fe concentrations were much higher comparing that of Bangladesh which is about 10 times approx. (Robinson et al., 2011) and in Arkansas, USA (Sharif et al., 2011). Considering 10% of the analyzed amorphous and more crystalline Fe (viz. ferrihydrite and goethite) has a surface property of Hfo. Since, the adsorption isotherm simulation with the PHREEQC highly over-predicted the adsorption of *As* onto the sediments, therefore the assumption of amorphous and crystalline Fe oxides possessing a 10% Hfo surface complexation property was justified.

As extracted in SSE step, which targets the amorphous and crystalline Fe-oxides, has good correlation with the extracted Fe (*Section 5.2.3*). The surface composition of the sediments was simulated in PHREEQC using the mean groundwater chemistry from the target tubewell-1 and tubewell-2. The model was run with the amount of ferrihydrite and goethite sorption sites available (Table 5.18-5.19) calculated from SSE. The reactions and thermodynamic constants for PHREEQC surface complexation model (Table 4.4-4.5) with Hfo_s (ferrihydrite_strong sites), Hfo_w (ferryhydrite_weak sites) and Goe_ (goethite single site) was used in the simulation.

The model results (Table 5.20-5.21) were found to be satisfactory when high Fe content sediments are curtailed from the samples. No depth profile changes between the modeled and extracted *As* was observed. The model output was very sensitive to the sediment type and the extraction methods used, which was used in the quantification of mineral phase and their surface site density and sorption intensity (Miller, 2001; Sharif et al., 2011; Robinson et al.,

2011). The model was very sensitive to groundwater composition with respect to which sorption with other ions (Alkalinity, PO_4^{3-}, Fe^{2+}) on reactive surface sites of sorbent occurs.

The discrepancies between the simulated and extracted *As* may be attributed to varying water chemistry at the specific location from where the sediment sample was collected and/or influence of other amorphous adsorbing phases including Mn(IV) oxides which was not considered. The reasonable match between the experimental and simulated data suggests that the competitive adsorption of *As* with ions PO_4^{3-}, CO_3^{2-}, Ca^{2+}, Mg^{2+} and Fe is well represented by the surface reactions and parameter values adopted (Table 4.5).

The saturation indices calculated from PHREEQC indicated that the sediments were supersaturated with respect Fe minerals viz. ferrihydrite ($Fe(OH)_3$), goethite ($FeO(OH)$), Magnetite (Fe_3O_4), siderite ($FeCO_3$) and vivianite ($Fe_3(PO_4)_2.8H_2O$). Therefore, the precipitation of the above mentioned minerals phases were anticipated and thus they increases the availability of adsorption sites and resulting in over-prediction of adsorption of *As*.

Table 5.20 Model output using *As* extracted from amorphous Fe-oxides for sample 1A.

Sl. no.	Sample Id	Extracted_*As*	Model_*As*	Difference (%) between Extracted and Modeled *As*
1	1A -10	2.1	1.6	23.8
2	1A -30	1.5	0.93	38.0
3	1A -50	1.47	0.61	58.5
4	1A -70	1.24	0.3	75.8
5	1A -90	1.57	0.5	68.2
6	1A -110	1.2	0.49	59.2
7	1A -130	1.7	0.42	75.3
8	1A -150	1.2	0.63	47.5

Table 5.21 Model output using *As* extracted from crystalline Fe-oxides for sample 1A.

Sl. no.	Sample Id	Extracted_*As*	Model_*As*	Difference (%) between Extracted and Modeled *As*
1	1A -10	6.24	11.63	-86.38
2	1A -30	3.05	3.19	-4.59
3	1A -50	2.1	1.9	9.52
4	1A -70	3.12	0.87	72.12
5	1A -90	2	2.53	-26.50
6	1A -110	1.2	1.14	5.00
7	1A -130	0.87	0.65	25.29
8	1A -150	1.67	2.1	-25.75

The model output was sensitive to the groundwater *As* concentration and other competing ions present in the groundwater. The output of SCM models shows that approx. 98% of the reactive sites are occupied with HCO_3^-, PO_4^{3-}, CO_3^{2-}, Ca^{2+}, Fe^{2+} and Mn^{2+}. The relative composition of the surface complex calculated from SCM for the aquifer sediment is shown in pie diagram (Figure 5.46). The Hfo_s (ferrihydrite_strong sites) shows negligible (~ 0.3%) adsorption of *As*. The weak adsorption sites (Hfo_w) are dominated by carbonate species (~ 55%), silica species (~ 14.7%), phosphate (~ 13%), OH_2^+ (~ 12%). *As* occupies about 1.3% surface sites. In comparing the surface composition of Bangladesh aquifer sediment, Swartz et al. (2004) reported the dominance of silica species (56%), carbonates (28%) and 6% of *As*(III). While Postma et al. (2007) calculated the surface composition of Vietnam aquifer sediment, and reported the dominance of carbonate species (48%), silica species (31%) and *As*(III) (~3%) of surface sites.

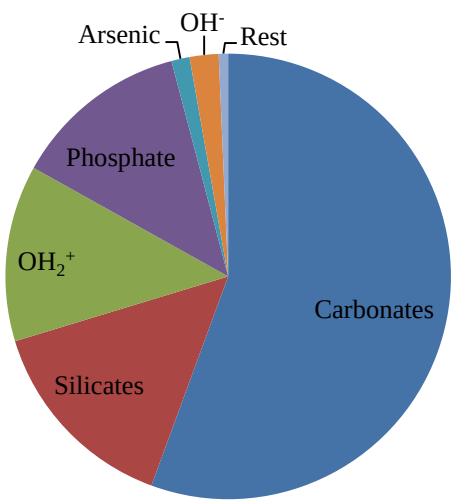

Figure 5.46 The relative composition of Surface complex calculated from the composition of groundwater quality of Site_1 using PHREEQC.

Thus, the concentration of these competing ions in the groundwater along with their respective thermodynamic constants plays an important role in limiting the complexation of *As* onto Hfo surfaces. The results indicate that the error due to neglecting competition of anions can be large. The magnitude of variation of percentage difference between modeled and observed *As* (Table 5.20-5.21) suggested that SCM could be used to predict the *As* sorbed onto the sediments satisfactorily. The model results showed that ferrihydrite phase (Hfo) have mean 51% and median 58%, and goethite phase model (Goe_) have mean 31% and median 26% of the percentage (%) difference between the model and the extracted *As*. There are

some discrepancies in the values of the intrinsic surface constants for the surfa1ce reactions of *As* related to HCO_3^-, H_4SiO_4, PO_4^{3-}, CO_3^{2-} and other ions in published references (Dzombak and Morel, 1990; Swedlund and Webster, 1999; Dixit and Hering, 2003, 2006; Wilkie and Hering, 1996). The selection of appropriate surface constants was critical because even a small change in the surface constant reaction for HCO_3^-, H_4SiO_4, PO_4^{3-}, CO_3^{2-} and other ions can produce a large difference in the model output.

The surface constants used in SCM model for simulating the metal ion adsorption on selected mineral phases (viz. ferrihydrite and goethite) are based on experimental datasets generated in simple electrolyte solutions, which is over simplistic compared to complex natural groundwater (Sharif et al., 2011). The adsorption of major ions and organic acids in natural waters is known to cause significant changes in the point-of-zero-charge and iso-charge point of mineral phases. The surface reactions used in the model are generated under different controlled environments in different laboratories, and under different electrolyte solutions. (Sharif et al., 2011). So, the surface reactions in the model are not truly applicable for complex electrolyte solution such as natural groundwaters. No evidence was found regarding the applicability of these surface reaction datasets under different redox conditions.

Thus, Surface Complexation Model (SCM) using Component Additivity (CA) predicted the arsenic distribution in the sediments from the surface-site densities, chemical extraction data, published sorbent-site densities from literatures, measured rock-water ratios and detailed chemical analysis of groundwater with two sorbent phases satisfactorily i.e. Ferrihydrite phase (Hfo_w and Hfo_s) and Goethite phase (Goe_).

Chapter 6

Summary and conclusions

Higher groundwater *As* concentration in parts of the alluvial plains of the Brahmaputra River of Assam state was evaluated by analyzing its hydrogeochemical conditions and sedimentary characteristics. High risk potential for toxicity as well as vulnerability of *As* contamination of the study areas were indicated to be of geogenic i.e. of natural origin.

Natural is believed to be derived from erosion of lithified sediments and crystalline rocks of Himalayan range or Tibetan Plateau, the eroded materials contains As bearing "primary minerals" transported by the large river systems of Brahmaputra. Yet, the specific sources of *As* could not be identified in the sediment phase. However, the mechanism of *As* mobilization could be reductive dissolution of Fe-oxides. The sinks of *As* in the sediment was recognized as the sediment from the alluvial plains containing Fe-oxide. The *As* sorbed on the Fe-oxides coatings of the sediments might have dissolved into the groundwater through complex biogeochemical conditions leading to reduced condition prevailing in the sub-surface, that subsequently produces *As* release and retardation mechanism in the aquifer.

217 groundwater samples were collected and analyzed for 20 water quality parameters. American Public Health Association (APHA, 1998) standard methods were used for the measurement of dissolved ion concentrations. In order to deduce the relationship between various water quality parameters analyzed and for identifying the patterns, multivariate statistical method i.e. Principal Component Analysis (PCA) was done using SPSS 17.0 statistical software package. The hydrochemical composition and saturation indices were calculated based upon the hydrochemical results with the PHREEQC program (Parkhurst and Appelo, 1999). Arsenic concentration in the Darrang district was with mean concentration of 20 µg/l, while Jorhat district had higher *As* concentration (mean ~ 100 µg/l). The groundwaters in these areas are characterized by high dissolved Fe, Mn, HCO_3^- and low concentrations of NO_3^- and SO_4^{2-}. The redox potential and the groundwater composition supported the reducing condition prevailing in the aquifers. The difference in the groundwater geochemistry from the two districts was noted to be mainly controlled by the redox condition in the subsurface. The hydrochemical conditions, minerals saturation and the redox environment suggested reductive dissolution of Fe-oxides as the dominant *As* releasing mechanism in both the study areas. Competition of adsorption sites by anions viz. PO_4^{3-} and

HCO_3^- to certain extent was also believed to be responsible for the release of *As* in some affected locations.

The sediment characteristics leading to the dissolution of *As* into the groundwater was studied by analyzing 13 drill core samples. The soil samples were analyzed for the chemical properties viz. pH, cation exchange capacity (CEC), organic matter content (Loss on Ignition method). The bulk mineralogy of the sediments, morphology, elemental composition and specific surface area (SSA) were determined using X-ray powder diffractometry (XRD), Scanning Electron Microscopy (SEM) and Energy Dispersive X-Ray (EDX) and laser particle size analyzer. Total metal concentrations of the sediments were analyzed using EPA-3052. The total *As* concentrations observed was not unusually higher than global normal range. The recovery of the Certified Reference Material (CRM) of Japanese Geological Survey JLk-1 and JSd-3 for *As* showed 97.3% and 106.5% respectively for the digestion procedure.

Sequential Selective Extraction (SSE) was used to assess *As* distribution into different chemical phases present in the sediments. As an internal check to SSE, mass balance was done by comparing the sum of concentrations for each step in the extraction divided by the total digestion of the trace metals. The *As* extracted by amorphous and crystalline Fe-oxides accounted for the highest fraction (32% to 50%) of total *As* extracted. High correlation was observed between the *As* extracted from Fe-oxides phases with the amount of Fe extracted in those phases (r^2: 0.4 – 0.9). The residual phase of *As* accounted for about 60% in the high contaminated areas of Site_1, while in the adjacent location (Site_2) with lower *As* groundwater (< 20 µg/l) had higher residual concentration fraction of 80%, i.e. the available *As* in natural environment is lesser than 20% of total *As* extracted. Since the total extracted *As* is not unusually high, dissolved *As* present in the groundwater may not be entirely due to the elevated total solid phase *As* concentrations in the sediments alone. The complex geochemical conditions causing higher reducing environment in the sub-surface i.e. redox, suboxic to anoxic condition as well as the hydro-geochemical condition that existed in the area must be favorable, which was found to be consistent with the mechanism of reductive dissolution of Fe-oxides via respiration of organic matter, thus releasing the associated adsorbed or co-precipitated *As*, as has been accepted in several other case studies.

To assess the attenuation processes in the sub-surface, batch experiment were conducted on three sediment soil samples collected from Site_1 drill-core 1C named as C_50, C_70 and C_150. The samples were characterized as: Reduced sediment (C_50) grayish colored with

low Fe and Mn, Oxidized sediment (C_70) brown colored with high Fe and Mn, Moderate sediment (C_150) ash-greenish colored with moderate Fe and Mn.

Arsenic removal kinetic tests for *As*(III) and *As*(V) by the sediment samples viz. C_50, C_70 and C_150 was carried under 50 ml polyethylene centrifuge tubes at room temperature (26 +/-2 ºC) with 1:20 soil/water ratio. About 80% of total *As* adsorption was observed at initial 30 minutes. Elovich adsorption kinetic model was found to be the best suitable kinetic model to describe the adsorption behavior of *As* on the sediment sample. Due to the heterogeneity of sediments with varying particle sizes, sorption sites and porosities promote transport processes; significant correlation was observed for intra-particle diffusion model. Thus, the adsorption mechanism suggested that the rate determining step was controlled by both surface sorption as well as intra-particle diffusion.

Batch experiments suggested that the sediment samples were able to adsorb *As*(V) and *As*(III) at circum-neutral pH, where the groundwater existed in the study area. Freundlich and Langmuir adsorption isotherm were fitted to the sorption experiment. Freundlich adsorption isotherm fits relatively better for both *As*(III) and *As*(V). The effect of increased in pH (6 to 8) resulted in minor reduction in adsorption of *As*(V) suggesting electrostatic repulsion due to soil surface charge density. The sediment sample C_70 demonstrated highest *As* adsorption capacity, as this sample had highest Fe and Mn content. PO_4^{3-} was found to have highest competition with *As*(V) adsorption on the reduced sediment (C_50) as well as moderate sediment (C_150) and showed lesser effects on oxidized sediment (C_70). The combined effects of anions showed highest reduction in the adsorption capacities of the sediment samples.

The oxidation of *As*(III) to *As*(V) by the sediment was studied as it not only decreased the toxicity of *As*, but also enhanced *As* removal from drinking water and sequestration to soils and sediments. The oxidized sediment (C_70) and moderate sediment (C_150) samples were found to have higher oxidation of aqueous *As*(III) on the oxidative site as solid *As*(V) than direct adsorption of aqueous *As*(III) as solid *As*(III). The reduced sediment sample (C_50) showed dominant adsorption of *As*(III) with lower amount of oxidation taking place. C_70 and C_150 had relatively higher Mn extractable and the oxidation of *As*(III) via MnO_2 is one the most effective pathway to reduce the toxicity as well as mobility of *As* in the subsurface environment.

The surface complexation model (SCM) using component additivity (CA) approach was used to predict solid phase *As* in the sediment samples. The equilibrium surface complexation model (SCM) of PHREEQC (Parkhurst and Appelo, 1999) with diffuse layer model (DLM) was used to predict the differences between sorbed *As* on ferrihydrite or hydrous ferric oxides (Hfo_ amorphous phases) as well as goethite (Goe_ more crystalline phase), which were derived from the selective sequential extraction (SSE) data and the modeled simulations. The reaction database for the model run were applied from published surface complex parameters including *As*(III) and *As*(V). The model output was expressed as the percentage difference between the extracted and modeled arsenic, where ferrihydrite phase (Hfo) model have mean 51% and median 58%, and goethite phase model (Goe_) have mean 31% and median 26%. The model was very sensitive to groundwater composition (i.e. HCO_3^-, PO_4^{3-}, SiO_2), which competes in sorption with other ions on reactive surface sites of sorbents. The relative composition of the surface complex calculated from SCM for the aquifer sediment shows that the Hfo_s (ferrihydrite_strong sites) showed negligible (~0.3%) adsorption of *As*. The Hfo_w (weak adsorption sites) are dominated by carbonate species (~55%), silica species (~14.7%), phosphate (~13%), OH_2^+ (~12%) and *As* occupies about 1.3% surface sites.

The major conclusions drawn from the study are:

- Groundwater geochemistry of the two study areas suggested strong reducing condition indicated lower redox potential (Eh) values validated by high concentration of HCO_3^-, Fe and low concentration of SO_4^{2-} and NO_3^-. The hydrogeochemical composition of the groundwater was characterized as Na-HCO_3 type, Ca-HCO_3 type to the transition zone of Ca-Na-HCO_3 type.
- Selective Sequential Extraction (SSE) demonstrated that reductive dissolution of Fe-oxides phase accounts for highest *As* extraction and substantial amount of *As* was extracted in specific sorption phase.
- The SSE, hydrogeochemical conditions, mineral saturation and the redox environment suggested reductive dissolution of Fe-oxides as the dominant *As* releasing mechanism in the study area. Competition of adsorption sites by anions viz. PO_4^{3-}, HCO_3^- and SiO_2 to certain extent might be responsible for the release of *As* in some affected areas.

- The total sediment *As* concentration from sediment digestion process was found to be in the range 6.5 mg/kg to 45 mg/kg with a mean of 14.5 mg/kg, which is comparable to global normal range. The amount of extractable *As* fractions (%) of the sediment in the selective sequential extraction (SSE) plays a major role in the enrichment of *As* in the groundwater.
- The batch attenuation kinetics study on sediment samples revealed that the main *As* adsorption mechanism takes place through chemisorption, and fitted well for the Elovich kinetic model. The rate determining step was found to be controlled by both surface sorption as well as intra-particle diffusion.
- The batch adsorption study showed that the oxidized sediment (C_70) sample had the highest *As* adsorption capacity with lesser effect of competing anions viz. PO_4^{3-}, HCO^{3-} and Si (silica). The reduced sediment (C_50) sample had lowest *As* adsorption capacity and high reduction in adsorption due to competitive anions. The competition of adsorption sites for the anions considered generally followed the order $PO_4^{3-} > SiO_2 > HCO_3^-$.
- The oxidation of *As*(III) to *As*(V) experiment showed that aqueous *As*(III) oxidation to solid *As*(V) in the oxidative sites of the sediments was the dominant *As* removal mechanism for oxidized sediment (C_70) and moderate sediment (C_150). The direct adsorption of aqueous *As*(III) on the adsorptive sites as solid *As*(III) was main process of *As* removal for reduced sediment sample C_50.
- A Surface Complexation Model (SCM) using Component Additivity (CA) predicted the arsenic distribution from surface-site densities, chemical extraction data, published sorbent-site densities, measured rock-water ratios and detailed chemical analysis of groundwater using two phases i.e. Ferrihydrite phase (Hfo_) and Goethite phase (Goe_) to a reasonable degree of satisfaction considering the complexities involved with such natural processes.

The findings of the study can be used for exploring integrated mitigation strategy for *As* contamination of groundwater e.g. through targeting oxidizing sediments by placing well screen at specific depths or to target specific aquifers with *As* free sediment architecture (low extractable fraction of *As* from SSE) to obtain *As* safe drinking water for rural communities. The findings suggested that natural aquifer materials might make natural attenuation of *As* viable.

References

1. Acharyya, S.K., Chakraborty, P., Lahiri, S., Raymahashay B.C., Guha, S., Bhowmick, A., 1999. As poisoning in the Ganges delta. *Nature* 401, 545-546.
2. Ahmann, D., Krumholz, L.R., Hemond, H.F., Lovley, D.R., Morel, F.M.M., 1997. Microbial mobilization of arsenic from sediments of the Aberjona watershed. *Environment Science and Technology* 31, 2923–30.
3. Ahmed, K.M., Bhattacharya, P., Hasan, M.A., Akhter, S.H., Alam, S.M.M., Bhuyian, M.A.H., 2004. Arsenic enrichment in groundwater of alluvial aquifers in Bangladesh: an overview. *Applied Geochemistry* 19, 181–200.
4. Ali, M.A., Dzombak, D.A., 1996. Interaction of copper, organic acid, and sulfate in goethite suspensions. *Geochimica et Cosmochimica Acta* 60, 5045–5053.
5. Allard, B., Hakanson. K., Karlson, S., 1986. The importance of sorption phenomena in relation to trace element speciation and mobility. *In speciation of metals in Water Sediment and Soil Systems*; Proceedings of an International Workshop. Sunne 15-16 October, 1986. Edited by L. Lander, New York: Springer-Verlag, 141-153.
6. Allison, J.D., Brown, D.S., Novo-Gradac, K.J., 1990. MINTEQA2/PRODEFA2 – A Geochemical Assessment Model for Environmental Systems. US Environmental Protection Agency, Athens, Georgia.
7. Amirbahman, A., Kent, D. B., Curtis, G. P., Davis, J. A., 2006. Kinetics of sorption and abiotic oxidation of arsenic(III) by aquifer materials. *Geochimica et Cosmochimica Acta* 70, 533–547.
8. Anawar, H.M., Akai, J., Komaki, K., Terao, H., Yoshioka, T., Ishizuka, T., Safiullah, S., Kato, K., 2003. Geochemical occurrences of arsenic in groundwater of Bangladesh: sources and mobilization processes. *Journal of Geochemical Exploration* 77, 109–131.
9. Anawar, H.M., Akai, J., Sakugawa, H., 2004. Mobilization of arsenic from subsurface sediments by effect of bicarbonate ions in groundwater. *Chemosphere*, 54, 753–762.
10. Andrea, M.O., 1980. Arsenic in rain and the atmospheric balance of arsenic. *Journal of Geophysical Research* 85, 4512-4518.
11. Anschutz, P., Dedieu, K., Desmazes, F., Chaillou, G., 2005. Speciation, oxidation state, and reactivity of particulate manganese in marine sediments. *Chemical Geology* 218, 265-279.
12. APHA, 1998. *Standard Methods for the Examination of Water and Wastewater*. American Public Health Association, Washington, D.C.
13. Appelo, C.A.J., Postma, D., 1999. A consistent model for surface complexation on birnessite (MnO_2) and its application to a column experiment. *Geochimica et Cosmochimica Acta* 63, 3039-3048.
14. Appelo, C.A.J., Postma, D., 2005. *Geochemistry, Groundwater and Pollution.* Balkema, Rotterdam.
15. Appelo, C.A.J., Van-Der-Weiden, M.J.J., Tournassat, C., Charlet, L., 2002. Surface complexation of ferrous iron and carbonate on ferrihydrite and the mobilization of arsenic. *Environmental Science and Technology* 36, 3096–3103.
16. Arai, Y., Elzinga, E.J., Sparks, D.L., 2001. X-ray absorption spectroscopic investigation of arsenite and arsenate adsorption at the aluminum oxide–water interface. *Journal of Colloid and Interface Science* 235, 80–88.
17. Arai, Y., Sparks, D.L., Davis, J.A., 2005. Arsenate adsorption mechanisms at the allophane–water interface. *Environmental Science and Technology*, 39, 2537–2544.
18. ARSAC, 1990a. *District report on Hydrogeomorphological studies, Darrang District, Assam*. Assam Remote Sensing Application Centre (ARSAC), Assam Science Technology & Environment Council.

19. ARSAC, 1990b. *District report on Hydrogeomorphological studies, Jorhat District, Assam*. Assam Remote Sensing Application Centre (ARSAC), Assam Science Technology & Environment Council.
20. Azeue, J.M. and Nriagu, J.O. 1995. Impact of abandoned mine tailing on the arsenic concentrations in Moira Lake, Ontario. *Journal of Geochemical Exploration* 52, 81-89.
21. Baig, J.A., Kazi, T.G., Arain, M.B., Afridi, H.I., Kandhro, G.A., Sarfraz, R.A., Jamal, M.K., Shah, A.Q., 2008. Evaluation of arsenic and other physic-chemical parameters of surface and groundwater of Jamshoro, Pakistan. *Journal of Hazardous Materials* 166, 662-669.
22. Baig, J.A., Kazi, T.G., Arain, M.B., Shah, A.Q., Sarfraz, R.A., Afridi, H.I., Kandhro, G.A., Jamali, M.K., Khan, S., 2009. Arsenic fractionation in sediments of different origins using BCR sequential and single extraction methods. *Journal of Hazardous Materials* 167, 745-751.
23. Barrachina, C.A., Carbonell, F.B., Beneyto, M.J., 1996. Kinetics of arsenite sorption and desorption in Spanish soils. *Communications in Soil Science and Plant Analysis* 27, 3101-3107.
24. Bardelli, F., Benvenuti, M., Costagliola, P., Benedetto, F.D., Lattanzi, P., Meneghini, C., Romanelli, M., Valenzano, L., 2011. Arsenic uptake by natural calcite: An XAS study. *Geochimica et Cosmochimica Acta* 75, 3011-3023.
25. Barringer, J.L., Bonin, J.L., Deluca, M.J,, Romagna, T., Cenno, K., Alebus, M., Kratzer, T., Hirst, B., 2007. Sources and temporal dynamics of arsenic in a New Jersey watershed, USA. *Science of the Total Environment* 379, 56-74.
26. Baruah, N.G., Borkakoty, P.K., 2003. *Soil tillage required for rain-fed rice production system*. National Agricultural Technology Project, ICAR New Delhi and Regional Agricultural Research Station, Titabor, Assam.
27. Bauer, M., Blodau, C., 2006. Mobilization of arsenic by dissolved organic matter from iron oxides, soils and sediments. *Science of the Total Environment* 354, 179–190.
28. Belzile, N., 1988. The fate of arsenic in sediments of the Laurentian Trough. *Geochimica et Cosmochimica Acta,* 52, 2293–2302.
29. Berg, M., Tran, H.C., Nguyen, T.C., Pham, H.V., Schertenleib, R., Giger, W., 2001. Arsenic contamination of groundwater and drinking water in Vietnam: a human health threat. *Environmental Science and Technology* 35, 2621–2626.
30. Berg ,M., Stengel, C., Trang, P.T.K., Viet, P.H., Sampson, M.L., Leng, M., 2007. Magnitude of arsenic pollution in the Mekong and Red River Deltas — Cambodia and Vietnam. *Science of the Total Environment* 372, 413–25.
31. Berg, M., Trang, P.T.K., Stengel, C., Buschmann, J., Viet, P.H., Dan, N.V., Giger, W., Stuben, D., 2008. Hydrological and Sedimentary controls leading to arsenic contamination of groundwater in the Hanoi area, Vietnam: The impact of iron-arsenic ratios, peat, river bank deposits and excessive groundwater abstraction. *Chemical geology* 249, 91-112.
32. Bhattacharya, P., Chatterjee, D., Jacks, G., 1997. Occurrence of arsenic contaminated groundwater in alluvial aquifers from Delta plains, Eastern India: options for safe drinking water supply. *Water Resource Development* 13, 79–92.
33. Bhattacharya, P., Jacks, G., Ahmed, K.M., Routh, J., Khan, A.A., 2002. Arsenic in groundwater of the Bengal delta plain aquifers in Bangladesh. *Bulletin of Environmental Contaminant Toxicology* 69, 538–45.
34. Bhattacharya, P., Claesson, M., Bundschuh, J., Sracek, O., Fagerberg, J., Jacks, G., 2006 Distribution and mobility of arsenic in the Rio Dulce alluvial aquifers in Santiago del Estero Province, Argentina. *Science of the Total Environment* 358, 97–120.
35. Bhattacharya, P., Welch, A.H., Stollenwerk, K.G., McLauhlin, M.J., Bundschuh, J., Panaullah, G., 2007. Arsenic in the environment: Biology and Chemistry. *Science of the Total Environment* 379, 109-120.
36. Bora, K., Chetia, M., Singh, S.K., 2008. Groundwater arsenic contamination in three blocks of Golaghat district of Assam. *Journal of Indian Water Works Association* 40, 150-154.

37. Brammer, H., Ravenscroft, P., 2009. Arsenic in groundwater: A threat to sustainable agriculture in South and South-east Asia. *Environment International* 35, 647-654.
38. Breit, G.N., Foster, A.L., Sanzalone, R.F., Yount, J.C., Whitney, J.W., Welch, A.H., Islam, M.N., 2001. Arsenic cycling in eastern Bangladesh: the role of phyllosilicates. Program Abstract *Geological Society of America, Annual Meeting*. 32, A192.
39. Breit, G.N., Whitney, J.W., Foster, A.L., Stollenwerk, K.G., Yount, J.C., Welch, A.H., 2003. Geochemical changes affecting arsenic in the sediment of the Ganges-Brahmaputra-Meghna river system. Program Abstract *Geological Society of America, Annual Meeting*, Seattle, WA.
40. Bundschuh, J., Bhattacharya, P., Chandrasekharam. D., 2005. *Natural arsenic in groundwater: occurrence, remediation and management*. London: A.A. Balkema. 339 pp.
41. Buschmann, J., Berg, M., Stengel, C., Sampon, M., 2007. Arsenic and manganese contamination of drinking water resources in Cambodia: Coincidences of risk areas with low relief topography. *Environment Science and Technology* 41, 2146-2152.
42. Catalano, J.G., Park, C., Fenter, P., Zhang, Z., 2008. Simultaneous inner- and outer-sphere arsenate adsorption on corundum and hematite. *Geochimica et Cosmochimica Acta,* 72, 1986-2004.
43. CGWB-Central Ground Water Board, 2004 "*Groundwater Resources of Assam*" CGWB, North East Region, Ministry of Water Resource, Guwahati.
44. Chakraborti, D., Sengupta, M.K., Rahaman, M.M., Ahamed, S., Chowdhury, U.K., Hossain, M.A., 2004. Groundwater arsenic contamination and its health effects in the Ganga–Megna–Brahmaputra Plain. *Journal of Environmental Monitoring* 6, 74–83.
45. Chakraborti, D., Rahman, M.M., Das, B., Murrill, M., Dey, S., Mukherjee, S.C., Dhar, R.K., Biswas, B.K., Chowdhury, U.K., Roy, S., Sorif, S., Selim, M., Rahman, M., Quamruzzaman, Q. 2010. Status of groundwater arsenic contamination in Bangladesh: A 14 year study report. *Water Research* 44, 5789-5802.
46. Chakraborti, D., Das, B., Murrill, M., 2011. Examining India's Groundwater Quality Management. *Environment Science and Technology* 45, 27-33.
47. Chakraborty, S., Wolthers, M., Chatterjee, D., Charlet, L., 2007. Adsorption of arsenite and arsenate onto muscovite and biotite mica. *Journal of Colloid and Interface Science* 309, 392–401.
48. Charlet, L., Chakraborty, S., Appelo, C.A.J., Roman-Ross, G., Nath, B., Ansari, A.A., Musso, M., Chatterjee, D., Mallick, S. B., 2007. Chemodynamics of an As "hotspot" in a West Bengal aquifer: a field and reactive transport modeling study. *Applied Geochemistry* 22, 1273–1292.
49. Cheng, L., Fenter, P., Sturchio, N.C., Zhong, Z., Bedzyk, M.J., 1999. X-ray standing wave study of arsenite incorporation at the calcite surface. *Geochimica et Cosmochimica Acta* 63, 3153-3157.
50. Cheng, Z., van Geen, A., Seddique, A.A., Ahmed, K.M., 2005. Limited temporal variability of arsenic concentrations in 20 wells monitored for 3 years in Araihazar, Bangladesh. *Environment Science and Technology* 39, 4759–4766.
51. Chui, V.Q., Hering, J.G., 2000. Arsenic adsorption and oxidation at manganite surface. 1. Method for simultaneous determination of adsorbed and dissolved arsenic species. *Environmental Science and Technology* 34, 2029–2034.
52. Davis, J.A., Coston, J.A., Kent, D.B., Fuller, C.C., 1998. Application of the surface complexation concept to complex mineral assemblages. *Environmental Science and Technology* 32, 2820–2828.
53. De Vitre, R., Belzile, N., Tessier, A., 1991. Speciation and adsorption of arsenic on diagenetic iron oxyhydroxides. *Limnology and Oceanography* 36, 1480-1485.

54. Dean, W.E. Jr., 1974. Determination of carbonate and organic matter in calcareous sediments and sedimentary rocks by loss on ignition: Comparison with other methods. *Journal of Sedimentary Petrology* 44, 242–248.
55. Deschamps, E., Ciminelli, V.S.T., Holl, W.H., 2005. Removal of As(III) and As(V) from water using a natural Fe and Mn enriched sample. *Water Research* 39, 5212-5220.
56. DGM, 1994a. *Basic Data of Tubewells, constructed in undivided Darrang district Assam*. Directorate of Geology and Mining, Govt. of Assam.
57. DGM, 1994b. *Basic Data of Tubewells, constructed in undivided Sibsagar district Assam*. Directorate of Geology and Mining, Govt. of Assam.
58. Dhar, R.K., Zheng, Y., Stute, M., van Geen, A., Cheng, Z., Shanewaz, M., Shamsudduha, M., Hoque, M.A., Rahman, M.W., Ahmed, K.M., 2008. Temporal variability of groundwater chemistry in shallow and deep aquifers of Araihazar. *Journal of Contaminant Hydrology* 99, 97-111.
59. Dixit, S., Hering, J.G., 2003. Comparison of arsenic(V) and arsenic(III) sorption onto iron oxide minerals: implications for arsenic mobility. *Environmental Science and Technology* 37, 4182–4189.
60. Dixit, S., Hering, J.G., 2006. Sorption of Fe (II) and As (III) on goethite in single- and dual-sorbate systems. *Chemical Geology* 228, 6–15.
61. Dowling, C.B., Poreda, R.J., Basu A.R., Peters S.L., Aggarwal P.K., 2002. Geochemical study of arsenic release mechanisms in the Bengal Basin groundwater. *Water Resource Research* 38, 1173–1190.
62. Drahota, P., Filippi, M., 2009. Secondary arsenic minerals in the environment: A review. *Environment International* 35, 1243-1255.
63. Dzombak, D.A., Morel, F.M.M., 1990. *Surface Complexation Modelling- Hydrous Ferric Oxide*. John Wiley, New York.
64. Eby, G.N., 2004. *Principal of Environmental Chemistry*. Brooks/Cole-Thomson publisher.
65. Edmunds, W.M., Cook, J.M., Kinniburgh, J.M., Miles, D.L., Trafford, J.M., 1989. *Trace elements occurrence in British groundwater*. British Geological Survey, Research Report SD/89/3.
66. Eiche, E., Neumann, T., Berg, M., Weinman, B., van Geen, A., Norra, S., Berner, Z., Trang, P.T.K., Hung Viet, P., Stüben, D., 2008.Geochemical processes underlying a sharp contrast in groundwater arsenic concentrations in a village on the Red River delta, Vietnam. *Applied Geochemistry* 23, 3143–3154.
67. Enmark, G., Nordborg, D. (2007). Arsenic in groundwater of Brahmaputra floodplain, Assam, India – source, distribution and release mechanism. Minor Field Study 131, Master of Science program in Aquatic and Environmental Engineering, Uppsala University.
68. Farooqi, A., Masuda, H., Firdous, N., 2007. Toxic fluoride and arsenic contaminated groundwater in the Lahore and Kasur districts, Punjab, Pakistan and possible contaminant sources. *Environmental Pollution* 145, 839-849.
69. Febrianto, J., Kosasih, A.N., Sunarso, J., Ju, Y., Indraswati, N., Ismadji, S., 2009. Equilibrium and kinetic studies in adsorption of heavy metals using biosorbent: A summary of recent study. *Journal of Hazardous Materials* 162, 616-645.
70. Fendorf, S.E., Eick, M., Grossl, P., Sparks, D.L., 1997. Arsenate and chromate retention mechanisms on goethite. 1. Surface structure. *Environmental Science and Technology* 31, 315–319.
71. Freundlich, H. 1906. Uber die adsorption in lusungen. *Journal of Physical Chemistry*. 57: 385 (in German).
72. Friedrich, B.P., Armienta, M.A., Merkel, B.J., 2001. Origin of arsenic in the groundwater of the Rioverde basin, Mexico. *Environmental Geology* 40, 1290-1298.
73. Gault, A.G., Polya, D.A., Lythgoe, P.R., Farquhar, M.L., Charnock, J.M., Wogelius, R.A., 2003. Arsenic speciation in surface waters and sediments in a contaminated

waterway: IC-ICP-MS and XAS based study. *Applied Geochemistry* 18, 1387–1397.

74. Goh, K.H., Lim, T.T., 2004. Geochemistry of inorganic arsenic and selenium in a tropical soil: effect of reaction time, pH, and competitive anions on arsenic and selenium adsorption. *Chemosphere* 55, 849-859.
75. Goh, K.H., Lim, T.T., 2005. Arsenic fractionation in a fine soil fraction and influence of various anions on its mobility in the subsurface environment. *Applied Geochemistry,* 20, 229–239.
76. Goldberg, S., 2002. Competitive adsorption of arsenate and arsenite on oxides and clay minerals. *Soil Science Society American Journal* 66, 413-421.
77. Goldberg, S., Glaubig, R.A., 1988. Anion sorption on a calcareous, montmorillonite soil – Arsenic. *Soil Science Society American Journal* 52. 1297–1300.
78. Grafe, M., Eick, M.J., Grossl, P.R., 2001. Adsorption of arsenate and arsenite on goethite in the presence and absence of dissolved organic carbon. *Soil Science Society of American Journal,* 65, 1680–1687.
79. Guo, H.M., Yang, S.Z., Tang, X.H., Li, Y., Shen, Z.L., 2008. Groundwater geochemistry and its implications for arsenic mobilization in shallow aquifers of the Hetao basin, Inner Mongolia. *Science of the Total Environment* 393, 131-144.
80. Guo, H.M., Zhang, B., Li, Y., Berner, Z., Tang, X., Norra, S., Stuben, D., 2011. Hydrogeological and biogeochemical constrains of arsenic mobilization in shallow aquifers from the Hetao basin, Inner Mongolia. *Environmental Pollution* 159, 876-883.
81. Gupta, S.S., Bhattacharyya, K.G., 2011. Kinetics of adsorption of metal ions on inorganic materials: A review. *Advances in colloid and Interface Science* 162, 39-58.
82. Halim, M.A., Majumder, R.K., Nessa, S.A., Hiroshiro, Y., Uddin, M.J., Rahman, S.H., Jinno, K., 2009. Hydrogeochemistry and Arsenic Contamination of Groundwater in the Ganges Delta Plain, Bangladesh. *Journal of Hazardous Material* 164, 1335-1345.
83. Halim, M.A., Majumder, R.K., Nessa, S.A., Oda, K., Hiroshiro, Y., Jinno, K., 2010. Arsenic in shallow aquifer in the eastern region of Bangladesh: insights from principal component analysis of groundwater compositions. *Environmental Monitoring and Assessment* 161, 453-472.
84. Han, X., Li, Y.L., Gu, J.D., 2011. Oxidation of As(III) by MnO2 in the absence and presence of Fe(II) under acidic conditions. *Geochimica et Cosmochimica Acta* 75, 368-379.
85. Harvey, C.F., Swartz, C.H., Badruzzaman, A.B.M., Keon, B.N., Yu, W., Ashraf, A.M., Jay, J., Beckie, R., Niedan, V., Brabander, D., Oates, P.M., Ashfaque, K.N., Islam, S., Hemond, H.F., Ahmed, M.F., 2002. Arsenic mobility and groundwater extraction in Bangladesh. *Science* 298, 1602–1606.
86. Harvey, C.F., Swartz, C.H., Badruzzaman, A.B.M., Keon, B.N., Yu, W., Ali, M.A., 2005. Groundwater arsenic contamination on the Ganges delta: biogeochemistry, hydrology, human perturbations, and human suffering on a large scale. *C R Geoscience* 337, 285–96.
87. Harvey, C.F., Ashfaque, K.N., Yu, W., C.H., Badruzzaman, Ashraf, A.M., Oates, P.M., Micheal, H.A., Neumann, R.B., Beckie, R., Islam, S., Ahmed, M.F., 2006. Groundwater dynamics and arsenic contamination in Bangladesh. *Chemical Geology* 228, 112-136.
88. Hendershot, W.H., Lalande, H., Duquette, M., 2008a. Soil Reaction and Exchangeable Acidity. In: Carter, M.R., Gregorich, E.G., editors. *Soil Sampling and Method of Analysis*. 2nd Edition. Canadian Society of Soil Science. CRC press, Taylor and Francis group.
89. Hendershot, W.H., Lalande, H., Duquette, M., 2008b. Ions exchange and Exchangeable cations. In: Carter, M.R., Gregorich, E.G., editors. *Soil Sampling and Method of Analysis*. 2nd Edition. Canadian Society of Soil Science. CRC press, Taylor and Francis group.

90. Herreweghea, S., Swennena, R., Vandecasteeleb, C., Cappuynsa, V., 2003. Solid phase speciation of arsenic by sequential extraction in standard reference materials and industrially contaminated soil samples. *Environmental Pollution* 122, 323–342.
91. Ho, Y.S., 2004. Selection of optimum sorption isotherm. *Carbon* 42, 2115–2116.
92. Ho, Y.S., 2006. Second-order kinetic model for the sorption of cadmium onto tree fern: A comparison of linear and non-linear methods. *Water Research* 40, 119 – 125.
93. Ho, Y.S., McKay, G., 2000. The kinetics of sorption of divalent metal ions onto sphagnum moss peat. *Water Research* 34, 735–742.
94. Ho, Y.S., McKay, G., 2003. Sorption of dyes and copper ions onto biosorbents. *Process Biochemistry* 38, 1047–1061.
95. Horneman, A., van Geen, A., Kent, D., Mathe, P.E., Zheng, Y., Dhar, R.K., O'Connell, S., Hoque, M.A., Aziz, Z., Shamsudduha, M., Seddique, A., Ahmed, K.M., 2004. Decoupling of arsenic and iron release to Bangladesh groundwater under reducing conditions. Part I: Evidence from sediment profiles. *Geochimica et Cosmochimica Acta* 68, 3459–3473.
96. Hossain, M.F., 2006. Arsenic contamination in Bangladesh – An overview. *Agriculture, Ecosystems and Environment* 113, 1-16.
97. Hudson-Edwards, K. A., Houghton, S. L., and Osborn, A., 2004. Extraction and analysis of arsenic in soils and sediments. *Trends in Analytical Chemistry* 23, 745–752.
98. Jain, A., Loeppert, R.H., 2000. Effect of competing anions on the adsorption of arsenate and arsenite by ferrihydrite. *Journal of Environmental Quality* 29, 1422-1430.
99. Jonsson, J., Sherman, D.M., 2008. Sorption of As(III) and As(V) to siderite, green rust (fougerite) and magnetite: Implication for arsenic release in anoxic groundwater. *Chemical geology* 255, 173-181.
100. Kaiser, K., Guggenberger, G., Zech, W., 1997. Dissolved organic matter sorption on subsoils and minerals studied by 13C-NMR and DRIFT spectroscopy. *European Journal of Soil Science* 48, 301-310.
101. Kazi, T.G., Arain, M.B., Jamali, M.K., Jalbani, N., Afridi, H.I., Sarfraz, R.A., Baig, J.A., Shah, A.Q., 2009. Assessment of water quality of polluted lake using multivariate statistical techniques: A case study. *Ecotoxicology and Environmental Safety* 72, 301– 309.
102. Kent, D.B., Fox, P.M., 2004. The influence of groundwater chemistry on arsenic concentrations and speciation in a quartz sand and gravel aquifer. *Geochemical Transaction* 5, 1-5.
103. Keon, N.E., Swartz, C.H., Brabander, D.J., Harvey, C., and Hemond, H.F., 2001. Validation of an arsenic sequential extraction method for evaluating mobility in sediments. *Environmental Science and Technology* 35**,** 2778–2784.
104. Kim, M.J., Nriagu, J.O., Haack, S.K., 2000. Carbonate ions and arsenic dissolution by groundwater. *Environment Science and Technology* 34, 3094-3100.
105. Kirk, M., Holm, T., Park, J., Jin, Q., Sanford, R., Fouke, B., Bethke, C., 2004. Bacterial sulfate reduction limits natural arsenic contamination in groundwater. *Geology* 32, 952-956.
106. Kirk, M.F., Roden, E.E., Crossey, L.J., Brealey, A.J., Spilde, M.N., 2010. Experimental analysis of arsenic precipitation during microbial sulfate and iron reduction in model aquifer sediment reactors. *Geochimica et Cosmochimica Acta* 74, 2538-2555.
107. Koretsky, C. 2000. The significance of surface complexation reactions in hydrologic systems: a geochemist's perspective. *Journal of Hydrology*. 230: 127-171.
108. Kotska, J.E., Luther III, G.W., 1994. Partitioning and speciation of solid phase iron in saltmarsh sediments. *Geochimica et Cosmochimica Acta* 58, 1701–1710.
109. Lagergren, S., 1898. About the theory of so-called adsorption of soluble substances. *Kungliga Svenska Vetenskapsakademiens Handlingar*. Band 24: 1-39.
110. Langmuir, D., 1997. *Aqueous Environmental Geochemistry*. Prentice-Hall, Upper Saddle River, NJ.

111. Lin, Z., Puls, R.W., 2000. Adsorption, desorption and oxidation of arsenic affected by clay minerals and aging process. *Environmental Geology,* 32, 753–759.
112. Lin, Z., Puls, R.W., 2003. Potential indicators for the assessment of arsenic natural attenuation in the subsurface. *Advances in Environmental Research* 7, 825-834.
113. Lopez, R., Álvarez-Valero, M., Nieto, J., Sáez, R., Matos, X., 2008. Use of sequential extraction procedure for assessing the environmental impact at regional scale of the São Domingos Mine (Iberian Pyrite Belt). *Applied Geochemistry* 23, 3452-3463.
114. Lowers, H.A., Breit, G.N., Foster, A.L., Whitney, J., Yount, J., Uddin, M.N., Muneem, A.A., 2007. Arsenic incorporation into authigenic pyrite Bengal Basin sediment, Bangladesh. *Geochimica et Cosmochimica Acta* 71, 2699-2717.
115. Mahanta, C., Dutta, A., Basu, S., Borah, P., Choudhury, R., Saikia, L., Alam, W., Dutta, R., 2010. Groundwater Arsenic Contamination in the Brahmaputra Floodplains: Outcome of a Comprehensive Field Investigation in Assam, India. Proc. Of the ASCE - *EWRI 3rd International Perspective on Current and Future State of Water Resource & the Environment* at IIT Chennai from 5th January – 7th January 2010.
116. Mallick, S., Rajgopal, N.R., 1996. Groundwater development in the arsenic-affected alluvial belt of West Bengal - some questions. *Current Science* 70, 956–958.
117. Mandal, B.K., Ogra, Y., Suzuki, K.T., 2003. Speciation of arsenic in human nail and hair from arsenic-affected area by HPLC-inductively coupled argon plasma mass spectrometry. *Toxicology and Applied Pharmacology* 189, 73–83.
118. Mandal, B.K., Suzuki, K.T., 2002. Arsenic around the world: a review. *Talanta* 580, 201-235.
119. Manning, B.A., Fendorf, S.E., Bostick, B., Suarez, D.L., 2002. Arsenic(III) oxidation and arsenic(V) adsorption reactions on synthetic birnessite. *Environmental Science and Technology* 36, 976–981.
120. Manning, B.A., Goldberg, S., 1996. Modeling competitive adsorption of arsenate with phosphate and molybdate on oxide minerals. *Soil Science Society American Journal* 60, 121–131.
121. Manning, B.A., Goldberg, S., 1997. Adsorption and stability of arsenic at the clay mineral–water interface. *Environmental Science and Technology* 31, 2005–2011.
122. Martin, J.M., Whitfield, M., 1983. The significance of the river input of chemical elements to the ocean. In: Wong, C.S., Boyle, E., Bruland, K.W., Burton, J.D., Goldberg., editors. *Trace metals in Seawater*. Plenium Press, New York, pp. 265-296.
123. Matschullat, J., 2000. Arsenic in the geosphere—a review. *Science of the Total Environment* 249, 297–312.
124. McArthur, J.M., Ravenscroft, P., Safiullah, S., Thirlwall, M.F., 2001. Arsenic in groundwater: testing pollution mechanisms for sedimentary aquifers in Bangladesh. *Water Resources Research*, 37,109–117.
125. McArthur, J.M., Banerjee, D.M., Hudson-Edwards, K.A., Mishra, R., Purohit, R., Ravenscroft, P., Cronin, A., Howarth, R.J., Chatterjee, A., Talukdar, T., Lowry, D., Houghton, S., Chadha, D.K., 2004. Natural organic matter in sedimentary basins and its relation to arsenic in anoxic groundwater: the example of West Bengal and its worldwide implications. *Applied Geochemistry* 19, 1255–1293.
126. McArthur, J.M., Ravenscroft, P., Banerjee, D.M., Milsom, J., Hudson-Edwards, K.A., Sengupta, S., Bristow, C., Sarkar, A., Tonkin, S., Purohit, R., 2008. How paleosols influence groundwater flow and arsenic pollution, A model from the Bengal Basin and its worldwide implication. *Water Resources Research* 44, W11411.
127. McArthur, J.M., Nath, B., Banerjee, D.M., Purohit, R., Grassineau, N., 2011. Palaeosol Control on Groundwater Flow and Pollutant Distribution: The Example of Arsenic. *Environmental Science and Technology* 45, 1376-1383.
128. Meng, X.G., Bang, S., Korfiatis, G.P., 2000. Effects of silicate, sulfate and carbonate on arsenic removal by ferric chloride. *Water Research* 34, 1255-1261.
129. Miller, G.P., 2001. Surface complexation modeling of arsenic in natural water and sediment systems. Doctoral Dissertation. New Mexico Institute of Mining and Technology, Socorro, NM, USA.
130. Morse, J.W., Luther, G.W., 1999. Chemical influences on metal-sulfide interactions in anoxic sediments. *Geochimica et Cosmochimica Acta* 63, 3373-3378.

131. Mukherjee, A.B., Bhattacharya, P., 2001. Arsenic in groundwater in the Bengal delta plain: slow poisoning in Bangladesh. *Environmental Reviews* 9,189–220.
132. Mukherjee, A.B., Bhattacharya, P., Jacks, G., Banerjee, D.M., Ramanathan, A.L., Mahanta. C., et al. 2006. Groundwater arsenic contamination in India: extent and severity. In: Naidu R, Smith E, Owens G, Bhattacharya P, Nadebaum P, editors. *Managing arsenic in the environment: from soil to human health*. Melbourne: CSIRO Publishing; p. 533–94.
133. Mukhopadhyay, D., Sanyal, S.K., 2004. Complexation and release isotherm of arsenic in arsenic-humic/fulvic equilibrium study. *Australian Journal Soil Research* 42, 815-824.
134. Mulligan, C., Fukue, M., Sato,Y., 2010. *Sediments contamination and sustainable remediation*. CRC press, Taylor and Francis Group, New York.
135. Nadakavukaren, J.J., Ingermann, R.L., Jeddeloh, G., Falkowski, S.J., 1984. Seasonal variation of arsenic concentration in well water in Lane County, Oregon. *Bulletin Environmental Contaminant Toxicology* 33, 264–269.
136. Naidu, R., Bhattacharya, P., 2006. Management and remediation of arsenic from contaminated water. In: Naidu, R., Smith, E., Owens, G., Bhattacharya, P., Nadebaum, P., editors. *Managing arsenic in the environment: from soil to human health*. Melbourne: CSIRO Publishing; p. 327–50.
137. Nath, B., Berner, Z., Chatterjee, D., Basu Mallik, S., Stueben, D., 2008. Mobility of arsenic in West Bengal aquifers conducting low and high groundwater arsenic Part II: comparative geochemical profile and leaching study. *Applied Geochemistry* 23, 996–1011.
138. Nath, B., Maity, J.P., Jean, J-S., Birch, G., Kar, S., Yang, H-J., Lee, M-K., Hazra, R., Chatterjee, D., 2011. Geochemical characterization of arsenic-affected alluvial aquifers of the Bengal Delta (West Bengal and Bangladesh) and Chianan Plains (SW Taiwan): Implications for human health. *Applied Geochemistry* 26, 705-713.
139. Nesbitt, H. W., Canning, G. W., Bancroft, G. M., 1998. XPS study of reductive dissolution of 7A˚ birnessite by H_3AsO_3, with constraints on reaction mechanism. *Geochimica et Cosmochimica Acta* 62, 2097–2110.
140. NHMRC/NRMMC (National Health and Medical Research Council/ Natural Resource Management Ministerial Council). National water quality management strategy. Australian drinking water guidelines186496118X; 2004.
141. Nickson, R.T., McArthur, J.M., Burgess, W.G., Ahmed K.M., Ravenscroft, P., Rahman, M., 1998. Arsenic poisoning of Bangladesh groundwater. *Nature,* 395, 338.
142. Nickson, R.T., McArthur, J.M., Ravenscroft, P., Burgess, W.G., Ahmed, K.M., 2000. Mechanism of arsenic release to groundwater, Bangladesh and West Bengal. *Applied Geochemistry,* 15, 403–413.
143. Nickson, R.T., McArthur, J.M., Shrestha, B., Kyaw-Mint, T.O., Lowry, D., 2005. Arsenic and other drinking water quality issues in Muzaffargarh District, Pakistan. *Applied Geochemistry* 20, 55–68.
144. Nickson, R., Sengupta, C., Mitra, P., Dave, S. N., Banerjee, A. K., Bhattacharya, A., 2007. Current knowledge on the distribution of arsenic in groundwater in five states of India. *Journal of Environmental Science and Health Part A, 42*: 1707–1718.
145. Nordstrom, D.K., 2002. Worldwide occurrences of arsenic in ground water. *Science* 296, 2143–2148.
146. Nriagu, J.O., Bhattacharya, P., Mukherjee, A.B., Bundschuh, J., Zevenhoven, R., Loeppert, R.H., 2007. Arsenic in soil and groundwater: an introduction. In: Bhattacharya, P., Mukherjee, A.B., Bundschuh, J., Zevenhoven, R., Loeppert, R.H., editors. Arsenic in soil and groundwater environment: biogeochemical interactions, health effects and remediation. *Trace Metals and other Contaminants in the Environment* vol. 9 (Series Editor Nriagu, JO), Elsevier, Amsterdam, The Netherlands 1–58.
147. Olias, M., Nieto, J.M., Sarmiento, A.M., Ceron, J.C., Canovas, C.R., 2004. Seasonal water quality variations in a river affected by acid mine drainage: the Odiel River (southwest Spain). *Science of the Total Environment* 333, 267–281.
148. Oremland, R.S., Dowdle, P.R., Hoeft, S., Sharp, J.O., Schaefer, J.F., Miller, L.G., Blum, J.S., Smith, R.L., Bloom, N.S., Wallschlaeger, D., 2000. Bacterial dissimilatory reduction of arsenate and sulfate in meromictic Mono Lake, California. *Geochimica et Cosmochimica Acta* 64, 3073–3084.

149. Oscarson, D.W., Huang, P.M., Defosse, D., Herbillion, A., 1981. Oxidative power of Mn(IV) and Fe(III) oxides with respect to As(III) in terrestrial and aquatic environments. *Nature* 291, 50-51.
150. O'Shea, B., Jankowski, J., Sammut, J., 2007. The source of naturally occurring arsenic in a coastal sand aquifer of eastern Australia. *Science of the Total Environment* 379, 151-166.
151. Pal, T., Mukherjee, P.K., Sengupte, S., 2002. Nature of arsenic pollutants in groundwater of Bengal Delta – a case study from Baruipur area, West Bengal, India. *Current Science* 82,554–561.
152. Parkhurst, D.L., and Appelo, C.A.J., 1999. User's guide to PHREEQC (Version 2)—A computer program for speciation, batch-reaction, one-dimensional transport, and inverse geochemical calculations. U.S. Geological Survey Water-Resources Investigations Report *99-4259*.
153. Pfeifer, H.R., Häussermann, A., Lavanchy, J.C., Halter, W. 2007. Distribution and Behavior of arsenic in soils and waters in the vicinity of the former gold-arsenic mine of Salanfe, Western Switzerland. *Journal of Geochemical Exploration* 93, 121-134.
154. Polizzotto, M.L., Harvey, C.F., Li, G., Badruzzman, B., Ali, A., Newville, M., Sutton, S., Fendorf, S., 2006. Solid-phases and desorption processes of arsenic within Bangladesh sediments. *Chemical Geology* 228, 97–111.
155. Polizzotto, M.L., Kocar, B.D., Benner, S.G., Sampson, M., Fendorf, S., 2008. Near surface wetland sediments as a source of arsenic release to ground water in Asia. *Nature* 454, 505–508.
156. Poots, Y.J.P., Mckay, G., Healy, J. 1976. The removal of acid dye from effluent using natural adsorbent – Peat. *Water Research* 10, 1061-1066.
157. Postma, D., Appelo, C.A.J., 2000. Reduction of Mn-oxides by ferrous iron in a flow system: column experiment and reactive transport modeling. *Geochimica et Cosmochimica Acta* 64, 1237–1247.
158. Postma, D., Larsen, F., Minh Hue, N.T., Thanh Duc, M., Viet, P.H., Nhan, P.Q., Jessen, S., 2007. Arsenic in groundwater of the Red River floodplain, Vietnam: Controlling geochemical processes and reactive transport modeling. *Geochimica et Cosmochimica Acta* 71, 5054–5071.
159. Postma, D., Jessen, S., Minh Hue, Duc, M. T., Koch, C.B., N.T., Viet, P.H., Nhan, P.Q., Larsen, F., 2010. Mobilization of arsenic and iron from Red River floodplains sediments, Vietnam. *Geochimica et Cosmochimica Acta* 74, 3367-3381.
160. Ranjan, D., Talat, M., Hasan, S.H., 2009. Biosorption of arsenic from aqueous solution using agriculture residue 'rice polish'. *Journal of Hazardous Materials* 166, 1050-1059.
161. Raven, P.R., Jain, A., Loeppert, R.H., 1998. Arsenite and arsenate adsorption on ferrihydrite: Kinetics, equilibrium, and adsorption envelopes. *Environmental Science and Technology* 32,344–349.
162. Ravencroft, P., McArthur, J.M., Hoque, B.A., 2001. Geochemical and palaeohydrological controls on pollution of groundwater by arsenic. In: Chappell W.R., Abernathy C.O. and Calderon R.L. (eds) *Arsenic Exposure and Health Effects IV*. Elsevier, Oxford, 53–77.0
163. Redman, A.D., Macalady, D.O.L., Ahmann, D., 2002. Natural organic matter affects arsenic speciation and sorption onto hematite. *Environmental Science and Technology* 36, 2889-2896.
164. Reza, A.H.M.S., Jean J.S., Lee, M.K., Liu, C.C., Bundschuh, J., Yang, H.J., Lee, J.F., Lee, Y.C., 2010a. Implications of organic matter on arsenic mobilization into groundwater: Evidence form northwestern (Chapai-Nawabganj), central (Manikganj) and southeastern (Chandpur) Bangladesh. *Water Research* 44, 5556-5574.
165. Reza, A.H.M.S., Jean, J.H., Lee, M.K., Yang, H.J., Liu, C.C., 2010b. Arsenic enrichment and mobilization in the Holocene alluvial aquifers of the Chapai-

Nawabganj district, Bangladesh: A geochemical and statistical study. *Applied Geochemistry* 25, 1280-1289.

166. Robinson, C., von Bromssen, M., Bhattacharya, P., Haller, S., Biven, A., Hossain, M., Jacks, G., Ahmed, K.M., Hasan, M.A., Thunvik, R., 2011. Dynamic of arsenic adsorption in the targeted arsenic-safe aquifers in Matlab, south-eastern Bangladesh: Insight from experimental studies. *Applied Geochemistry* 26, 624-635.
167. Romero F. M., Armienta M. A., Chavez A.C., 2004. Arsenic sorption by carbonate-rich aquifer material, a control on arsenic mobility at Zimapan, Mexico. *Archives of Environmental Contaminant Toxicology* 47, 1–13.
168. Rowland, H.A.L., Gault, A.G., Lythgoe, P., Poyla, D.A., 2008. Geochemistry of aquifers sediments and arsenic-rich groundwater from Kandal Province, Cambodia. *Applied Geochemistry* 23, 3029-3046.
169. Santana, S.P., Alfonso, M.P., Tagle, M.V., Icart, M.P., Brunori, C., Morabito R. 2007. Total and partial digestion of sediments for the evaluation of trace element environmental pollution. *Chemosphere* 66, 1545-1553.
170. Saunders, J.A., Lee, M-K., Wolf, L.A., Morton, C.M., Feng, Y., Thomson, I., Park, S., 2005. Geochemical, microbiological, and geophysical assessments of anaerobic immobilization of heavy metals. *Bioremediation Journal* 9, 33–48.
171. Saunders, J.A., Lee, M.K., Shamsudduha, M., Dhakal, P., Uddin, A., Chowdhury, M.T., Ahmed, K.M., 2008. Geochemistry and mineralogy of arsenic in (natural) anearobic groundwaters. *Applied Geochemistry* 23, 3205-3214.
172. Scott, M.J., Morgan, J.J., 1995. Reactions at oxide surfaces. 1. Oxidation of As(III) by synthetic birnessite. *Environmental Science and Technology* 29, 1898–1905.
173. Sengupta, S., McArthur, J.M., Sarkar, A., Leng, M.J., Ravencroft, P., Howarth, R.J., Banerjee, D.M., 2008. Do ponds cause arsenic-pollution of groundwater in the Bengal basin? An answer from West-Bengal. *Environmental Science and Technology* 42, 5156-5164.
174. Shamsudduha, M., Uddin, A., Saunders, J.A., Lee, M.-K., 2008. Quaternary stratigraphy, sediment characteristics and geochemistry of arsenic contaminated alluvial aquifers in the Ganges–Brahmaputra floodplain in central Bangladesh. *Journal of Contaminant Hydrology* 99, 112–136.
175. Sharif, M.U., Davis, R.K., Steele, K.F., Kim, B., Kresse, T.M., Fazio, J.A., 2008. Inverse geochemical modeling of groundwater evolution with emphasis on arsenic in the Mississippi River Valley alluvial aquifer, Arkansas, USA. *Journal of Hydrology* 350, 41–55.
176. Sharif, M.S.U., Davis, R.K., Steele, K.F., Kim, B.K., Hays, P.D., Kresse, T.M., Fazio, J.A., 2011. Surface complexation modeling for predicting solid phase arsenic concentrations in the sediments of the Mississippi River Valley alluvial aquifer, Arkansas, USA. *Applied Geochemistry* 26, 496-504.
177. Sharma, V.K., Sohn, M., 2009. Aquatic arsenic: Toxicity, speciation, transformation and remediation. *Environment International* 35, 743-759.
178. Shimada, N., 1996. Geochemical conditions enhancing the solubilization of arsenic into groundwater in Japan. *Applied Organometallic Chemistry* 10, 667–674.
179. Shrestha, R.R., Surestha, M.P., Upadhyay, N.P., Pradhan, R., Maskey, A., Maharjan, M., 2003. Groundwater arsenic contamination, its health impact and mitigation program in Nepal. *Journal Environmental Science and Health* A 38,185–200.
180. Sigg, L.M., 1979. Die Wechselwirkung von Anionen und schwachen Säuren mit a-FeOOH (Goethit) in wässriger Lösung. Doctoral Dissertation. Swiss Federal Institute of Technology (Eidgenössische Technische Hochschule), Zurich.
181. Silveira, M.L., Alleoni, L.R.F., O'Connor, G.A., Chang, A.C., 2006. Heavy metal sequential extraction methods-A modification for tropical soils. *Chemosphere* 64, 1929-1938.

182. Singh, A.K., 2004. Arsenic contamination in groundwater of North Eastern India. *National seminar on hydrology*, Roorkee, November 22-23, 2004.
183. Smedley, P.L., Kinniburgh, D.G., 2002. A review of the source, behavior and distribution of arsenic in natural waters. *Applied Geochemistry* 17, 517–68.
184. Smith, J.V.S., Jankowski, J., Sammut, J., 2006. Natural occurrences of inorganic arsenic in the Australian coastal groundwater environment: implications for water quality in Australian coastal communities. In: Naidu, R., Smith, E., Owens, G., Bhattacharya, P., Nadebaum, P., Editor Nriagu, J.O., Elsevier, Amsterdam, The Netherlands, 2007;editors. *Managing arsenic in the environment: from soil to human health*. Melbourne, Australia: CSIRO Publishing; pp. 129–54.
185. Sø, H.U., Postma, D., Jakobsen, R., Larsen, F., 2008. Sorption and desorption of arsenate and arsenite on calcite. *Geochimica et Cosmochimica Acta* 72, 5871-5884.
186. Sparks, D.L., 1999. *Soil physical chemistry*. CRC press, Taylor and Francis group.
187. Sposito, G., 1989. *The Chemistry of Soils*. Oxford University Press, New York.
188. SPSS Inc., 1998. SPSS BASE 8.0 – Application Guide. SPSS Inc., Chicago, USA.
189. Sracek, O., Bhattachary, P., Jack, G., Gustafsson, Bromssen, M.V., 2004. Behavior of arsenic and geochemical modeling of arsenic enrichment in aqueous environments. *Applied Geochemistry* 19, 169-180.
190. Stachowicz, M., Hiemstra, T., van Riemsdijk, W.H., 2008. Multi-competitive interaction of As(III) and As(V) oxyanions with Ca^{2+}, Mg^{2+}, PO_4^{3-} and CO_3^{2-} ions on goethite. *Journal of Colloid and Interface Science* 320, 400-414.
191. Stollenwerk, K.G., Breit, G.N., Welch, A.H., Yount, J.C., Whitney, J.W., Foster, A.L., Uddin, M.N., Majumder, R.K., Ahmed, N., 2007. Arsenic attenuation by oxidized aquifer sediments in Bangladesh. *Science of the Total Environment* 379, 133-150.
192. Stuben, D., Berner, Z., Chandrashekharam, D., Julie, K., 2003. Arsenic enrichment in groundwater of West Bengal, India: geochemcal evidence for mobilization of As under reducing conditions. *Applied Geochemistry* 18, 1417-1434.
193. Stumm, W., 1992. *Chemistry of the solid-water interface*. Wiley and Sons, New York.
194. Stumm, W., Morgan, J.J., 1996. *Aquatic chemistry*. 3rd edition, Wiley and Sons, New York.
195. Suter, D., Siffert, C., Sulzberger, B. and Stumm, W., 1988. Catalytic dissolution of iron (III)-(hydr)oxide by oxalic acid in the presence of Fe(II). *Naturwissenschaften*, 75, 571-573.
196. Swartz, C.H., Blute, N.K., Badruzzman, B., Ali, A., Brabander, D., Jay, J., Besancon, J., Islam, S., Hemond, H.F., Harvey, C., 2004. Mobility of arsenic in a Bangladesh aquifer: inferences from geochemical profiles, leaching data, and mineralogical characterization. *Geochimica et Cosmochimica Acta* 68, 539–4557.
197. Swedlund, P.J., Webster, J.G., 1999. Adsorption and polymerization of silicate acid on ferrihydrite, and its effect on adsorption. *Water Research* 33, 3413–3422.
198. Tan, K.H., 2011. *Principles of soil chemistry*. CRC press, Taylor and Francis group.
199. Tessier, A., Campbell, P.G.C., Bisson, M., 1979. Sequential extractions for separation of particulate trace metals. *Analytical Chemistry* 51, 844-851.
200. Thornton, I., 1996. Sources and pathways of As in the geo-chemical environment: health implications. In: Appleton, J.D., Fuge, R., McCall, G.J.H. (Eds.), *Environmental Geochemistry and Health* 113, 153-161.
201. Tournassat, C., Charlet, L., Bosbach, D., Manceau, A., 2002. Arsenic(III) oxidation by birnessite and precipitation of manganese(II) arsenate. *Environmental Science and Technology* 36, 493–500.
202. Uddin, A., Shamsudduha, A., Saunders, J.A., Lee, M-K., Ahmed, K.M., Chowdhury, M.T., 2011. Mineralogical profiling of alluvial sediments from arsenic affected

Ganges-Brahmaputra floodplain in central Bangladesh. *Applied Geochemistry* 26, 470-483.

203. van Geen, A., Robertson, A.P., Leckie, J.O., 1994. Complexation of carbonate species at the goethite surface: implications for adsorption of metal ions in natural waters. *Geochimica et Cosmochimica Acta* 58, 2073-2086.
204. van Geen, A., Rose, J., Thoral, S., Garnier, J.M., Zheng, Y., Bottero, J.Y., 2004. Decoupling of As and Fe release to Bangladesh groundwater under reducing conditions. Part II: evidence from sediment incubations. *Geochimica et Cosmochimica Acta* 68, 3475–3486.
205. van Geen, A., Zheng, Y., Cheng, Z., Aziz, Z., Horneman, A., Dhar, R.K., Mailloux, B., Stute, M., Weinman, B., Goodbred, S., Seddique, A.A., Hoque, A., Ahmed, K.M., 2006. A transect of groundwater and sediment properties in Araihazar, Bangladesh: further evidence of decoupling between As and Fe mobilization. *Chemical Geology* 228, 85–96.
206. van Geen, A., Radloff, K., Aziz, Z., Cheng, Z., Huq, M.R., Ahmed, K.M., Weinman, B., Goodbred, S., Jung, H.B., Zheng, Y., Berg, M., Trang, P.T.K., Charlet, L., Metral, J., Tisserand, D., Guillot, S., Chkraborty, S., Gajurel, A.P., Upreti, B.N., 2008. Comparison of arsenic concentrations in simultaneously-collected groundwater and aquifer particles from Bangladesh, India, Vietnam, and Nepal. *Applied Geochemistry* 23, 3244–3251.
207. Varsanyi, I., Kovacs., 2006. Arsenic, iron and organic matter in sediments and groundwater in the Pannonian Basin, Hungary. *Applied Geochemistry*, 21, 949–963.
208. Walther, J.V., 2010. *Essential of Geochemistry*. 2nd Edition, Jones & Bartlett.
209. Wang, S., Mulligan, C.N., 2006. Occurrence of arsenic contamination in Canada: Sources, behavior and distribution. *Science of the Total Environment* 366, 701– 721.
210. Wang, S., Mullingan, C.N., 2008. Speciation and surface structure of inorganic arsenic in solid phases: A review. *Environment International* 34, 867 – 879.
211. Wang, S.W., Liu, C.W., Jang, C.S., 2007. Factors responsible for high arsenic concentrations in two groundwater catchments in Taiwan. *Applied Geochemistry* 22, 460-476.
212. Wang, Y., Deng, Y., 2009. Environmental Geochemistry of High-Arsenic Aquifer Systems. In: Wang, L.K., Chen, J.P., Hung, Y.T., Shammas, N.K., editors. *Heavy Metal in the Environment*. Taylor and Francis group, CRC press.
213. Welch, A.H., Stollenwerk, K.G., 2003. *Arsenic in ground water: geochemistry and occurrence*. Norwell, Massachusetts: Kluwer Academic Publishers 475 pp.
214. Welch, A.H., Westjohn, D.B., Helsel, D.R., Wanty, R.B., 2000. Arsenic in groundwater of United States: Occurrence and geochemistry. *Groundwater* 22, 589-604.
215. Wenzel, W.W., Kirchbaumer, N., Prohaska, T., Stingeder, G., Lombic, E., Adriano, D.C., 2001. Arsenic fractionation in soils using an improved sequential extraction procedure. *Analytical Chimica Acta* 436, 309–323.
216. WHO (World Health Organization), 1996. Guideline for Drinking-Water Quality Health Criteria and Other Supporting Information. 2nd Edition, WHO. Geneva, pp. 940-949.
217. Wilkie, J.A., Hering, J.G., 1996. Adsorption of arsenic onto hydrous ferric oxide: Effects of adsorbate/adsorbent ratios and co-occuring solutes. *Colloids Surfaces A* 107, 97-110.
218. Wu, F.C., Tseng, R.L., Juang, R.S., 2009. Initial behavior of intraparticle diffusion model used in the description of adsorption kinetics. *Chemical Engineering Journal* 153, 1‑8.
219. Xie, X., Wang, Y., Su, C., Liu, H., Duan, M., Xie, Z., 2008. Arsenic mobilization in shallow aquifers of Datong Basin: Hydrochemical and mineralogical evidences. *Journal of Geochemical Exploration* 98, 107-115.

220. Yu, W. H., Harvey, C. M., Harvey, C.F., 2003. "Arsenic in groundwater in Bangladesh: A geostatistical and epidemiological framework for evaluating health effects and potential remedies." *Water Resources Research* 39, 1146.
221. Zheng, Y., Stute, M., van Geen, A., Gavrieli, I., Dhar, R., Simpson, H.J., Schlosser, P., Ahmed, K.M., 2004. Redox control of arsenic mobilization in Bangladesh groundwater. *Applied Geochemistry* 19, 201–14.
222. Zheng, Y., van Geen, A., Stute, M., Dhar, R., Mo, Z., Cheng, Z., Horneman, A., Gavrieli, I., Simpson, H.J., Versteeg, R., Steckler, M., Grazioli-Venier, A., Goodbred, S., Shahnewaz, M., Shamsudduha, M., Hoque, M.A., Ahmed, K.M., 2005. Geochemical and hydrogeological contrasts between shallow and deeper aquifers in two villages of Araihazar, Bangladesh: implications for deeper aquifers as drinking water sources. *Geochimica et Cosmochimica Acta* 69, 5203–5218.

Appendix - A 1

Groundwater Quality from the Study Areas

A 1.1 Groundwater Quality Data of Pub Mangaldai Block - Darrang District (mg/l)

Sl. No.	X	Y	pH	EC	Na	Ca	Mg	Fe	K	Mn	HCO_3^-	SO_4^{2-}	Cl	NO_3^-	PO_4^{3-}	As
1	26.482933	92.1185	7.20	157.2	6.34	30.28	5.99	0.38	2.80	0.52	120	3.72	6.00	0.10	1.10	bdl
2	26.479333	92.131867	7.40	431	4.76	75.00	18.30	3.22	4.98	0.49	350	8.87	26.49	4.80	0.24	bdl
3	26.484367	92.1148	7.20	421	8.25	60.50	22.08	1.10	4.42	1.20	264	11.68	15.50	0.30	1.36	bdl
4	26.4873	92.116667	7.10	118.1	5.92	23.58	3.80	0.99	2.58	0.55	84	0.62	4.50	0.20	1.96	0.0221
5	26.5005	92.12405	6.10	160	5.82	38.96	5.76	5.20	5.35	2.10	126	8.73	10.00	0.60	1.02	0.003
6	26.500368	92.13525	6.80	133.2	5.30	25.78	4.28	6.45	3.00	0.26	96	2.11	8.00	0.50	0.02	0.001
7	26.5061	92.1489	6.50	380	22.21	37.26	7.88	10.96	5.25	1.53	122	34.23	44.49	0.50	0.08	0.004
8	26.502233	92.15505	6.80	197.1	10.94	36.81	5.69	5.76	4.48	1.03	128	5.21	18.49	0.40	0.04	0.0011
9	26.495483	92.152367	7.00	193.8	9.77	45.08	5.68	2.41	3.83	1.00	158	1.89	10.00	0.60	0.52	0.0190
10	26.494067	92.151367	6.80	331	13.36	51.12	7.91	1.43	4.09	1.84	190	0.53	17.49	0.10	1.08	0.001
11	26.488167	92.1472	6.90	364	11.00	57.88	9.81	5.40	4.52	1.42	250	0.20	10.50	0.10	0.86	0.1120
12	26.506733	92.157117	6.90	144.7	11.42	40.88	4.07	3.54	4.00	0.24	132	4.42	5.00	0.20	0.98	bdl
13	26.505633	92.084633	6.50	130.5	6.96	20.48	2.45	20.59	2.90	0.84	72	0.62	11.50	1.20	0.12	0.0064
14	26.503067	92.085267	6.30	102.4	7.07	19.40	2.45	25.11	2.78	0.64	62	2.48	11.50	4.80	0.42	bdl
15	26.508683	91.833383	7.10	168.8	14.24	34.06	4.93	15.91	1.46	0.40	130	8.87	5.50	5.30	0.12	0.0024
16	26.485883	91.8405	6.70	176.5	23.01	30.96	4.11	11.97	1.37	0.49	144	2.53	2.50	0.60	0.28	0.0886
17	26.485617	91.841483	6.70	199	25.63	35.66	5.10	11.53	1.38	0.71	162	2.17	3.00	1.10	0.48	0.1200
18	26.5171	91.833367	6.80	146.2	15.83	13.52	3.91	8.01	1.17	0.31	120	4.50	7.00	0.90	0.40	0.0288
19	26.518333	91.824883	6.80	191.7	22.95	67.25	4.60	5.00	1.23	0.13	110	5.00	8.00	2.30	0.53	0.0021
20	26.51764	91.83452	6.70	170	24.28	59.67	5.05	0.40	1.36	0.03	115	6.20	10.00	2.80	0.14	bdl
21	26.471967	92.069983	6.96	304	9.77	24.451	6.83	19.03	3.10	1.50	115	10.36	4.00	0.10	2.10	0.0436
22	26.48905	92.066033	7.06	233	9.84	21.424	4.02	20.18	4.00	0.53	81	25.61	6.00	0.01	1.10	0.0730
23	26.4874	92.082	6.92	276	16.71	21.969	5.57	5.19	12.60	0.07	63	18.71	36.99	1.30	0.24	0.006
24	26.405617	92.11675	7.59	204	6.56	25.572	4.22	1.70	4.20	0.26	88	2.78	9.00	0.01	1.36	0.0465
25	26.488283	92.116283	7.47	216	6.34	25.214	4.58	1.43	8.10	0.58	93	3.95	8.00	0.10	1.96	0.0825
26	26.487483	92.116483	7.38	346	9.12	35.009	11.35	6.71	14.50	1.36	150	11.64	24.99	0.20	1.02	0.0438
27	26.485617	92.1148	7.8	397	6.68	45.502	16.83	0.42	5.80	0.73	229	17.04	14.00	0.50	0.02	0.0010
28	26.486667	92.115133	7.85	424	10.76	61.344	19.49	3.95	8.00	1.16	190	8.41	24.99	0.01	0.08	0.0062

29	26.4843	92.11465	7.9	449	12.41	60.59	18.53	1.03	6.50	0.54	240	14.48	21.99	0.01	0.04	0.007
30	26.505483	92.160167	7.57	220	9.33	25.318	4.40	1.42	5.70	0.20	108	1.56	8.00	0.01	0.52	0.0027
31	26.492833	92.151067	7.58	286	13.63	32.1	5.32	5.82	4.70	0.33	136	8.35	11.00	0.20	1.08	0.0140
32	26.493233	92.15077	7.5	339	13.89	40.494	7.45	6.76	5.50	0.27	146	4.18	22.99	0.01	0.86	0.0175
33	26.49555	92.152317	7.72	278	11.98	29.946	4.25	2.99	5.00	0.26	128	3.12	8.00	0.01	0.98	0.0267
34	26.50125	92.154583	7.51	355	12.54	38.956	8.72	3.86	6.20	0.64	136	12.64	38.99	0.01	0.12	0.0075
35	26.504433	92.1437	7.75	437	13.79	72	10.34	0.79	7.50	0.37	220	6.46	26.99	0.10	0.42	0.0017
36	26.503517	92.141017	7.48	237	9.20	19	2.82	0.79	4.00	0.19	60	20.27	28.99	0.01	0.12	0.003
37	26.502933	92.139167	7.55	192	10.40	21.492	2.43	4.34	4.00	0.04	74	16.76	24.99	1.40	0.28	0.0013
38	26.50035	92.13525	7.46	191	6.69	23.337	2.50	6.61	4.00	0.07	86	8.80	6.00	0.01	0.48	0.009
39	26.4999	92.135017	7.5	284	8.48	27	8.75	0.30	5.20	0.39	140	1.17	16.99	0.01	0.40	0.0021
40	26.506033	92.141083	6.45	618	16.44	98.3	25.28	3.75	7.90	0.14	372	2.56	43.99	0.80	1.36	0.0310

A 1.2 Groundwater Quality of Sipajhar Block - Darrang District (mg/l)

Sl. No.	X	Y	pH	EC	Na	Ca	Mg	Fe	K	Mn	HCO_3^-	SO_4^{2-}	Cl	NO_3^-	PO_4^{3-}	As
1	26.52445	91.853	6.4	173.5	19.35	33.02	4.78	13.42	1.22	0.57	120	11.03	10.00	2.50	1.20	0.0185
2	26.529722	91.855	6.7	148.7	17.08	18.89	3.84	9.83	1.20	0.33	104	4.84	10.50	2.40	1.40	bdl
3	26.530556	91.855556	6.3	178.5	17.24	9.48	4.73	15.78	1.32	0.51	114	7.83	9.00	0.20	1.20	0.0066
4	26.49	91.850833	6.7	146	15.77	28.08	5.69	7.98	1.23	0.28	128	3.36	9.00	0.90	0.80	0.0126
5	26.496333	91.843056	6.8	144.2	16.67	30	4.79	7.41	1.18	0.29	118	9.73	9.00	2.70	0.80	0.0019
6	26.499333	91.83765	6.6	185.4	21.95	20.14	5.79	9.40	1.38	0.59	138	3.31	9.00	2.90	1.40	0.0058
7	26.49305	91.849833	6.4	148.5	16.56	20.11	4.17	8.08	1.12	0.32	114	7.67	9.50	2.40	1.00	0.0609
8	26.502683	91.8615	6.6	180.5	17.17	27.13	4.18	7.58	1.15	0.28	114	8.20	11.50	2.90	1.00	0.0094
9	26.509167	91.845	6.7	156.4	19.13	15.91	4.03	7.87	1.12	0.35	120	9.71	11.00	3.50	1.00	0.0146
10	26.506417	91.834722	6.6	168.5	20.39	22.01	3.48	7.38	1.12	0.39	122	14.58	9.00	3.60	0.60	0.0225
11	26.521667	91.834167	6.4	167.4	21.06	18.7	4.64	10.99	1.05	0.43	130	17.33	11.50	4.10	1.20	0.0055
12	26.52045	91.82475	6.4	167.6	18.88	19.99	4	10.26	1.06	0.39	118	6.37	9.00	3.00	1.60	0.0180
13	26.523333	91.821267	6.3	159	14.31	11.78	3.39	20.31	1.12	0.59	106	8.88	11.50	0.40	0.80	0.0014
14	26.5256	91.839767	6.4	148.1	16.87	16.3	3.99	10.28	0.94	0.38	120	8.60	9.50	2.50	1.20	0.0104
15	26.54	91.853933	6.4	142.4	16.58	18.45	3.51	9.58	0.91	0.32	102	7.21	9.00	1.30	1.00	0.0095
16	26.519444	91.854183	6.5	150.5	17.11	27.27	4.24	8.11	0.98	0.43	118	0.74	13.00	1.30	1.00	0.0133
17	26.4708	91.876133	6.6	148.1	17.07	23.22	4.31	8.55	1.07	0.39	114	7.74	12.00	2.20	1.20	0.0121
18	26.475567	91.876567	6.4	157.7	19.62	11.8	4.73	11.10	1.11	0.40	114	13.02	10.00	3.90	1.40	0.0171
19	26.491389	91.868817	6.5	153.6	18.60	14.5	4.34	9.64	1.30	0.41	124	8.83	11.50	2.30	0.10	bdl

20	26.459167	91.886917	6.5	169.2	21.53	14.79	5.38	13.55	1.05	0.59	124	1.90	10.00	0.10	1.00	0.0135
21	26.457367	91.886967	6.4	150.4	19.33	18.44	4.87	9.41	1.02	0.32	108	7.04	9.50	1.00	1.20	0.0109
22	26.4584	91.902583	6.4	145.4	18.59	20.87	4.85	9.00	0.93	0.34	114	9.69	11.00	2.90	1.20	0.0077
23	26.476944	91.883611	6.5	143.4	18.77	17.2	4.9	10.09	0.98	0.32	114	10.73	13.50	2.80	1.40	0.0104
24	26.476389	91.882222	6.4	148	19.03	16.5	4.75	11.80	0.92	0.31	112	8.71	10.50	3.20	1.20	0.0142
25	26.472778	91.895278	6.4	168	23.33	14.7	5.93	11.66	1.08	0.44	138	16.99	10.00	3.80	1.20	0.0323
27	26.480833	91.895556	6.5	178.9	22.33	19.81	6.41	15.37	1.34	0.60	138	8.30	12.00	0.20	1.80	0.0236
28	26.480556	91.890556	6.4	161.7	21.47	18.2	4.82	14.96	1.95	0.65	130	10.61	14.00	2.10	1.20	0.0264
29	26.491667	91.8875	6.5	162.3	21.45	15.41	5.29	15.60	1.82	0.69	124	8.97	10.50	1.80	1.00	0.0126
30	26.49	91.894167	6.6	159	21.09	15	5.11	14.51	1.90	0.68	126	10.98	13.50	3.00	1.20	0.0170
31	26.488611	91.894444	6.5	167.5	22.86	24.55	5.6	13.91	2.18	0.74	134	8.69	17.00	2.50	1.20	0.0089
32	26.488056	91.894167	6.5	174	23.74	22.54	5.93	13.73	1.92	0.80	138	10.38	12.50	1.90	1.20	0.0145
33	26.499167	91.881389	6.6	162	22.78	22.55	3.63	14.21	2.17	0.74	136	5.24	10.00	1.50	1.40	0.0142
34	26.425833	91.904833	6.5	170	23.26	24.5	4.67	11.69	1.73	0.67	138	5.84	16.50	1.60	1.00	0.0075
35	26.419433	91.915833	6.8	179	26.04	23.16	5.5	10.30	1.85	0.82	156	6.54	13.50	2.50	1.00	0.0120
36	26.418783	91.90515	6.6	269	26.37	15	7.64	12.96	1.65	0.82	174	11.75	15.00	0.40	1.80	0.0147
37	26.42245	91.903633	6.7	149	21.10	14.4	3.89	11.19	1.50	0.60	122	7.02	15.50	1.70	1.40	0.0533
38	26.405317	91.9058	6.5	151	21.90	22.66	3.71	10.53	1.62	0.57	118	10.34	12.00	2.50	1.20	0.0229

A 1.3 Groundwater Quality of Site_1 of Jorhat District (mg/l)

Sl. No.	X	Y	pH	EC	Na	Ca	Mg	Fe	K	Mn	HCO_3^-	SO_4^{2-}	Cl	NO_3^-	PO_4^{3-}	As
1	26.594917	94.2483	6.7	191	44.77	22.13	7.38	9.40	2.41	0.08	200	10.49	36.99	2.60	0.30	0.3176
2	26.59195	94.258233	6.3	197	117.20	26.95	10.72	1.10	2.24	0.02	392	1.60	5.00	1.00	0.40	0.4366
3	26.688533	94.463383	6.8	172	46.55	21.63	5.3	5.62	3.27	0.10	180	6.12	7.00	3.90	0.30	0.2440
4	26.59515	94.247783	6.8	196.4	46.97	21.5	5.93	5.35	2.40	0.08	210	6.32	18.99	2.20	0.20	0.2666
5	26.595417	94.25095	6.3	311	20.51	20.7	4.84	14.47	1.90	0.17	132	19.11	13.00	2.10	0.30	0.1097
6	26.59355	94.252567	5.8	195.4	4.71	14.11	0.84	5.26	1.79	0.50	48	1.65	75.98	0.01	0.01	0.0125
7	26.5932	94.25385	6.3	329	82.99	25.31	6.39	0.68	1.91	0.05	312	0.97	31.99	1.60	0.30	0.1335
8	26.59235	94.257617	6.4	335	18.92	15.84	4.75	26.49	2.04	0.77	156	15.79	14.00	0.80	0.10	0.0464
9	26.59215	94.2566	6.4	311	94.22	24.47	14.18	4.18	1.93	0.35	356	2.25	9.00	2.10	0.40	0.1811
10	26.596717	94.251767	6.6	382	68.85	26.55	13.96	4.19	2.00	0.06	276	2.12	17.99	8.20	0.10	0.2038
11	26.596817	94.252917	6.3	327	32.97	19.74	4.45	8.75	1.69	0.20	164	10.27	14.00	2.40	0.20	0.2145
12	26.599	94.255333	6.3	388	28.95	16.58	4.15	12.26	1.81	0.17	176	17.99	16.00	2.30	0.20	0.1978
13	26.599117	94.256767	6.4	328	33.78	24.12	4.88	9.70	2.03	0.14	196	14.74	9.00	2.60	0.30	0.2692

Sl. No.	X	Y	pH	EC	Na	Ca	Mg	Fe	K	Mn	HCO_3^-	SO_4^{2-}	Cl	NO_3^-	PO_4^{3-}	As
14	26.598867	94.25745	6.6	340	39.60	23.26	4.25	6.30	2.42	0.13	168	6.00	8.00	3.10	0.10	0.2309
15	26.59995	94.2569	6.7	366	39.49	21.22	4.95	5.88	2.16	0.12	208	6.62	6.00	2.30	0.10	0.1759
16	26.611267	94.262017	6.7	179.9	36.81	25.43	6.62	12.27	3.02	0.17	196	11.04	6.00	1.40	0.10	0.4156
17	26.617667	94.259583	6.7	73.3	39.50	21.48	4.87	6.08	4.80	0.07	160	9.49	73.98	2.20	0.20	0.2247
18	26.608533	94.463303	6.8	200	37.38	21.89	5.29	9.82	2.03	0.15	176	12.07	59.98	2.00	0.30	0.3256
19	26.59525	94.247763	6.8	200	41.54	21.48	5.79	5.72	3.98	0.13	224	8.74	15.00	2.30	0.40	0.3391
20	26.594918	94.24823	6.7	200	41.56	25.84	5.19	7.02	1.67	0.10	172	7.87	17.99	1.80	0.20	0.3221
21	26.59542	94.25195	6.3	160	25.99	26.8	5.42	40.52	3.27	0.55	164	24.23	29.99	1.80	0.10	0.0483
22	26.59055	94.242567	6.9	452	46.39	18.8	10	11.02	3.27	0.07	232	3.16	5.96	12.30	0.60	0.4082
23	26.59312	94.253085	7.1	411	50.26	19.8	8.41	5.91	2.40	0.08	228	5.06	9.93	13.50	0.80	0.2800
24	26.59335	94.25676	7.0	408	48.44	18.4	7.65	5.88	2.41	0.10	216	7.22	3.97	13.10	1.00	0.2325
25	26.591905	94.258213	7.0	340	35.42	18.14	6.71	7.48	1.90	0.19	196	4.60	5.96	9.40	0.80	0.1691
26	26.592105	94.25566	6.8	335	31.23	10.77	6.71	12.89	1.79	0.17	164	4.98	5.96	9.40	0.80	0.1290
27	26.59672	94.2519	7.0	328	38.00	15.46	7.18	8.17	1.91	0.12	188	7.03	7.94	12.10	0.80	0.1689
28	26.59682	94.25292	7.0	378	40.93	15.71	7.43	6.72	2.04	0.13	208	41.44	3.97	9.40	1.00	0.1807
29	26.5992	94.2554	7.0	382	38.75	18.11	8.72	10.96	2.24	0.17	208	71.86	5.96	12.70	0.90	0.2460
30	26.59912	94.25678	7.0	349	40.90	14.57	6.86	6.52	1.93	0.07	184	4.49	5.96	9.70	0.70	0.1452
31	26.59888	94.257405	7.1	370	38.35	13.81	7.64	8.68	2.00	0.11	196	3.23	15.88	8.40	0.90	0.2234
32	26.6001	94.25569	7.0	352	42.15	15.53	6.89	3.96	1.69	0.12	204	3.23	3.97	10.30	0.80	0.1037
33	26.61103	94.262023	7.1	381	44.68	16.67	8.28	6.17	1.81	0.13	224	2.93	3.97	10.50	1.20	0.1190
34	26.617701	94.25956	7.1	378	44.90	13.68	7.7	7.61	2.03	0.10	208	4.56	3.97	13.60	1.30	0.1562
35	26.5989	94.25746	6.9	392	42.42	16.97	8.17	8.91	2.42	0.12	208	7.11	3.97	12.70	1.00	0.0980
36	26.59985	94.256905	6.6	486	23.11	13.76	7.12	26.83	2.16	0.53	256	8.97	11.91	11.80	0.30	0.0238
37	26.611301	94.262	6.3	427	29.53	9.63	8.39	19.78	3.02	0.35	220	11.79	5.96	16.50	2.10	0.0516
38	26.618001	94.259579	6.2	353	21.21	8.99	6.66	19.50	4.80	0.41	180	9.92	7.94	14.90	1.90	0.0693
39	26.6085	94.4633	6.5	473	38.43	15.63	10.85	14.76	2.03	0.22	308	12.36	1.99	13.50	1.30	0.1489
40	26.595125	94.247756	6.5	358	14.62	16	6.74	31.66	3.98	0.64	160	1.98	5.96	43.00	0.20	0.1581
41	26.594908	94.248123	6.6	487	45.36	17	11.07	17.48	1.67	0.52	280	6.65	5.96	19.80	1.00	0.1136
42	26.595402	94.25196	7.0	433	51.52	10.3	8.89	6.64	3.59	0.23	268	4.07	7.94	11.80	1.20	0.2906
43	26.59056	94.24261	6.4	384	21.94	16.6	6.42	29.27	2.57	0.51	192	2.47	5.96	6.50	0.90	0.0499
44	26.599094	94.255467	6.1	83	3.92	12.4	1.25	8.55	1.97	0.58	48	2.47	5.96	0.70	0.01	0.0100

A 1.4 Groundwater Quality of Site_2 of Jorhat District (mg/l)

Sl. No.	X	Y	pH	EC	Na	Ca	Mg	Fe	K	Mn	HCO_3^-	SO_4^{2-}	Cl	NO_3^-	PO_4^{3-}	As
1	26.575167	94.22595	6.5	143	14.34	15.5	5.39	33.17	0.29	0.57	142	2.51	14.00	1.10	0.50	0.0262
2	26.575617	94.225317	6.6	171	29.90	24.2	5.43	13.62	1.00	0.14	182	10.36	9.00	3.40	0.60	0.0315
3	26.575217	94.226317	6.6	166	20.67	14.6	6.36	13.90	1.00	0.22	158	15.52	6.00	3.80	0.70	0.0604
4	26.57415	94.226883	6.6	168	23.15	20.0	6.28	14.29	1.00	0.15	164	13.72	7.00	3.40	0.60	0.0793
5	26.574833	94.228517	6.6	166	24.74	18.9	6.13	14.27	0.50	0.13	164	10.16	9.00	2.60	0.50	0.0507
6	26.57495	94.229183	6.6	169	25.39	23.4	6.8	21.95	1.21	0.40	164	4.55	13.00	2.40	0.50	0.0596
7	26.575867	94.22975	6.6	166	27.04	16.0	5.91	14.73	0.86	0.08	160	10.77	9.00	3.10	0.70	0.0357
8	26.575783	94.23055	6.6	168	21.83	17.6	6.31	15.62	1.28	0.32	156	11.83	17.00	3.30	0.70	0.0785
9	26.576233	94.2312	6.7	166	22.51	13.0	6.48	15.38	0.65	0.18	160	17.90	12.00	2.90	0.60	0.0770
10	26.57735	94.230417	6.7	166	29.82	16.0	5.64	15.72	0.96	0.11	164	10.48	11.00	3.30	0.60	0.0426
11	26.57885	94.230367	6.5	161	18.77	19.8	6.33	17.73	0.73	0.20	172	14.78	14.00	3.40	0.60	0.0566
12	26.579417	94.230917	6.3	138	14.55	16.7	5.67	24.72	0.11	0.33	148	6.29	15.00	4.40	0.50	0.0382
13	26.580267	94.230617	6.6	172	31.65	19.3	5.71	12.88	1.01	0.08	172	8.73	14.00	3.70	0.60	0.0418
14	26.575667	94.231867	6.4	166	16.14	18.6	6.25	21.18	1.01	0.24	146	18.22	14.00	3.50	0.60	0.0513
15	26.576267	94.233067	5.7	131	11.56	18.6	4.54	30.23	1.04	0.69	96	4.26	36.00	0.30	0.20	0.0051
16	26.5763	94.233817	6.5	162	27.11	21.7	6.15	14.64	1.07	0.19	170	10.68	14.00	3.40	0.60	0.0551
17	26.57635	94.235033	5.8	106	9.21	15.1	3.73	29.73	0.77	0.64	100	2.14	19.00	0.40	0.30	0.0060
18	26.576345	94.23503	6.6	162	21.78	14.8	6.6	13.78	0.68	0.16	176	12.17	10.00	3.20	0.80	0.0654
19	26.576183	94.236083	6.7	166	27.70	9.6	6.15	12.21	0.70	0.12	166	8.53	14.00	4.00	0.60	0.0461
20	26.57525	94.236817	6.7	182	27.44	11.9	6.03	12.96	0.92	0.09	176	10.19	18.00	4.20	0.50	0.0373
21	26.577167	94.236517	6.7	167	19.09	14.3	6.68	12.05	1.00	0.13	160	13.34	11.00	3.60	0.60	0.0613
22	26.577367	94.236867	6.7	194	31.26	18.0	5.58	10.83	1.26	0.15	192	8.96	19.00	3.30	0.60	0.0305
23	26.575017	94.2381	6.5	147	14.46	18.5	5.36	19.41	1.26	0.21	156	18.96	15.00	5.30	0.60	0.0393
24	26.5741	94.238833	6.5	149	16.58	16.2	5.86	21.06	1.00	0.22	154	19.99	25.00	4.00	0.60	0.0538
25	26.576333	94.2165	6.8	167	30.18	10.9	5.24	11.97	1.11	0.11	178	11.34	30.00	3.80	0.60	0.0378
26	26.47975	94.121733	6.9	302	29.07	8.5	6.13	16.46	1.62	0.12	156	2.60	8.00	5.20	1.00	0.0389
27	26.513017	94.105717	6.6	265	23.51	10.5	6.06	15.18	0.93	0.07	160	3.30	7.00	4.90	1.40	0.0255
28	26.474667	94.124183	6.6	302	30.97	11.1	6.04	11.85	1.42	0.16	188	7.60	10.00	8.70	1.60	0.0183
29	26.467217	94.156833	6.6	255	18.05	20.1	7.27	11.83	0.46	0.17	140	8.82	10.00	9.80	1.10	0.0378
30	26.4804	94.161583	6.3	170	8.23	5.7	3.5	25.44	0.89	0.77	68	42.90	17.00	1.20	0.01	0.0071
31	26.48165	94.161767	6.6	256	25.80	8.0	6.07	0.61	0.88	0.10	160	8.00	8.00	8.60	1.20	0.0105

32	26.481633	94.161983	6.5	262	14.53	12.9	6.19	19.88	0.89	0.31	140	2.78	8.00	3.40	1.40	0.0410
33	26.4819	94.1622	6.6	262	18.78	8.1	6.61	15.01	1.36	0.33	140	4.03	9.00	5.20	0.90	0.0430
34	26.481933	94.1622	6.6	266	19.96	12.2	7.1	12.95	1.11	0.20	132	5.10	8.00	6.40	1.30	0.0438
35	26.481945	94.16219	6.6	268	18.85	14.7	6.5	15.95	0.88	0.29	140	5.70	12.00	8.30	1.50	0.0509

A 1.5 Groundwater Quality of Site_3 of Jorhat District (mg/l)

Sl. No.	X	Y	pH	EC	Na	Ca	Mg	Fe	K	Mn	HCO_3^-	SO_4^{2-}	Cl	NO_3^-	PO_4^{3-}	As
1	26.4883	94.109967	7.16	350	78.40	17.85	12.07	3.08	2.08	0.05	364	4.47	5.00	3.10	3.00	0.0582
2	26.488307	94.109963	7.22	340	79.00	19.35	12.75	2.59	2.04	0.04	366	4.76	4.00	2.70	2.80	0.0626
3	26.488298	94.109967	7.29	390	85.90	21.57	16.42	3.03	2.33	0.05	430	4.37	5.00	3.70	2.60	0.0460
4	26.487567	94.1124	7.24	290	62.70	18.65	15.77	4.08	1.91	0.08	346	4.76	7.00	3.20	0.80	0.0945
5	26.479817	94.121767	7.41	310	67.80	17.55	15.40	3.01	2.55	0.05	368	4.32	3.00	3.30	1.60	0.1504
6	26.474683	94.12435	6.81	250	45.00	16.44	10.20	8.68	2.18	0.32	262	9.23	9.10	5.30	2.80	0.0799
7	26.455633	94.1425	7.16	210	52.95	15.85	10.22	3.51	1.69	0.06	278	4.57	4.00	2.60	2.10	0.1500
8	26.455632	94.142502	7.26	250	49.00	15.77	14.05	3.12	1.28	0.06	280	4.66	7.00	1.20	1.20	0.0734
9	26.455634	94.142498	7.13	255	45.95	18.53	13.00	3.45	1.24	0.09	274	5.88	3.00	1.30	1.20	0.0726
10	26.46975	94.157217	6.99	280	79.25	19.27	19.10	5.70	2.44	0.06	446	6.27	1.00	4.50	3.00	0.0719
11	26.47975	94.12173	7.3	471	69.92	15.04	15.41	3.84	1.62	0.05	362	0.68	12.00	3.50	1.00	0.0992
12	26.51302	94.10572	7.4	586	97.12	23.71	16.7	3.35	0.93	0.05	500	0.15	14.00	5.20	1.20	0.0477
13	26.47467	94.12418	6.8	402	44.80	16.57	9.44	9.68	1.42	0.26	276	3.46	20.00	5.40	1.30	0.0498
14	26.46722	94.15683	6.85	260	27.70	16.87	8.07	12.86	0.46	0.25	184	1.77	25.00	1.80	0.50	0.0241
15	26.4804	94.16158	7.02	301	48.75	16.02	7.22	6.05	0.89	0.14	240	2.77	18.00	4.10	1.20	0.0300
16	26.48165	94.16177	6.96	301	46.32	18.25	5.88	1.11	0.88	0.14	224	1.82	11.00	3.70	1.20	0.0347
17	26.48163	94.16198	6.91	301	46.48	16.29	6.5	5.92	0.89	0.15	222	14.43	11.00	3.70	1.20	0.0392
18	26.4819	94.1622	7.4	370	44.98	15.38	9.44	27.29	1.36	0.92	296	3.14	19.00	4.30	0.80	0.0341
19	26.48193	94.1622	7.02	365	46.94	11.34	8.54	8.13	1.11	0.18	280	2.37	13.00	3.60	1.00	0.0491
20	26.600533	94.256783	7.8	740	140.00	15.13	11.2	0.89	2.39	0.02	420	3.04	3.97	5.90	1.40	0.1268
21	26.60047	94.2568	7.2	550	72.36	12.2	13.95	3.62	1.94	0.79	320	3.10	5.96	4.10	0.90	0.1242
22	26.405467	94.15695	6.4	421	47.03	15.18	10.76	7.36	1.44	0.14	228	5.17	5.96	4.70	0.80	0.0711
23	26.4079	94.156333	6.9	385	44.54	17.12	9.13	8.20	1.52	0.29	212	3.90	25.81	3.70	0.90	0.0737
24	26.4086	94.157833	6.4	299	16.05	9.51	8.11	18.15	1.29	1.31	140	2.60	3.97	1.50	0.20	0.0324
25	26.4122	94.16335	6.6	276	26.81	12.41	6.65	6.47	0.88	0.29	176	5.20	5.96	5.10	1.70	0.0539

26	26.41345	94.16605	6.6	411	48.35	19.12	11.51	7.99	1.67	0.16	244	5.60	3.97	4.30	1.20	0.0646
27	26.413617	94.16605	6.6	308	31.54	21	7.17	5.96	0.89	0.21	180	5.20	5.96	6.80	1.30	0.0816
28	26.413583	94.165833	6.8	590	74.00	30.67	17.35	7.01	2.17	0.46	348	2.80	5.96	3.50	0.80	0.1142
29	26.419233	94.1652	6.9	560	67.97	22.74	14.96	8.62	2.06	0.32	332	4.20	5.96	4.00	1.00	0.0977
30	26.421933	94.165367	6.8	291	21.47	13.45	8.93	6.87	0.73	0.50	180	4.60	3.97	2.50	0.90	0.0287
31	26.421933	94.1555	6.8	327	31.56	18.73	9.34	7.81	0.74	0.57	184	6.20	5.96	2.40	1.00	0.0396
32	26.422533	94.164417	6.7	336	36.72	12	8.41	7.39	1.09	0.90	204	7.30	9.93	4.30	1.40	0.0455
33	26.42255	94.164983	6.9	344	38.72	15.15	8.86	6.76	1.00	0.72	212	6.60	3.97	4.40	1.40	0.0495
34	26.429983	94.163933	6.8	393	37.69	15.17	10.58	5.52	1.20	0.44	216	4.40	5.96	3.70	0.30	0.0529
35	26.4398	94.163633	7.3	597	98.91	15.66	10.08	6.36	1.68	0.20	360	2.30	5.96	2.30	1.50	0.0413
36	26.440033	94.163667	6.4	360	33.95	11.83	9.53	5.61	1.15	0.49	212	4.60	5.96	5.70	1.60	0.1105
37	26.45475	94.166367	6.8	358	35.21	16.89	9.09	6.85	1.13	0.13	208	2.30	3.97	5.00	1.40	0.1177
38	26.454967	94.16635	6.8	345	33.90	12.52	9.15	6.75	1.14	0.12	200	2.40	3.97	3.90	1.10	0.1623
39	26.461317	94.167117	7.1	464	48.88	12.54	16.69	5.15	1.12	0.13	260	2.20	5.96	6.50	0.50	0.1582

A 1.6 Groundwater Quality of Site_4 of Jorhat District (mg/l)

Sl. No.	X	Y	pH	EC	Na	Ca	Mg	Fe	K	Mn	HCO_3^-	SO_4^{2-}	Cl	NO_3^-	PO_4^{3-}	As
1	26.5974	94.27245	6.9	524	42.48	14	19.0	18.34	1.68	0.14	300	6.00	4.00	18.70	1.00	0.0430
2	26.597033	94.270867	7.3	466	63.83	21.2	12.0	1.20	1.15	0.22	288	3.00	8.00	8.60	0.60	0.0770
3	26.59685	94.268783	7.4	466	64.87	10.8	10.6	1.90	1.13	0.23	296	2.00	6.00	8.80	0.70	0.0771
4	26.597167	94.267183	7.4	453	59.95	20.7	10.4	1.65	1.14	0.27	280	2.50	6.00	7.30	0.70	0.0681
5	26.5975	94.2646	7.4	445	64.31	18.7	10.0	1.29	1.12	0.32	272	3.20	6.00	11.10	1.30	0.0676
6	26.59855	94.2615	7.4	445	59.43	12.4	9.9	0.95	3.02	0.27	284	2.00	4.00	9.50	0.90	0.1005
7	26.617533	94.259367	7.1	444	57.09	11.9	10.4	0.59	4.80	0.31	280	1.30	8.00	11.20	0.80	0.0794
8	26.582467	94.146283	6.7	417	50.39	14	11.8	9.63	2.03	0.21	232	5.00	4.00	17.60	1.70	0.0848
9	26.581217	94.151167	7.4	446	58.49	16.3	10.5	1.59	1.97	0.19	268	1.30	8.00	7.10	0.50	0.1236
10	26.583367	94.155633	7.4	448	62.27	10.1	10.1	9.00	1.00	0.23	268	3.30	6.00	9.30	1.20	0.0863
11	26.583967	94.157333	7.3	412	54.04	13.5	9.8	3.19	1.20	0.20	240	2.70	8.00	8.10	0.90	0.1300
12	26.58485	94.159317	6.7	288	8.30	9.6	11.2	16.85	1.68	1.13	120	3.30	25.00	4.50	0.50	0.0404
13	26.584817	94.159383	7.1	383	50.42	14.2	9.1	1.98	1.15	0.17	228	2.40	8.00	7.50	0.70	0.0899
14	26.587233	94.158167	7.3	397	51.29	9.1	9.4	1.35	1.13	0.16	232	19.40	6.00	8.30	14.00	0.0749
15	26.5869	94.158367	7.4	498	64.57	14	10.5	0.76	1.14	0.06	292	1.60	10.00	7.50	1.80	0.0413
16	26.56985	94.158533	6.9	352	42.51	7.6	8.1	10.11	1.12	0.11	204	6.00	8.00	18.50	1.50	0.0600
17	26.585467	94.160783	6.4	290	21.01	20.4	8.9	15.13	3.02	0.18	164	15.00	8.00	29.50	2.20	0.0389

Sl. No.	X	Y	pH	EC	Na	Ca	Mg	Fe	K	Mn	HCO_3^-	SO_4^{2-}	Cl	NO_3^-	PO_4^{3-}	As
18	26.598	94.153367	7.1	440	62.07	13.8	10.8	0.69	4.80	0.14	296	2.00	10.00	10.60	1.40	0.0829
19	26.596567	94.155433	7.4	530	85.82	22	8.9	0.83	2.03	0.05	312	2.00	8.00	8.90	1.40	0.0514
20	26.595883	94.158883	7.2	349	38.37	11.8	7.6	4.69	1.97	0.20	196	2.70	10.00	6.90	1.00	0.0176
21	26.593783	94.158883	7.1	363	39.77	14.1	7.0	9.47	1.00	0.17	200	3.30	28.00	7.70	1.50	0.0487

Appendix - A 2

Scanning Electron Microscopy (SEM) and Energy Dispersive X-Ray (EDX) figures has been shown for drillcore 1A location of Site_1.

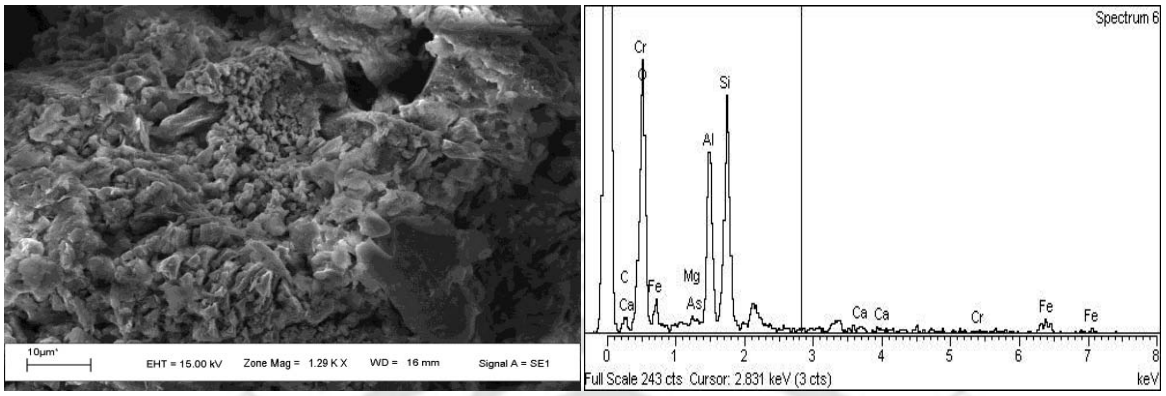

Figure A 2.1 SEM and EDX of sediment sample 1A_10 at depth 3 m.

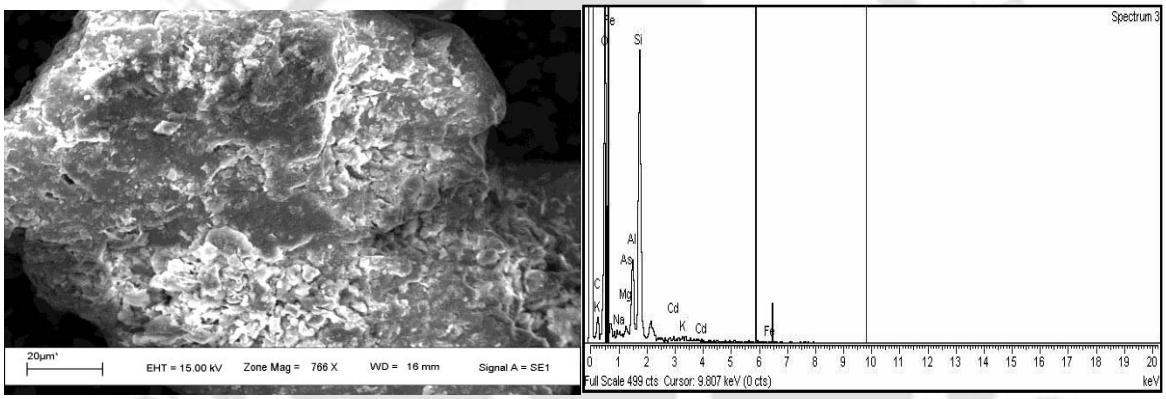

Figure A 2.2 SEM and EDX of sediment 1A_30 at depth 9 m.

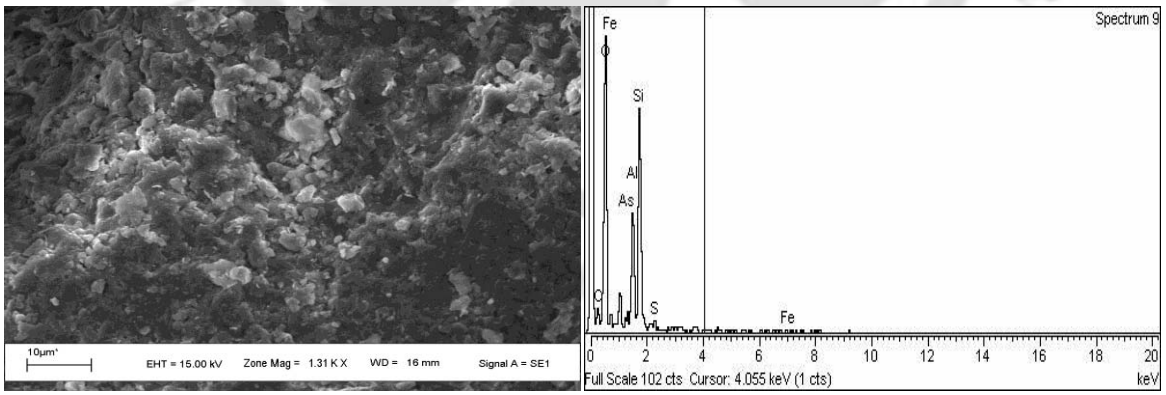

Figure A 2.3 SEM and EDX of sediment 1A_50 at depth 15 m.

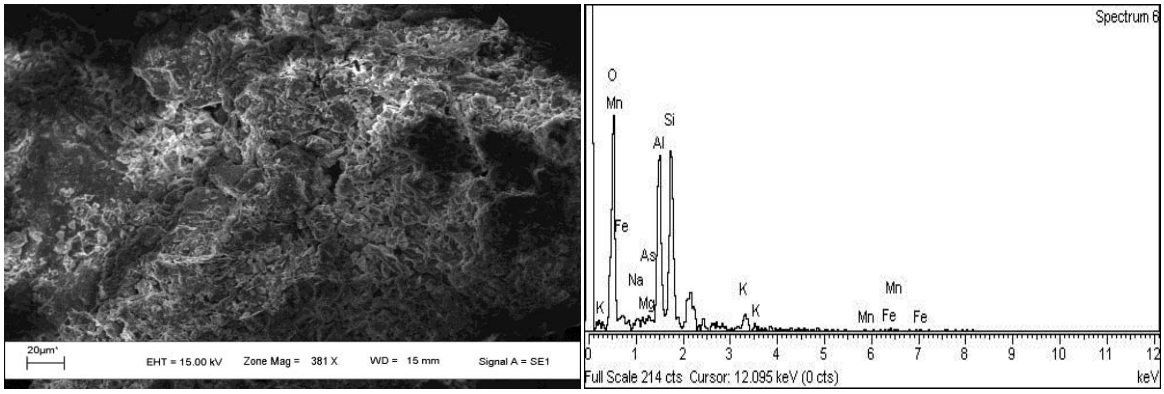

Figure A 2.4 SEM and EDX of sediment 1A_70 at depth 21 m.

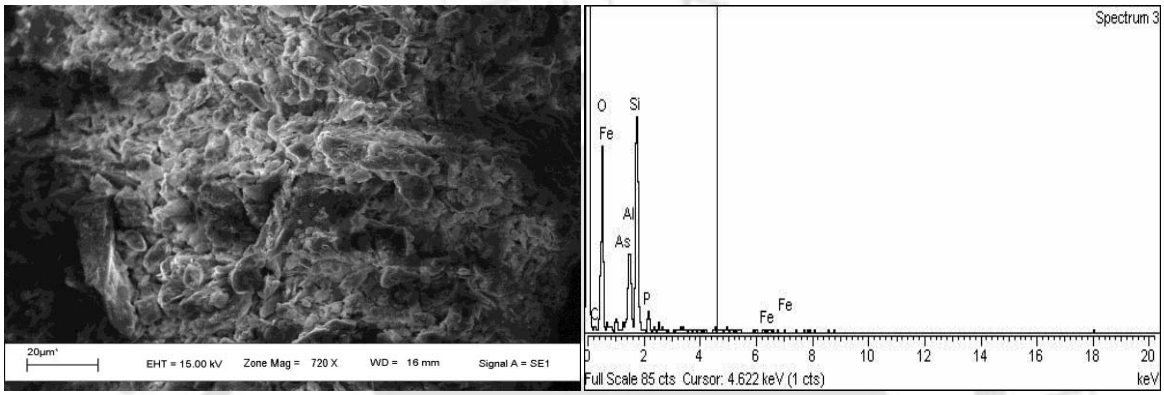

Figure A 2.5 SEM and EDX of sediment 1A_90 at depth 27.5 m.

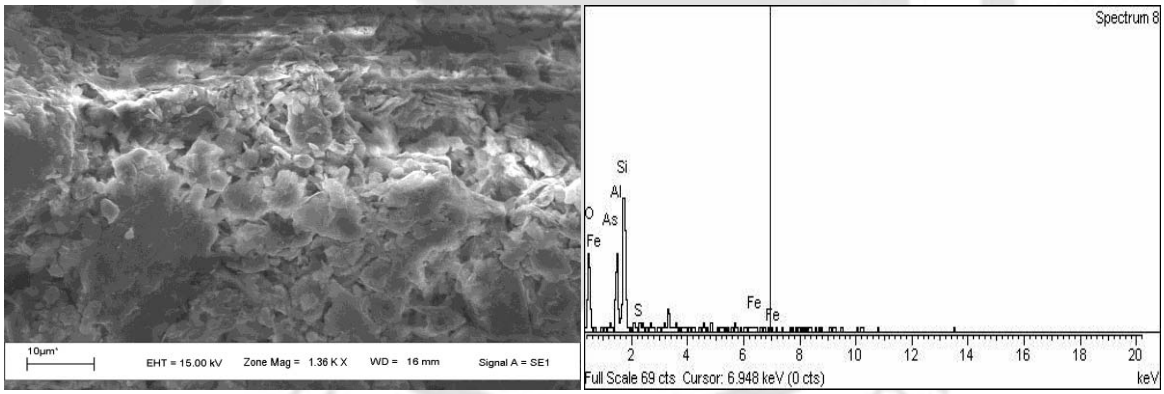

Figure A 2.6 SEM and EDX of sediment 1A_110 at depth 33.5 m.

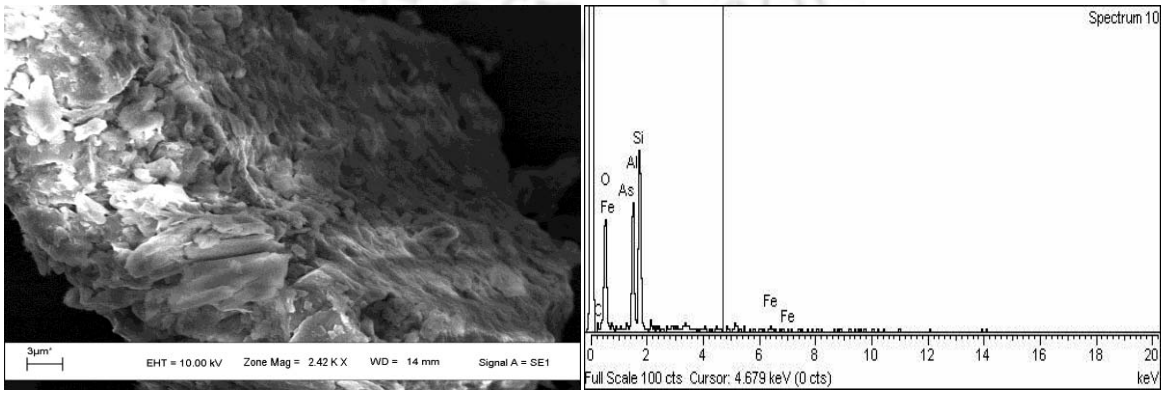

Figure A 2.7 SEM and EDX of sediment 1A_150 at depth 47 m.

Appendix – A 3

X-Ray Diffractograms (XRD) for drillcore 1A location of Site_1.

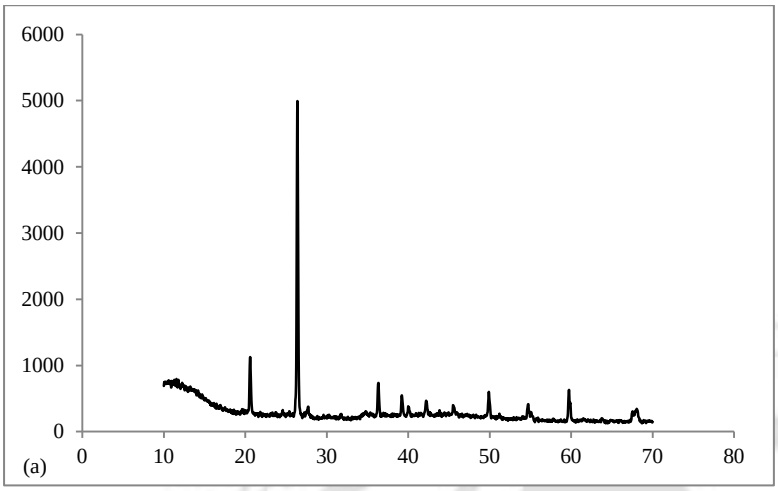

Figure A 3.1 XRD of sediment sample 1A_10 at depth 3 m.

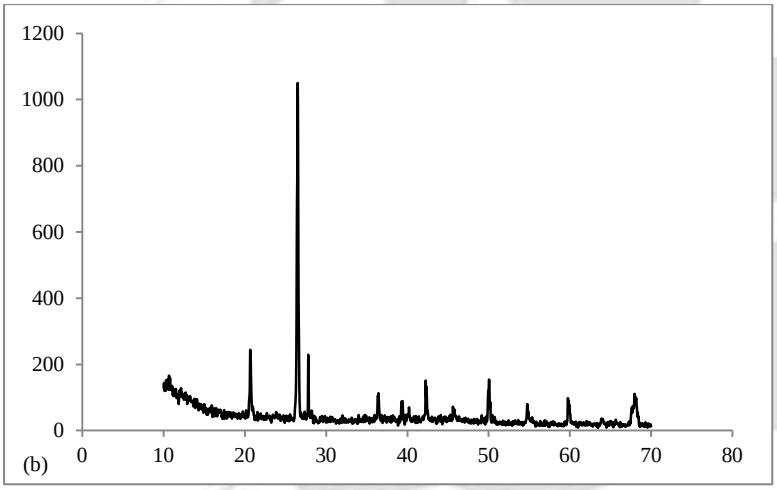

Figure A 3.2 XRD of sediment 1A_30 at depth 9 m.

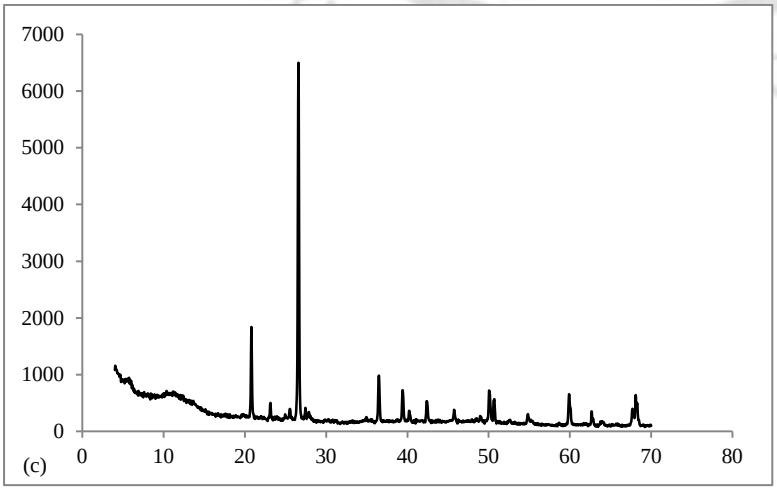

Figure A 3.3 XRD of sediment 1A_50 at depth 15 m.

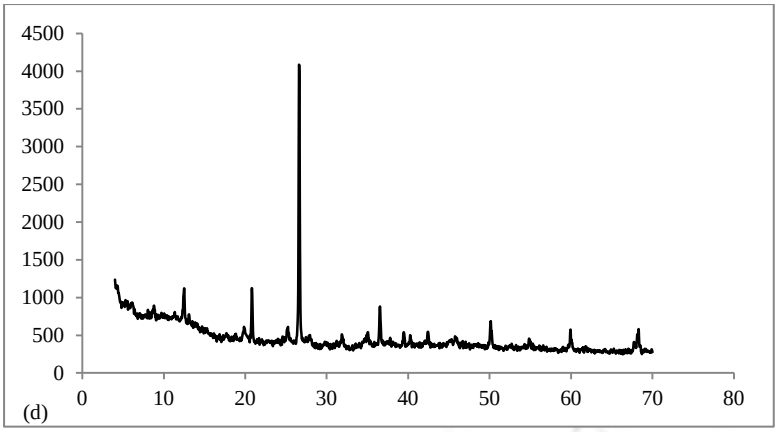

Figure A 3.4 XRD of sediment 1A_70 at depth 21 m.

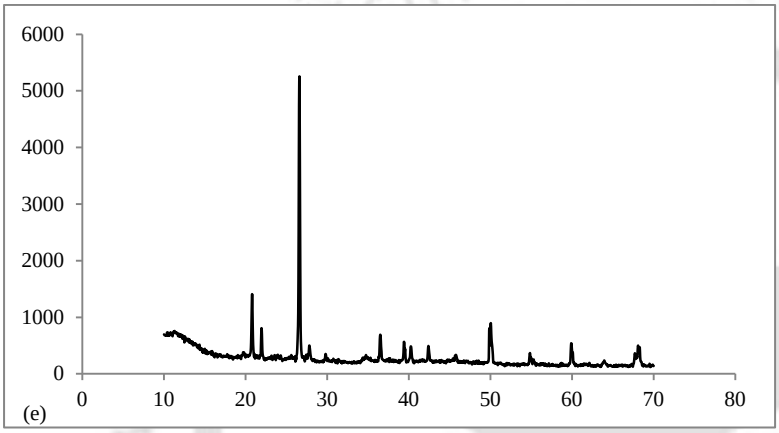

Figure A 3.5 XRD of sediment 1A_90 at depth 27.5 m.

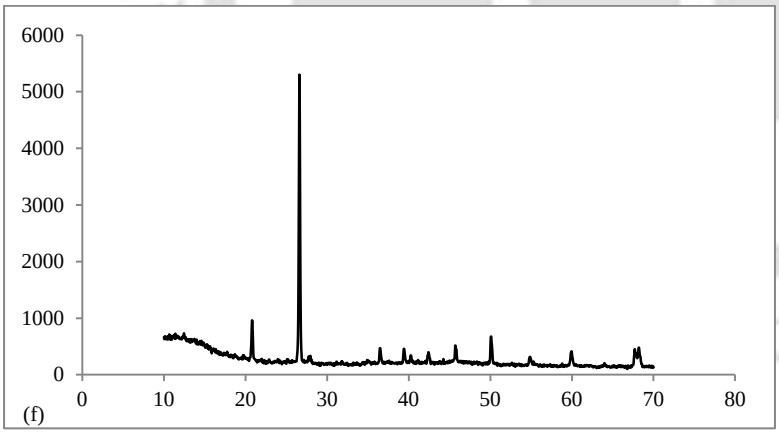

Figure A 3.6 XRD of sediment 1A_110 at depth 33.5 m.

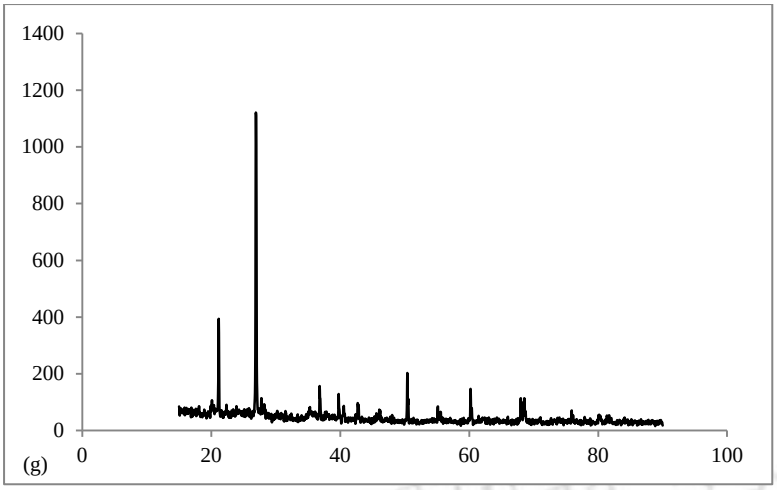

Figure A 3.7 XRD of sediment 1A_130 at depth 40 m.

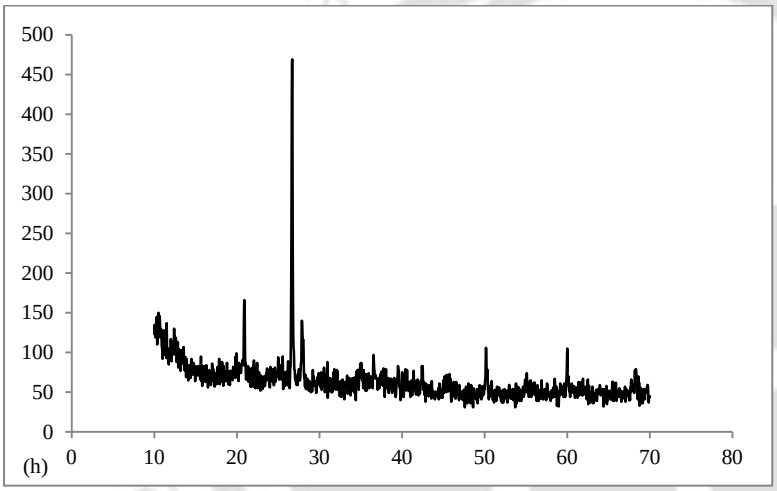

Figure A 3.8 XRD of sediment 1A_150 at depth 47 m.

Appendix - A 4

Total metal concentration in the sediments analyzed using EPA-3052 digestion procedure for Copper (Cu), Zinc (Zn), Cadmium (Cd), Chromium (Cr), Sodium (Na), Magnesium (Mg), Calcium (Ca) and Potassium (K).

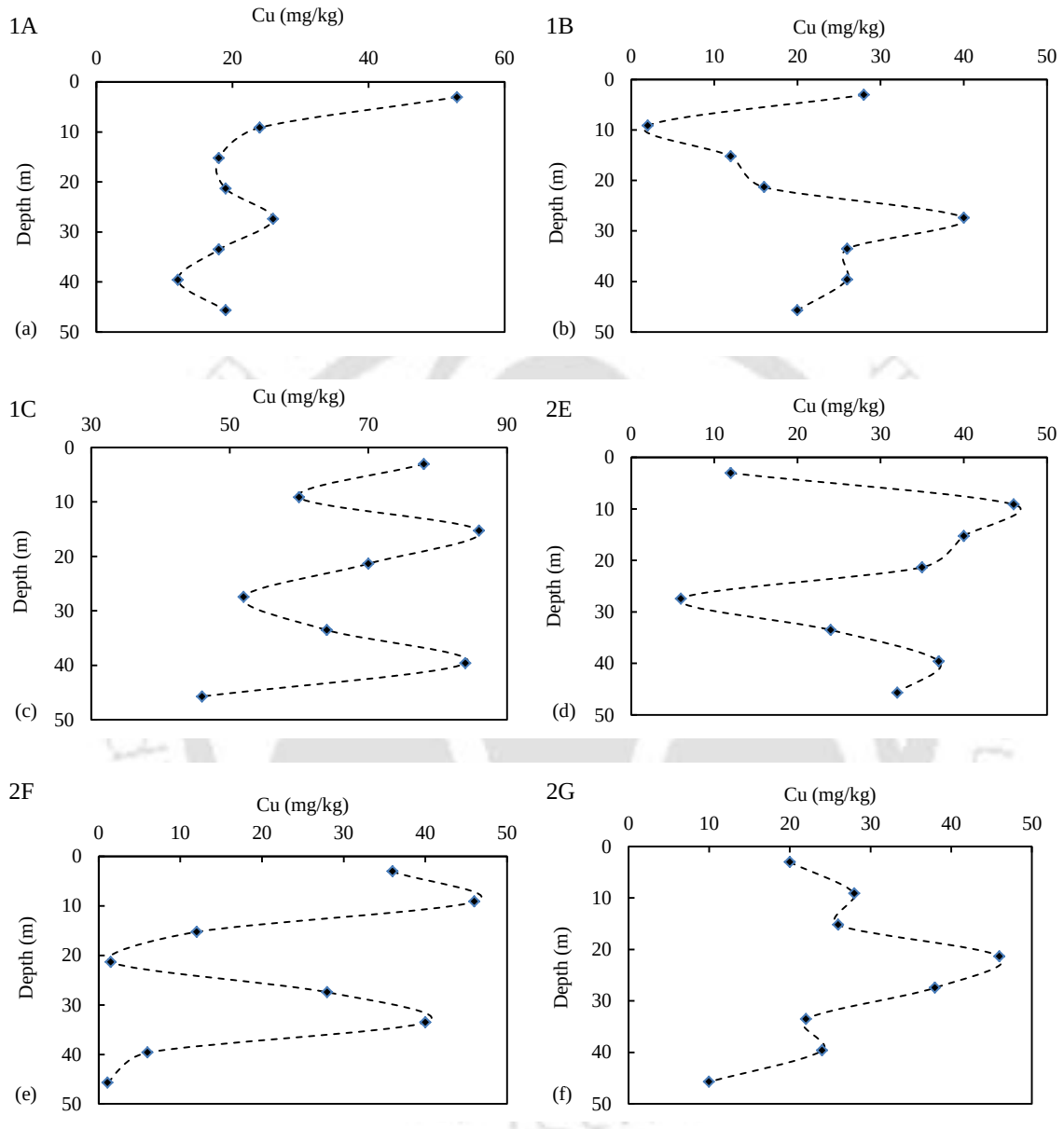

Figure A 4.1 Total Copper (Cu) concentration in the sediment core samples along the depth profile at locations (a) 1A (b) 1B (c) 1C (d) 2E (e) 2F (f) 2G.

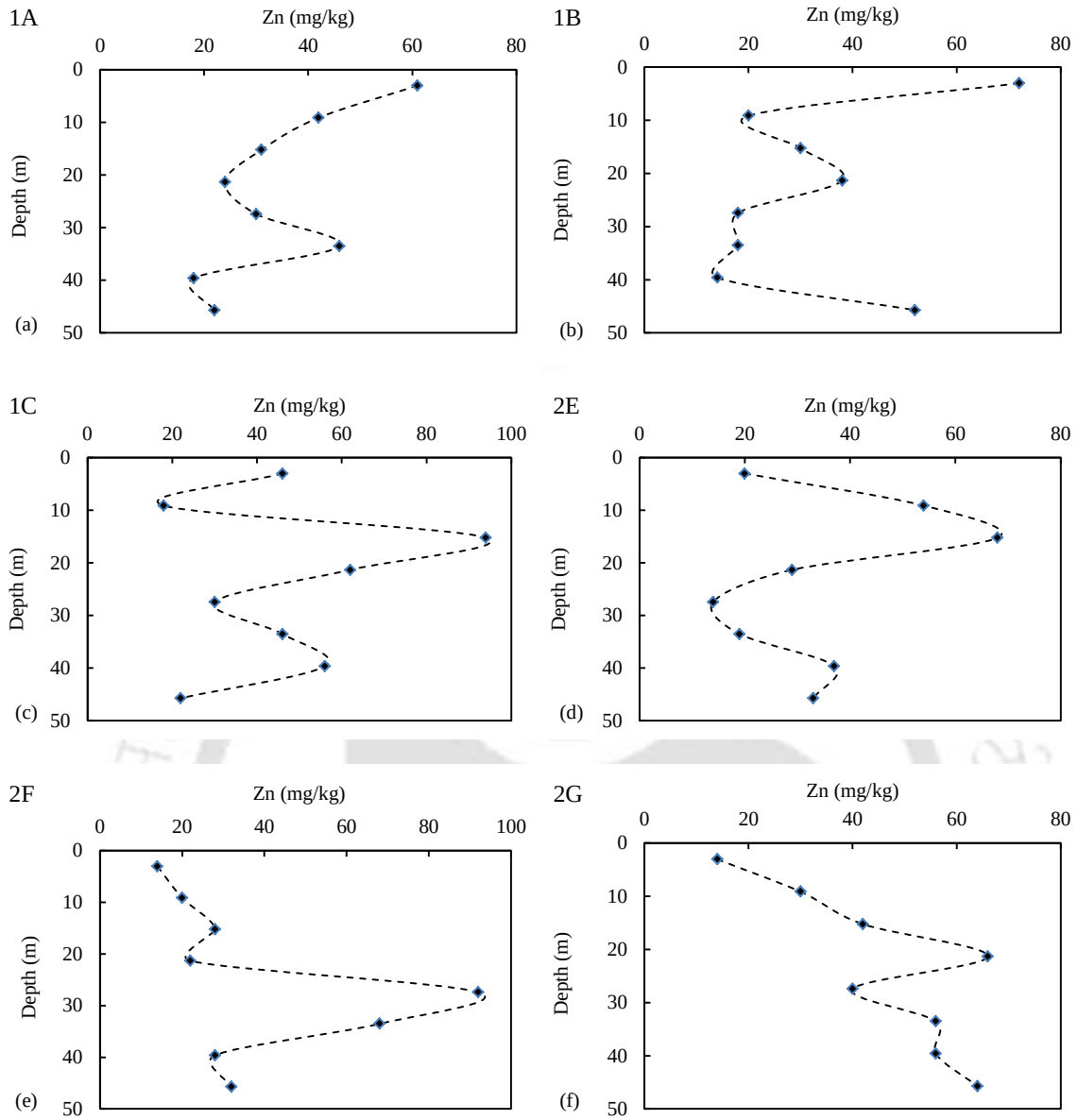

Figure A 4.2 Total Zinc (Zn) concentration in the sediment core samples along the depth profile at locations (a) 1A (b) 1B (c) 1C (d) 2E (e) 2F (f) 2G.

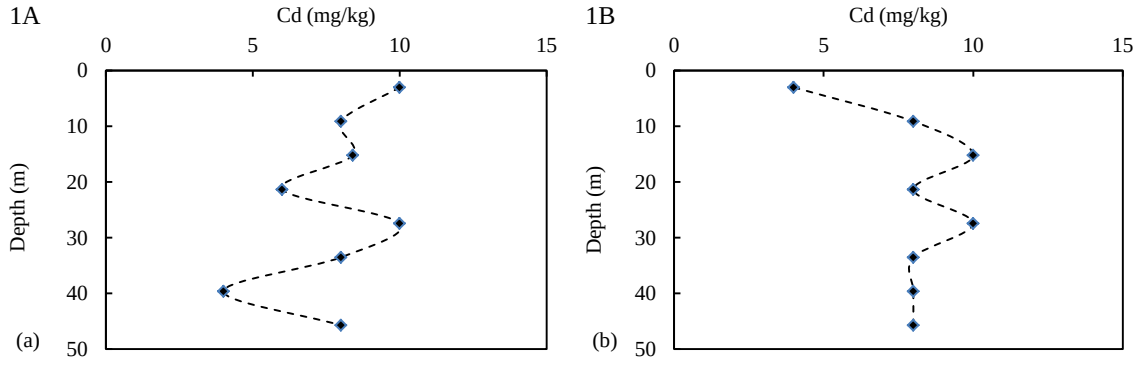

Figure A 4.3 Total Cadmium (Cd) concentration in the sediment core samples along the depth profile at locations (a) 1A (b) 1B.

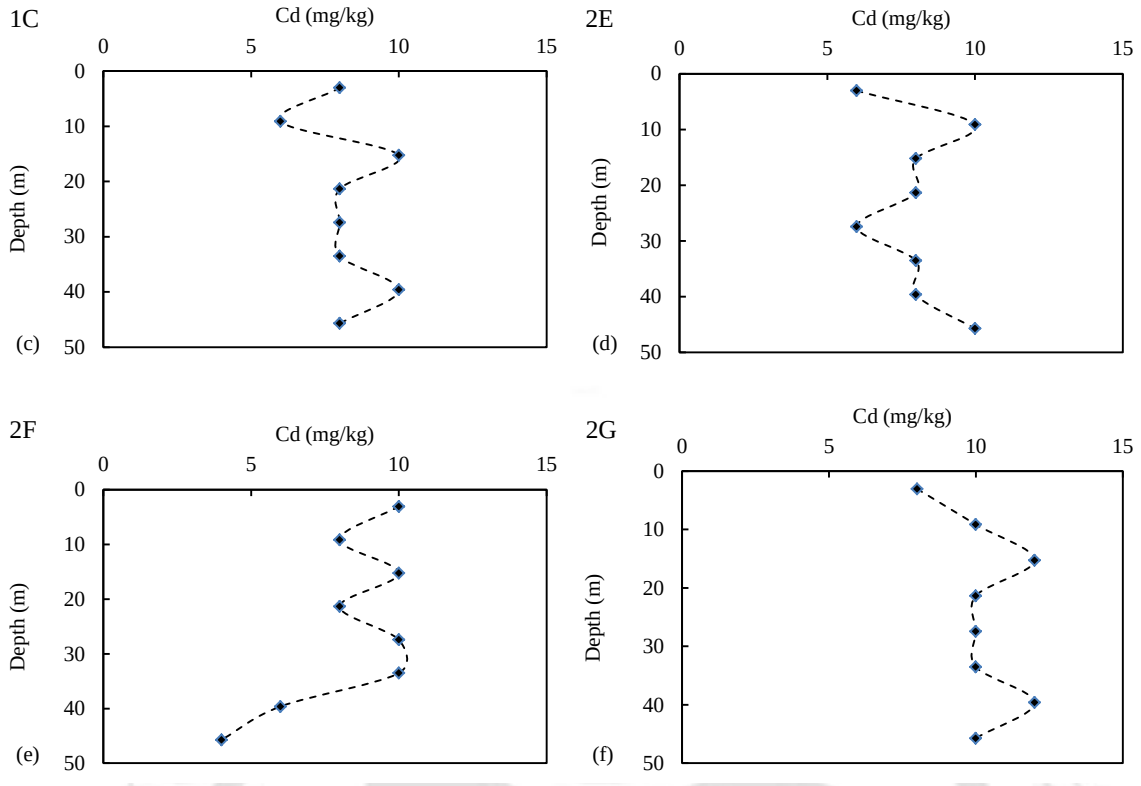

Figure A 4.3 Total Cadmium (Cd) concentration in the sediment core samples along the depth profile at locations (c) 1C (d) 2E (e) 2F (f) 2G.

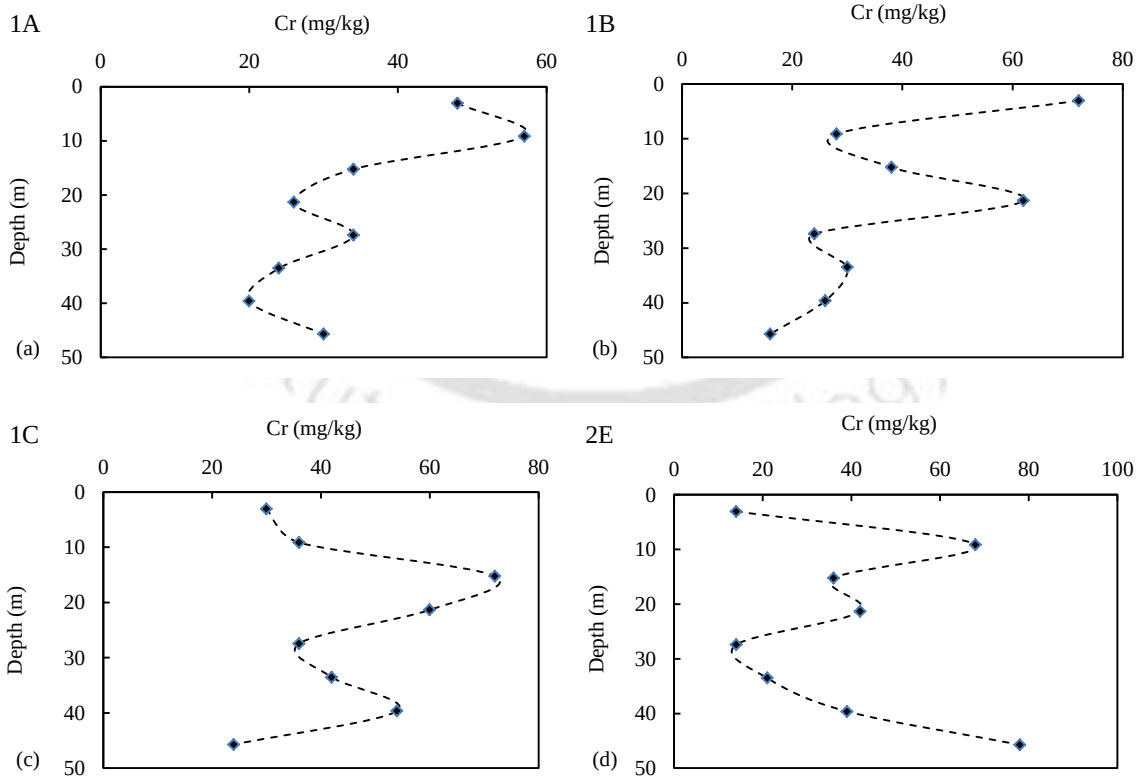

Figure A 4.4 Total Chromium (Cr) concentration in the sediment core samples along the depth profile at locations (a) 1A (b) 1B (c) 1C (d) 2E.

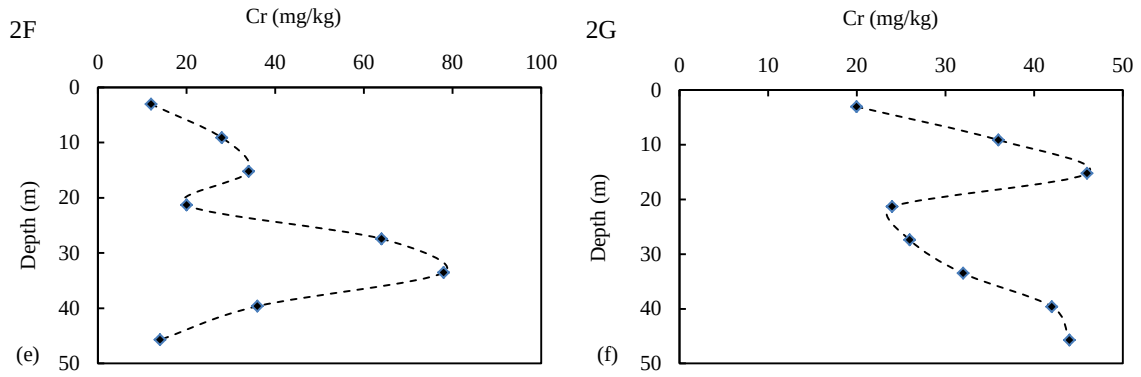

Figure A 4.4 Total Chromium (Cr) concentration in the sediment core samples along the depth profile at locations (e) 2F (f) 2G.

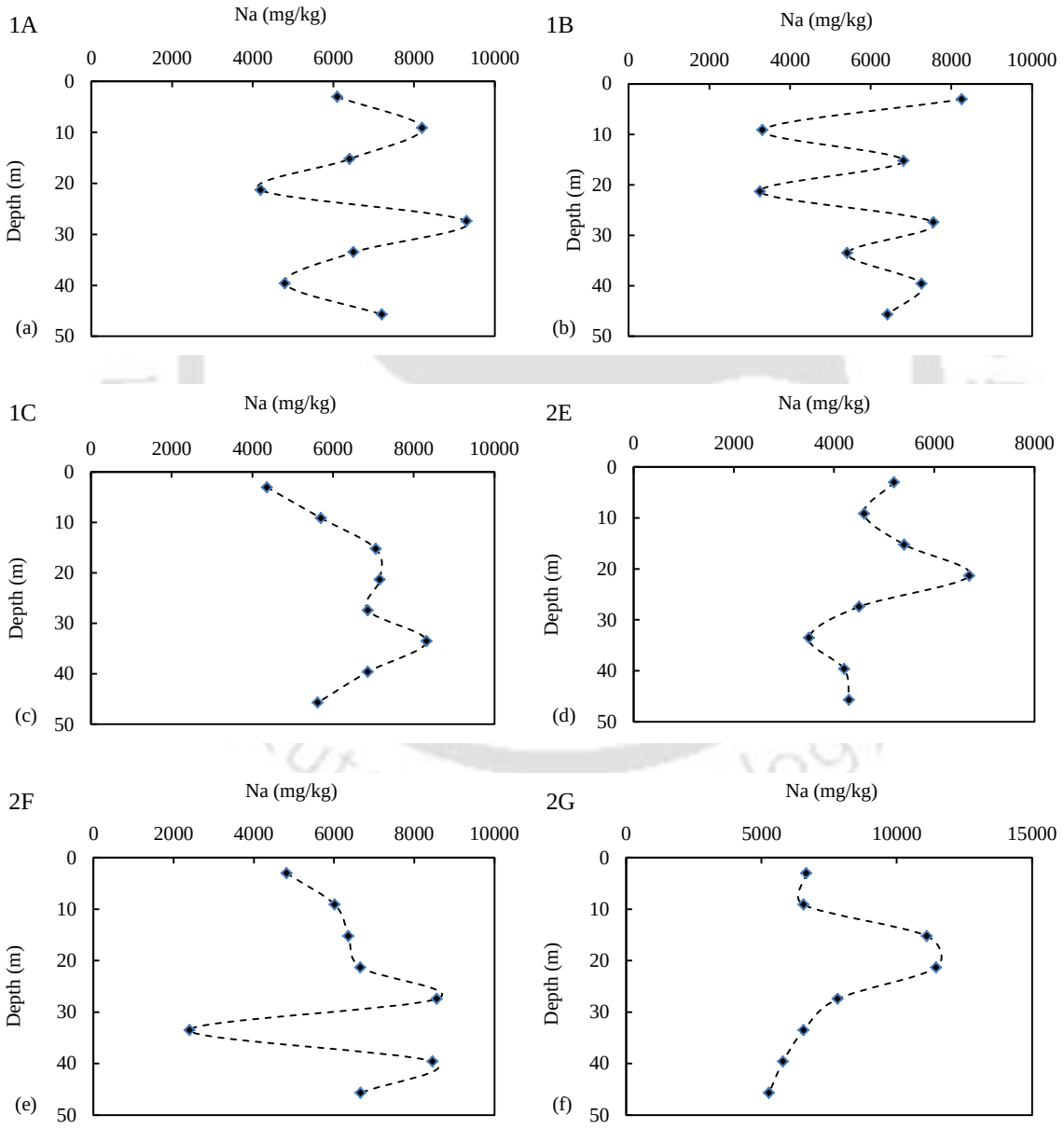

Figure A 4.5 Total Sodium (Na) concentration in the sediment core samples along the depth profile at locations (a) 1A (b) 1B (c) 1C (d) 2E (e) 2F (f) 2G.

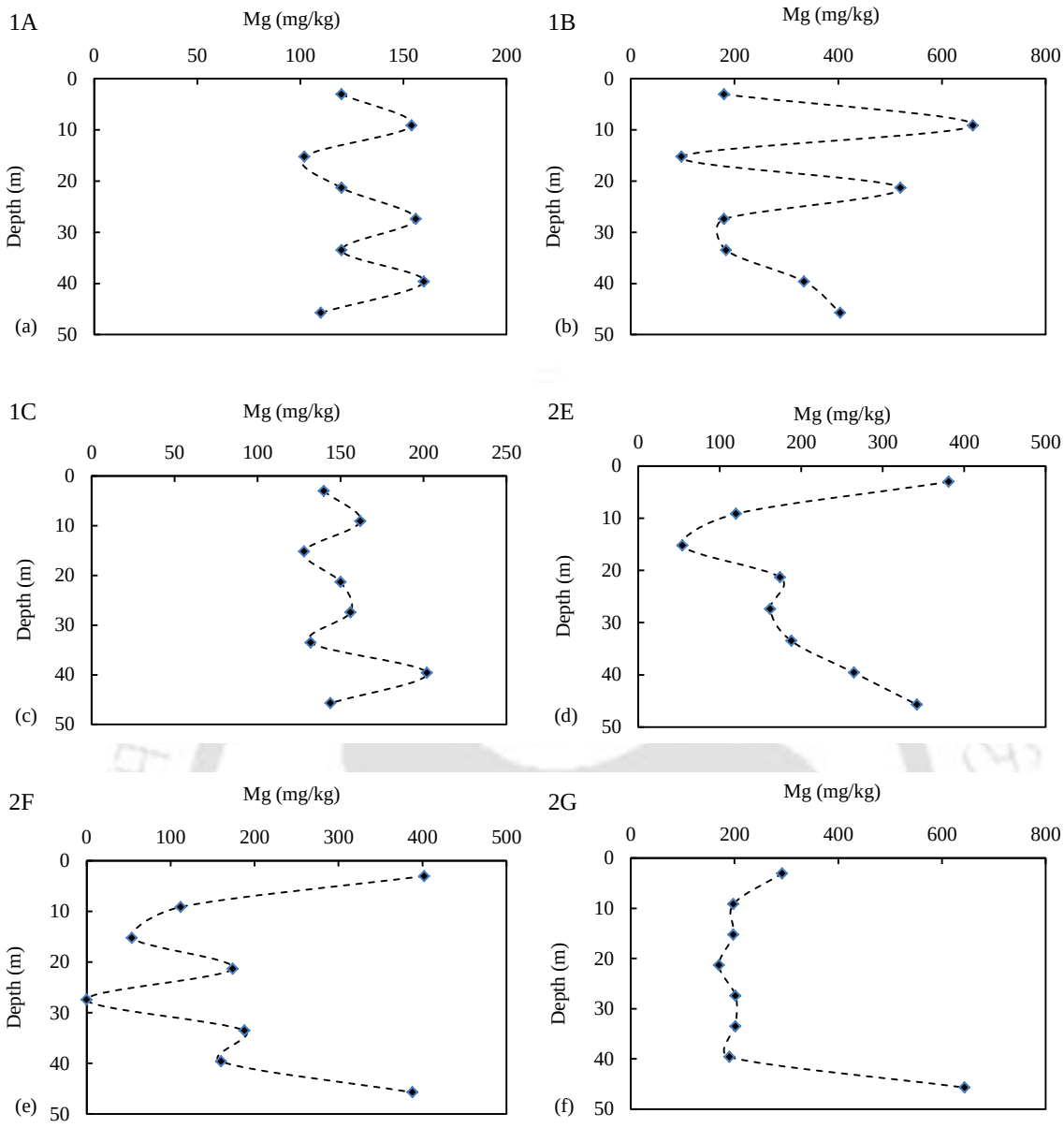

Figure A 4.6 Total Magnesium (Mg) concentration in the sediment core samples along the depth profile at locations (a) 1A (b) 1B (c) 1C (d) 2E (e) 2F (f) 2G.

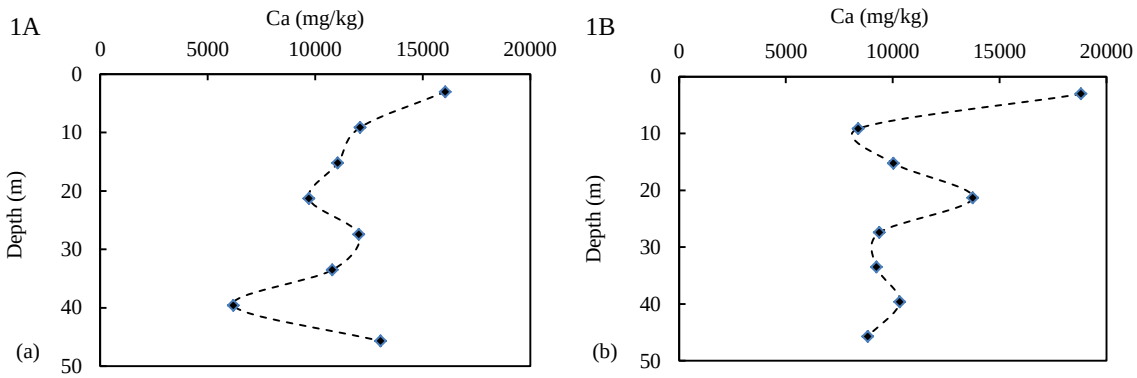

Figure A 4.7 Total Calcium (Ca) concentration in the sediment core samples along the depth profile at locations (a) 1A (b) 1B.

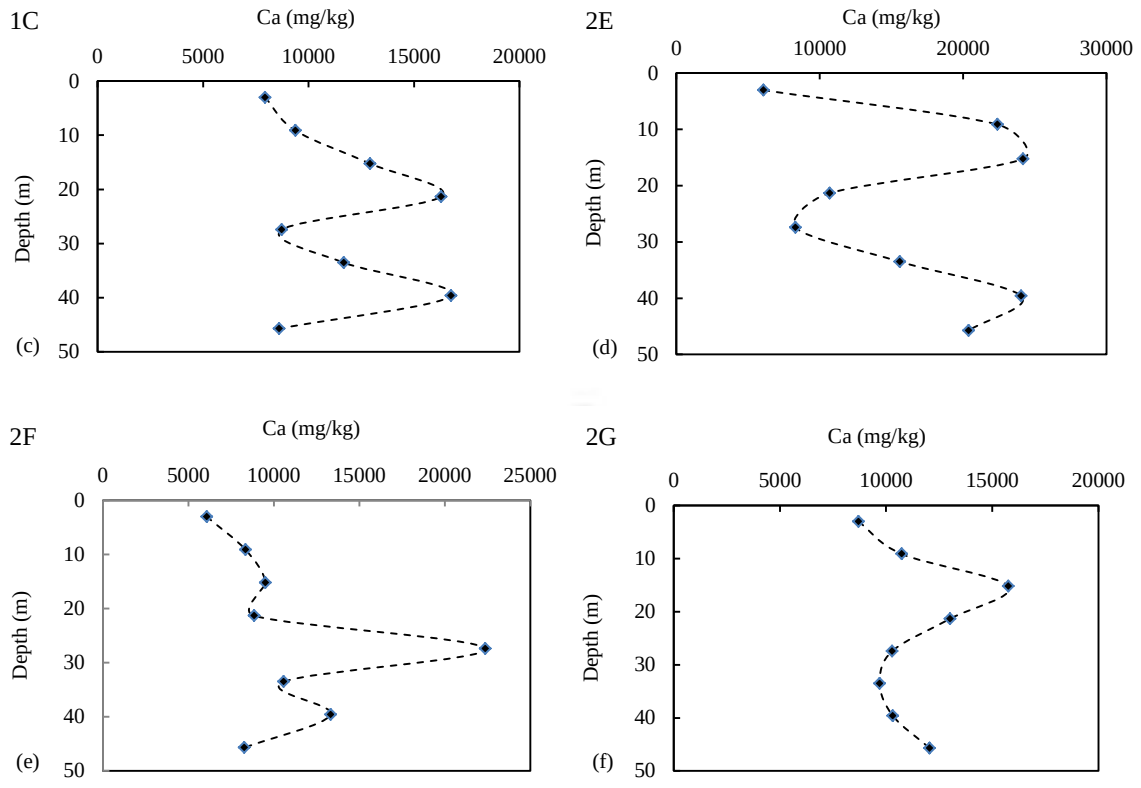

Figure A 4.7 Total Calcium (Ca) concentration in the sediment core samples along the depth profile at (c) 1C (d) 2E (e) 2F (f) 2G.

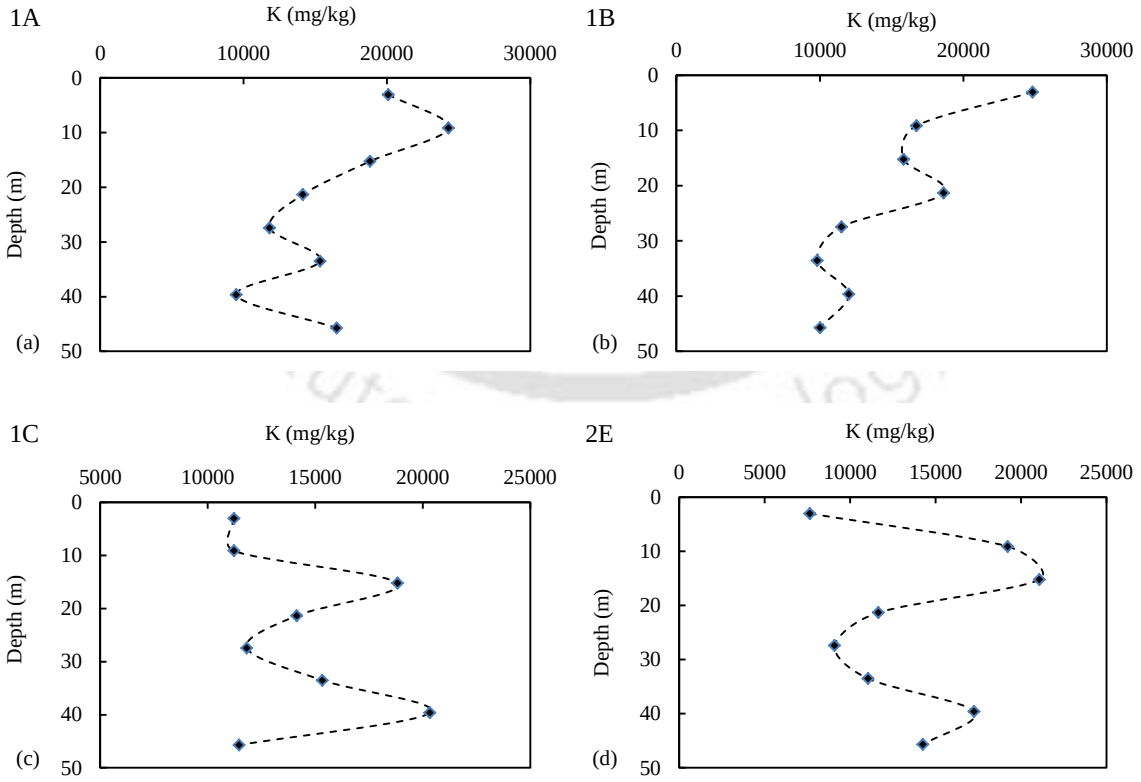

Figure A 4.8 Total Potassium (K) concentration in the sediment core samples along the depth profile at locations (a) 1A (b) 1B (c) 1C (d) 2E.

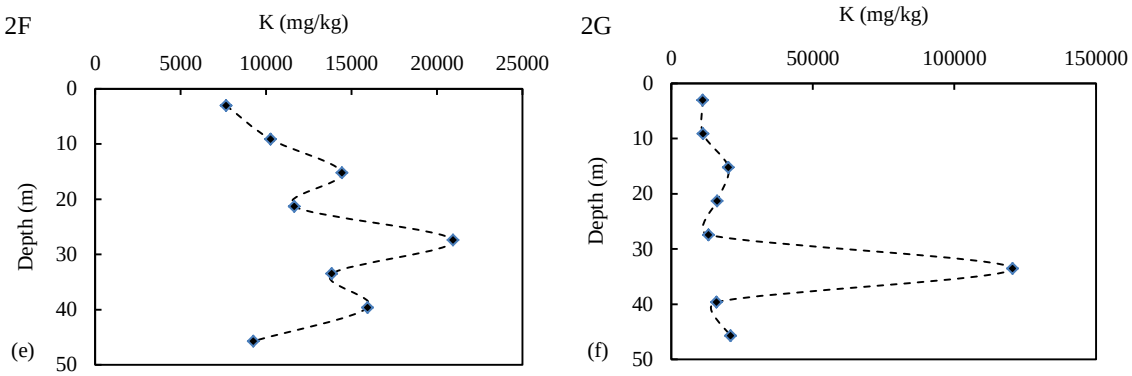

Figure A 4.8 Total Potassium (K) concentration in the sediment core samples along the depth profile at locations (e) 2F (f) 2G.

Appendix - A 5. Results of Selective Sequential Extraction (SSE) in mg/kg for the sediment samples of Site_1.

Samples	Ext_1	Ext_2	Ext_3	Ext_4	Ext_5	Ext_6	Ext_7
1A_10	0.020	1.600	0.060	0.109	1.50	2.54	4.03
1A_30	0.070	1.250	0.005	0.037	1.50	3.20	3.83
1A_50	0.043	0.150	0.015	0.021	1.47	2.10	4.32
1A_70	0.109	0.720	0.020	0.037	2.70	3.12	8.00
1A_90	0.005	0.200	0.027	0.065	2.54	2.00	4.63
1A_110	0.110	1.500	0.141	0.061	1.20	1.20	4.40
1A_130	0.030	1.000	0.029	0.019	1.70	0.87	4.85
1A_150	0.060	0.750	0.038	0.018	1.20	1.00	4.18

Samples	Ext_1	Ext_2	Ext_3	Ext_4	Ext_5	Ext_6	Ext_7
2E_10	0.263	0.332	0.056	0.016	1.00	1.40	4.50
2E_30	0.425	0.358	0.099	0.045	2.00	4.00	6.30
2E_50	0.238	0.484	0.107	0.067	6.00	2.90	6.00
2E_70	0.370	0.353	0.107	0.069	1.78	3.70	4.94
2E_90	0.275	0.924	0.128	0.126	2.00	4.20	7.06
2E_110	0.626	0.785	0.197	0.164	1.66	2.40	4.17
2E_130	0.516	1.406	0.174	0.126	2.60	2.40	6.42
2E_150	0.293	0.525	0.093	0.126	1.20	1.94	4.18

Samples	Ext_1	Ext_2	Ext_3	Ext_4	Ext_5	Ext_6	Ext_7
1B_10	0.642	0.703	0.113	0.237	6.00	3.00	7.35
1B_30	0.340	0.582	0.100	0.100	0.81	0.88	9.58
1B_50	0.377	0.633	0.098	0.076	0.59	0.66	10.43
1B_70	0.435	0.900	0.090	0.067	1.32	3.30	11.95
1B_90	0.456	0.966	0.123	0.150	3.33	0.99	7.03
1B_110	0.281	0.992	0.135	0.125	4.32	3.79	7.30
1B_130	0.325	1.135	0.100	0.145	1.99	3.92	5.58
1B_150	0.374	0.923	0.100	0.135	1.42	3.00	8.53

Samples	Ext_1	Ext_2	Ext_3	Ext_4	Ext_5	Ext_6	Ext_7
2F_10	0.252	0.505	0.123	0.080	0.50	0.23	6.00
2F_30	0.292	0.830	0.163	0.079	2.40	0.30	11.07
2F_50	0.321	0.809	0.109	0.050	3.40	1.47	10.30
2F_70	0.313	0.559	0.128	0.050	0.67	0.37	9.50
2F_90	0.901	1.200	0.077	0.040	6.50	12.71	22.00
2F_110	0.352	1.717	0.124	0.100	5.67	5.72	17.00
2F_130	0.348	1.560	0.111	0.091	1.65	2.75	12.50
2F_150	0.358	0.565	0.041	0.060	1.01	1.45	8.00

Samples	Ext_1	Ext_2	Ext_3	Ext_4	Ext_5	Ext_6	Ext_7
1C_10	0.215	0.627	0.113	0.237	1.64	0.78	8.30
1C_30	0.183	0.646	0.100	0.100	2.66	0.79	8.90
1C_50	0.263	0.950	0.098	0.076	2.00	0.67	13.25
1C_70	0.221	0.761	0.090	0.067	8.00	4.35	25.00
1C_90	0.611	2.805	0.123	0.150	1.98	0.90	11.45
1C_110	0.261	0.800	0.135	0.125	1.80	3.50	11.00
1C_130	0.269	1.281	0.100	0.145	3.24	1.10	15.00
1C_150	0.259	0.637	0.100	0.135	2.01	0.80	7.00

Samples	Ext_1	Ext_1	Ext_1	Ext_1	Ext_1	Ext_1	Ext_1
2G_10	0.025	0.783	0.027	0.028	1.25	2.00	10.55
2G_30	0.050	0.450	0.078	0.095	1.20	3.40	11.30
2G_50	0.075	1.750	0.089	0.082	4.00	3.00	14.00
2G_70	0.100	1.340	0.067	0.075	1.00	4.01	10.30
2G_90	0.125	0.375	0.042	0.058	3.40	1.27	8.00
2G_110	0.150	1.450	0.087	0.089	1.50	2.89	8.00
2G_130	0.175	0.425	0.067	0.092	3.27	3.50	10.00
2G_150	0.200	0.450	0.089	0.045	1.40	2.89	10.00

Table A 6.5 Elovich Kinetics model for 1C_50 300 µg/l Initial As(III) concentration

Time (mins)	As(III)	qt	ln(T)	X=qt/qe	ln(1-X)	Model qtm	(qtm-avgqt)^2	(qtm-qt)^2	r2
5	220	1.6	1.609	0.320	-0.657	1.701	0.656	0.010	0.97
10	203.9	1.9215	2.303	0.192	-0.864	1.895	0.379	0.001	
20	193	2.14	2.996	0.107	-1.034	2.089	0.178	0.003	
30	187	2.26	3.401	0.075	-1.141	2.202	0.095	0.003	
60	170	2.6	4.094	0.043	-1.527	2.396	0.013	0.041	
120	173	2.54	4.787	0.021	-1.447	2.590	0.006	0.003	
240	164	2.72	5.481	0.011	-1.709	2.785	0.075	0.004	
360	153.2	2.936	5.886	0.008	-2.155	2.898	0.150	0.001	
600	146.5	3.07	6.397	0.005	-2.583	3.041	0.281	0.001	
1440	134	3.32	7.272	0.002	-8.108	3.286	0.601	0.001	

Plot of qt versus t1/2
Fig 5.34
intercept
slope
b=1/slope
a=exp(inercept*b)/b

Table A 6.6 Intra-particle diffusion model for 1C_50 300 µg/l Initial As(III) concentration

Time (mins)	As(III)	qt	t1/2	X=qt/qe	ln(1-X)	Bt	model qtm=(A-B)	(qtm-avgqt)^2	(qtm-qt)^2	r2
5	220	1.6	2.236	0.320	-0.657	0.160	0.243	0.027	0.006	0.80
10	203.9	1.9215	3.162	0.192	-0.864	0.366	0.188	0.012	0.000	
20	193	2.14	4.472	0.107	-1.034	0.536	0.150	0.005	0.002	
30	187	2.26	5.477	0.075	-1.141	0.643	0.129	0.003	0.003	
60	170	2.6	7.746	0.043	-1.527	1.030	0.070	0.000	0.001	
120	173	2.54	10.954	0.021	-1.447	0.950	0.081	0.000	0.004	
240	164	2.72	15.492	0.011	-1.709	1.212	0.049	0.001	0.001	
360	153.2	2.936	18.974	0.008	-2.155	1.657	0.012	0.004	0.000	
600	146.5	3.07	24.495	0.005	-2.583	2.085	-0.011	0.008	0.000	
1440	134	3.32	37.947	0.002	-8.108	7.610	-0.054	0.018	0.003	

Plot of qt versus t1/2
Fig 5.35

1.250
0.280
3.571
24.321

Appendix - A 7

Table A 7.1 Input parameters for PHREEQC surface complexation model in amorphous Fe-oxides for surface site densities (mol sites/mol Fe) for sample 1B-2G.

Sl. no.	Sample Id	Depth m	Amor. Fe(mg/kg)	Ferrihydrite g/kg	HFO_ w	HFO_s	Goe_
1	1B -10	3	5697	38.03	8.55E-02	2.14E-03	6.35E-03
2	1B -30	9	3529	23.56	5.29E-02	1.32E-03	3.93E-03
3	1B -50	15	2564	17.11	3.85E-02	9.62E-04	2.86E-03
4	1B -70	21	3329	22.22	4.99E-02	1.25E-03	3.71E-03
5	1B -90	27	3157	21.07	4.74E-02	1.18E-03	3.52E-03
6	1B -110	33	950	6.34	1.43E-02	3.56E-04	1.06E-03
7	1B -130	40	3459	23.09	5.19E-02	1.30E-03	3.86E-03
8	1B -150	46	2100	14.02	3.15E-02	7.88E-04	2.34E-03
9	1C -10	3	2416	16.13	3.62E-02	9.06E-04	2.69E-03
10	1C -30	9	9058	60.46	1.36E-01	3.40E-03	1.01E-02
11	1C -50	15	1257	8.39	1.89E-02	4.71E-04	1.40E-03
12	1C -70	21	21545	143.81	3.23E-01	8.08E-03	2.40E-02
13	1C -90	27	2602	17.37	3.90E-02	9.76E-04	2.90E-03
14	1C -110	33	5880	39.25	8.82E-02	2.21E-03	6.55E-03
15	1C -130	40	13661	91.19	2.05E-01	5.12E-03	1.52E-02
16	1C -150	46	2604	17.38	3.91E-02	9.77E-04	2.90E-03
17	2E -10	3	174	1.16	2.61E-03	6.53E-05	1.94E-04
18	2E -30	9	2113	14.1	3.17E-02	7.92E-04	2.35E-03
19	2E -50	15	1426	9.52	2.14E-02	5.35E-04	1.59E-03
20	2E -70	21	1337	8.92	2.01E-02	5.01E-04	1.49E-03
21	2E -90	27	778	5.19	1.17E-02	2.92E-04	8.67E-04
22	2E -110	33	833	5.56	1.25E-02	3.12E-04	9.29E-04
23	2E -130	40	2130	14.22	3.20E-02	7.99E-04	2.37E-03
24	2E -150	46	3410	22.76	5.12E-02	1.28E-03	3.80E-03
25	2F -10	3	333	2.22	5.00E-03	1.25E-04	3.71E-04
26	2F -30	9	2487	16.6	3.73E-02	9.33E-04	2.77E-03
27	2F -50	15	4183	27.92	6.27E-02	1.57E-03	4.66E-03
28	2F -70	21	1359	9.07	2.04E-02	5.10E-04	1.51E-03
29	2F -90	27	6949	46.38	1.04E-01	2.61E-03	7.75E-03
30	2F -110	33	6829	45.58	1.02E-01	2.56E-03	7.61E-03
31	2F -130	40	14179	94.64	2.13E-01	5.32E-03	1.58E-02
32	2F -150	46	3705	24.73	5.56E-02	1.39E-03	4.13E-03
33	2G -10	3	468	3.12	7.02E-03	1.76E-04	5.21E-04
34	2G -30	9	2528	16.87	3.79E-02	9.48E-04	2.82E-03
35	2G -50	15	2541	16.96	3.81E-02	9.53E-04	2.83E-03

36	2G -70	21	849	5.67	1.27E-02	3.18E-04	9.47E-04
37	2G -90	27	2288	15.27	3.43E-02	8.58E-04	2.55E-03
38	2G -110	33	1517	10.13	2.28E-02	5.69E-04	1.69E-03
39	2G -130	40	1643	10.97	2.46E-02	6.16E-04	1.83E-03
40	2G -150	46	3890	25.97	5.84E-02	1.46E-03	4.34E-03

Table A 7.2 Input parameters for PHREEQC surface complexation model in crystalline Fe-oxides for surface site densities (mol sites/mol Fe) for sample 1B-2G.

Sl. no.	Sample Id	Depth m	Cryst. Fe (mg/kg)	Ferrihydrite g/kg	HFO_ w	HFO_s	Goe_
1	1B -10	3	18100	120.82	2.72E-01	6.79E-03	2.02E-02
2	1B -30	9	3523	23.52	5.28E-02	1.32E-03	3.93E-03
3	1B -50	15	2453	16.37	3.68E-02	9.20E-04	2.73E-03
4	1B -70	21	4750	31.71	7.13E-02	1.78E-03	5.29E-03
5	1B -90	27	1849	12.34	2.77E-02	6.93E-04	2.06E-03
6	1B -110	33	3240	21.63	4.86E-02	1.22E-03	3.61E-03
7	1B -130	40	3957	26.41	5.94E-02	1.48E-03	4.41E-03
8	1B -150	46	3721	24.84	5.58E-02	1.40E-03	4.15E-03
9	1C -10	3	4246	28.34	6.37E-02	1.59E-03	4.73E-03
10	1C -30	9	3388	22.61	5.08E-02	1.27E-03	3.78E-03
11	1C -50	15	1906	12.72	2.86E-02	7.15E-04	2.12E-03
12	1C -70	21	4347	29.02	6.52E-02	1.63E-03	4.85E-03
13	1C -90	27	1120	7.48	1.68E-02	4.20E-04	1.25E-03
14	1C -110	33	3253	21.71	4.88E-02	1.22E-03	3.63E-03
15	1C -130	40	4835	32.27	7.25E-02	1.81E-03	5.39E-03
16	1C -150	46	5198	34.7	3.91E-02	9.77E-04	2.90E-03
17	2E -10	3	1476	9.85	2.21E-02	5.54E-04	1.65E-03
18	2E -30	9	4378	29.22	6.57E-02	1.64E-03	4.88E-03
19	2E -50	15	5662	37.79	8.49E-02	2.12E-03	6.31E-03
20	2E -70	21	4554	30.4	6.83E-02	1.71E-03	5.08E-03
21	2E -90	27	1775	11.85	2.66E-02	6.66E-04	1.98E-03
22	2E -110	33	3789	25.29	5.68E-02	1.42E-03	4.22E-03
23	2E -130	40	3542	23.64	5.31E-02	1.33E-03	3.95E-03
24	2E -150	46	4773	31.86	7.16E-02	1.79E-03	5.32E-03
25	2F -10	3	348	2.32	5.22E-03	1.31E-04	3.88E-04
26	2F -30	9	1039	6.94	1.56E-02	3.90E-04	1.16E-03
27	2F -50	15	4254	28.4	6.38E-02	1.60E-03	4.74E-03
28	2F -70	21	967	6.45	1.45E-02	3.63E-04	1.08E-03
29	2F -90	27	21779	145.37	3.27E-01	8.17E-03	2.43E-02
30	2F -110	33	8743	58.36	1.31E-01	3.28E-03	9.75E-03

31	2F -130	40	10347	69.07	1.55E-01	3.88E-03	1.15E-02
32	2F -150	46	2519	16.81	3.78E-02	9.45E-04	2.81E-03
33	2G -10	3	2831	18.9	4.25E-02	1.06E-03	3.16E-03
34	2G -30	9	3115	20.79	4.67E-02	1.17E-03	3.47E-03
35	2G -50	15	4556	30.41	6.83E-02	1.71E-03	5.08E-03
36	2G -70	21	1677	11.19	2.52E-02	6.29E-04	1.87E-03
37	2G -90	27	3501	23.37	5.25E-02	1.31E-03	3.90E-03
38	2G -110	33	1870	12.48	2.81E-02	7.01E-04	2.08E-03
39	2G -130	40	1943	12.97	2.91E-02	7.29E-04	2.17E-03
40	2G -150	46	3574	23.86	5.36E-02	1.34E-03	3.98E-03

Table A 7.3 Model output using *As* extracted from amorphous Fe-oxides for sample 1B- 2G.

Sl. no.	Sample Id	Extracted_*As*	Model_*As*	Difference (%) between Extract and Modeled *As*
1	1B -10	4.1	1.84	55.1
2	1B -30	1.84	1.13	38.6
3	1B -50	1.75	0.83	52.9
4	1B -70	2.42	1.07	55.8
5	1B -90	2.14	1.08	49.5
6	1B -110	1.78	0.33	81.5
7	1B -130	3.24	1.17	63.9
8	1B -150	1.42	0.63	55.6
9	1C -10	1.64	0.78	52.4
10	1C -30	2.66	2.92	-9.8
11	1C -50	2	0.41	79.5
12	1C -70	8	6.93	13.4
13	1C -90	2	0.84	58.0
14	1C -110	1.8	1.89	-5.0
15	1C -130	3.24	4.4	-35.8
16	1C -150	0.8	0.82	-2.5
17	2E -10	0.54	0.06	89.6
18	2E -30	2	0.68	66.1
19	2E -50	2.1	0.46	78.1
20	2E -70	1.78	0.43	75.8
21	2E -90	0.64	0.25	60.9
22	2E -110	1.02	0.27	73.5
23	2E -130	2.6	0.69	73.5
24	2E -150	2.71	1.1	59.4
25	2F -10	0.5	0.11	78.0
26	2F -30	2.4	0.8	66.7
27	2F -50	3.4	1.35	60.4

Sl. no.	Sample Id	Extracted_*As*	Model_*As*	Difference (%) between Extract and Modeled *As*
28	2F -70	0.67	0.44	34.2
29	2F -90	6.5	2.32	64.3
30	2F -110	5.67	2.2	61.2
31	2F -130	7.25	4.47	38.3
32	2F -150	1.01	1.19	-17.4
33	2G -10	0.41	0.15	63.4
34	2G -30	1.75	0.81	53.7
35	2G -50	2.01	0.82	59.2
36	2G -70	0.51	0.28	45.1
37	2G -90	2.4	0.74	69.2
38	2G -110	1.75	0.49	72.0
39	2G -130	1.05	0.53	49.5
40	2G -150	2.55	1.25	51.0

Table A 7.4 Model output using *As* extracted from crystalline Fe-oxides for sample 1B-2G.

Sl. no.	Sample Id	Extracted_*As*	Model_*As*	Difference (%) between Extracted and Modeled *As*
1	1B -10	6.04	9.6	-58.94
2	1B -30	1.75	1.86	-6.29
3	1B -50	0.97	1.3	-34.02
4	1B -70	3.3	2.51	23.94
5	1B -90	0.64	0.97	-51.56
6	1B -110	3.15	1.7	46.03
7	1B -130	2.84	2.1	26.06
8	1B -150	2.48	1.97	20.56
9	1C -10	3.07	2.25	26.71
10	1C -30	2.75	1.79	34.91
11	1C -50	0.67	1	-49.25
12	1C -70	4.35	2.3	47.13
13	1C -90	0.9	0.59	34.44
14	1C -110	3.5	1.73	50.57
15	1C -130	3.75	2.55	32.00
16	1C -150	2.01	1.67	16.92
17	2E -10	1.4	0.78	44.29
18	2E -30	2.75	2.3	16.36
19	2E -50	2.9	3	-3.45
20	2E -70	2.94	2.41	18.03
21	2E -90	1.75	0.94	46.29
22	2E -110	2.4	2	16.67
23	2E -130	2.4	1.87	22.08
24	2E -150	2.55	2.53	0.78

Sl. no.	Sample Id	Extracted_*As*	Model_*As*	Difference (%) between Extracted and Modeled *As*
25	2F -10	0.22	0.18	18.18
26	2F -30	0.3	0.55	-83.33
27	2F -50	1.47	2.25	-53.06
28	2F -70	0.37	0.51	-37.84
29	2F -90	12.7	11.54	9.13
30	2F -110	5.72	4.63	19.06
31	2F -130	2.75	5.46	-98.55
32	2F -150	1.45	1.33	8.28
33	2G -10	1.45	1.5	-3.45
34	2G -30	2.45	1.65	32.65
35	2G -50	3	2.41	19.67
36	2G -70	1.05	0.88	16.19
37	2G -90	2.15	1.85	13.95
38	2G -110	1.45	0.98	32.41
39	2G -130	1.79	1	44.13
40	2G -150	2.75	1.89	31.27